EFFECTS OF POOL VOLUME ON WET MILLING EFFICIENCY

François Mulenga Katubilwa

A thesis submitted to the Faculty of Engineering and the Built Environment, University of the Witwatersrand, Johannesburg, in fulfilment of the requirements for the degree of Doctor of Philosophy.

Johannesburg, 2012

I declare that this thesis is my own, unaided work. It is being submitted for the Degree of Doctor of Philosophy to the University of the Witwatersrand, Johannesburg. It has not been submitted before for any degree or examination in any other University.

François Mulenga Katubilwa

…… day of ……. year ……..

Abstract

The volume of slurry in a rotary mill has a bearing on the presence of a pool of slurry and therefore on milling efficiency. Load behaviour was investigated at different volumes of slurry. The insight gained was then used to evaluate the implications of slurry pooling on milling.

First, the effects of viscosity on mill charge behaviour were measured using photographic techniques applied to a Perspex mill. A model of the angular location of the free surface of the slurry pool, as affected by slurry filling was proposed. Next, a real ore was used and the load behaviour was measured using non-invasive sensors fitted to a pilot mill. At this point, the angular position of the pool and the net power draw were correlated to the volume of slurry for mill speeds ranging from 65 to 85 % of critical. An additional series of tests was carried out on a mill filled with grinding media only, for speeds spanning from approximately 24 to 110 % of critical. The aim here was to isolate and study the media charge. Lastly, a laboratory mill was used to run batch grinding tests on a Platinum ore for slurry fillings U between 1.0 and 3.0 and at 65 % solids content. Two ball fillings were considered for identical slurry volumes: J = 20 % and 30 %.

Results showed that not only did the proposed pool model work well using an artificial slurry in the Perspex mill, but it also worked for the Platinum ore tested in the Wits pilot mill. The behaviour of the media charge was not substantially affected by slurry viscosity and slurry filling. The net power drawn by the 'dry mill' compared well with DEM prediction for non-centrifuging speeds. The effect of slurry pooling on net power draw, on the other hand, was best accounted for using a Torque-arm model and an empirical model developed to this end. As for milling kinetics, results suggested that the slurry pool should be avoided because milling efficiency deteriorated as a result. However, the production of fines was not largely altered.

Dedications

This work is dedicated to the two dearest people of my life: my wife Rose M. Chanda and my son Enoch B. Mulenga.

I believe this PhD thesis is a reward for your patience!

Acknowledgements

First and foremost, praise be to the Almighty GOD who gave me the opportunity to do a PhD thesis. My Lord, Jehovah Jireh, you have always been there to support, guide, encourage and strengthen me in each and every step of my life.

Achieving a PhD has always been a dream, and with the proper mentorship it has become a reality. As would say Antoine de Saint-Exupéry: "A goal without a plan is just a wish". Many thanks to Prof. Michael H. Moys, my supervisor, for being so understanding especially during the hard time this project had to face. Your valuable advices, assistance in proof-reading the draft, and availability in orientating me when things could not break through are highly appreciated.

To the love of my life Rose M. Chanda and our offspring Enoch B. Mulenga, you have been my inspiration and motivation when the tunnel was dark. Your countless prayers will never be rightfully valued; only I can deeply feel what it has been like being supported spiritually.

Comments and feedback from the Comminution Group of the Centre of Materials and Process Synthesis (COMPS), University of the Witwatersrand, Johannesburg, have been valuable. Dr. Matthew J. Metzger in particular has been helpful in the analysis of our results using the Attainable Region method.

I am also indebted to Dr. Murray M. Bwalya, Consulting Engineer with Prof Moys' Mineral Processing Research Group for his assistance in the use of SimView, the DEM simulator.

Lastly, Prof. Diane Hildebrandt and David Glasser, Directors of the Centre of Materials and Process Synthesis (COMPS), University of the Witwatersrand, Johannesburg are acknowledged for the financial assistance and for allowing the publication of these results.

Katubilwa, François Mulenga

Table of contents

List of publications

The articles below have been published or submitted to peer-reviewed journals in fulfilment of the requirements for the degree of Doctor of Philosophy. They are either directly related or relevant to the present thesis:

Katubilwa, F.M., Moys, M.H., 2011. Effects of filling degree and viscosity of slurry on mill load orientation. Minerals Engineering, vol. 24, no. 13, pp. 1502 – 1512

Katubilwa, F.M., Moys, M.H., Glasser, D., Hildebrandt, D., 2011. An attainable region analysis of the effect of ball size on milling. Powder Technology, vol. 210, no. 1, pp. 36 – 46

Chimwani, N., Glasser, D., Hildebrandt, D., Metzger, M.J., **Mulenga, F.K.**[1], 2012. Determination of the milling parameters of a platinum group minerals ore to optimize product size distribution for flotation purposes. Minerals Engineering, in press

Mulenga, F.K., Moys, M.H., 2012. Effects of slurry filling and mill speed on load behaviour. The Southern African Institute of Mining and Metallurgy, Abstracts submitted for the Southern African Mineral Beneficiation and Metallurgy Conference, MINPROC 2012

Mulenga, F.K., Moys, M.H., 2012. Effects of slurry volume on net power draw of a tumbling ball mill. International Journal of Mineral Processing, Submitted manuscript

The article below was published during the first author's research work towards his Masters degree at the University of the Witwatersrand in Johannesburg:

Katubilwa, F.M., Moys, M.H., 2009. Effects of ball size distribution on milling rate. Minerals Engineering, vol. 22, no. 15, pp. 1283 – 1288

[1] Prior to the edition of this paper, the full name of the first author was changed from François Mulenga Katubilwa (Katubilwa, F.M.) to François Katubilwa Mulenga (Mulenga, F.K.). New regulations in his country of origin now stipulate that middle name and surname be swapped around and changed accordingly.

List of figures

List of tables

List of Symbols

a	Selection function parameter which is mainly a function of milling conditions, see Equation (2.3)
a_1	Fitting parameter allowing for the mass of balls M_b in the mill
a_2	Fitting parameter which is a strong function of the volumetric concentration of powder in slurry for $0.3 \leq C_v \leq 0.55$
a_3	Fitting parameter which is a strong function of the volumetric concentration of powder in slurry for $0.3 \leq C_v \leq 0.55$
A	Curve fitting parameter dependent on the fractional ball filling J, see Equation (2.13)
A_0	Area between the bisect line and the product distribution line in the definition of the Size Reduction ratio, see Equation (6.1)
A_1	Fitting parameter used to represent the piece-wise function in Equation (5.15)
A_2	Fitting parameter used to represent the piece-wise function in Equation (5.15)
b	Fitting parameter used to represent the piece-wise function in Equation (5.15)
$b_{i,j}$	Primary breakage distribution function of a particle of size j breaking into size i
B	Curve fitting parameter function of the fractional mill filling J, see Equation (2.13)
$B_{i,j}$	Cumulative breakage function
c	Constant given the value of 1.32, see Equation (2.10)
C_0	Fitting parameter in Equation (4.2)
C_d	Damping matrix as defined in Equation (2.12)
C_v	Volumetric concentration of powder in slurry in percent
d	Diameter of grinding balls in m
D	Diameter of the mill inside liners in m
D_{eff}	Effective diameter due to the prematurely centrifuged layer
E	Curve fitting parameter dependent on the fractional speed of the mill ϕ, see Equation (2.14)
E_m	Margin of error or maximum error of the estimate
f	Piece-wise function used as the empirical model for the effect of slurry pooling on mill power in Equation (5.15)
F	Curve fitting parameter function of the fractional speed of the mill ϕ, see Equation (2.14)

$\vec{F}_i$	Force vector applied on particle i
g	Constant of gravity, that is, 9.81 m/s^2
GI	Grinding index
i	Integer defining the different size intervals, the largest being 1
I	Moment of inertia of particle in Equation (2.12)
J	Ball filling or fraction of mill volume occupied by grinding balls at rest including interstices
J_{eff}	Effective ball filling
k	Fitting parameter in Equation (4.2)
K	Stiffness matrix as defined in Equation (2.12)
K_1	Constant allowing for liner design and slurry properties. It is given the value of 12.262 by Bond, see Equation (5.1)
K_2	Constant function of liner design and slurry properties, see Equation (5.4)
L	Length of the mill inside liners in m
$\vec{L}_i$	Position vector considered from the centroid of the grinding ball to the resultant force $\vec{F}_i$ applied on it
m	Mass of particle in interaction as defined in Equation (2.12)
M_b	Mass of balls in the mill in kg
M_i *or* m_i	Mass fraction of particles in size class i
M_L	Mass of the load in kg, that is, media charge filled with slurry
M_p	Mass of the pool of slurry in kg
$\vec{M}$	Moment about the centroid of particle i
n	Size class corresponding to the sink fraction in the Population Balance Modelling (PBM) of milling
N	Number of data points in a sample or size of the sample
N_c	Theoretical critical speed of the mill in revolutions per second
N_{eff}	Effective speed of the mill in percent of critical speed
N_m	Rotational speed of the mill in revolutions per second
N_r	Angular speed of the grinding media at radial position r
$P_{expt}(t)$	Measured particle size distribution after grinding time t
$P_{model}(t)$	Predicted particle size distribution after grinding time t
P_{net} or m_p	Net power draw by the mill in Watts
P_0	Parameter representing the net power drawn by the mill at slurry filling U = 0 in Equation (5.14)
r	Radial position inside the mill in m
r_i	Inner surface radius of the charge marking the boundary between the active and the inactive kidney-shaped ball charges in m

$\vec{r}_i$	Position vector of particle i in interaction as defined in Equation (2.12)
r_m	Internal radius of the mill given by $r_m = D/2$ in m
R^2	Coefficient of determination
S_D	Percent passing a specified size in the mill discharge
s_e	Standard error of estimate
S_F	Percent passing a specified size in the mill feed
S_i	Selection function or rate of disappearance of particles of material in size class i
SSE	Sum of Squares of Errors in Equation (4.3)
SR	Degree of size reduction or Size Reduction index
t	Actual grinding time as measured during laboratory batch tests
$T_{shoulder}$	Exit time in seconds corresponding to the shoulder position of the media charge
T_{toe}	Time of entry in seconds of the proximity probe corresponding to the detection of the toe of the media charge
U	Slurry filling or ratio of volume of slurry loaded to the volume of ball interstices available within the static bed of grinding media
U_0	Initial slurry filling considered for batch testing
U_t	Actual slurry filling at a given grinding time t
V_{balls}	Volume of balls occupied by the static bed of grinding balls inside the mill
V_{mill}	Volume of the mill in m^3
V_{sl}	Volume of slurry needed to make up a slurry filling U
w_i or $w_i(t)$	Mass fraction present in the size interval i after grinding time t
x	Independent variable or parameter inducing a response y
x_i	Upper size of the particle size interval i under consideration
x_L	Centre of mass of the media charge filled with slurry
x_p	Centre of mass of the pool of slurry
y	Measurement of the response or dependent variable
y_i	Experimental value of y measured for a given x_i (x-value)
y_{mdl}	Predicted value of y obtained using a regression equation
z	Empirical parameter equated to $z = (1 - J)^{0.4532}$, see Equation (2.18)
$z_{\alpha/2}$	Critical statistical value as defined in Equation (5.6)
α	Selection function parameter which is material-dependent
α_d	Dynamic angle of repose of the load in radians

β	Breakage function parameter characteristic of the material used. Its values generally range from 2.5 to 5
β_0	Bond model parameter determining at which load volume maximum power occurs. It is given a value of 0.937 by Bond
δ_c	Thickness of the prematurely centrifuging layer expressed as a fraction of the mill diameter (D)
ε	Porosity of the bed of grinding media at rest inside the mill. The average value is assumed to be 0.4
Δ_J	Parameter that governs the strength of the dependence of δ_c on J. It is a strong function of liner profile, see Equation (5.3)
Δ_N	Parameter that is a strong function of liner profile and slurry viscosity in Equation (5.3). It is related to the number of lifters
Δt	Time step used for the numerical integration of the DEM equations, see Equation (2.12)
ϕ	Mill speed expressed as a fraction of theoretical critical speed
ϕ^*	Parameter in Equation (5.3) found to be approximately constant at a value of 136 but could vary between 134 and 138. The parameter is virtually independent of liner design
ϕ_c	Experimentally determined fraction of the theoretical critical speed at which centrifuging is fully established, i.e. the majority of the charge is centrifuging
ϕ_{100}	Speed of the mill in percent of critical speed
Φ_j	Fraction of fines produced in a single fracture event. It is dependent on the material being crushed
γ	Breakage function parameter which is material-dependent. Its typical values lie between 0.5 and 1
η	Parameter given a value of 9 by Bond in Equation (5.1). It determine the position of the maximum power and reflects the tendency of the mill charge to centrifuge at speeds nearing the critical speed
Λ	Selection function parameter which is material-dependent
μ	Selection function parameter which is primarily a function of milling conditions
θ	Angular position in radians
θ_{mdl}	Predicted pool angle θ_{pool} obtained using Equation (4.3)
θ_{pool}	Angular position of the free horizontal surface of the pool of slurry in radians
$\theta_{pool,\,i}$	Average pool angle measured for a slurry filling U_i as defined in Equation (4.3)

θ_S or θ_{sh}	Angular position of the shoulder of the media charge in radians
θ_T or θ_{toe}	Angular position of the toe of the media charge in radians
θ_{TO}	Slurry toe angle for overflow discharge mills which is equal to θ_T for grate discharge mills [in radians]
$\vec{\theta}$	Angular position vector or rotational position vector of particle i in interaction, see Equation (2.12)
ρ_c	Average density of the grinding charge in kg/m^3
ρ_L	Bulk density of the mill load in kg/m^3
ρ_p	Density of slurry in kg/m^3
σ	Standard deviation for N values of the toe or shoulder positions collected for the N revolutions considered in the series of test
σ_i	Standard deviation on $\theta_{pool,\,i}$ in Equation (4.3)
ζ	Parameters given a value of 10 by Bond in Equation (5.1). It determines the position of the maximum power and also reflects the tendency of the mill charge to centrifuge at speeds nearing the critical speed

Chapter 1 Introduction

Except in applications such as the cement and the coal industry, milling is generally done wet. Slurried material is fed to the inlet of the cylindrical mill and is discharged from the outlet. Two main forms of product discharge exist: the overflow discharge and the grate discharge. In the first design, the discharge trunnion which has a larger diameter than the inlet enables the creation of a hydraulic gradient along the rotational axis of the cylindrical drum. In fact, slurry is allowed to accumulate until it can overflow at the discharge end via the discharge trunnion. The gradient then drives the slurry through the mill such that the product is collected at the other end of the mill. In a grate discharge system, however, an internal grate and a pulp lifter are placed at the end of the mill. The pulp lifter lifts the product and discharges it into the discharge trunnion. The product is typically discharged into a sump. As a consequence of this, the slurry level is normally lower in a grate discharge mill. But in some cases where the inflow exceeds the pulp lifter capacity, the slurry level will be as high as in overflow mills. Excess slurry is therefore present in the form of a pool resulting in a phenomenon known as ‘slurry pooling’.

The implications of slurry pooling on milling as well as the conditions propitious to its formation are investigated in the present thesis. In-depth analysis is envisaged to better understand the phenomenon.

1.1 Background

Slurry pooling in grinding mills is an important problem which is not fully understood. Though challenging, a careful study of the phenomenon, even under laboratory conditions, may be relevant to the design and the operation of tumbling mills.

Hogg and Rogovin (1982) were amongst the first to have investigated the problem. They proposed a model that describes the dynamics of material transport within the load as well as the exchange taking place between pool of slurry and charge of media balls. Figure 1.1 below illustrates the proposed model.

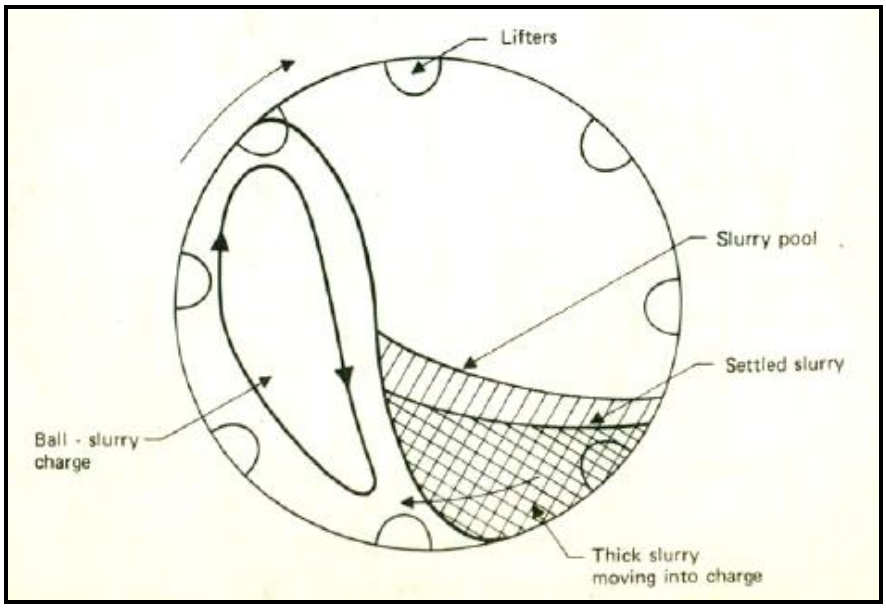

Figure 1.1 Schematic description of slurry transport between pool and media charge in a tumbling ball mill (after Hogg and Rogovin, 1982)

Under conditions favourable to slurry pooling, that is by overfilling the mill with slurry, slurry is entrained in the rising mill load and fills up the voids between balls. Any excess results in the formation of a pool of slurry around the toe region of the media charge.

In general, the presence of a pool depends on the flowrate of slurry and the type of discharge mechanism used. The first factor is typically true for grate discharge mills. In other words, the transport of material through the mill will determine the level of slurry hold-up and pool inside the mill (Morrell and Stephenson, 1996). By comparison, a pool of slurry is inevitable in overflow mills irrespective of the flowrate. Here, the diameter of the discharge trunnion and ball filling will determine the volume of the pool. The flowrate and viscosity of slurry will

contribute towards slurry pooling to a lesser extent, since the level of the pool will increase slightly with both these variables.

With reference to mill power, the pool of slurry has been showed to be the reason for the lower power drawn by overflow mills compared to grate discharge mills under similar conditions. However, larger pools of slurry imply longer residence time (Napier-Munn *et al.*, 1996); hence, lower throughput and possibly over-grinding.

If one defines the 'specific energy consumption' as the amount of energy consumed per unit mass of product of given fineness, then experience seems to suggest that the smaller the pool, the more energy intensive the process is. This view is shared by researchers such as Latchireddi and Morrell (2003) who believe that optimum milling conditions are reached when slurry is held up completely inside the grinding media without a pool of slurry. And as we shall see later, concordant findings by Tangsathitkulchai (2003), though on a laboratory scale, have demonstrated this to be reasonably valid. The problem is that statements by Latchireddi and Morrell (2003) are based on their experience with semi-autogenous (SAG) and autogenous (AG) mills in which the grinding media charge is composed of a mixture of large rocks and steel balls. They are therefore not necessarily applicable to ball milling. As for Tangsathitkulchai (2003), he observed a proportional relationship between the net power of a mill and the milling rate of particles of average size of 1 mm, also called specific rate of breakage. However, the milling rate of a particle size interval does not equate in a proportionate production of fines; and therefore, in 'efficient' grinding.

Although some might argue that grate discharge mills offer more flexibility in getting the 'optimum', mineral processing engineers have not been stopped from using overflow mills. The dilemma has even prompted Lux and Clermont (2003) to conduct some comparative pilot experiments. What they found is that, in an open circuit, despite a 10 – 15 % drop in power, a gain of 4 % in milling

efficiency was incurred in the overflow configuration. It is argued that this gain is statistically insignificant, and even meaningless, in an industrial situation.

That is why it is believed that a better understanding of the changing load behaviour with pool volume is worth investigating. To this end, the interrelation between slurry and media charge have been investigated. The effect that the pool of slurry has on the general behaviour of the load has also been studied. Finally, an attempt has been made to understand how milling parameters relate to pool volume in a laboratory mill.

1.2 Statement of the problem

The design of the discharge has a direct impact on the ore transportation pattern (Rogovin and Hogg, 1988) and consequently on the retention time (residence time distribution) and on milling kinetics (fineness of product). Longer residence time implies larger pool of slurry, which in turn implies higher slurry hold-up with variable axial distribution (Moys, 1986).

On the milling side, however, the reduction in power draw is likely to result in a coarse grind. The dynamics of the mill charge are known to govern milling kinetics. For argument's sake, if the position of slurry influences the orientation of the media charge, the pool will affect, to some extent, milling kinetics. With regard to the efficiency of a mill, if this happens, one would wonder whether the presence of a pool in the mill is an important factor in the determination of milling kinetics. From this, a key question arises: How does the pool of slurry contribute to milling efficiency and to the whole load behaviour of the mill?

In addressing the issue at hand, it would be argued that the combined effects of all the above could be perceived as the reason for similar performance in the two discharge designs. It is therefore believed that the pool of slurry has more to reveal. In an investigative effort to elucidate this, attention has been focused on evaluating the impact that mill power as affected by pool volume has on energy

consumption for grinding and on product size distribution. Specifically, the contribution of the pool of slurry to milling efficiency has been studied. The relationship between the volume of the pool and the size distribution of the product has also been established for different slurry fillings. This was done with the objective of determining whether it is any better to control power by means of pool volume whilst getting a product fine enough for downstream operations. Finally, the load orientation was modelled in order to help make sense of forthcoming results.

1.3 Research objectives

Tangsathitkulchai (2003) suggested that in order to optimise milling efficiency, the effect of load behaviour on particle breakage required particular attention. He also demonstrated through well planned experiments that mill power alone does not define breakage. He then postulated that the load orientation dictates milling kinetics. The present thesis is intended to find out the extent to which the level of the pool affects milling efficiency. It is indeed believed that pool volume affects the impact energy distribution and therefore milling kinetics. A direct consequence of this would be a change in milling efficiency. The underlying hypothesis is that pool volume has a strong influence on product grind. Assuming some level of truth in this, one might show that the pool volume is an important parameter in the control and design of ball mills.

By and large, milling kinetics is more the result of load behaviour than mill power. Load behaviour can primarily be modified by changing mill speed and lifter profile. Mill speed has the potential to be regarded as an optimisation variable more flexible than lifter profile. This is true especially if one considers that the profile of lifters changes with time due to wear mechanisms. In addition to this, mill speed is more precisely related to mill power (Morrell, 2003) than to lifter profile (Moys, 1993).

In line with this, Lux and Clermont (2004) attempted to control load orientation using mill speed. They observed that the extra power input incurred by increasing the speed from 65 to 90 % of critical did not result in a finer grind. One would therefore question the industrial operating conditions generally used to seemingly optimise grinding. It is however possible that higher speed may increase of milling capacity but not efficiency.

The complexity of the problem at hand increases when one thinks about possible parameters directly influencing milling kinetics. The following are accepted to have major impact on milling kinetics: ball filling, ball size and ball size distribution, mill speed, liner profile, powder filling, pulp density (slurry density), slurry rheology and ore transportation. Slurry density (solids concentration) and media size are probably the most frequently considered factors in the optimisation of ball mill efficiency. But little attention has been paid to studying the pool volume.

In wet milling, the flowrate at the inlet determines the presence of a pool. But for an overflow discharge configuration, there is always a pool that counterbalances the torque due to the mill charge, thereby lowering mill power. As to whether the decrease in power contributes to milling kinetics is yet to be established. That is the reason why we attempt to understand the influence that the pool has on milling.

The pool of slurry reduces power consumption in ball mills. We evaluate the impact that this reduction in mill power has on grinding efficiency and product size distribution. The relationship between the position of the pool (or rather slurry filling) and the product size distribution is also established for a given mill speed.

At this stage of the knowledge the link between load behaviour and power draw has been proved and widely accepted (Moys, 1993; Dong and Moys, 2003; Morrell, 1993). Nonetheless, whether maximum grinding occurs at maximum power draw is still yet to be ascertained.

All in all, it is envisaged in this research project to use a set of sensors to measure the interaction between slurry and media charge in detail. The aim was to further the fundamental understanding of mill behaviour and specifically the behaviour of the pool of slurry in tumbling ball mills. Next to this, the effect of slurry on mill load behaviour under slurry pooling conditions was assessed. The contribution of slurry pooling to mill power draw was also measured. Sensors mounted on the shell of a pilot scale mill were extensively utilised in this regard. Then, a series of batch grinding tests was carried out on slurries of constant density but different filling volumes. It was then possible to create pools of different volumes. In doing so, milling kinetics was studied as a function of slurry volume. And from there, the effects that the pool volume has on milling efficiency were measured. This set of tests was carried out in a laboratory grinding mill.

1.4 Envisaged contribution to knowledge

The aggressive environment of tumbling mills has made it difficult to get a clear description of the dynamics of a mill charge. A set of sensors developed at the University of the Witwatersrand provide an opportunity to monitor online the behaviour of the mill load (Moys, 1985; Kiangi and Moys, 2006 & 2008). The sensors are intended to be used simultaneously to collect signals representing the positions of both media charge and slurry. The collected data can then help draw a clear picture of the in-mill load behaviour. This in turn has a bearing on milling kinetics. That is why, the main focus of the work is to characterise the effect of pool volume on milling. Once a clear understanding of the relationship is fairly established, it is believed that doors will be opened to designing better mills. A moving plug fitted in the trunnion of an overflow discharge mill would be a good example (Clermont *et al.*, 2008). In addition, knowing the mill internal dynamics in terms of grinding balls and pulp slurry positions could lead to improved discharge design (Moys, 1987). Signals of load behaviour can also be

used in the control of continuous mills. As a result, milling could be appropriately controlled through the discharge design. Ways of altering transportation of ore through the mill could be devised to control milling optimally. Finally, it is anticipated that a better understanding of the relationship between the slurry pool volume and milling efficiency (power efficiency) will be gained.

1.5 Layout of the thesis

Besides the introduction, the thesis is organised in seven chapters. The second chapter highlights the main findings published in the field of wet milling. It looks at the current state of knowledge on slurry pooling and the advances in the measurement of the load behaviour.

The experimental design, equipment and methods used in this thesis are presented in the third chapter. Strategies implemented in the collection of data are discussed. Difficulties encountered throughout the course of the laboratory work are also highlighted.

Chapters four through seven constitute the core of the thesis. Tests using a transparent mill to observe the motion of the load are described in the fourth chapter. Results are presented and a model of the position of the pool is proposed. The interrelation between media charge and slurry position is also measured for different viscosities of an artificial fluid. The validation of these findings using an instrumented pilot mill and a natural ore is presented in chapter five. Four models of mill power are used to ascertain the effects of pool volume on net power draw. The Discrete Element Model (DEM), and models respectively by Bond (1962), Moys (1993), and Morrell (1993) are compared against measured net power of a dry mill. Three known power models are used to make sense of the contribution of the pool to power draw: Morrell (1993), Tangsathitkulchai (2003), and the Torque-arm model by Moys and Smit (1998). In addition, an empirical power model that accounts for slurry pooling is proposed.

Experiments in a small laboratory mill are described in chapter six where milling kinetics are determined as a function of slurry filling. The data is analysed using the Population Balance Model (PBM) applied to grinding and relevant parameters are determined. To underscore the effect of slurry pooling on milling, a discussion of the significance of the findings is undertaken in what could be called a 'microscopic approach'. The very same results are later analysed in a 'telescopic way' using the attainable region method in chapter seven. Attempts to optimise the size reduction process are made to determine how far the pool of slurry can be used to control milling.

The Population Balance Model is applied to milling to assess the mechanics of breakage and perform a mass balance of the system. As such, this analysis can be viewed as very detailed or 'microscopic'. The Attainable Region technique, on the contrary, relates the feed in to the product out; as a result, it regards milling as a black box and is only interested in the relationship between what comes in (feed) and what comes out (product), and to a great extent, the energy expended to perform the work. That is why the Attainable Region method is considered to be a 'telescopic or macroscopic' approach to milling.

Chapter 2 Literature review

Comminution, and ball milling in particular, has been the centre of research and development since the 1920's. It does not come as a surprise that the field is well endowed with publications of scientific value in the form of technical notes and original papers.

A review of past works is done with focus on the phenomenon of slurry pooling in tumbling mills. Next to this, the underlying breakage mechanisms believed to occur in tumbling ball mills and the modelling aspect of size reduction are reviewed. The main factors influencing wet milling and the developments made in the study of load behaviour are also highlighted. Then, several methods of describing milling and mill power draw are discussed. Finally, a novel technique – know as the 'Attainable Region' – is presented. The method has been intensively used for the graphical analysis of chemical reactions and is now penetrating the minerals processing world.

2.1 Introduction

Comminution modelling has rapidly grown from an empirical understanding of breakage to a phenomenological description of the micro-processes taking place. In the first instance, energy-size relations by Von Rittinger, Kick and Bond epitomise the early trends in comminution modelling (Wills and Napier-Munn, 2005). Although having served the purpose probably until the middle of the last century, the drawback these comminution theories suffer is that they are unable to predict the full size distribution of comminuted products. This limitation prompted a significant shift in comminution modelling.

Early works by Epstein (1947 & 1948) opened the way to a more mechanistic description of the process. The approach brought about a set of integro-

differential equations that are today referred to as the Population Balance Model (PBM), more appropriately called size-mass balance model (Yekeler, 2007).

To fill the gap between the mathematical description of milling and the product size distribution, diverse solutions have been proposed, sometimes overlapping or complementing in some aspects. First attempts to solving the integro-differential equations were made by Reid (1965) using size discretisation. Years of experimentation have consolidated and brought to maturity the Population Balance Model as well as the proposed solution. In this regard, King (2001) provided a very comprehensive review of works and modelling methods applied to mineral processing in general, and comminution in particular.

Important milestones reached in the history of comminution modelling which are relevant to our research project are presented. Factors that play a significant role in wet milling and highlight models associated with them if available are discussed.

Next to rigorous mathematical modelling, process engineers have also resorted to graphical techniques in the description of milling, and specifically particle size distribution. In line with this, we present a newcomer that has joined the family of graphical analysis techniques of size reduction: the Attainable Region (AR).

2.2 Breakage mechanisms in tumbling ball mills

Several mechanisms contribute to the grinding action that takes place inside a rotary mill. These include impact or compression, chipping, and abrasion. These mechanisms deform particles beyond their limits of elasticity and cause them to break (Wills and Napier-Munn, 2005).

The relative motion between media is responsible to a great extent for the grinding action. Ball media are entrained in a tumbling motion which engenders some interactions. During these interactions media collide or roll over each other. Depending on the type and the magnitude of the interaction, particles

break following a certain pattern. King (2001) argued that particles break primarily by impact or crushing and attrition in a ball mill. It seems however that impact breakage is predominant at coarser particle sizes whilst attrition is the main reduction mechanism at finer sizes in tumbling ball mills (Austin *et al.*, 1984). Between these two extremes, breakage is composed of some combination of impact and abrasion. For the purpose of this thesis, breakage is considered to be the result of impact, abrasion, and attrition only (Figure 2.1). Other types of breakage that can be considered as a combination of any or all of the three mechanisms mentioned above are not discussed here.

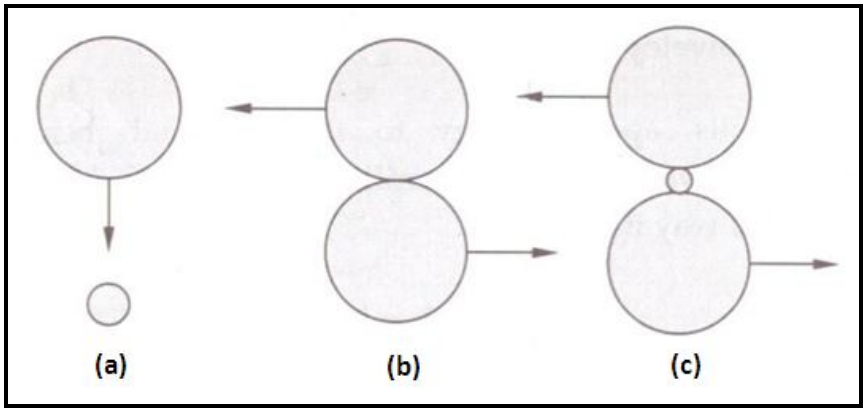

Figure 2.1 Principal breakage mechanisms inside a tumbling ball mill: (a) impact, (b) abrasion, and (c) attrition (after Napier-Munn *et al.*, 1996)

2.2.1 Impact breakage

Breakage by impact occurs when forces are normally applied to the particle surface (Figure 2.1a). It is also referred to as breakage by compression. King (2001) expounded this mechanism of fracture and showed that it encompasses shatter and cleavage.

Fracture by cleavage occurs when the energy applied is just sufficient to load comparatively few regions of the particle to the fracture point, and only a few particles result. The progeny size is comparatively close to the original particle size. This type of fracture occurs under conditions of slow compression where

the fracture relieves the loading on the particle immediately. Fracture by shatter, on the other hand, occurs when the applied energy is well in excess of that required for fracture. Under these conditions many areas in the particle are over-loaded; the result is a comparatively large number of particles with a wide spectrum of sizes. This occurs under conditions of rapid loading such as in a high velocity impact (Kelly and Spottiswood, 1982).

2.2.2 Abrasion breakage

Abrasion is regarded as a surface phenomenon which takes place when two particles move parallel to their plane of contact (Figure 2.1b). Small pieces of each particle are broken or torn out of the surface, leaving the parent particles largely intact. Abrasion fracture occurs when insufficient energy is applied to cause significant fracture of the particle. Rather, localized stressing occurs and a small area is fractured to give a distribution of very fine particles (effectively localized shatter fracture) (Kelly and Spottiswood, 1982).

2.2.3 Breakage by attrition

When a ball mill is running at low speed, grinding is a result of rubbing action within the ball mass and between the ball mass and the mill liners. The size reduction depends mainly on the surface areas of the media in interaction (Hukki, 1954). This breakage mechanism is known as attrition. It is caused by the relative movement between powder and individual grinding media components in the mill (Figure 2.1c).

In the relative motion of particles and media, very small particles happen to be nipped between large balls or between large balls and mill liner, particularly at low speed. The rubbing of particles between two media or between media and liner will result in the production of a significant number of very fine particles compared to the parent size. For that reason, it would be fair to assume that

attrition is largely responsible for the breaking of particles that have become smaller than the voids between the grinding media and that the stresses induced in the particles nipped between the two media or between the media and the liners are not large enough to cause fracture (King, 2001).

2.3 Modelling the milling process

The objective of any operation of size reduction is to break large particles down to the required size. In tumbling ball mills for instance, this operation is achieved through repetitive actions of breakage. Modelling such a mechanism necessitates a detailed understanding of the grinding process itself. Then, allowing for all the operating variables and machine characteristics the feed and product size distributions can be related.

Fragments from each particle that appear after first breakage consist of a wide range of particle sizes. Some of the daughter fragments are still coarse and require further breakage. The probability of further breakage depends on the machine design and particle size.

The underlying physics suggests that the breakage process is seemingly a combination of two actions taking place simultaneously inside the mill: selection of the particle for breakage, and actual breakage resulting in a particular distribution of fragment sizes after the particle has been selected (Gupta and Yan, 2006). A size-mass balance inside the mill that takes into account the two aforementioned reactions will make the full description of the grinding process possible. And eventually, mathematical relations between feed size and product size, after comminution, can be developed.

In the following sections, the basic principle of the Population Balance Model (PBM) as applied to batch milling is summarised. The two fundamental breakage processes (i.e. selection of particles for breakage and actual breakage) as well as their mathematical description are then discussed.

2.3.1 Population balance model for batch milling

Consider particles with size x at time t within a given feed size distribution; denote their mass fraction as $w(x, t)$. Now, take a time interval dt small enough to allow only single breakage to occur on a fraction of $w(x, t)$.

If the fraction selected for single event breakage per unit time is $S(x)$, then $S(x).dt$ represents the mass fraction broken after the time interval dt. This mass breaks into a wide range of children particles the size of which spans from the parent size x down to 0 (theoretically). In a batch grinding reactor, the flow of material within an infinitesimal class interval $[x, x + dx]$ can be categorised into three: (1) the mass fraction accumulated because not selected for breakage, (2) the mass fraction leaving the class interval as a result of single breakage events, and (3) the mass fraction coming in through breakage of particles larger than x. After time interval dt, the second category of particles is given by $S(x).dt$ whilst the third necessitates the determination of the mass fraction reporting to $[x, x + dx]$ as a result of breakage of selected particles of initial sizes larger than x.

To this end, let us symbolically call y any particle size larger than x (that is, $0 \leq y \leq x$). It is clear that selected particles of size y for breakage give birth to particles of sizes spanning from y down to 0 (theoretically). After choosing infinitesimal class intervals $[x, x + dx]$ and $[y, y + dy]$ to represent particles respectively of size x and y, one can determine the fraction of children particles formed after breakage of a unit mass $S(y)$ of parent particles has been selected for breakage from a mass fraction $w(y, t)$.

Now, if one considers $b(x, y)$ to be the mass fraction of children particles from $S(y).w(y, t)$ reporting to $[x, x + dx]$ after unit time, then for time interval dt, the mass of particles breaking from $[y, y + dy]$ and reporting to $[x, x + dx]$ is given by $b(x, y).S(y).w(y, t).dt$. Because there exists an infinitely large number of particles with size larger than x in the considered feed, the generation of particles of size x

will be the contribution of particles of sizes y with $x \leq y < +\infty$ which symbolically will be written as $dt.\int_{x}^{+\infty} b(x,y).S(y,t).w(y,t).dy$

In the final analysis, the variation in the mass fraction of particles in class interval $[x,\ x + dx]$ at time t (or symbolically $\frac{\partial w(x,t)}{\partial t}$) is due to the death of selected particles of size x through breakage (given by $-S(x).w(x,\ t)$ where the minus sign represent the disappearance of particle from the class interval) and by particles generated from larger particles (given by $\int_{x}^{+\infty} b(x,y).S(y,t).w(y,t).dy$).

It becomes possible to describe the flow of material in any class interval $[x,\ x + dx]$ in a batch milling reactor using the following integro-differential equation:

$$\frac{\partial w(x,t)}{\partial t} = -S(x).w(x,t) + \int_{x}^{+\infty} b(x,y).S(y,t).w(y,t).dy \qquad \textbf{(2.1)}$$

Equation (2.1) is known as the 'size-continuous, mass density-size formulation of the Population Balance Model for a well-mixed batch grinding process' (Bilgili *et al.*, 2006). Because size is conventionally measured using a series of sieves with mesh apertures arranged in a geometric sequence (generally $2^{1/2}$ or $2^{1/4}$), it is better to discretise Equation (2.1) to accommodate results from laboratory batch testing. The widely used discrete form considers a discrete size and a continuous time; to achieve this, variables such as x and y in Equation (2.1) are replaced by their discrete version x_i and y_j. In this new notation, the largest size class interval is named x_1 and is limited by screens of sizes x_1 and x_2; this way, the mass fraction of particles falling in size class interval $[x_1,\ x_2]$, or in class 1 for short, at time t becomes $w_1(t)$ or $w(x_1,\ t)$. In the same way, the discrete form of $b(x,\ y)$ becomes $b(x_i,\ y_j)$ or simply $b_{i,j}$. The last size class interval known as the 'sink' and composed of the smallest particles is termed $[x_n,\ 0]$ while particles in that class are of size x_n.

It shall be seen later that the size-discrete, time-continuous version of Equation (2.1) reduces to Equation (2.8) better known as the 'batch grinding equation'.

2.3.2 Selection function

It is generally accepted that the rate of disappearance of particles being ground in a mill is proportional to the amount of particles present. This assumption known as the first order breakage law, results in a similarity between milling and chemical reactions.

For a single size feed material, the description of the grinding kinetics can be written as follows

$$\frac{dw_i}{dt} = -S_i . w_i(t) \qquad \textbf{(2.2)}$$

where S_i is the rate of disappearance of particles or selection function

w_i is the mass fraction present in the size interval i after grinding time t

i is an integer defining the different size intervals, the largest being 1.

In order to define the variation of the selection function with particle size, Austin *et al.* (1984) proposed the following empirical model:

$$S_i = a.x_i^{\alpha} \frac{1}{1+\left(\frac{x_i}{\mu}\right)^{\Lambda}} \qquad \textbf{(2.3)}$$

where x_i is the upper size of the particle size interval i under consideration

a and μ are parameters which are mainly function of milling conditions

α and Λ are material-dependent parameters.

Equation (2.3) is only valid for materials milled at constant speed with a charge constituted of balls of same diameter. Under these milling conditions, parameters a and μ are constant and not function of particle size. However, their values will be revised accordingly, should mill speed or charge composition (i.e. ball size, ball filling, powder filling) change (Austin *et al.*, 1984).

Because the population balance model is based upon the first order grinding law, it is sometimes referred to as the 'first order rate model' (Napier-Munn *et al.*, 1996).

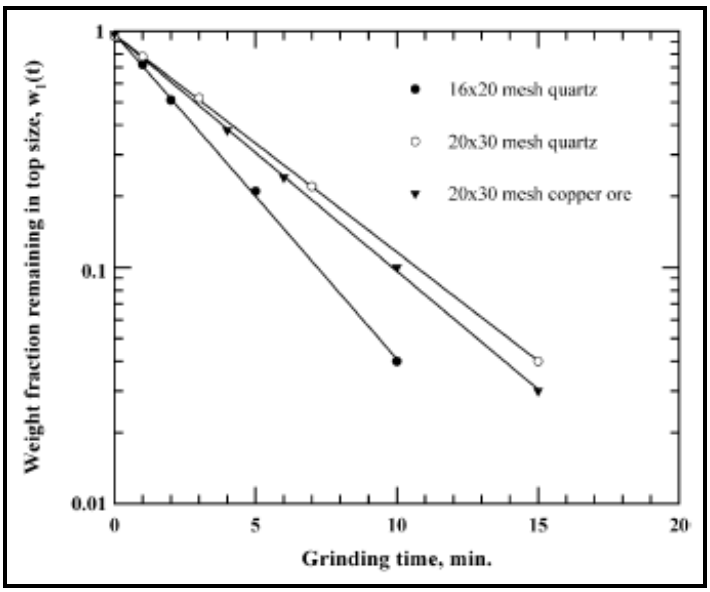

Figure 2.2 Illustration of first order reaction model applied to milling: Normal breakage (Tangsathitkulchai, 2002)

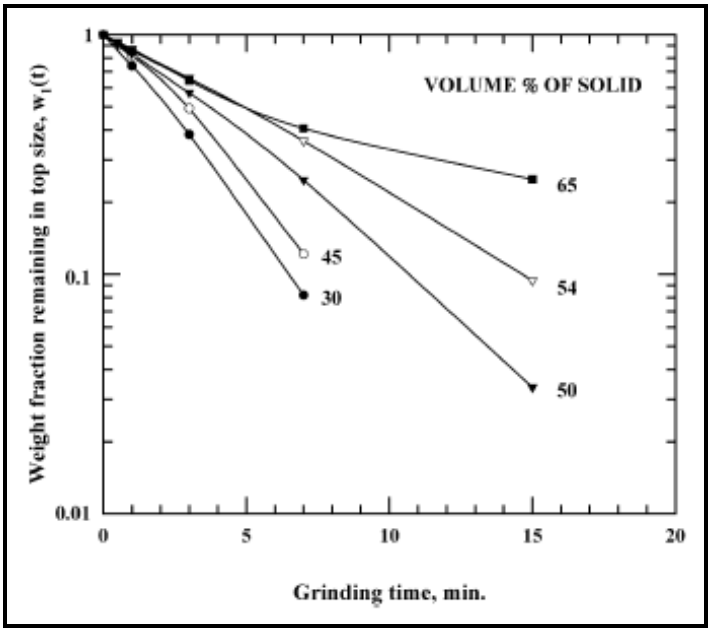

Figure 2.3 Variation in milling kinetics with solids concentration showing departure from first order reaction model (Tangsathitkulchai, 2002)

Figure 2.2, for instance, illustrates a case in which there is good agreement between the first-order breakage model and laboratory batch grinding results for a given material. However, substantial deviations from the first-order law can be recorded especially for relatively concentrated slurries (Tangsathitkulchai, 2002) or for coarser feeds (see Figure 2.3). When non-linear breakage is due to the size of particles being crushed, breakage is said to occur in the abnormal region.

Despite its simplicity the first-order law has proven to apply to numerous materials so far especially for fine sizes. Research is currently underway in order to get much insight in the foundation of this assumption (Bilgili *et al.*, 2006). But until that is fully achieved, the model will remain reasonably good for many materials over a wide range of operation (Austin *et al.*, 1976; Austin *et al.*, 1984, Bilgili *et al.*, 2006). Departure from the first-order breakage pattern has been comprehensively addressed by several researchers. Detailed analysis and description of non-first-order milling kinetics can be found from the following list of articles: Austin *et al.*, 1973; Austin *et al.*, 1977; Bilgili and Scarlett, 2005; Bilgili *et al.*, 2006; Bilgili, 2007; Capece *et al.*, 2011.

Perhaps the most important point is that for finer materials, Equation (2.3) readily becomes

$$S_i = a.x_i^{\alpha} \qquad \textbf{(2.4)}$$

This reduced equation geometrically represents on log-log scale a straight line the characteristics of which are the slope α and the breakage rate a at the standard particle size of 1 mm.

The parameter α is a positive number normally in the range 0.5 to 1.5. It is a characteristic of the material and does not vary with rotational speed, ball load, ball size or mill hold-up over the normal recommended test ranges (Austin and Brame, 1983) for dry milling, but the value of a varies with mill conditions.

2.3.3 Breakage function

The breakage function, better called the primary breakage distribution function, can be defined as the average size distribution resulting from the fracture of a single particle (Kelly and Spottiswood, 1990).

The function is used to describe the size distribution of the children particles produced after a single step of breakage of a parent particle of the material under consideration. To put it another way, if a parent particle is hit by a grinding ball, the resulting child product will consist of broken particles of a wide range of sizes. The description of this breakage event (single step of breakage) is made possible through a clear definition of the breakage function of the material being broken. And typically, but not always, for a given material, particles break following the same pattern. Provided this is the case, the material is referred to as 'normalisable'.

It is now understood that the relative distribution of each size fraction after breakage gives a full description of the product. Such a distribution is in fact the basis of the breakage function. And symbolically, the primary breakage distribution function of a particle of size *j* breaking to size *i* is defined as follows:

$$b_{i,j} = \frac{mass\ of\ \ particles\ \ from\ class\ \ j\ broken\ to\ size\ i}{mass\ of\ \ particles\ of\ \ class\ \ j\ broken} \qquad \textbf{(2.5)}$$

A more convenient way of describing the breakage distribution function is to use the cumulative breakage function defined as follows (Austin *et al.*, 1984):

$$B_{i,j} = \sum_{k=n}^{i} b_{k,j} \qquad \textbf{(2.6)}$$

With the new definition of the breakage distribution function, Austin *et al.* (1984) proposed an empirical model relating the cumulative breakage function to particle size. The general fitting model of the cumulative breakage function for a non-normalisable material is given below

$$B_{i,j} = \Phi_j \left(\frac{x_{i-1}}{x_j} \right)^{\gamma} + (1 - \Phi_j) \left(\frac{x_{i-1}}{x_j} \right)^{\beta} \quad \textbf{(2.7)}$$

where β is a parameter characteristic of the material used the values of which generally range from 2.5 to 5

γ is also a material-dependent characteristic the values of which are typically found to be between 0.5 and 1.5

Φ_j represents the fraction of fines that are produced in a single fracture event. It is also dependent on the material used.

Recent trends show that ranges of β-values found have been consistently exceeding the value of 5 advocated by Austin *et al.* (1984). So, it should not come as a surprise if values for β are reported to float around 5 – 15, especially for particles finer than 600 microns in wet milling (Yekeler, 2007).

Equation (2.7) represents an empirical model relating the cumulative breakage function to particle size and can be plotted as illustrated in Figure 2.4.

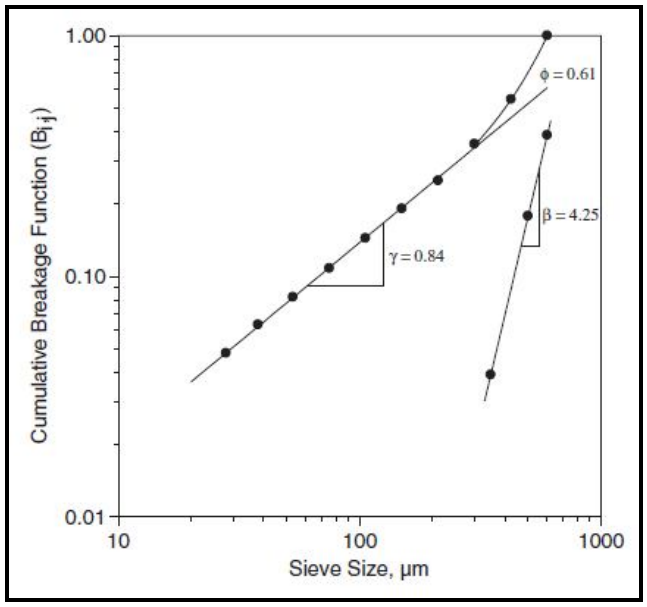

Figure 2.4 Example of the cumulative breakage function versus product size (Ozkan and Yekeler, 2003)

A simple but effective assumption is to consider the breakage distribution function as independent of the initial particle size. In other words, the breakage function is assumed to be normalisable. In this case, Φ_j is not a function of the parent size j but a constant. Though arguable in essence, this assumption has proven to be acceptable for many materials and for simulation purposes (Austin *et al.*, 1984; King, 2001).

2.3.4 Batch grinding equation

Breakage kinetics is usually investigated by means of batch grinding tests. An important point to make is that the primary objective of the batch grinding method is to measure and characterise the material in terms of breakage rate and breakage function.

To come back to batch grinding tests, a series of laboratory tests, generally in a small mill, are performed using a procedure known as the one-size-fraction method (Austin *et al.*, 1984). A sample in one size class is prepared. Then, the material is loaded in the mill together with the ball media. Grinding is performed for several suitable grinding time intervals. After each interval, the product is sieved, then further milled. Thus, the disappearance rate of feed size material is monitored for the different grinding time intervals chosen a priori. Lastly, laboratory results are analysed for the material to be characterised in terms of breakage rate and breakage function as stated in the previous paragraph.

Using the breakage characteristics of the material, a size-mass balance can be performed for each size interval. Basically, the amount of material being broken into and out of the size interval of interest, and the starting feed mass are simultaneously considered around the size of interest. This is symbolically expressed in the following equation (Austin and Bhatia, 1971/72):

$$\frac{dw_i(t)}{dt} = -S_i w_i(t) + \sum_{\substack{j=1 \\ i>1}}^{i-1} b_{i,j} S_j w_j(t), \text{ on condition that } n > i > j > 1, \qquad \textbf{(2.8)}$$

where S_i is the selection function of the material considered of size i

$w_i(t)$ is the mass fraction of size i present in the mill at time t

$b_{i,j}$ is the mass fraction from breakage of size interval j reporting to size i

n is the sink size class.

From then on, the particle size distribution of the material being milled can be predicted for any grind time along the process using Equation (2.8). To put it another way, from Equation (2.8), n differential equations can be generated. They are then solved and particle size distributions calculated.

2.4 Factors influencing wet milling

Ball milling has been the subject of intensive research for the past few decades. It is indeed the mineral processing operation used most frequently for size reduction. Known as the most energy inefficient process, focus has mainly been on ways of reducing energy consumption incurred by the operation.

Indeed, a large amount of energy is needed to break particles. But, the degree of size reduction required is to be carefully monitored to avoid over-grinding. Otherwise, this would imply a waste of energy that could have been saved. That is why several researchers have come up with various recommendations for the efficient operation of ball mills. Kelsall *et al.* (1968 – 1973) were amongst the first to systematically study five milling parameters; namely, ball size, slurry filling, residence time distribution, grinding media filling and density, and media shape. Based on their preliminary work and that of others, researchers such as Austin *et al.* (1984) and Yekeler (2007) have proposed models describing the effects of the typical grinding parameters on the milling process. Grinding media, slurry properties, lifter geometry and mill speed are presented. The dynamics and implications of slurry pooling on milling in general are discussed.

2.4.1 Ball filling and slurry filling

Load filling is arguably one of the most influential factors used in the control of milling, whether be it in terms of energy consumption or milling capacity. Common sense readily suggests that an increase in either ball filling or slurry filling results in a larger mill load. To deal with this, the mill will draw more power because more momentum is required to lift and rotate the whole load (see Figure 2.5 below).

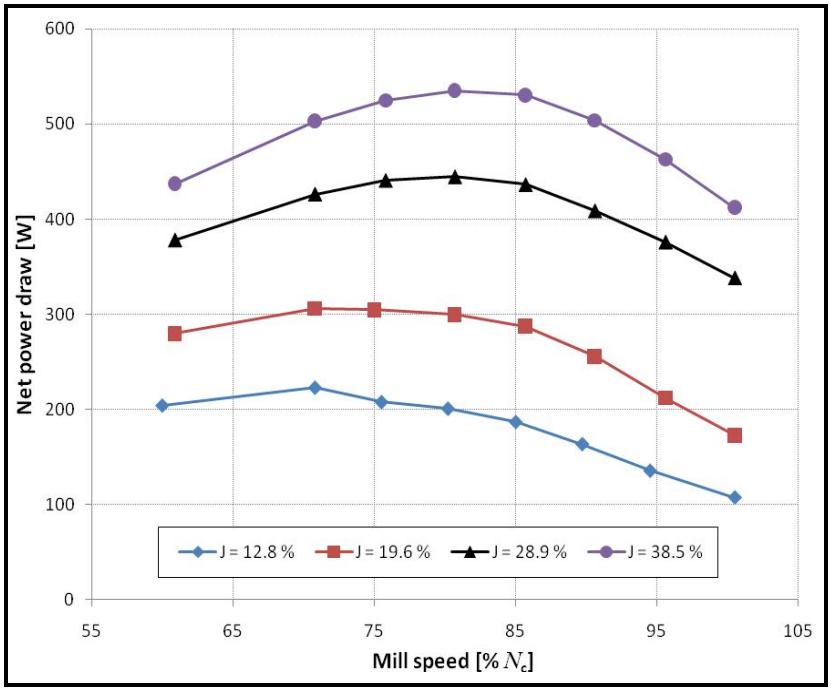

Figure 2.5 Effects of ball filling on mill power draw (data from Moys, 1993)

If one considers a ball mill of internal volume V_{mill}, it is clear that the mill can theoretically carry an equal volume of grinding media to its own volume. In practice, however, only a fraction of the volume V_{balls} is occupied by grinding balls. The ratio of volume occupied by balls at rest to the mill volume is defined as ball filling J.

In addition to the bed of balls, and specifically in wet milling, slurry (which is a mixture of ore particles and water in some proportion) is also loaded into the mill. Depending on the volume loaded, slurry occupies first the interstices between grinding balls before immersing the bed of balls at rest. The ratio of

volume of slurry loaded to the volume of ball interstices available within the bed at rest is the slurry filling U.

A limitation to the gradual increase in ball filling is that the maximum power occurs when the media filling is approximately 45 % of the mill volume; after that, power tends to decrease. By the same token, slurry should preferably be loaded in a way that ensures that most of the material is held in the media interstices (Latchireddi and Morrell, 2003). The charge is more likely to experience ball-ball contact and waste energy if the level of slurry is low. On the other hand, if there is more slurry than media charge can hold within, a pool of slurry will form. As a result, impact breakage becomes less pronounced.

Both ball filling and slurry filling affect milling. Shoji *et al.* (1980) proposed an empirical equation that relates milling rate to powder filling. The equation was produced using results of different works in small mills at fixed ball filling:

$$S_i(U) \propto a \propto \left(2.80e^{-4.1U} + e^{-0.8U}\right),\ 0.3 \le U \le 2.0 \qquad \textbf{(2.9)}$$

As for ball filling, further analysis of data compiled by Shoji *et al.* (1980) later showed that milling kinetics could be expresed as follows (Shoji *et al.*, 1982)

$$S_i(J,U) \propto a \propto \frac{1}{1+6.6J^{2.3}}.\exp(-cU) \qquad \textbf{(2.10)}$$

where c is a constant given the value of 1.32.

Equation (2.10) works for $0.5 \le U \le 1.5$ and $0.2 \le J \le 0.6$

Equations (2.9) and (2.10) are indicative of the effects that mill loading (that is, ball filling and slurry filling) has on milling kinetics.

Note that Shoji and co-workers (1980 & 1982) modelled the dependency of the milling rate on milling conditions for a dry mill. Tangsathikulchai (2003), on the other hand, carried out batch tests using a wet mill. Good agreement was found between his findings in wet milling and findings by Shoji and colleagues in dry milling. This is a clear demonstration that ball filling and slurry filling (or powder filling) affect milling rate whether milling is done dry or wet.

2.4.2 Properties of slurry

Slurries are basically a mixture of a liquid carrier and small particles in some proportion. As far as milling is concerned, the liquid carrier is generally water, and the proportion of solids-water widely varies from very dilute solutions to mud-like pastes. It is therefore understood that the most important properties of slurry would be its rheology and particle concentration.

Slurry rheology in essence encompasses the study of slurry deformation and flow (Napier-Munn *et al.*, 1996). To put it another way, studying the behaviour of slurries in motion by understand how they deform while in motion and how they flow under different conditions is part of determining the rheology of slurry. The commonly used way of describing slurry rheology is by means of what is called a 'flow curve' (i.e., a line chart showing the dependency of shear stress applied to slurry upon shear rate). It should be noted that shear rate is another word for velocity gradient created within the fluid due to the relative motion of layers of liquid. From a milling point of view, studying slurry rheology would simply reduce to investigating the effects of viscosity and slurry composition on milling.

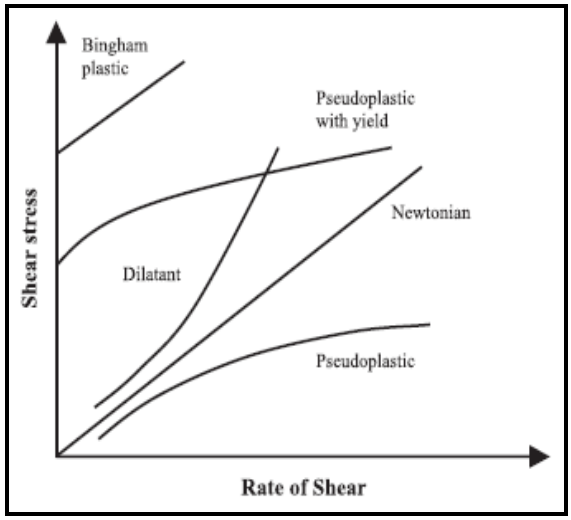

Figure 2.6 Types of slurries by flow curve (He *et al.*, 2004)

Shi and Napier-Munn (2002) and Bazin and Chapleau (2005) showed that the composition of the slurry affects viscosity. The gradually increasing fineness of the product as the ore is being milled, results in changing rheological

characteristics of slurry from one type to another (see Figure 2.6) in a complex fashion.

One of the many studied parameters is the change in viscosity with solids concentration. As shown in Figure 2.7, not only does viscosity increase exponentially with solids concentration, but it also changes with particle size distribution.

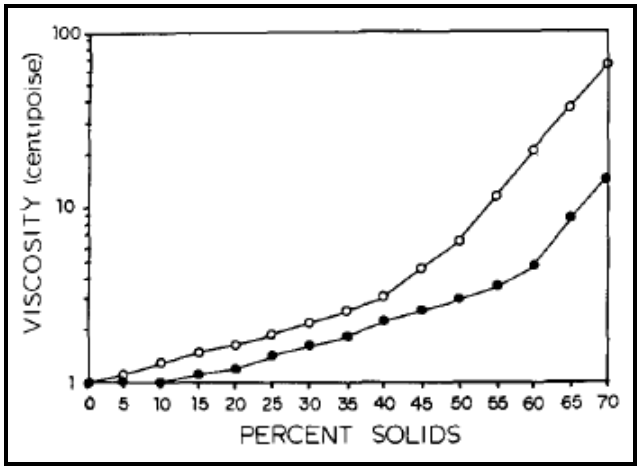

Figure 2.7 Example of variation in apparent slurry viscosity with percent solids for an iron ore at 80 % passing respectively 75 microns for filled data points and 45 microns for open ones (after Kawatra and Eisele, 1988)

Appreciating the importance of a full understanding of this problem, Shi and Napier-Munn (1996) researched on slurry viscosity, solids concentration and particle size distribution intensively. Though a definite model correlating the three parameters was not proposed, the two researchers diagrammatically demonstrated the interrelation, giving a more intuitive picture of slurry rheology in milling (Figure 2.8). Furthermore, Shi and Napier-Munn (2002) were able to show that slurry viscosity has a complex dependence on the concentration of solids in the slurry. In fact, a number of combined factors individually contribute to slurry exhibiting some form of rheological characteristics. They essentially reported that the most influential one was the changing fineness of the product as it is being milled. That is why it is generally recommended to remove fines as

they are being produced to limit changes in the rheological characteristics of slurry within a reasonable range.

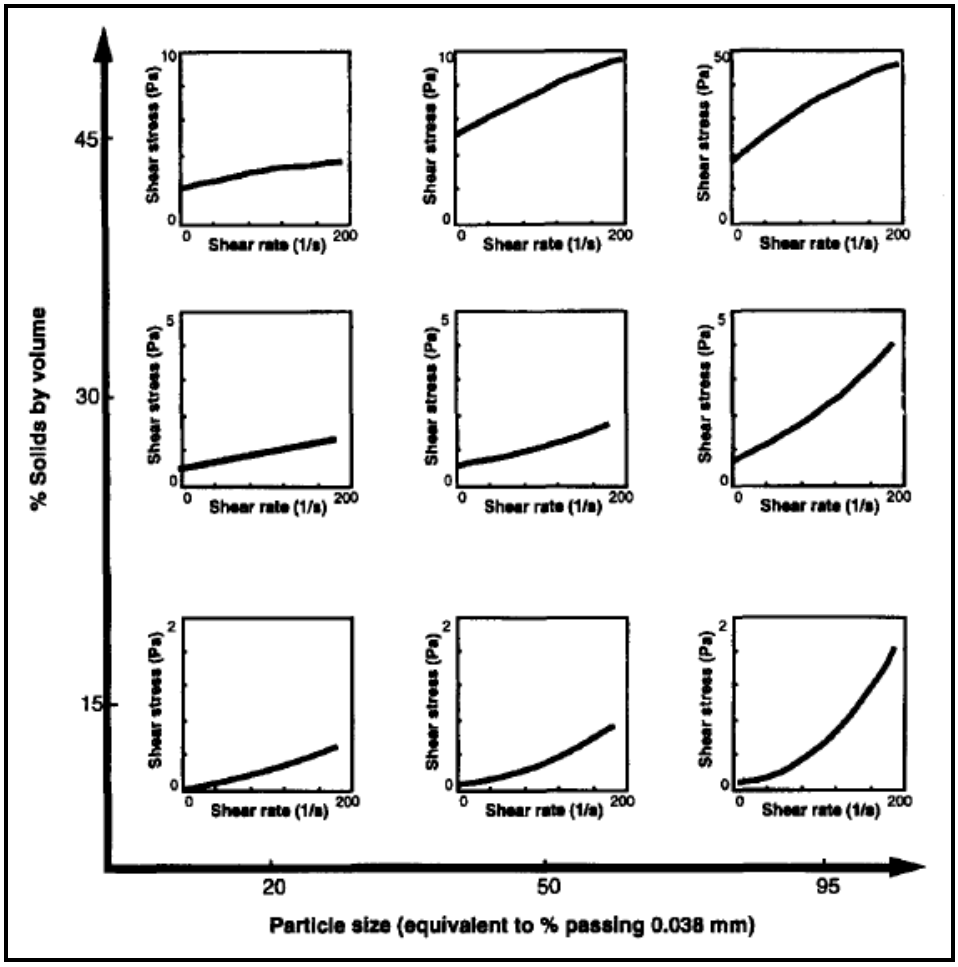

Figure 2.8 Rheological behaviour of slurry for different solids concentrations and particle sizes in ball milling (Shi and Napier-Munn, 1996)

Figure 2.8 summarises the results of their investigation and shows the shift in rheological behaviour of slurry as milling proceeds. One can clearly see that for the same particle size distribution, diluted slurry is essentially dilatant. In more concentrated slurries, the rheology becomes pseudoplastic with yield increasing with solids concentration. The transition from dilatant to pseudoplastic is more rapid for coarser particles (i.e. 20 % passing 38 microns in Figure 2.5) than it is for finer ones. In the latter case (i.e. 50 % and 95 % passing 38 microns), slurries are still dilatant even at 30 % solids volumetric concentration before becoming pseudoplastic. On the other hand, for the same solids concentration, there is no

significant change in rheological classification of slurry. That is to say, slurry remains pseudoplastic or dilatant as grinding proceeds. A detailed look indicates that levels of apparent viscosity and yield stress are varying on a case basis. This simply means that milling does little to slurry rheology except increasing the apparent viscosity for given shear rate.

Perhaps the most important point to make is that slurries are generally never Newtonian. Their nonlinear flow curve epitomises the inherent difficulty of measuring slurry rheology itself. Suffice it to say that this factor, on its own, renders the study of slurry properties quite challenging. Particularly, understanding the individual contributions of viscosity and slurry concentration to milling has been limited.

It is worth mentioning that some references and text books such as Chhabra and Richardson (2008) also use the terms shear-thickening and shear-thinning for dilatant and pseudoplastic respectively.

2.4.3 Liner/lifter profile

The essence of liners in tumbling mills is primarily to protect the mill shell from wearing down, thereby extending the life span of the mill. Lifters on the other hand limit the level of slippages of the mill load against the liners. Lifters come in different profiles with the same purpose. While performing their duty, their profile has a significant effect on load behaviour and in particular on the actual critical speed of the mill.

Depending on their geometry, lifters can be perceived as more aggressive if they tend to promote cataracting, and less aggressive if cascading is more involved under normal operating conditions. In the first case, particles are thrown in the air and execute a free-fall motion before landing either on the mill liners or the lower region of the load. If the imparted momentum is high enough, particles will stick to the mill wall for a full revolution, the load is thus said to ‘centrifuge’.

In the second case, particles tumble down the dynamic load in a rolling motion. Figure 2.9 gives a pictorial example of how load behaviour shifts from cascading with moderate cataracting to cataracting with great tendency to centrifuging for the same lifter profile but difference lifting angles. Photographs were taken for a dry laboratory mill running at 75 % of critical speed and 30 % ball filling.

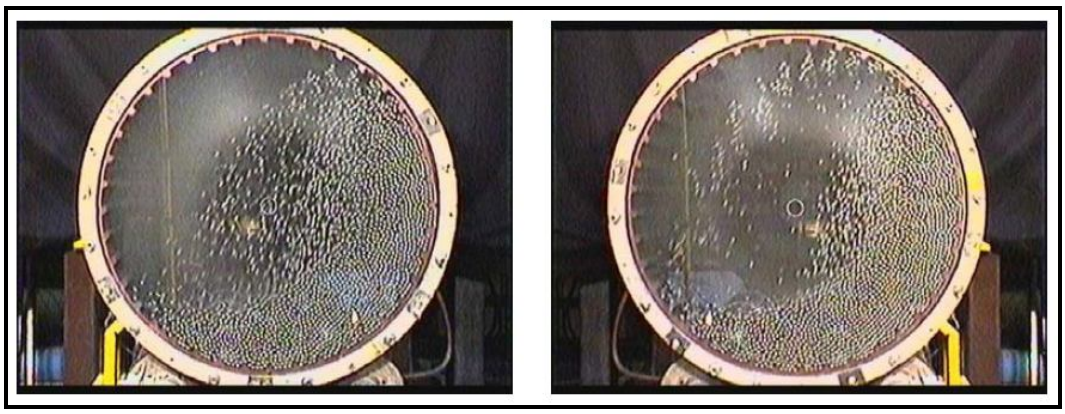

Figure 2.9 Snapshots showing the effects of lifter profile on load behaviour: soft (30°) angle of attack – on the left; and aggressive (5°) angle of attack – on the right (after Clermont *et al.*, 2008)

The photographic evidence above lends itself to repercussions of paramount significance, the first and foremost being that power draw will certainly change with lifter design. This has been experimentally demonstrated by Moys (1993).

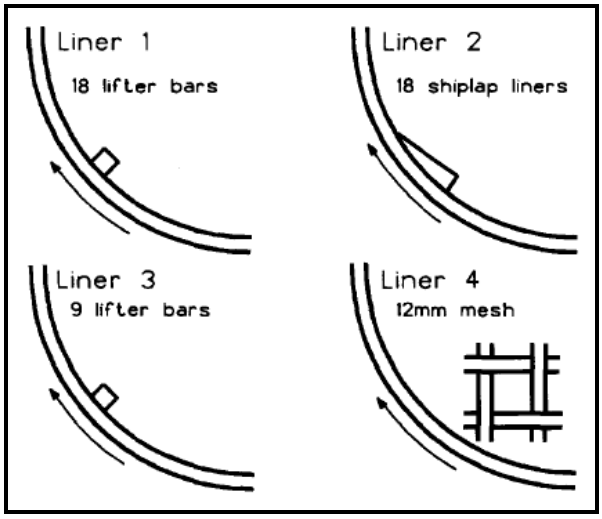

Figure 2.10 Types of lifters used by Moys (1993)

Figure 2.10 presents the four types of lifters Moys (1993) used to assess the effects of lifter design on mill power whereas Figure 2.11 shows their corresponding power as mill speed was varied. It is clear that lifters have a significant impact on mill power and therefore on load behaviour.

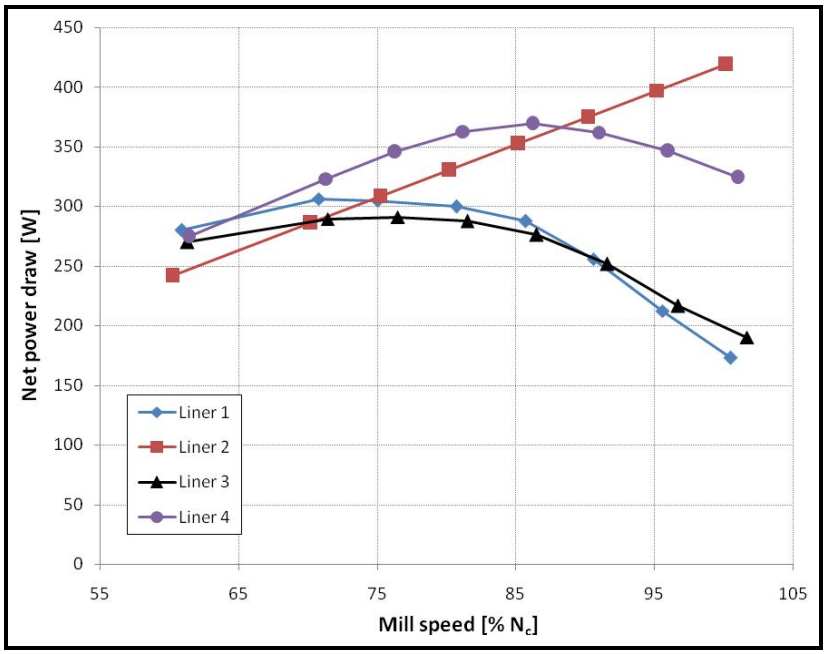

Figure 2.11 Effects of lifter configuration on mill power draw (data from Moys, 1993)

It is also observed from Figure 2.11 that the maximum power is reached at different speeds (compare Liner 3 and Liner 4), or not reached at all within the range of speeds investigated (see Liner 2). This is a clear indication that the actual critical speed depends also on the geometry of the lifter used. It is worth mentioning that the theoretical critical speed may be defined as the speed at which a single ball starts to centrifuge. The actual critical speed is in fact the speed experimentally measured with the load present and not theoretically calculated using the assumed motion of only one ball.

2.4.4 Mill rotational speed

The speed at which the mill is run is an important parameter in controlling/designing mills. It determines whether the load is predominantly

cascading, cataracting or centrifuging. Selection of gears will determine mill speed and a gear change cannot be done easily. However, some newer mills use variable speed to control the mill in response to changes in ore hardness.

Concordant studies have however demonstrated the ability of mill speed to control milling to some extent. Equation (2.11) proposed by Austin *et al.* (1984) illustrates this well. This empirical model relates the breakage rate of a mono-sized feed S_i to the fractional speed of the mill ϕ and in a sense gives an indication of the effects of mill speed:

$$S_i \propto (\phi - 0.1)\left(\frac{1}{1+\exp[15.7(\phi - 0.94)]}\right) \qquad \textbf{(2.11)}$$

where ϕ is the fraction of the theoretical critical speed N_c of the mill.
This equation is valid only for mill speeds in the range $0.4 < \phi < 0.9$

2.4.5 Slurry pooling

Mill throughput is closely related to load filling. The amount of balls and ore that the mill can take up generally determines its capability to process a large volume of ore. Intuitively, throughput would be proportional to ore hold-up: the more the mill takes up, the more material will come out and the faster this will happen. However, overfilling the mill is not advisable. The ability of the mill to hold up more material therefore depends on the volume of voids between media balls. So, if the mill is supplied with more slurry than the media interstices can take, the extra material will form a pool of slurry around the lower region of the media charge known as the toe (see Section 2.5.1).

Media interstices are defined using the notion of static porosity of the bed of balls. Recent work by Sichalwe *et al.* (2011) showed that the dynamic bed porosity increases with mill speed and does not remain constant at approximately 40 % as generally reported (Austin *et al.*, 1984). This tells us that

the mill can hold up more slurry than predicted with a direct implication: addition of pulp residence time, outside the grinding zone, in a pool.

On another note, an overflow discharge mill will invariably have a pool of slurry. In this case, slurry hold-up is not entirely determined by ball filling but by the diameter of the discharge trunnion. Furthermore, the presence of the pool modifies the pattern of material transport along and across the charge. Rogovin (1983) argued that a layer of slurry of thickness δ taken from the pool is entrained in the rising mill charge, then enters back into the pool through cascading motion. Figure 2.12 schematically illustrates what is believed to be the flow of material across the mill.

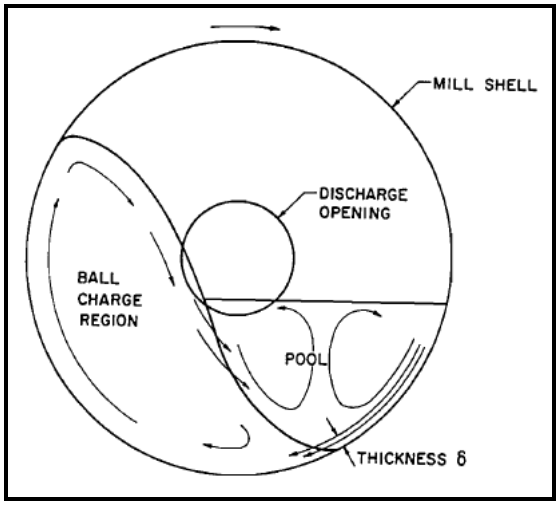

Figure 2.12 Schematics of transverse flow patterns in an overflow ball mill. A layer of slurry, of effective thickness δ, is carried out of the pool by the rotating mill shell (after Rogovin, 1983)

Experimental work on a pilot mill has showed that slurry hold-up in a discharge mill is mainly influenced by mill speed and charge volume. In their discussion, Latchireddi and Morrell (2003) explained that the influence of mill speed on slurry hold-up is highly dependent on voidage, being minimum at high charge volumes and maximum at lower charge volumes. One reason for this is the variation in bulk density which effects the dilation of the tumbling charge.

Tangsathitkulchai (2002), on his side, hypothesised the following to be happening (see Figure 2.13): For an overfilled mill, a pool of slurry (1) will form at the base of ball charge. A fraction of the ball mass (2) is submerged in the slurry. This fraction works against the stationary suspension of slurry causing a liquid drag on the interstitial particles. Around the shoulder of the media charge, balls (3) moving out from the slurry suspension tumble down in either a cascading or cataracting motion towards the pool at the toe of the load. For a cascading motion, coarse particles trapped (4) in the interstices are preferentially milled by attrition. Fine particles coating balls are also milled by attrition due to the relative motion of balls in this zone but not to the same extent as larger particles.

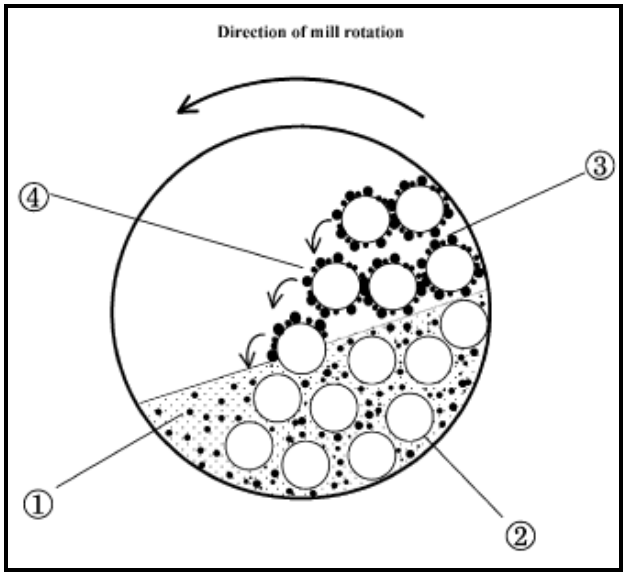

Figure 2.13 Sub-processes promoting preferential breakage of coarser particles in wet ball mills (after Tangsathitkulchai, 2002)

In terms of grinding mechanisms, whilst changing the discharge mechanism of industrial mills, Latchireddi and Morrell (2006) identified the predominant mechanisms that are believed to occur inside the mill under normal operating conditions. They compared two discharge configurations: the first that encourages slurry pooling and the other suppressing it. What they found is that attrition and impact are the prevailing breakage mechanisms with or without a

pool of slurry (see Figure 2.14). However, in the first case, the magnitude of breakage is low whereas it is more pronounced in the second.

Though this study was conducted on SAG mills, it shows at least qualitatively that the presence of a pool leads to poor impact and poor attrition breakage. We would argue that submerged balls are continuously lubricated, reducing the effectiveness of contact and friction between particles and balls. In addition, cataracting balls are damped by buoyancy and cushioning caused by the pool.

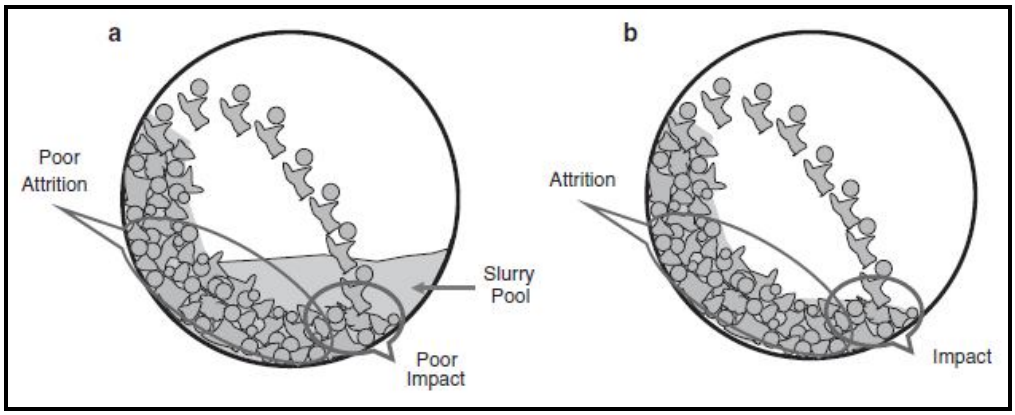

Figure 2.14 Grinding mechanisms present in a mill load a) with and b) without a pool of slurry (after Latchireddi and Morrell, 2006)

The key points to remember here as far as slurry pooling is concerned are: First, estimates of the variation in dynamic porosity of the tumbling charge are necessary to provide the maximum slurry hold-up that can be held in grinding media without a slurry pool (Latchireddi and Morrell, 2003).

Second, slurry pooling tends to encourage preferential breakage of coarse particles by attrition. Tangsathitkulchai (2002) was able to show that the preferential breakage is responsible for the phenomenon of breakage rate acceleration of top-size particles.

Last, even if overlapping works seem to suggest that the presence of a pool is undesirable, the throughput offered by this situation is high and could proportionately compensate the reduced grinding rate.

2.5 Load behaviour in wet milling

2.5.1 Introduction

Early works on the internal motion of the charge of a tumbling mill have been done using cinematographic techniques. The simplicity inherent to the implementation of this technique is one of its advantages. The technique is well-suited for preliminary works where great accuracy in measurement is not required. In this technique, the front plate of the mill is made of a transparent material to enable the motion of the mill to be observed. A high speed camera was then used to capture all the events. The only problem was the poor quality of the images that may result with the transparent plate being scratched as the operation proceeds. A brightly-coloured ore and/or an artificial liquid is generally required to obtain photographs of good quality that will ensure an easy determination of the position of the charge. However, the method becomes cumbersome or impossible when there is a need to investigate pilot and industrial mills.

Experience shows that a better understanding of load behaviour and its interrelation with milling efficiency is the answer to efficient operation. In this regard, Moys (1985) pioneered the use of a set of sensors capable of detecting the position of media charge and slurry. He proposed a proximity sensor for the detection of the position of the media charge. The study of the position of the slurry necessitates a conductivity probe.

A proximity probe works under the principle of inductance. To put it another way, whenever a steel ball moves into the field of detection of the inductive proximity sensor, eddy currents build up in the ball which in turn affect the field generated by the probe. This variation is converted into electrical information that will be interpreted as the presence of the media charge. The conductivity probe, on the other hand, is made of an electrode which establishes an electric connection with the ground when in contact with water present in slurry. The

voltage signal generated is translated into presence/absence of slurry. In fact, the magnitude of the signal at any instant is related to the amount of slurry in the conduction path.

The Sensomag® mentioned earlier works under similar principle except for slight modifications. The main one being that the two sensors are imbedded in the same casing. And, instead of using conductivity to detect slurry, electrochemical properties are used (De Haas, 2008).

To come back to the proximity probe, Kiangi and Moys (2006 & 2008) described in a comprehensive fashion the use of the sensor. They explored with great detail the effects of the particle filling and size on load behaviour. To a large extent, their work epitomises the success of the sensor in dry milling.

As far as wet milling is concerned, the proximity probe needs to be coupled with a conductivity probe. In doing so, the relationship between media charge and slurry behaviour can be completely described as shown in Figure 2.15. It is basically a superimposition of the media charge, here termed (1) and defined by the angles (5) and (6) for media toe and shoulder, with the slurry subtended by the slurry toe (3) and shoulder (4) angles. It is therefore understood that to unambiguously define the load behaviour, one has to define the positions of the media charge and the slurry in terms of toe and shoulder angles. The pool of slurry (2) is located between the slurry toe (3) and toe of media charge (5).

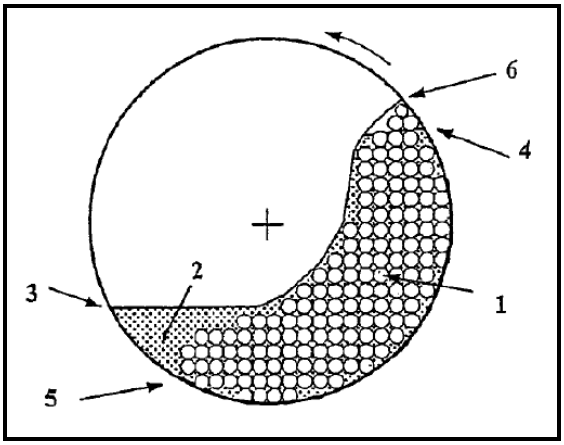

Figure 2.15 Definition of load behaviour in a wet ball mill (after De Haas, 2008)

The idea of using a single device to study media charge and slurry simultaneously has been considered by some researchers. Tano (2005) for example proposed the use of a single strain gauge mounted in a lifter to determine the profile of the load. The problem with such an arrangement is that the output signal is quite noisy and sensitive to many external factors. In fact, cataracting balls landing in the pool region blur the signal. This renders specifically the location of the pool quite tricky and unclear. It is believed that measuring media charge and slurry separately offers more flexibility and improves the quality of the information obtained from the signals. The reason for this is the absence of interference between the physical properties being detected, and so between the two output signals.

In summary, each key position, namely media charge toe and shoulder as well as slurry toe and shoulder have to be carefully measured in order to understand the role played by load behaviour in milling. Moreover, the measuring techniques are to be appropriately chosen and their quality assessed.

2.5.2 Description of load behaviour

There are several ways of defining the position of the load. Moys *et al.* (1996a) for example use the 12 o'clock position for the reference position while Morrell (1993) prefers the 3 o'clock position as the zero reference. Whichever way one would define the sets of reference axes, the position of the pool will correspond to the angle θ_{pool} of the intercept between the free surface of the slurry and the inner shell of the mill. The shoulder is the angle θ_{sh} from which balls exit the media charge in cascading or free fall motion and land around the toe θ_{toe} (see Figure 2.16).

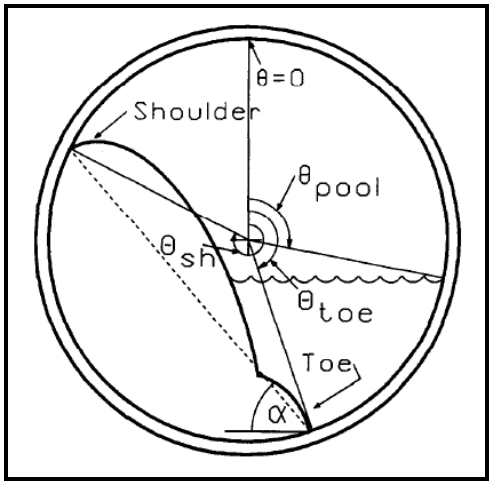

Figure 2.16 Load behaviour of a wet ball mill

In wet milling, and depending on the mill discharge configuration but also on the volume of slurry held up in the mill, there can be a pool of slurry above the toe region defined by the pool angle θ_{pool}.

2.5.3 Measurement of load behaviour: Developments

Numerous measurement techniques of load behaviour exist. They can be categorised in two: off-the-shell and on-the-shell methods. Only the latter shall be discussed comprehensively as they provide a better insight on the internal load behaviour. Off-the-shell methods, however, have been reported to be more appropriate for measurements of the total volumetric filling of a mill (Tano, 2005). Two off-the-shell measurement techniques are widely used. The first consists in measuring the bearing back-pressure on the mill's feed or discharge end (Kolacz, 1997). The pressure which is related to the weight of the mill load can be correlated to the filling level of the mill. The second technique uses microphones placed in the vicinity of the ball mill to pick up the sound level and infer the total mill filling (Watson, 1985; Hosseini *et al.*, 2011). In fact it determines the weight of the in-mill load via processed data representing the detected vibrations created by the mill shell (Zhi-gang Su *et al.*, 2008; Huang *et*

al., 2009). Both techniques are non invasive and therefore do not give a good idea of load behaviour.

The next paragraphs discuss on-the-shell techniques and their developments. In this family, sensing the position of media charge is generally done by means of exerted force on the mill shell, change in conductive or magnetic properties associated with the material grinding media are made off. Slurry, on the other hand, will be identified by a signature that comes with the fluid carrier in the form of electrical conductivity or some form of electrochemical property.

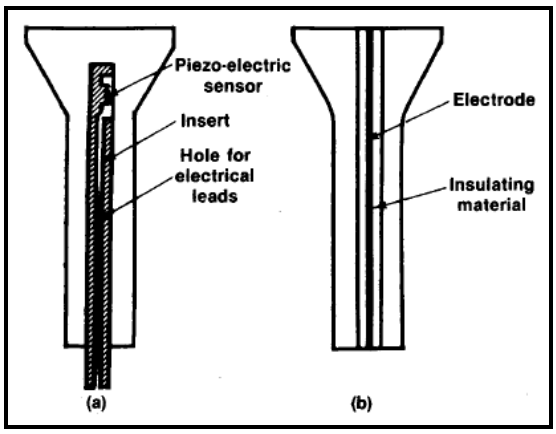

Figure 2.17 Instrumented bolts showing (a) a bolt with piezo-electric sensor for detecting mechanical disturbances, and (b) a bolt for measuring electrical conduction (Vermeulen *et al.*, 1984)

Figure 2.17 shows a diagram of one of the first set of on-the-shell sensors to have been successfully used to measure load behaviour of a tumbling ball mill. The first is a bolt fitted inside with a piezo-electric sensing device that basically translates any mechanical pressure or force into an electric signal, thereby detecting primary the media charge and to limited extent slurry. The other bolt has got an inside wire that acts as a live electrode and the bolt itself is the ground. All that needs to happen is for this arrangement to be bridged by the conducting liquid resulting in a drop in resistance between the two electrodes.

Another relevant set of sensors is presented in Figures 2.18 and 2.19 where slurry is detected by a conductivity probe set up a little differently. As shown in

Figure 2.18, the bolt is used as the live electrode while the mill shell plays the role of the electric ground.

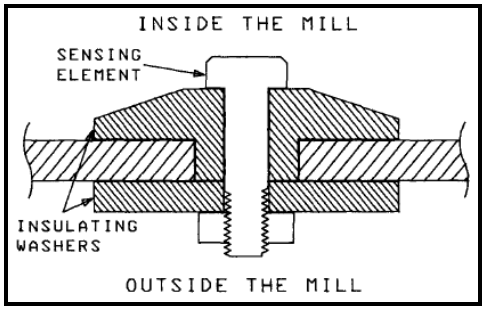

Figure 2.18 Conductivity probe (Montini and Moys, 1988)

The presence of media charge is in this case detected using the magnetic properties of grinding media (Figure 2.19). While this has some advantages of sensing only grinding media, it is limited to steel-based ones. The piezo-electric sensor mentioned earlier does not suffer this limitation.

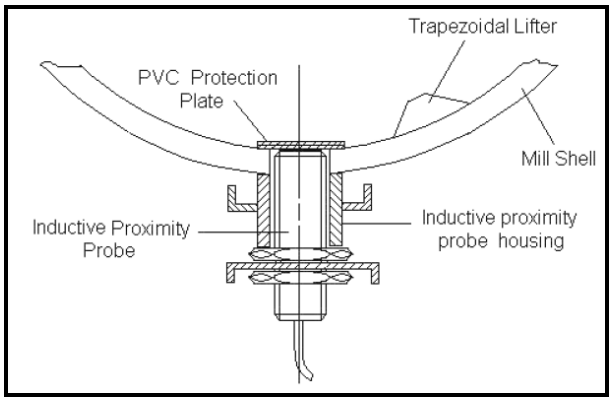

Figure 2.19 Proximity probe (Kiangi and Moys, 2006)

The other prominent idea is to embed within one single matrix a sensing system that unambiguously and simultaneously detects grinding balls and slurry. The strain gauge by Tano (2005) is one such implementation. The sensor is enclosed in a rubber liner fitted on one lifter of the mill (Figure 2.20). Rubber is used to give flexibility to the sensing lifter while absorbing some of the impact energy, thereby protecting the sensor. The rubber used should be flexible enough to deform under the influence of slurry, but robust enough to limit the level of impact that needs to be sensed.

The system is elegant and attractive despite the fact that interference can be important, reducing the quality of the signal and making the interpretation challenging especially if the mill vibrations are high.

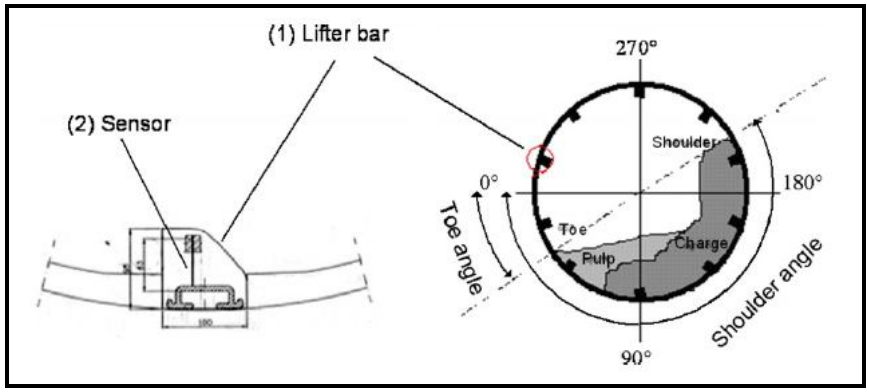

Figure 2.20 To the right a cross section of a mill with a horizontal reference line, the left part shows the lifter bar (1) with a strain gauge sensor embedded (2), (Tano, 2005)

In a more recent publication, Clermont *et al.* (2008) introduced the use of a set of sensors called Sensomag®. It is basically a tool that allows simultaneous determination of both the slurry and media charge positions inside the mill. Using the Sensomag®, they investigated the impact that changing the discharge configuration of a 4.8 m diameter ball mill has on power drawn. Measurements of the media charge and slurry orientations were taken both for the grate and overflow discharge configurations. Their work demonstrated the ability of the Sensomag® to detect the pool of slurry.

2.5.4 Discrete Element Method in wet milling

A dry mill can be regarded as a particulate system in which balls collide against each other and against the lining of the mill. It becomes evident that this environment can be modelled using a numerical approach known as the 'Discrete Element Method' or DEM for short.

Mishra and Rajamani (1990) were amongst the first to propose DEM as a tool for modelling tumbling mills. Since then, the method has gained popularity in the scientific community especially for design purposes and process improvements.

As far as DEM is concerned, two aspects of utmost importance are to be considered: the first being the assumption on the particulate entities while the second is the modelling of contact points (or collision events).

To put this into perspective, in the case of ball milling, particles are first modelled as spherical in 3D or circular in 2D depending on the level of accuracy needed and the complexity of the system at hand. Next, Newton's dynamic laws of motion are applied to individual balls during the mill rotation. That is to say, each ball is treated as a separate entity which experiences combined translation and rotation. The two types of motion are modelled for all the grinding media as shown in Equation (2.12) where the first represents the differential equation of the translation motion and the second the rotation one (Datta *et al.*, 1999):

$$\begin{cases} m\ddot{\vec{r}}_i + C_d.\dot{\vec{r}}_i + K.\vec{r}_i = \vec{F}_i \\ I.\ddot{\vec{\theta}} + \sum_i \vec{L}_i \wedge \left(K.\vec{r}_i + C_d.\dot{\vec{r}}_i\right) = \vec{M} \end{cases} \qquad \textbf{(2.12)}$$

In Equation (2.12), m, I, C_d, and K are the mass, moment of inertia, damping, and stiffness matrix respectively; $\vec{F}_i$ is the applied force vector; $\vec{M}$ is the moment about the centroid of the considered particle i. In the equation of the rotation motion, $\vec{L}_i$ represents the position vector considered from the centroid of the grinding ball to the resultant force $\vec{F}_i$ applied on it while '$\wedge$' is the cross-multiplication operator used to calculate the kinetic moment of the dissipative force $K.\vec{r}_i + C_d.\dot{\vec{r}}_i$ about the centroid of the ball.

Concerning the contact events, the widely accepted approach is to allow particles to overlap at the contact point so that the extent of overlapping determines the magnitude of relative velocities of particles for each contact. Relative velocities in the normal (along the line drawn through their centres) and

shear directions as well as the extent of overlapping are used to calculate the resulting forces (Mishra and Rajamani, 1990). Afterwards, Equation (2.12) is solved to determine the new acceleration vector; then, follows the first integration to calculate the next linear velocity v of the particle, and the second integration to update its position using appropriate time step Δt. Once all this is done, the cycle is repeated in an algorithmic fashion with the updated data. From this, information such as the trajectory of particles (see Figure 2.21) and collision events can be generated.

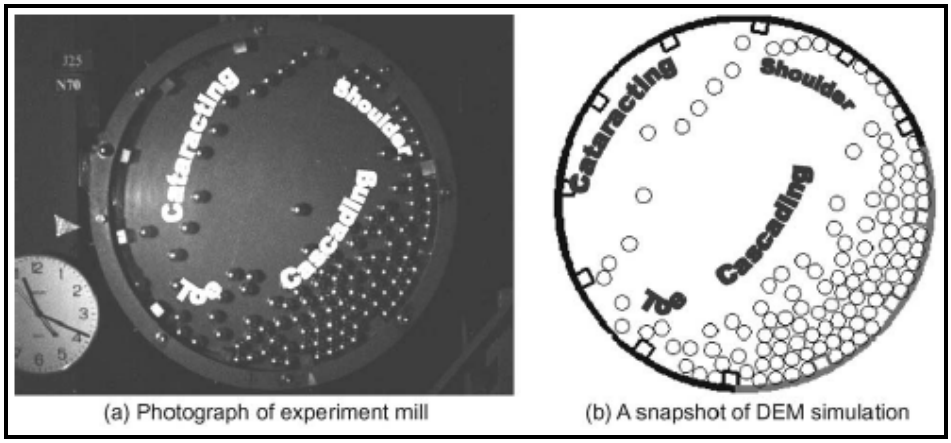

Figure 2.21 Example of load behaviour as measured on a glass-ended laboratory mill alongside the DEM simulated version (Hlongwani *et al.*, 2003)

Now, at each step of the numerical simulation, accelerations can be used to update acting forces. With position vectors and rotational speeds of grinding balls known, individual instantaneous torque can be calculated. This way, the total power can be determined. And at the end of the simulation, the average power can be calculated which corresponds to the DEM version of mill power draw.

The DEM technique has great application potential in comminution modelling at micro-process level (Napier-Munn *et al.*, 1996). It provides an astounding amount of information: boundary stresses, wear rates, collision forces, power consumption and torques, etc. However, its application is limited to dry milling.

Mori *et al.* (2004) proposed a method of simulating motions of balls in a wet environment. The effects of the slurry were taken into account through the drag force and buoyancy experienced by balls. These forces were included in the applied force vector $\vec{F}_i$ and in the moment $\vec{M}$ about the centroid of the particles immersed into the slurry (see Equation 2.12). Slurry was assumed horizontal and undisturbed (Figure 2.22). With this simplifying assumption, it was possible to locate balls below the slurry level and apply to them the addition forces exerted by slurry. The modified DEM algorithm enabled them to study wet milling and extract useful information amongst which the energy spectrum.

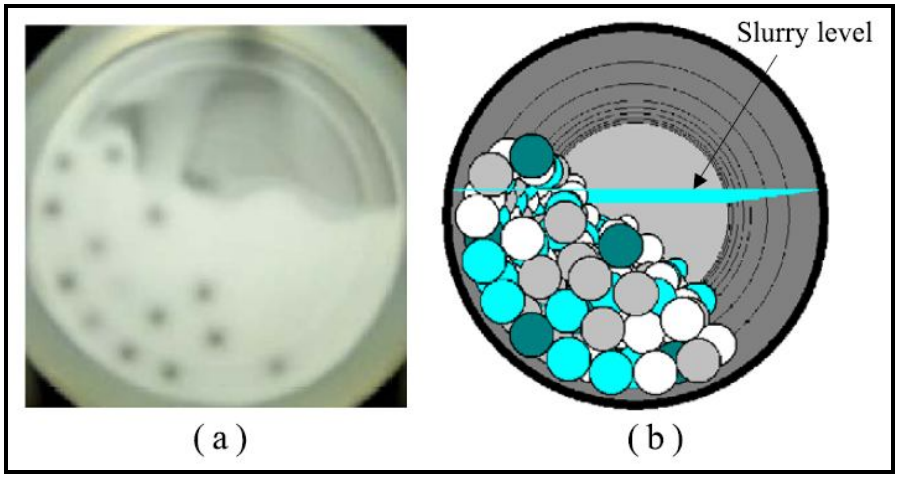

Figure 2.22 Application of DEM technique to wet milling: (a) experimental and (b) simulated (after Mori *et al.*, 2004)

The group of researchers then attempted to use the information provided by the energy spectrum to predict breakage rate of particles. They found insightful results that correlated well with laboratory findings.

Later on, Gudin *et al.* (2007) revisited the method and improved the description of the models describing the interactions amongst particles. They managed to back up the results of their simulation with laboratory experiments. They showed for instance that friction during contact between particles is a parameter of paramount importance. This implies that in order to get good simulation, friction needs to be adjusted and calibrated using laboratory tests beforehand.

At this point in time, confidence in the DEM technique has been gained through the many published works: Abd El-Rahman *et al.* (2001), Bwalya *et al.* (2001), Cleary (1998 – 2009), Datta *et al.* (1999), Mishra (2003), Powell *et al.* (2011), and Radziszewski, (1999) to name a few. And it is undeniably a promising tool; however, computational costs are still high and remain the main drawback. Moreover, the tool is mostly appropriate for dry milling. To use it for wet milling, better knowledge of the position of slurry with respect to media charge is required. Once this is achieved, more realistic algorithm constructed following the model by Mori *et al.* (2004) and Gudin *et al.* (2007) will follow. Combining the DEM to some other tool able to describe liquids is another option; one such approach is succinctly presented in Section 2.5.7.

2.5.5 Variations in media charge orientation

Measurements of the load orientation through photographic and on-the-shell techniques have shed more light on what is happening in the heart of a ball mill. Testing and modelling by Morrell *et al.* (1992) have shown that the position of the toe of the media charge remains the same for low speeds of the mill then noticeably varies for speeds nearing centrifuging (Figure 2.23). Note that angles are read following the direction of rotation of the mill with the reference located at 3 o'clock if the mill rotates anti-clockwise and at 9 o'clock otherwise.

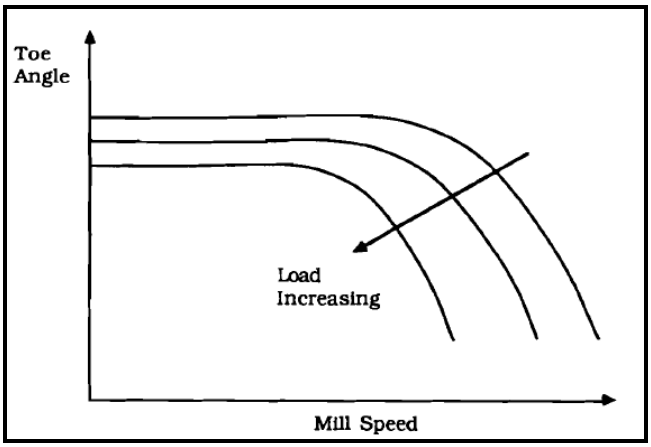

Figure 2.23 Variation of toe angle with ball filling and mill speed (Morrell *et al.*, 1992)

As far as load filling is concerned, Morrell *et al.* (1992) observed a decrease in the media toe angle for increasing ball filling consistent with a corresponding increase in bed depth, but also early centrifuging. The latter could be due to frictional forces present inside the load that modify the dynamics of energy transfer from mill shell to charge. The same trend is also observed with the shoulder at centrifuging speeds. Conversely, the shoulder angle goes up as load filling is increased as illustrated in Figure 2.24 for similar reasons as for the toe position.

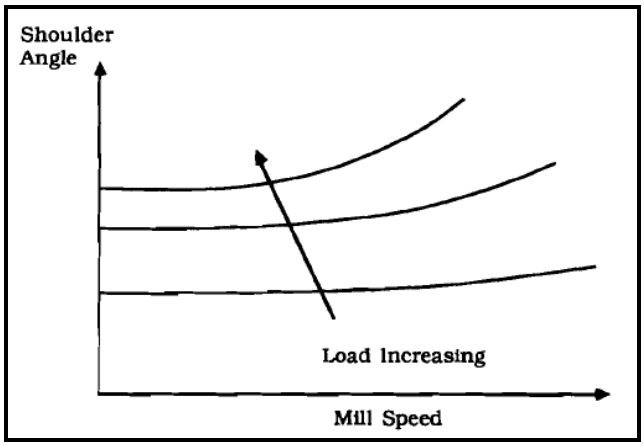

Figure 2.24 Variation of shoulder position with ball filling and mill speed (Morrell *et al.*, 1992)

The general empirical equations that describe the variations of the load orientation are given below. By load orientation, we mean the angular positions of the toe and shoulder of the media charge.

Variations in the position of the toe θ_T as shown in Figure 2.22 are given by

$$\theta_T = A.\left[1 - e^{-B.(\phi_c - \phi)}\right] + \frac{\pi}{2} \qquad \textbf{(2.13)}$$

where A, B are parameters that are function of the fractional volumetric ball filling J of the mill

ϕ_c is the experimentally determined fraction of the theoretical critical speed at which centrifuging is fully established, that is, when the

majority of the charge is centrifuging. It is a function of J and is further expected to be greater that the theoretical critical speed.

ϕ is the fraction of theoretical critical speed N_c at which the mill is run. The theoretical critical speed [revolutions per minute] for grinding balls of maximum diameter d [in metres] loaded in a mill of diameter D [in meters] is given by $N_c = \frac{42.3}{\sqrt{D-d}}$

θ_T is the toe angle [in radians]

To ensure that at centrifuging speed the angular displacement of the toe and shoulder converged to the same value ($\pi/2$ radians), the shoulder angle (θ_S) is chosen to be expressed as a function of θ_T. The general equation form that can be used is given below:

$$\theta_S = \frac{\pi}{2} - \left(\theta_T - \frac{\pi}{2}\right) \times \left(E + F.J\right) \qquad \textbf{(2.14)}$$

where E and F are parameters that are function of the fraction of theoretical critical speed ϕ

θ_S is shoulder angle in radians

J is the fractional ball filling.

2.5.6 Distribution of slurry in ball mill charge

Efficient milling operation is generally the result of good distribution of slurry within the load. Moys (1987) argued that viscosity is the most determining factor of the in-mill dynamics of slurry. He suggested that low-viscosity slurry is expected to drain down through the load faster. Conversely, viscous solutions will be entrained in the load and held much longer. And if a large and viscous pool of slurry is present, balls will settle more slowly in the toe region, thereby reducing impact of balls in the toe. The viscous slurry also causes the load to expand, reducing the interaction between the media, thereby causing them to

'float'. As a consequence of this, he hypothesised that the mill is likely to 'go off the grind'.

Testing these claims experimentally is quite a challenge. That is the reason why some researchers have resorted to the use of numerical techniques. Work by Cleary *et al.* (2006) is applicable even though simulations were intended for SAG mills. In this work, the researchers introduced a different approach to the problem of wet milling altogether. In order to explore the interaction between media charge and slurry, they modelled the mill load as a continuum fluid system (the slurry) flowing through a dynamic porous bed (the grinding balls).

On the one hand, the Discrete Element Method (DEM) was used to describe the motion of individual balls forming the charge, their mutual interaction, and the general motion of the media charge. This information is then interpreted as a bed with heterogeneous porosity. And on the other hand, the Smoothed Particle Hydrodynamics (SPH) was employed to model the slurry as a fluid of given rheological properties. Through appropriate coding, they combined the two concepts under what is called 'DEM-SPH framework' to allow for the interaction between the two systems. In doing so, they managed to describe the entire system constituting the wet mill load. The porosity of the bed as well as the motion and the distribution of slurry within the load are amongst the most insightful information one can get from the simulations.

Cleary *et al.* (2006) used the DEM-SPH framework to explore how the degree of filling and the viscosity of slurry shape the mill load. Figures 2.25 and 2.26 give an insight on what is believed to happen inside a SAG mill when slurry filling and viscosity are varied respectively. By slurry filling U (also referred to in this thesis as filling degree of slurry), we mean the volume fraction of the spaces between the balls at rest (that is the formal porosity of the bed of balls) which is filled with slurry (Austin *et al.*, 1984). These simulated snapshots are colour-coded by volume concentration of fluid present in a particular location. In this way, the dark blue colour represents slurry the fluid fraction of which is 0.35 whilst red is

pure slurry corresponding to a fluid fraction of 1.0. The distribution of the blue colour surely gives an indication of how the media charge is positioned. The position of the balls is known from the DEM simulations, but due to the limited information provided in the paper, we have assumed that most of the slurry is held in the media charge. Consequently, the blue coloration provides a fairly good indication of the position of balls. Furthermore, on the colour scale used, yellow represents slurry with a fluid fraction of 0.7.

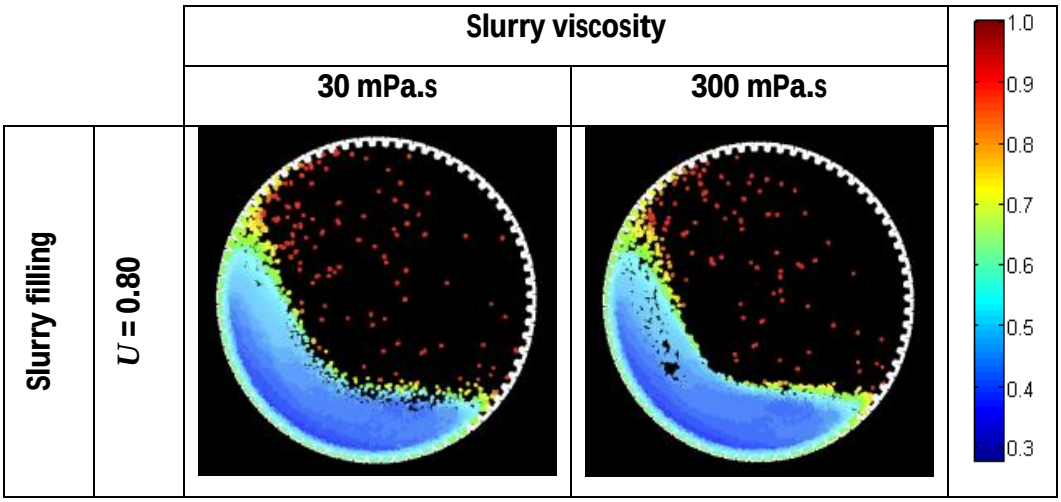

Figure 2.25 DEM-SPH simulation of slurry distribution in the load of a SAG mill for a slurry filling U of 0.8 and two levels of viscosity (after Cleary *et al.*, 2006). A colourmap provides values for fluid fractions of slurry and their corresponding colours.

It is important to emphasise here the fact that in rendering their simulations (Figures 2.25 and 2.26), Cleary *et al.* (2006) coloured the slurry by its volume fraction. As such, when the slurry is in free space (that is, no other particle is present in an elementary volume of the mill but slurry), the fluid is bound to occupy all of the space available and so is coloured red for a fluid fraction of 1.0. This explains why, for instance, fluid particles in free flight are coloured in red (see Figure 2.25).

As the fluid soaks into the media charge, it is only able to fill the interstices in the porous media bed and so only fills a decreasing fraction of the space available.

And in the case where the fluid percolates into the bed of grinding media and occupies completely the volume of voids available in the volume of interest, this region is then coloured dark blue reflecting the fluid fraction of 0.35. If the fluid partially filled the voids, the colour is anything going from yellow, green to light blue, depending upon the degree of occupancy of the pores in the media bed.

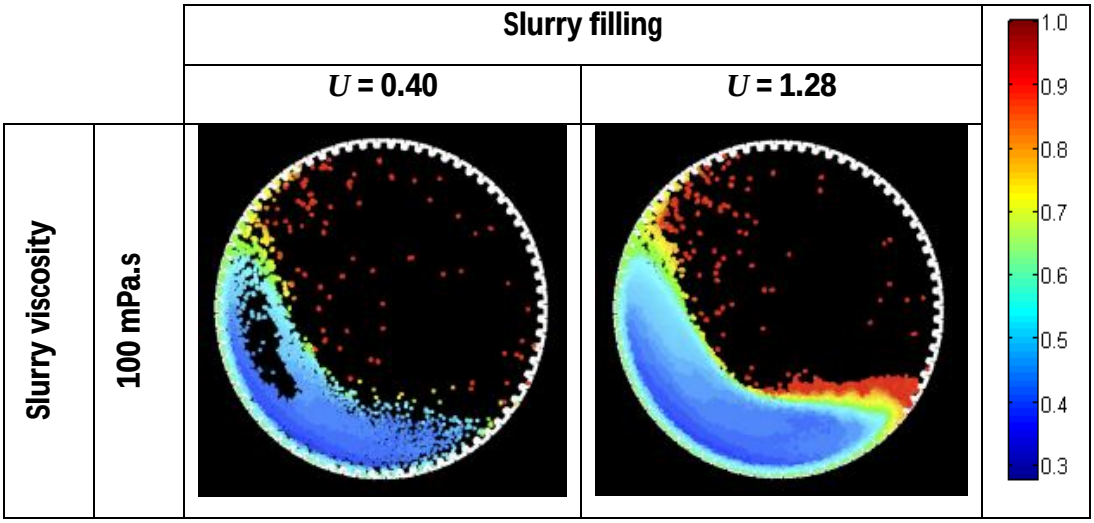

Figure 2.26 DEM-SPH simulation of slurry distribution in the load of a SAG mill for 100 mPa.s viscosity and two slurry filling levels (after Cleary *et al.*, 2006). A colourmap provides values for fluid fractions of slurry and their corresponding colours.

As far as the dependence of slurry distribution upon slurry viscosity is concerned, Figure 2.25 clearly shows that the position of the media charge (blue kidney-shaped region) does not change much with slurry viscosity. This outcome is in general realistic in view of the fact that grinding balls are heavy for their motion to be notably hindered by industrially-used slurries. That is why SPH-DEM framework proposed by Cleary *et al.* (2006) can be considered as a one-way simulation. This is because the SPH-DEM model does not allow slurry to affect grinding balls. New research has proposed a framework enabling two-way simulations to be implemented; in other words, slurry is given more freedom and cause balls to experience 'hindered motion'. However, preliminary findings do not show a big difference between the two approaches. The main strength of

two-way simulations is that the approach is far more realistic than its predecessor (Naidoo, 2012).

It should also be noted that a viscosity of 300 mPa.s is very high in practice and has therefore been used in the thesis for argument's sake.

Similarly, Figure 2.26 shows that for two different slurry fillings, media charge position remains almost unchanged.

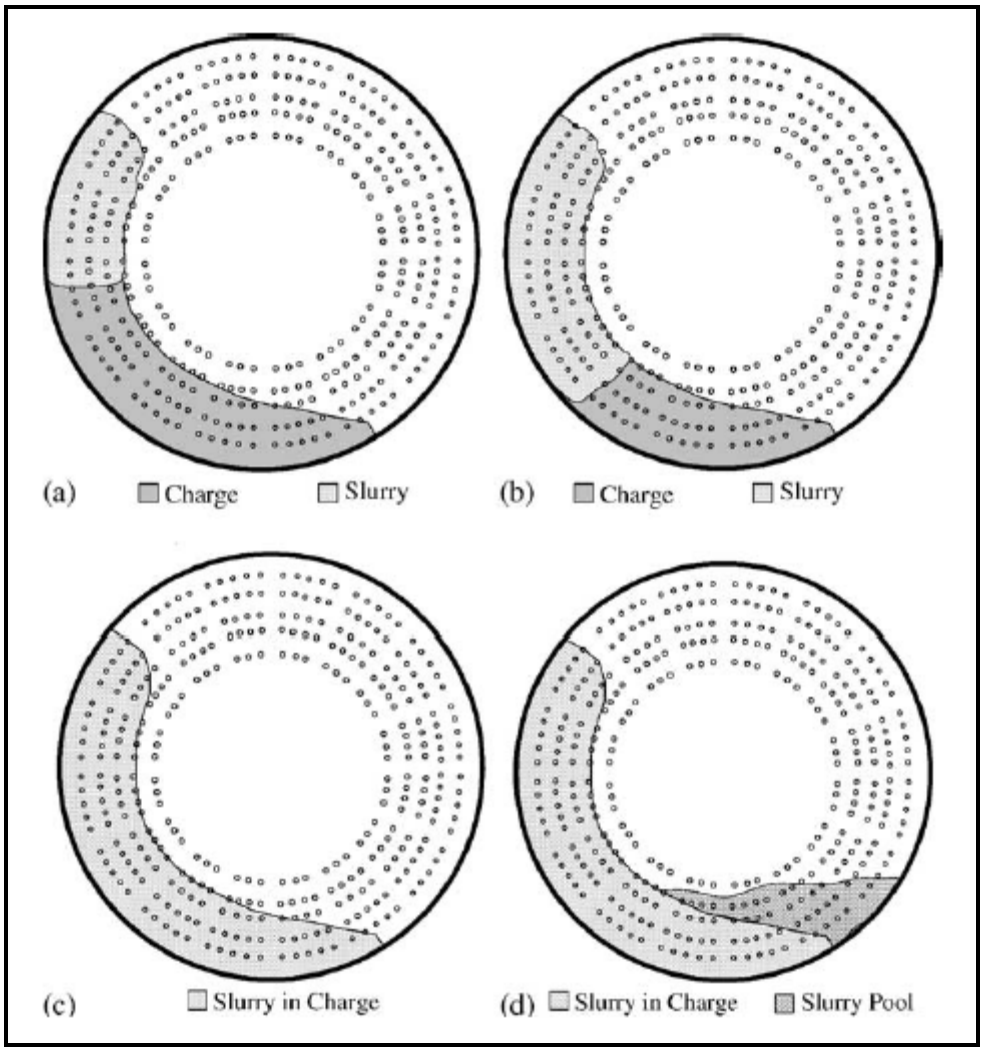

Figure 2.27 Evolution of slurry build-up with the level of internal filling of slurry in a grate discharge mill (after Latchireddi and Morrell, 2003). (a) Low flowrate, (b) Medium flowrate, (c) High flowrate, (d) Very high flowrate

It is good to appreciate here that the formation of a pool of slurry (red region in the toe region in Figure 2.26) is subject to an increase in slurry volume in the mill. In a sense, this observation complements the experimental work by Latchireddi and Morrell (2003) in which the distribution of slurry inside a grate discharge mill was studied for different slurry fillings. The slurry was found to build up from the shoulder to the toe as illustrated in Figure 2.27 as slurry filling increases. Experiments by Latchireddi and Morrell (2003) indicate that an increase in the volume of slurry causes the material to build-up from the shoulder to the toe inside the media charge, thereby leading to the eventual appearance of a pool of slurry. And simulations by Cleary *et al.* (2006) reveal that the position of the media charge toe region is about the same irrespective of the viscosity and the volume of slurry.

Of interest is the recent work by Naidoo (2012) presented at the International Conference, Comminution '12, in which grinding balls and liquid (slurry) were more realistically simulated in a tumbling ball mill. This work, still in its infancy, is ongoing and, as pointed out by the author, needs real data to be validated. Amongst other things that require careful attention are load behaviour (positions of both media charge and slurry) and power draw. However, the real contribution of this work is that the interaction between balls and liquid is bidirectional. In other words, the motion of individual balls is influenced by other surrounding balls and by the presence of a liquid; conversely, the fluid is affected by the presence of grinding media. Simulations by Cleary and Morrison (2012) for instance in which the DEM-SPH framework is used do not cater for this two-way interaction.

2.6 Net power draw of a ball mill as affected by slurry pool

2.6.1 Introduction

To our knowledge, there has not been a parameter that has drawn so much attention over the past century like mill power. This is still true even today. And

despite huge research investments, there is no unanimous consensus on the matter. However, significant progress has been made; specifically in establishing the link between load behaviour and mill power.

In line with this, the simplest conceptualisation of load behaviour is to consider the shape of the load as a rigid circular segment inclined at an angle equal to the dynamic angle of repose of the mill load. The chord limiting the circular segment connects the toe and shoulder of the load and is referred to as the surface of the idealised load in Figure 2.28.

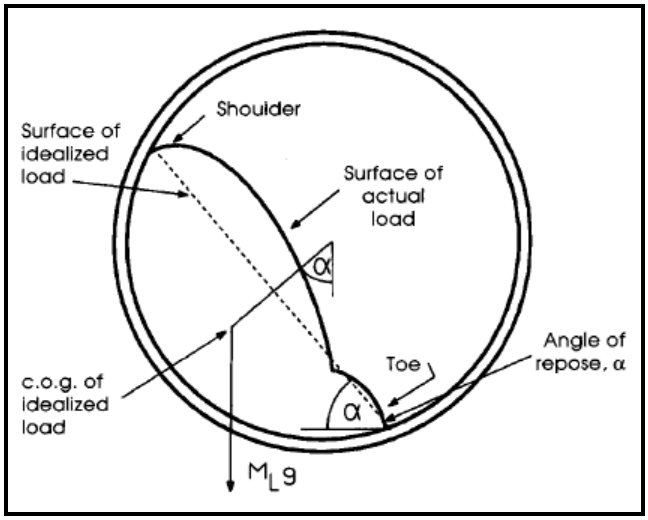

Figure 2.28 Rationale behind the torque-arm approach (Moys, 1993)

All that is now left to do is to determine the centre of gravity of the idealised load, calculate the torque of the load about the centre of rotation of the mill, and finally the mill power. Similarly, the potential energy can be considered in the calculation in lieu of the torque and will yield similar equations. Equations of mill power such as Hogg and Fuerstenau (1972), Arbiter and Harris (1982) are fruits of the idealised profile of the mill load.

It is important to remember that with better models of the load behaviour, the torque-arm approach can be applied more realistically depending on the operating conditions. Morrell (1993) is one such case where the load was shown to assume a crescent shape. The next two sections describe two classes of power

models that have been successfully applied to load behaviour under slurry pooling conditions.

2.6.2 Torque-arm approach

The torque-arm paradigm illustrated in Figure 2.28 generally applies to ball mills in which a pool of slurry is inexistent. One of the assumptions is that the load is locked inside a circular segment and that its weight applied at the gravity centre of this shape is responsible for the torque and power draw. This simplified load orientation generally works well for low mill speeds. Indeed under these operating conditions, the load assumes a cascading shape which is close to the circular segment shape.

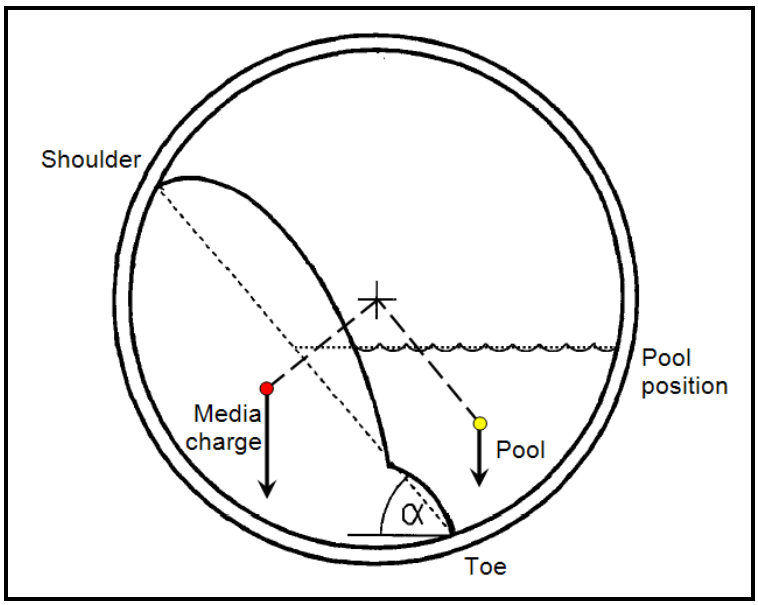

Figure 2.29 Torque balance applied to an idealised media charge and a horizontal free surface of the pool of slurry (after Moys *et al.*, 1996b)

Situations in which a pool is present have to be dealt with differently: the mill is in this case filled with more slurry than the media charge can contain. A fraction of slurry will be therefore held between the grinding balls while the remaining fraction will form a pool of slurry in the toe region. Moys and co-workers (Moys *et al.*, 1996a and 1996b, Moys and Smit, 1998) proposed to use a circular

segment for the media charge saturated with slurry and a horizontal surface for the pool of slurry (Figure 2.29). They then applied a torque balance to the full mill load.

As shown in Figure 2.29, the saturated media charge exerts a counter-clockwise torque whereas the weight of the pool acts clockwise. As a result, the total torque and power drawn drop owing to the presence of the pool. This way, it is possible to model the effects of slurry pool on mill power for cascading loads.

2.6.3 Energy balance approach: Morrell's model

Morrell's model of power is an elegant solution to mill power modelling. It has the merit of treating autogenous, semi-autogenous, and ball mills as one single class of devices the power draw of which could be predicted with the same equations. Furthermore, Morrell's model was initially intended for wet milling, but recent work has proved that it works also well for dry mills (Erdem *et al.*, 2004; Kiangi, 2011).

2.6.3.1 Active charge of the mill

Up until 1990, the prominent model of load behaviour has been that of an inclined circular segment the chord of which connects the toe and shoulder of the media charge. This oversimplified model has laid the foundation of most power models and paved the way to minor improvements (Liddell, 1986; Fuerstenau *et al.* 1990; Moys, 1990). It is to be highlighted that this model presents severe limitations; amongst others, it lacks the ability to describe high-speed mills.

To fill the gap between the actual and modelled behaviour of the load, Morrell (1993) advocated a crescent-like shape in order to approximate the kidney of the mill load. He posited that the load is comprised of two fractions: the active charge of the mill and a dead space (Figure 2.30). The active charge is basically the fraction of the load that rotates with the mill; hence, is responsible for the

power draw. The remainder encompasses the cataracting and centrifuging parts and has no effect on the mill power. He further assumed that the energy recovered from particles landing in the toe region was null.

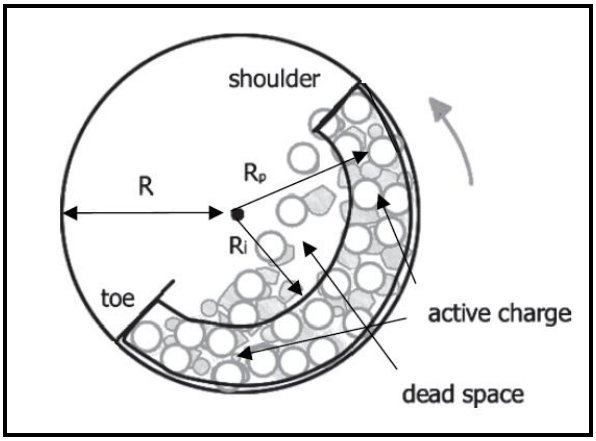

Figure 2.30 Definition of the active mill charge (redrawn after Morrell, 1993)

The active charge can be seen as a collective body within which interactions between particles are present. To this end, Morrell (1993) measured the velocity field of the load using photographs of a laboratory mill. In doing so, he managed to model the change in angular velocity of particles due to slip which occurs within the charge itself. To put it simply, not only does the mill load reduce to a crescent shape, but also friction between concentric layers of the active charge is modelled. In the end, the model of the load is locked in a defined shape but unlike what was done in the past with other models (Hogg and Fuerstenau, 1972; Arbiter and Harris, 1982; Fuerstenau *et al.*, 1990; Moys, 1990), particles are not glued to each other inside the shape. Instead, they are able to move in an en-mass motion. This makes the entire system to be dynamic (and not static) within the boundary of the crescent shape of the load.

Note that the Discrete Element Model (Mishra and Rajamani, 1992) of load behaviour is the only exception to the rule together with Morrell's crescent shape that actually takes the free motion of particles into account when calculating power draw.

Taking a different route from those presented in the two previous sections, Morrell (1993) developed a model of power based on the actual motion of charge, although presuming the motion to be confined between fixed shoulder and toe angular positions. He assumed that the active zone of the charge (see Figure 2.31 below) occupies the region between an inner radius (r_i) and the mill radius (r_m). The extent of this region is limited by the toe (θ_T) and shoulder (θ_S) of the media charge.

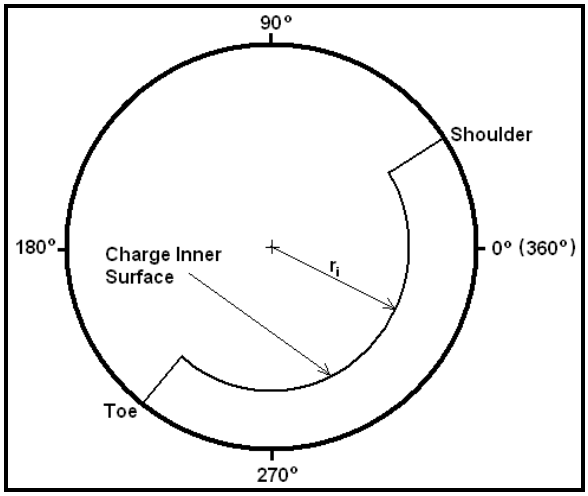

Figure 2.31 Active charge of the mill (after Morrell, 1993)

If the angular speed (velocities of upward and downward moving balls) of the balls is N_r, the power draft of a mill of length L and bulk density ρ_L of the charge is given by

$$P_{net} = 2\pi g L \rho_L . \int_{r_i}^{r_m} dr . \int_{\theta_T}^{\theta_S} N_r . r^2 \cos\theta . d\theta \qquad \textbf{(2.17)}$$

In Equation (2.17), the following variables r_i, r_m, θ_T and θ_S are calculated for given operating conditions using a few empirical correlations. In addition, Morrell carefully included slippage between layers of balls by expressing N_r as a function of radial position r. The model can also take care of charges with materials of different densities, as is the case in semi-autogenous mill. All these advanced features make the model quite comprehensive. However, the toe and shoulder positions of industrial mills are calculated using the same correlation obtained with the laboratory mill Morrell used which could be inappropriate. This is

because the intensity of forces at the ball-ball and ball-wall interface is not the same for two different mills. Nevertheless, despite its simplified approach the model claims greater degree of accuracy than the previous empirical models.

2.6.3.2 Window of applicability of the active charge model

Morrell (1993) used measurements of load behaviour in a glass-sided mill to develop and parameterise a model for load behaviour (as quantified by toe and shoulder position and slip of layers of media within the load). While the model he developed is based on a substantial approximation to actual load behaviour (Figure 2.31), it was nonetheless shown to predict the power drawn by a wide range of mills of the Australian design (mainly high D/L ratio and with mill speeds near 75 % of the critical speed) with exceptional accuracy. The crescent-like shape of the load which is the foundation of Morrell's model of mill power is the main reason for such a success.

By contrast, Moys and Smit (1998) stated that the model needed testing on tube mills (low D/L) and mills operating at high speed (e.g. 90 % of critical as is typical in the South African gold industry; Powell *et al.*, 2001). Recent work by Erdem *et al.* (2004) is another successful application of Morrell's model to industry. However, the speeds they investigated were limited to average speeds of about 70 – 78 % of critical.

Lastly, it is worth mentioning that the angular positions of the toe and shoulder in the crescent-shaped load are determined using Equations 2.13 and 2.14.

2.6.3.3 Velocity profile of the mill charge

The underlying assumption of Morrell's power model resides in the crescent shape of the load responsible for power draw shown in Figure 2.31. Morrell (1993) demonstrated that the load could be considered as a series of concentric layers piled from the mill shell to the charge inner surface and subtended between the toe θ_T and the shoulder θ_S of the media charge.

The momentum imparted by the lifters to the load makes the outermost layer rotate at the same speed N_m as the mill shell (r_m). As one gradually moves closer to the inner surface (r_i), slippage between layers occurs; as a result, the rotational speed of the concentric layers decreases, becomes null and eventually turns negative due to the down-falling cascading particles. Using a glass-ended laboratory mill, Morrell (1993) carefully measured slippage and modelled the velocity of layers of balls N_r as a function of their radial position r.

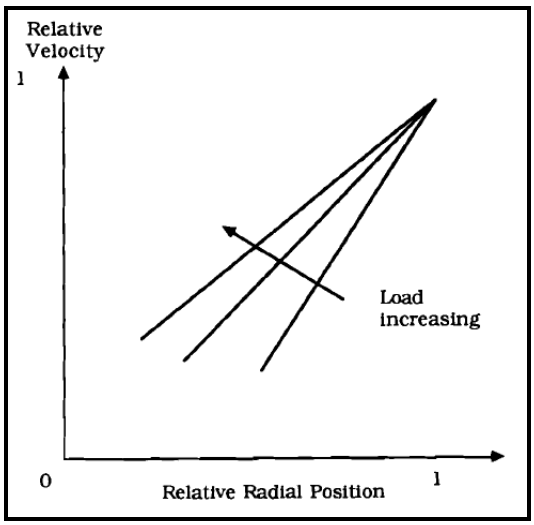

Figure 2.32 Variation in tangential velocity of particle with radial position within the load (after Morrell *et al.*, 1992)

Figure 2.32 indicates that there is a linear relationship between velocity and radial position of balls. It also shows that this relationship is subject to ball filling.

It is understood that for a constant ball filling, the influence of the mill shell linearly decreases as one moves towards the centre of the mill. The velocity field becomes even negative at lower ball fillings suggesting the presence of a cascading fraction of the mill in the active charge. Conversely, high ball fillings tend to have a more uniform velocity field due to the increasing pressure exerted by the bed onto the mill shell. This confined environment transfers the momentum of the mill more efficiently, thereby causing less slippage and therefore lower losses in rotational speed.

2.6.3.4 Net power draw of the mill

The integration of Equation (2.17) is the key to finding a mathematical expression of the net power. To this end, Morrell (1993) considered the crescent shape (Figure 2.31) and the velocity profile (Figure 2.32) of the load to come up with a power model applicable to both grate discharge and overflow discharge mills. He incorporated the effect of the slurry pool by assuming that the grinding charge is subjected to the buoyancy force as it falls through the slurry pool. This part of its motion occurs between the surface of the pool and the grinding charge toe as defined by θ_{TO} and θ_T respectively (see Figure 2.33).

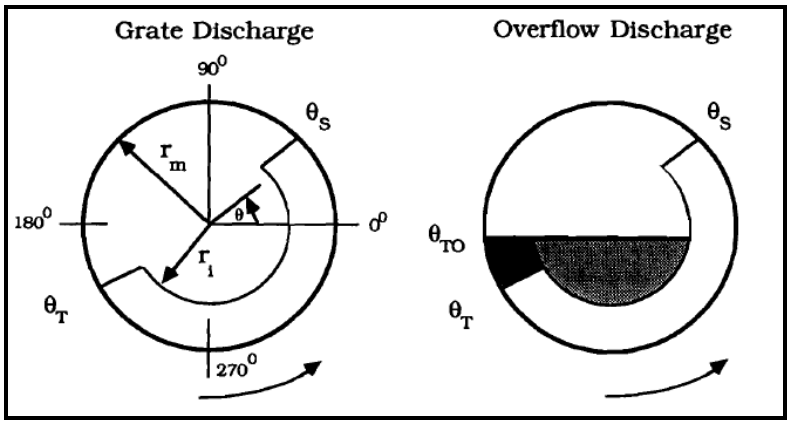

Figure 2.33 Simplified shape of the mill charge (Morrell *et al.*, 1992)

This eventually resulted in the following equation of power which describes both grate and overflow mills:

$$P_{net} = \frac{\pi g L N_m r_m}{3(r_m - z r_i)}\left[2r_m^3 - 3z r_m^2 r_i + r_i^3(3z-2)\right]\times\left[\rho_c(\sin\theta_S - \sin\theta_T) + \rho_p(\sin\theta_T - \sin\theta_{TO})\right] + L\rho_c\left[\frac{N_m r_m \pi}{(r_m - z r_i)}\right]^3\left[(r_m - z r_i)^4 - r_i^4(z-1)^4\right] \quad \textbf{(2.18)}$$

where ρ_p is the density of the slurry

ρ_c is the average density of the grinding charge

θ_{TO} slurry toe angle for overflow discharge mills which will be equal to θ_T for grate discharge mills

r_m is the internal radius of the mill given by $r_m = D/2$

r_i charge inner surface radius which marks the boundary between the active part of the charge and the inactive kidney-shaped media charge

z is an empirical parameter that Morrell (1993) equates to $z = (1 - J)^{0.4532}$

N_m is the rotational speed of the mill in revolutions per second

L is the mill length

g is the constant of gravity

The general empirical equations that describe the angular positions of the toe and shoulder of the media charge are respectively given by Equations 2.13 and 2.14 above. In these two equations, parameters A, B, E, and F were measured experimentally using photographs of the load in a laboratory mill (300 $\times$ 150 mm). The glass ended mill was rotated in the range 73 – 112 % of critical speed, for three geometries of lifters: the bevelled, the double wave and the Noranda designs. On these grounds, Morrell (1993) proposed the following:

$$\begin{aligned} A &= 2.5307 \times (1.2796 - J) \\ B &= 19.42 \\ E &= 0.3386 + 0.1041\phi \\ F &= 1.54 - 2.5673\phi \end{aligned} \qquad \textbf{(2.19)}$$

As for parameter ϕ_c, Equation (2.20) expresses its dependency upon mill speed ϕ and ball filling J:

$$\begin{cases} \phi_c = \phi, & \text{for } \phi > 0.35 \times (3.364 - J) \\ \phi_c = 0.35 \times (3.364 - J), & \text{for } \phi \le 0.35 \times (3.364 - J) \end{cases} \qquad \textbf{(2.20)}$$

Equations (2.13), (2.14), and (2.18) through (2.20) represent a comprehensive energy balance-based model of the net power draw by a cylindrical ball mill, or in short Morrell's power model. The model does not account for the following: energy losses due to friction, attrition and abrasion breakage, energy recovered through cataracting, reduction in the effective ball filling due to cataracting and/or premature centrifuging (Napier-Munn, 1996).

Perhaps the most important note to make is that Morrell's model (Equation 2.18) has remarkably worked on a large industrial database; however, its window of applicability should be restricted to non-supercritical tumbling mills.

2.6 Interrelation net power draw and milling efficiency

The work input to a mill is known to increase with speed providing the mill charge does not start centrifuging (see Figures 2.2 and 2.8). Normally, the optimal speed is 70 – 80 % of the critical speed (Wills and Napier-Munn, 2005). High speeds are often used to increase the amount of cataracting whereas low speeds produce more cascading. This explains why, for the same ball filling, speed can be used to modify mill power, and so load behaviour. This is particularly true with dry milling where the contribution of powder is generally insignificant. But, wet ball mills exhibit a strong dependence on slurry density and powder filling besides mill speed.

Figure 2.34 below summarises this statement well (Tangsathitkulchai, 2003). And to understand this, take a 40 % volumetric concentration in solids. For a gradually increasing slurry filling, the net mill power steadily increases; then reaches a maximum at a slurry filling U of approximately 1.0 before starting to decline. The argument for this behaviour is that the contribution of slurry through its pool is quite significant compared to dry milling. There is therefore strong evidence to suggest that for each slurry concentration, the net mill power changes with slurry filling. Furthermore, the optimum value of slurry filling giving maximum power is a function of slurry density. Be that as it may, Tangsathitkulchai's study is limited in that the resulting product size distributions were not analysed in great detail. At this stage, it is hard to ascertain whether the product might have not varied significantly despite dramatic changes in net power. If this were true, one would be tempted to overfill the mill with slurry until significant variations are observed.

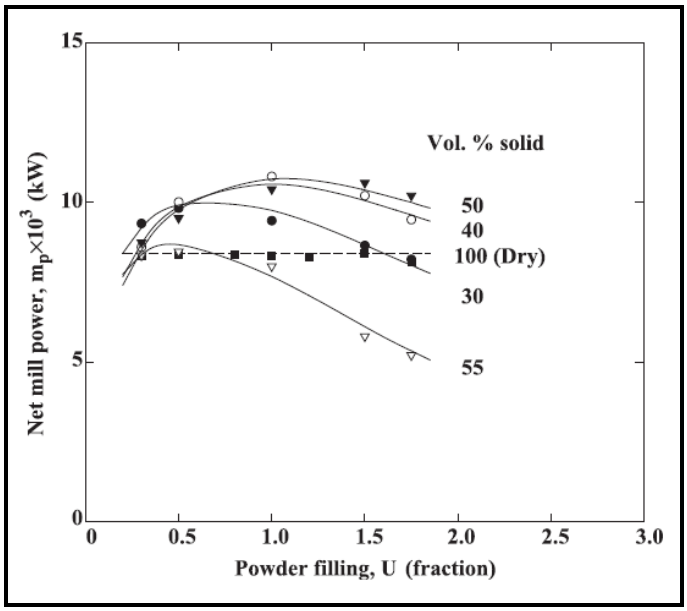

Figure 2.34 Variation of net power with slurry concentration and powder filling in a wet laboratory ball mill (after Tangsathitkulchai, 2003)

Perhaps the most important point is that Tangsathitkulchai (2003) came up with an empirical equation relating mill power (in *kW* per tons of balls used) to slurry concentration and powder filling – valid for slurry fillings in the range $0.3 \le U \le 1.75$:

$$\frac{m_p}{M_b} = a_1 U^{a_2} \exp\left(-a_3 U\right) \qquad \textbf{(2.21)}$$

where M_b is the mass of balls in the mill

a_1, a_2 and a_3 are fitting parameters that were found to be strong functions of the volumetric concentration of powder in the slurry in the range $0.3 \le C_v \le 0.55$

U and C_v are the slurry filling and slurry concentration respectively.

He then reported in the same article that at a constant powder load and for the quartz used, there was a linear relationship between specific rate of breakage and net mill power; and this, for the different slurry concentrations tested. However, under an artificial liquid other than water the relationship failed. This mystifying behaviour forced him to believe that besides slurry rheology, load behaviour influences the net mill power.

All and above, Tangsathitkulchai (2003) hypothesised that both bed expansion and changes in load orientation are involved in the milling process. But the data he produced were too limited to predict the load behaviour and link it to the observed results. Nonetheless, this quote taken from his paper says it all: “mill power alone does not define the breakage action”.

2.8 Attainable Region methodology applied to milling

2.8.1 Attainable Region: What is it?

Glasser and Hilderbrandt (1997) defined the Attainable Region (AR) as ‘the set of all physically realisable outcomes using only the processes of reaction and mixing in steady-state systems for some given feed(s)’. In other words, given the feed and the reaction kinetics, the set of all possible outputs of a chemical reaction can be found. And from there, the best combination subject to some operating constraints can be deduced not only in terms of the kinetics but also as an optimal reactor structure.

The first-order breakage rate model suggests that ball milling can be regarded as a chemical reaction and that the AR analysis can be used to study comminution processes. To this end, Khumalo *et al.* (2006) developed a technique in which they related breakage to the specific energy input. They then went on to experimentally showing that AR is applicable to ball milling (Khumalo *et al.*, 2007).

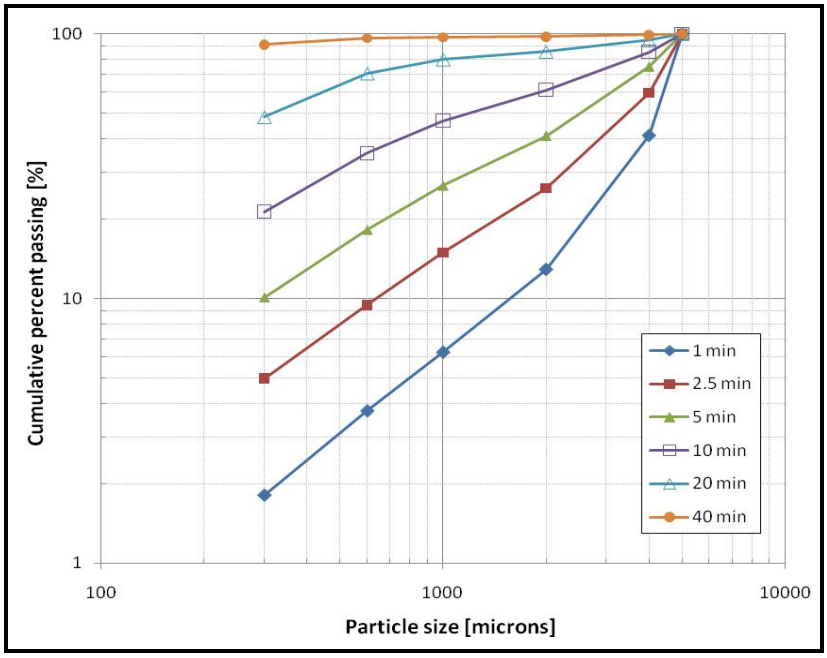

Figure 2.35 Particle size distribution of a silica sand tested in the laboratory (data from Khumalo, 2007)

To illustrate the methodology, suppose that we start off with a narrow-sized feed material $x_1 \leq x \leq x_2$ where x_1 and x_2 are two successive screen sizes taken from a given sequence. If after batch-grinding the feed sample for a grind time t a complete particle size analysis is performed from x_1 down to x_n, the type of graph shown in Figure 2.35 above can be plotted. Here, not only does Figure 2.35 present the PSD for t = 1 min, but it also shows the PSD's corresponding to several other grinding times ranging from 2.5 to 40 min and for which particle size analyses were performed in a similar fashion as for t = 1 min.

Consider grinding the initial material in order to get a product size distribution (PSD) with, say, a given sieve size x_k where $x_k \in \{x_i \text{ with } 1 \leq i \leq n\}$. Because of this specification, it is better but not compulsory to group mass fractions as follows:

(i) The feed size class defined as the material of size x which falls between x_1 and x_2. This class will be termed m_1

(ii) The middling size class constituted of particles of size x between x_2 and x_k. This second class will be termed m_2

(iii) The fines size class m_3 is defined as the mass fraction of material passing screen size x_k.

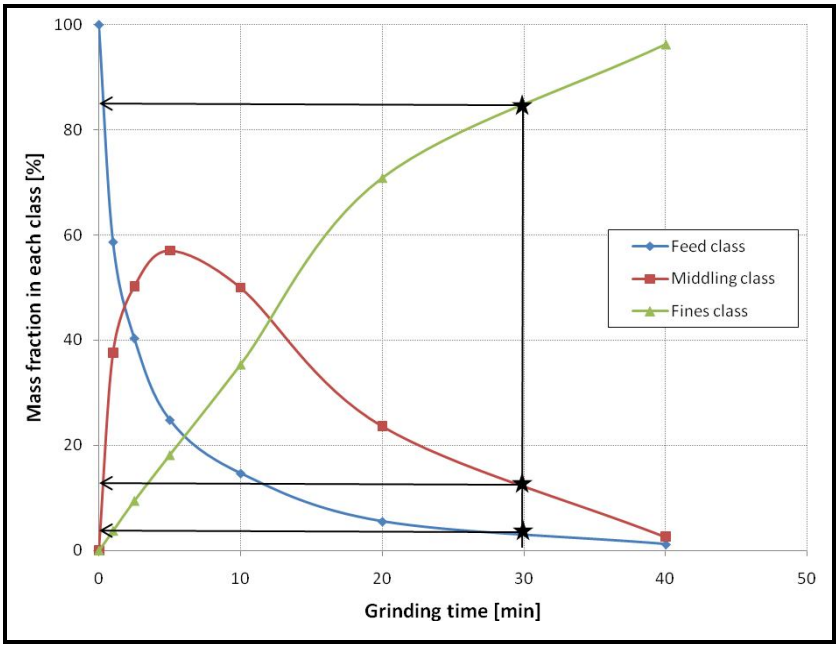

Figure 2.36 Grinding kinetics as plotted for the three size classes m_1, m_2 and m_3

After arbitrarily choosing x_2 and x_k as 4000 and 600 microns respectively, we can now track the change in mass fraction in each size class as a function of grinding time. This will look something like Figure 2.36 above.

If the objective is for instance to produce as much middlings as possible, Figure 2.36 shows that grinding the material for 5 min would be the way to go. And as one see with the AR analysis illustrated here, no model is needed to find such an optimum. Instead, a straightforward exercise of interpreting and reading graphs does the work.

On another note, following the reported mass fractions at different grinding times, it is now envisaged to present the data in the last format which is of much interest in the AR technique. To illustrate the transformation, respective mass fractions are read off Figure 2.36 at grinding time 30 min. They are then 'mapped' onto a 2-dimensional phase/concentration space, that is, (m_1, m_2). The

process is repeated for all the data points; and finally, after mapping, the AR plot is produced as shown in Figure 2.37.

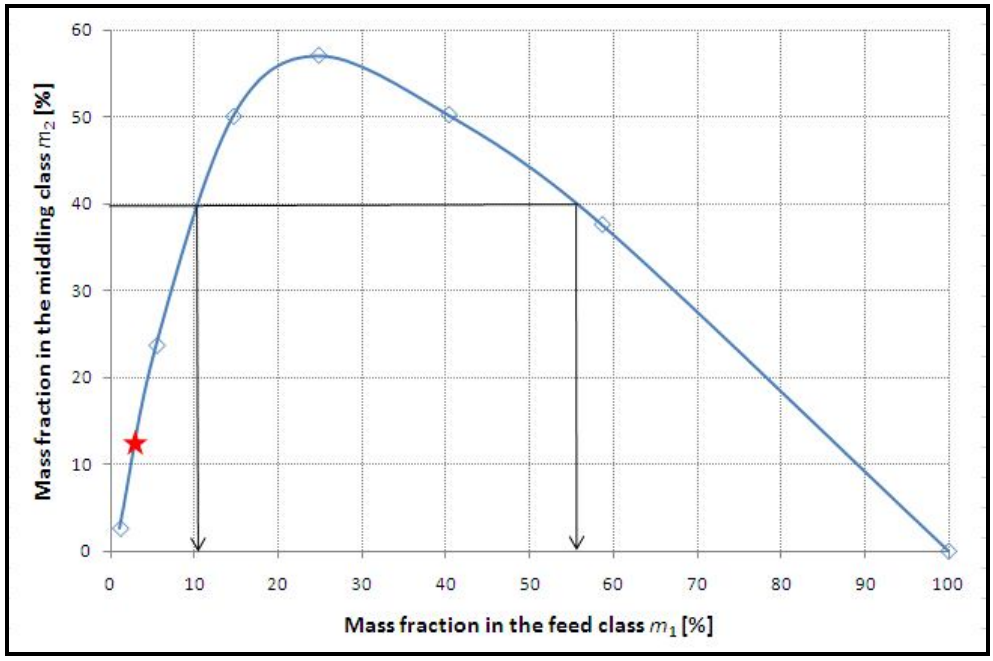

Figure 2.37 AR plot relative to the same silica sand tested with x_k = 600 microns

Figure 2.37 presents the same data produced from the silica sand material that is shown in Figure 2.36 but this time in the 2D space (m_1, m_2). It should be recalled that m_3 can be inferred by mass balance at any stage of the process. The plot presented here and drawn as a result of successive batch tests represents the path followed by the milling process to achieve the specified objective function from the system feed. It is referred to as the 'Attainable Region plot'.

The star marker on the plot (see Figure 2.37) corresponds to the 30 min grinding time considered earlier. From an AR perspective, one would say that about 97 % of the feed is needed to produce approximately 13 % of middling, and this after 30 min of grinding. It is therefore apparent that after 30 min, only 3 % mass fraction is left in the feed class m_1 whilst 13 % of middling m_2 is produced.

Now, if the objective is to produce at least 40 % of m_2, the AR plot indicates that between 44 and 89 % of the feed material is required. The graph in fact shows that for the objective to be met, between 11 % and 56 % of material should

remain in class m_1. This translates in a mass fraction between 89 and 44 % of material that needs to be ground out. Nonetheless, information such as the specific energy to be used or some other operating constraint will orientate the process engineer in the choice of the right mass fraction to be milled.

All and above, it appears that AR plots make it possible to characterise the selectivity of the process. In other words, the fraction of the initial feed material that will report to the class of interest can be determined under some operating conditions. Finally, note that the AR analysis as presented here is for illustration purposes and that each case study will require particular attention of its own.

2.8.2 Rationale of the Attainable Region methodology

The idea behind the term 'Attainable Region' can be conceived as follows: Take Figure 2.38 (created from Figure 2.36), point **A** represents a fresh feed not yet ground whilst point **B** represents a product milled for some time that consists of 15 % m_1 and 50 % m_2. It is possible to mix a fraction of **A**, say 25 %, and combine it with 75 % of **B** to get a composite material **C**. We can carry on with this exercise and fill up the region between the AR plot and the x-axis with dots for different combinations.

The dots represent all the possible (or attainable) composite materials that can be obtained by mixing principle out of the milling system. In other words, the stripped region in Figure 2.38 is called the 'Attainable Region'.

If the concavity is turned upwards (the region in Figure 2.38 is convex), mixing will present an advantage in that more material can be produced on top of the grinding process itself. Most importantly, the maximum turning point **M** (shown in Figure 2.38) can only be achieved if the class of interest is defined with upper and lower screen size boundaries. As a corollary, the sink fraction and the feed fraction never experience such a maximum. The bottom line is that a definite class (as opposed to a semi-infinite one) is required when one needs to optimise

the process. Sink and feed fraction are seen here as semi-infinite classes because they only have upper and lower sieve size limits respectively.

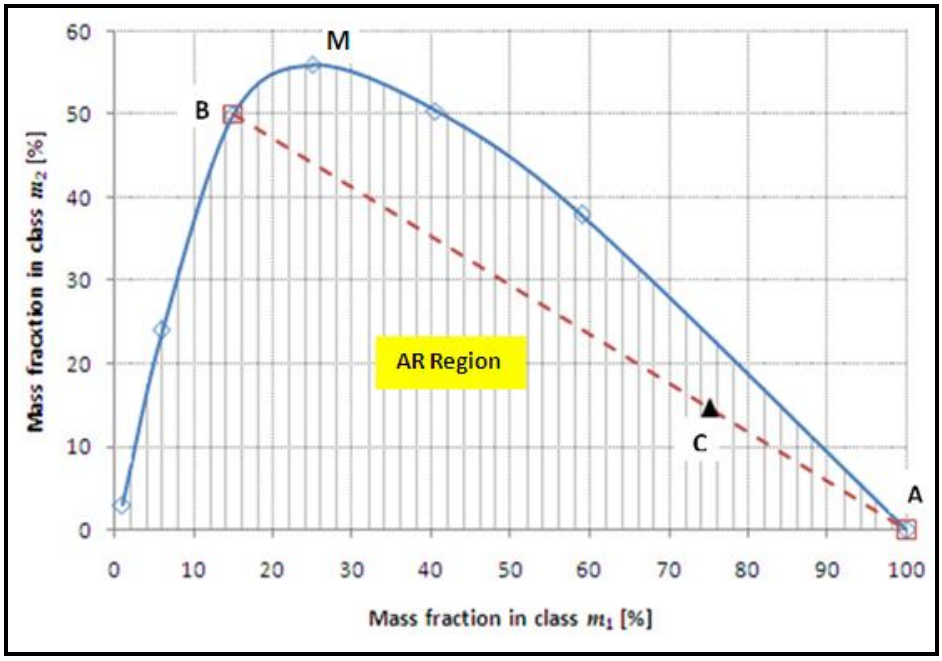

Figure 2.38 Principle of mixing in the AR space

2.8.3 Where to from here

It must be reckoned that the Attainable Region technique as applied to milling has now reached maturity. The confidence gained has however been built on laboratory work (Khumalo, 2007; Khumalo *et al.*, 2006 – 2008; Metzger, 2011; Metzger *et al.*, 2007 – 2012; Katubilwa *et al.*, 2011; Chimwani *et al.*, 2012; Chimwani, 2012). The next logical step should be in our opinion to find ways of validating it on industrial milling circuits. One possible route is to resort to commercial software packages (e.g. JKSimMet or MODSIM) and generate data for AR optimisation. Owing to the flexibility of simulators (Napier-Munn and Lynch, 1992), modifications of flowsheets should not be a problem.

2.9 Summary

Modelling approaches in the description of milling have been reviewed. In this regard, the Population Balance Model (PBM) articulated around the first-order

kinetics assumption has proven to be the most widely used technique. Despite attempts of incorporating non-first-order grinding kinetics into the population balance approach, first-order breakage (or linear breakage) is largely preferred owing to its simplicity and flexibility. This is true especially when breakage parameters are to be back-calculated through the PBM framework. Moreover, nonlinear models of breakage kinetics need to be expanded to full-scale applications to be as useful as linear models.

Next to the phenomenological analysis of milling is its graphical analysis. It has been found that graphical modelling has not been left behind; it has in a way reinvented itself and has given birth to the Attainable Region analysis. It is a technique that has the potential of complementing the PBM framework in the analysis of milling in particular.

Talking about slurry pooling, the review of past work has shown that slurry pooling in ball mills is not widely covered. The phenomenon has been studied mostly in autogenous and semi-autogenous mills. The review has therefore demonstrated the pertinence of slurry pooling in ball milling, especially when one considers its poor understanding. That is why the present thesis proposes to shed some light on the matter. Based on results obtained in autogenous milling, the following hypotheses will be tested for ball milling:

- The formation of slurry pool is the result of excess slurry that cannot be held up inside the media charge. Initially, the slurry is entrained within the mill charge so that the load behaves reasonably as a well-mixed entity; then, as the volume of slurry is progressively increased, it first remains within the perfectly mixed load, and eventually, the excess slurry drains off the load to form a pool of slurry.
- The reduction in power due the presence of a slurry pool should translate into a proportionate decrease in the production of fines.

Chapter 3 Experimental programme and equipments used

3.1 Introduction

The scientific method generally involves the following steps: the problem statement, a background research, the formulation of hypotheses and identification of key variables to be investigated, the design of experiments for testing the hypotheses constructed, and the analysis of results.

In the previous chapters, a problem statement has been formulated and the review of past work done. The identified research problem proposed to determine the contribution of slurry pooling to milling efficiency and to mill load behaviour. To answer this question, two hypotheses were constructed and measurable variables identified. First, it was posited that that the slurry pool phenomenon is the result of excess slurry that cannot be contained inside the media charge. Initially, the slurry is entrained within the mill charge to form with it a perfectly mixed load; then, once the volume of slurry exceeds a certain limit, the excess slurry drains off the load to form a pool of slurry. The second hypothesis pertains to the reduction in power due to slurry pooling: the power drop is also posited to affect the quality of the final product.

To test the two hypotheses above, the following structure was set:

1. Exploration of the phenomenon of slurry pooling in ball mills
2. Validation of the exploratory findings with a naturally occurring ore
3. Determination of the effects of power reduction due to the presence of a pool of slurry on milling kinetics.

To this end, three ball mills were used: a Perspex mill, the Wits pilot mill, and a laboratory batch mill. The next sections describe in detail the individual features of the mills and their respective programme of work. Expected outputs are also discussed.

3.2 Preliminary experiments

The experimental work aimed to study of the slurry pooling phenomenon is outlined in this section. The preparation of the artificial slurry to make up a range of viscosities is discussed. The Perspex laboratory mill, its technological characteristics and testing conditions are also presented. A great deal is made in the collection of data relative to charge motion by means of a high speed cinematographic technique.

3.2.1 Description of the Perspex mill

The first set of laboratory tests was qualitative. The basic aim was to observe the load behaviour and understand fundamentally what drives the phenomenon of slurry pooling.

The experimental setup was centred on a mill made of a Perspex material (Figure 3.1). To guarantee good quality of pictures of the load, a clear solution the viscosity of which could accurately be prepared was needed. Solutions of glycerol diluted in water were used.

Figure 3.1 Snapshot of the Perspex mill

Two milling parameters were considered: the viscosity and the level of slurry filling U. The effect of viscosity on load behaviour was to be investigated.

Different concentrations of glycerol were prepared for viscosity ranging from 1 mPa.s (pure water) to approximately 60 mPa.s (viscous solution). Media of approximately 10 mm in diameter were used to mimic the full charge of the mill. The choice for small balls was motivated by the fact that bigger ones were likely to damage the Perspex material or scratch it.

Finally, a cinematographic technique was used to capture on a video camera the motion of the load. The transparent mill was videoed for a ball filling J of 20 %, and a mill fractional speed ϕ of 60 %. Slurry filling U was varied from 0 to 3.0. The volume of artificial slurry V_{sl} to make up a given slurry filling U was determined as follows $V_{sl} = \varepsilon.U.J.V_{mill}$ where ε represents the porosity of the bed of grinding media at rest assumed to be 0.4 and V_{mill} is the volume of the mill.

The captured movies were to be later uploaded on a computer, then analysed to get an accurate measurement of the angular position of the pool and the toe and shoulder positions of the media charge.

Following the collection and processing of data, it was expected to come up with a model describing the relationship between slurry filling U and pool position θ_{pool} for changing viscosity. Added to this, a clear understanding of the interaction between slurry and media charge could be gained.

3.2.2 Specifications of the Perspex mill

The whole set of preliminary experiments was carried out using a transparent laboratory mill made of Perspex. The mill, the specifications of which are listed in Table 3.1, was mounted on rollers driven by a constant speed motor. Table 3.1 also gives a summary of the operating conditions considered. A photograph of the Perspex mill at rest loaded with grinding media at J = 20 % filling is also shown in Figure 3.1 above.

One thing to note is that the motor was not powerful enough to run at higher ball fillings. Because of technical limitations of the motor, it was only possible to consider no more than about 20 % ball filling for 60 % of the critical speed.

Table 3.1 Operating conditions of the Perspex mill

Mill dimensions	*Diameter, D* *Length, L*	*552 mm (inside liners)* *180 mm*
Lifter configuration	*Number* *Shape*	*18* *Trapezoidal* *25 mm height* *25 mm base width* *20 degrees face angle*
Test conditions	*Ball diameter* *Ball filling, J* *Slurry filling, U* *Mill speed, ϕ*	*10 mm only* *20 %* *0 – 3.0* *60 % of critical speed*

3.2.3 Preparation of the viscous solutions

Glycerol was used to investigate the effect of viscosity on load behaviour. Mixtures of water and glycerol of different concentrations (Table 3.2) were prepared to get solutions of viscosity ranging from 1 mPa.s (pure water) to approximately 60 mPa.s (viscous solution).

Volumetric proportions of water and glycerol used to make up the different viscosities are listed in Table 3.2. The average densities of the solutions prepared were determined at 20°C with the help of the Manufacturer's Specification Data Sheet (MSDS) provided by the supplier (Merck Chemicals Pty Ltd) of the glycerol used in this work. In addition, the supplier took care to report in his MSDS a set of curves relating the expected viscosity of the mixture to the volumetric concentration of glycerol for different temperatures. This way, it was possible to determine the volumetric fractions of water and glycerol needed to obtain a given viscosity.

Table 3.2 Water-Glycerol mixtures used

Glycerol [%]	Water [%]	Viscosity [mPa.s]	Average density [kg/m^3]
0	100	1	1000
42	58	4	1082
59	41	10	1130
69	31	20	1162
73	27	30	1176
80	20	60	1202

3.2.4 Programme of preliminary test work

The essence of milling is the reduction of particle size using grinding media. This implies that throughout the process, particle size is going finer as time proceeds. In rheological terms, the viscosity of slurry is expected to increase with grinding time. With this in mind, a series of tests was initiated with the objective of assessing the effects of viscosity on load behaviour. To this end, the transparent Perspex mill was taken advantage of.

Media of approximately 10 mm in diameter were used to mimic the charge of the mill. Using a video camera, the transparent mill was videoed for a ball filling J of 20 %, and a speed of 60 % of critical. Slurry filling U was varied from 0 to 3.0 for 6 levels of viscosity respectively (Table 3.2).

Initially, the mill was filled with balls. And after the viscous solution of known viscosity was prepared, the chosen volume was poured into the mill to make up a slurry filling U = 0.5. The mill was switched on while the sequences unfolding were videoed for 5 to 10 seconds. The mill was then stopped and the appropriate amount of solution added to make up the next level of slurry filling, that is, U = 1.0. The mill was started again and filmed. The next volume of slurry was added this time to get a slurry filling U = 1.1. The process was repeated until a slurry filling U of 3.0 was reached. Between tests, the temperature of the solution was monitored and recorded. Measured temperatures were found to vary in the range 16 – 19°C. From the MSDS, this change in temperature would reduce the highest viscosity (i.e. 60 mPa.s) by about 8 %.

Once the full series of tests was completed, the video was stored on a computer for later image analysis.

3.3 Pilot experiments

3.3.1 Description of the Wits pilot mill

The Perspex mill, though useful for preliminary work, had some major limitations. The motor driving the rollers on which the drum sat was not powerful enough to run more than 25 % ball filling. Slippages became inevitable; that is why, after trial and error, it was decided to settle for ball filling J = 20 %. The other problem was the low speed of the mill (60 % N_c).

To address some of these technological limitations, the Wits pilot mill was brought in. The mill was fitted with two non-invasive sensors for the study of load behaviour: the conductivity probe and the inductive proximity probe. The first was used to accurately measure the position of pulp whereas the second took care of the media charge. Here, the sophistication of the Wits pilot mill provides a facility for speed adjustment over a wide range (0 – 120 % N_c). The other important thing is that a Platinum ore was used instead of the glycerol solution. Owing to its darkish colour, a glass-ended plate fitted on the mill front was inappropriate. That is the reason why the two aforementioned sensors were used and not to the video camera any more.

Figure 3.2 shows a diagrammatic representation of the setup for the Wits pilot mill. The measuring facilities are numbered along in Figure 3.2 and their labels listed in Table 3.3 thereafter.

The mill (2) is constructed from a steel drum mounted on a mill rig (11). It is driven by a 2.5 kW variable speed motor (10) via a chain drive (9). The speed of the motor is controlled electronically through a speed controller (tachometer) and can run up to approximately 100 rpm. The milling cylinder (2) measures 550

mm in diameter (inside liners) by 400 mm long (inside liners) and is fixed to the mill axle (8) on which the load beams (6 and 13) are connected for torque measurements. The mill is lined with 18 lifters. The adopted shape of the lifters is a right-angled trapezium with the following characteristics: 25 mm height, 25 mm long base and 17 mm short base. The lifter profile was a geometric scale-down of lifters used in an industrial grinding mill in South Africa. The ratio between industrial and pilot mill diameters was used as the scale-down factor; hence, lifters and ball diameter were calculated accordingly.

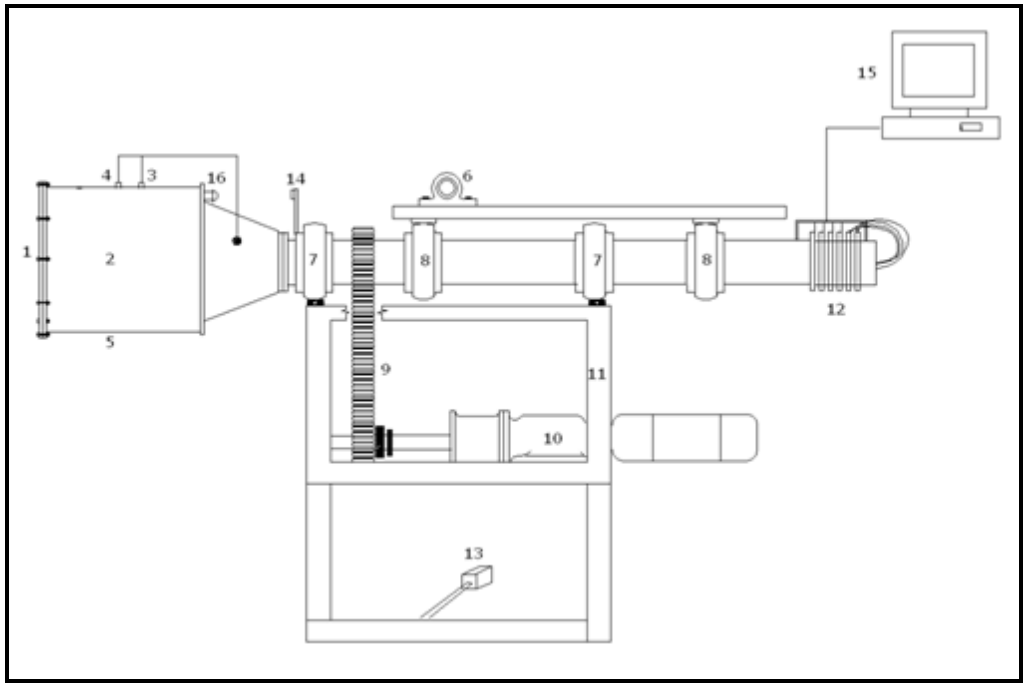

Figure 3.2 Setup of the Wits pilot mill

Table 3.3 Summary of features and measuring facilities of the Wits pilot mill

1	Front plate (PVC)	9	Chain drive
2	Milling chamber	10	Motor and Gear box
3	Conductivity sensor	11	Support frame
4	Inductive proximity probe	12	Slip rings
5	Mill shell	13	Axial load beam
6	Pivot load beam	14	Glass mirror
7	Motor gage bearings	15	Computer for data acquisition
8	Axle bearings	16	Phototransistor and LED

A 10 mm thick PVC disc was used to close the front side (1) of the mill with a provision for feeding and discharging the mill content. The torque yielded by the load beam (13) as a result of the tumbling load is detected as a voltage, processed and fed to the computer (15). The latter is interfaced with a Waveview© program from Eagle Appliances (Pty) Ltd (trading as Eagle Technology) for real time data acquisition. Both the signals from the proximity (4) and conductivity (3) sensors are transmitted off the mill to the computer by means of slip rings (12) mounted on the mill axle.

Broadly speaking, with the Wits pilot mill, one can measure the net power drawn to the mill, the positions of the slurry and the media charge inside the mill, and the speed of the mill.

As far as load behaviour is concerned, data pertaining to the media charge position and the pool level was collected without paying attention to milling. This was used to define a picture of the media charge behaviour and slurry position, as well as their interrelation. A validation of the preliminary findings was made and new insight brought to the surface. On top of that, net power was modelled to further establish the contribution of slurry pooling on mill power.

In short, the test work with the Wits pilot mill was conducted with the expectation to relate mill power to slurry pooling. Results were also used to validate the preliminary tests done with the Perspex mill.

3.3.2 Pilot mill commissioning

The set of pilot experiments was primarily intended to reproduce the preliminary tests done with the Perspex mill, but using a Platinum ore. Owing to the degree of rheological difficulty brought by the ore, it is expected to produce a marked difference in behaviour compared to glycerol solutions. Indeed, the apparent viscosity of slurry increases with milling and definitely the ore will not reflect the behaviour expected from the artificial liquid presented in the previous section.

To carefully collect as much information as possible with a reasonable amount of tests, the programme below was used: The experimental work involved the measurement of the load behaviour under similar conditions used during preliminary tests. Except for the Platinum ore, the same range of slurry fillings was considered: U = 0.0 – 3.0. Mill speed was varied from 65 to 85 % of the critical speed by increments of 5 %. One ball filling was investigated, that is, J = 20 %. With this filling degree, slurry volumes were calculated for slurry filling U in the range 0 – 3.0.

The proximity and conductivity probes were intensively used in the determination of the mill load behaviour. One thing though, only 10 mm balls was used so as not to damage the proximity probe. As shown in Figure 3.3, the shell of the Wits pilot mill was drilled to make provision for the proximity and the conductivity sensors. The two probes were placed side by side to measure load behaviour almost in the middle of the mill length, but also for easy reference and comparison during data processing.

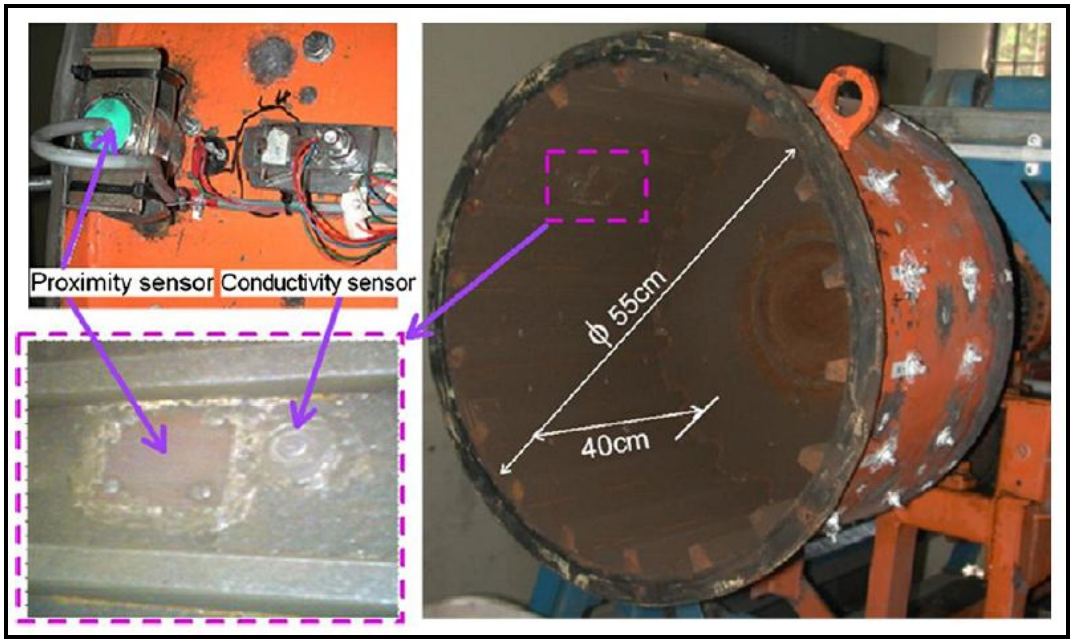

Figure 3.3 Installation of the proximity and conductivity sensors through the shell of the Wits pilot mill (Figure taken from Makokha and Moys, 2012)

The concentration of solids in the slurry was maintained at 65 % due to the size of balls; otherwise the slurry might be too viscous and entrain the grinding media in the flow. The collected data served in the correlation of slurry filling U and pool level θ_{pool}. At this stage of the work, it was expected to see how preliminary results compared to results produced during pilot mill commissioning.

Later on, the load behaviour was measured for a 'dry mill'; that is, a mill filled with balls only. The speed was varied from about 20 to 110 % of critical speed. The 'dry mill' was compared to DEM simulations as described in the next section.

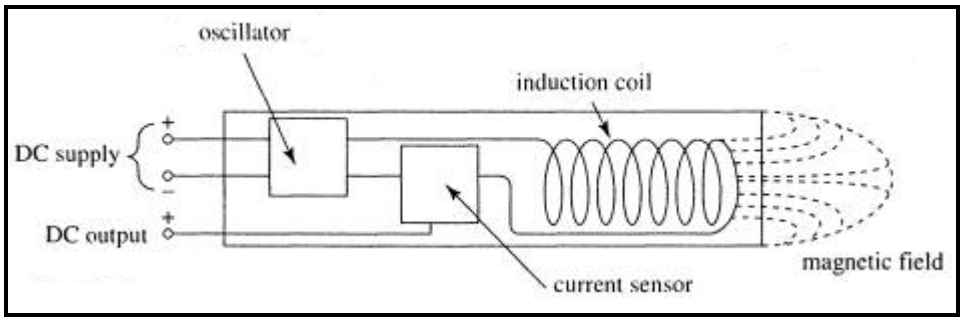

Figure 3.4 Block diagram of an inductive proximity probe

Here, only with the inductive proximity probe was used to measure the position of the media charge. This sensor operates under the principle of electrical inductance. A fluctuating current generated by an oscillator (Figure 3.4) powers an induction coil. This becomes energised and creates a magnetic field sensitive to metal. Any ball that falls within the metal sensing region of the probe develops an electromotive force that is then detected by the sensing device.

3.3.3 Programme of pilot test work

The Wits pilot mill described in Section 3.3.1 was used for the investigative work. It was fitted on the shell with two non-invasive sensors: the proximity probe and the conductive probe.

The work was twofold: First the mill was filled with 10 mm media balls only. The mill speed ϕ was then varied from 24.6 % to 106.1 % of critical. In the process,

the following information was recorded: the load behaviour (positions of shoulder and toe of the media charge), mill speed, and power draw. In the second part of the experiment, slurry was added to the media charge. The slurry was prepared with a solids concentration of 65 % by mass. Slurry filling U was varied from 0 to 3.0. Here as well, mill speed and net power draw were measured; measurements were taken for 30 sec on average. In terms of slurry behaviour, the position of the pool was determined with the conductivity probe. Mill speed was varied from 65 to 85 % of critical.

Table 3.4 below summarises the work that was done with the Wits pilot mill.

Table 3.4 Wits pilot mill – Experimental conditions

	'Dry mill'	**Wet mill**
Speed, ϕ [% of critical]	24.6 – 106.1	65 – 85
Mill diameter, D [mm]	552	552
Mill length, L [mm]	400	400
Ball filling, J [%]	20	20
Slurry filling, U [-]	0	0 – 3.0
Ball diameter, d [mm]	10	10
Ball density, ρ_b [kg/m^3]	7800	7800
Lifter geometry		
Number	18	18
Shape	Trapezoidal	Trapezoidal
Height [mm]	25	25
Base width [mm]	25	25
Face angle [°]	20	20

It should be mentioned that the term 'dry mill' adopted in the thesis specifically refers to the Wits pilot mill loaded with grinding media only. Neither ore in the form of powder or slurry, nor water is added to the charge of the mill.

It is also important to mention that the Wits pilot mill was set as a scale-down version of an industrial mill in which 40 mm balls and 18 trapezoidal lifters of 100 mm in height were used. The diameters of the industrial and pilot mills were used as the rescaling factor. That is the reason why, after calculations, it was decided to use 10 mm balls and 18 small lifters of 25 mm in height.

3.4 Batch grinding experiments

The test work done in the laboratory to investigate milling kinetics is described below. In a comprehensive fashion, feed preparation, batch testing, and particle size analysis are presented. The measurement of milling power is also briefly explained.

3.4.1 Description of the laboratory grinding mill

The last part of the programme sought to study milling kinetics. A laboratory mill was used to carry out a series of batch grinding tests. Upon completion of the batch tests, the selection function and breakage function parameters were to be determined for modelling purposes. It is worth mentioning that mill power was also recorded in order to determine energy consumption.

Figure 3.5 View of the laboratory ball mill

Figure 3.5 shows a photograph of the laboratory batch mill installed on a steel structure that carries all the control and measurement facilities. An electronic speed meter enables one to set and control the motor speed (see Figure 3.6), and thereby mill speed.

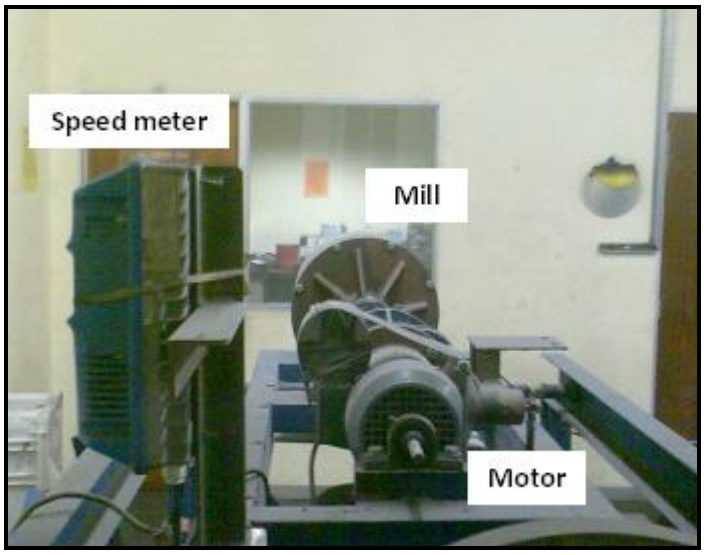

Figure 3.6 Rear view of the mill equipment set-up

The milling cylinder can take up to 20.2 litres in volume and is fitted with 8 rectangular lifters. Besides the net power and the speed of the mill, no other information can be measured online. The data acquisition system is similar to that of the Wits pilot mill presented earlier.

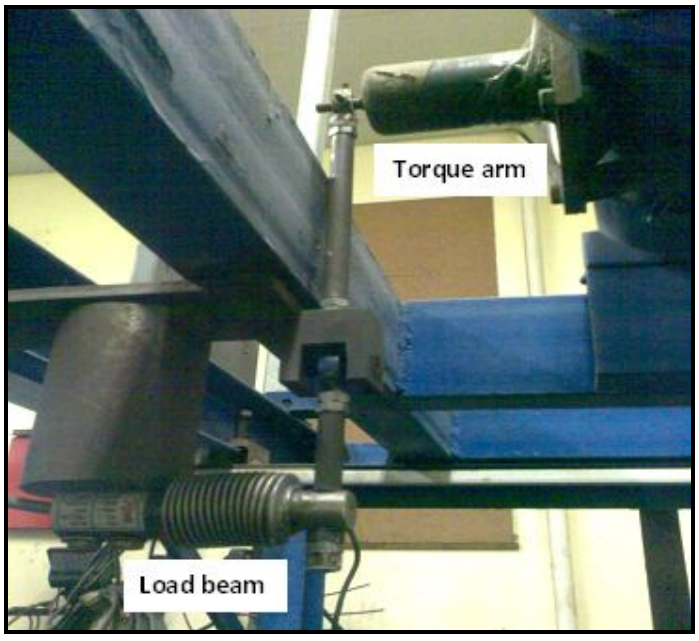

Figure 3.7 Power measurement system of the laboratory mill

The facility used to measure mill power is shown in Figure 3.7. It comprises a load beam that converts the force exerted onto it into corresponding voltage. A

piece of rod is attached on one of its ends to create a force as a result of the torque due to the rotation of the mill.

All in all, the batch mill is expected to supply enough information pertaining to milling kinetics and power draw for different slurry fillings; and thereby different pool volumes.

3.4.2 Batch milling conditions

The final set of experimental work for this thesis was carried out using a laboratory mill. The batch milling conditions and some of the technological features of this mill are listed in Table 3.5 below.

Table 3.5 Laboratory mill operating conditions

Mill dimensions	*Diameter D* *Length L*	*302 mm (inside liners)* *282 mm*
Lifter configuration	*Number* *Shape*	*8* *Rectangular* *13 mm height* *25 mm width*
Test conditions	*Ball diameter, d* *Ball filling, J* *Slurry filling, U* *Mill speed ϕ*	*20 mm only* *20 % and 30 %* *0 – 3.0 (basis J = 20 %)* *75 % of critical speed*

The most important thing to understand in Table 3.6 is that the mass of slurry remained constant while changing ball filling J. To put it another way, using the dimensions of the mill, the mass of balls needed to load the tumbling cylinder at 20 % of its volumetric capacity were calculated. After that, the masses of slurry at 65 % solids concentration by mass required were worked out to make up the following slurry fillings: U = 1.5; 2.0; 2.5; 3.0.

But, for a 30 % ball filling, the same masses of slurry were used, thereby dropping the actual slurry fillings to U = 1.0; 1.3; 1.7; 2.0 respectively.

Also note that 20 mm balls were used to speed up the batch grinding kinetics and therefore save up on experimental time for the many tests considered.

Table 3.6 Compositions of different slurries used

Actual slurry filling		Mass of ore [g]	Mass of water [g]
J = 20 %	J = 30 %		
1.5	1.0	3246.7	1748.24
2.0	1.3	4329.0	2330.99
2.5	1.7	5411.2	2913.73
3.0	2.0	6493.5	3496.48
	Total mass [g]	19480.4	

Table 3.6 gives a summary of the mass composition used in the preparation of different levels of slurry U at 65 % solids content. Identical masses of slurry were prepared for two ball fillings (20 and 30 %) which led to different slurry fillings.

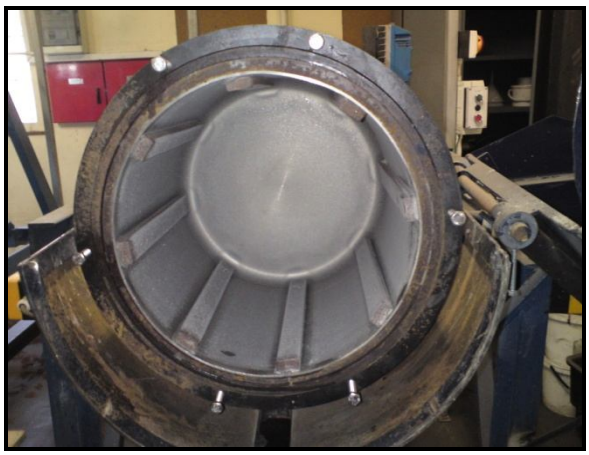

Figure 3.8 Photograph of the laboratory mill showing the lifters

Finally, a general view of the inside of the laboratory batch mill is presented in Figure 3.8 where the eight (8) rectangular lifters can be clearly seen.

3.4.3 Preparation of feed samples

The feed that was chosen for the pilot programme is a South African Platinum-bearing ore known as UG2 ore. It is one of the platinum-rich layers in an intrusion named the Bushveld Igneous Complex. About 60 % of the Platinum in

the Bushveld Complex is in the UG2 reef. Consequently, a lot of research and development has been concentrated on milling. That is why the availability of the UG2 ore has made it our preferred choice.

The feed material used for this work was a Platinum ore from the Western Bushveld Igneous Complex (Republic of South Africa) which had been subjected to primary milling. Internal references from a South African concentrator reported that the specific density on the UG2 used as established in routine inspection is 3.47 kg/cm^3. The ore was a fine material of size distribution less than 850 microns. Figure 3.9 provides the size distribution obtained after conventional sieving of one of the representative samples prepared. The particle size analysis consisted of a wet-sieving of the lot on a 25 microns sieve, then drying of the oversized fraction followed by its dry-sieving for 20 minutes. Note that 0.73 % of the initial mass passed through a 25 microns sieve while 93.93 % passed through sieve size 600 microns (see Appendix A.3.2).

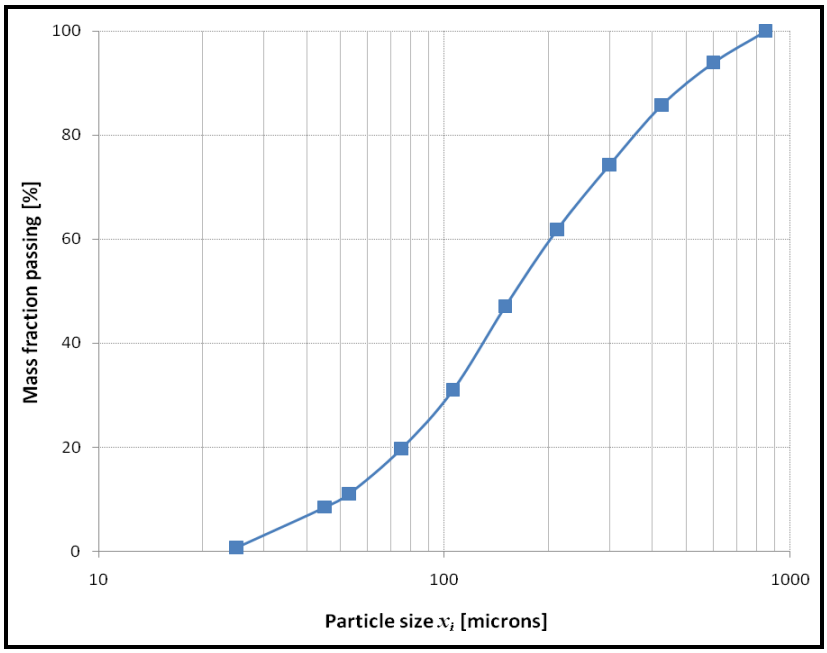

Figure 3.9 Representative feed size distribution used

Sample preparation involved cone and quartering of a heap of material to homogenise it. 60 kg sample of the material was progressively split into two fractions using Jones rifflers. The splitting was done in batches of approximately

1 – 2 kg, one at a time. Each one of the two fractions was then split with a rotating splitter into 10 smaller fractions; subsequently, these smaller fractions were split using a small splitter to prepare a total of 20 parts. Each part was weighed so that the 18 parts close to 582.75 g were retained for future use. The 4 rejected candidates from both larger fractions were kept for size analysis. Finally, the 18 parts were systematically combined to make up the masses of ore reported in Table 3.6 above. It is therefore understood that for U = 1.5, three (3) parts were needed whereas 5 parts were combined to prepare the ore for U = 2.0, and so on. Through this iterative process and within the experimental errors inherent to the sampling method, it was possible to obtain samples similar in size distribution.

The long preparation process explains why equal masses of slurry were used for different ball fillings J. Finally, the requirement for equally representative and similar feed samples was the motivation to devise and implement this systematic laboratory procedure.

3.4.4 Sampling procedure for mill product

Sampling of slurry is generally a challenge as it is known to be an inconsistent process. This is also true when dry powder is involved. A sampling method using slurried silica sand was tested. First, approximately 1 kg of powder (silica sand) was prepared by screening it through a 850 microns sieve. The undersized material was then divided into 10 fractions using a rotating splitter. Four of the ten samples were arbitrarily taken for analysis. The first sample (termed here 'dry sand') was wet-washed on a 38 microns sieve, then the oversized fraction dried in an oven at 50°C overnight before dry-sieving it through a stack of sieves from 850 down to 38 microns. The remaining three samples of powder were then combined and mixed with water to make up a slurry (termed here 'slurried sand') at 65 % solids content by mass. After this, the slurried sand was stirred up with an electric stirrer and a sample was quickly taken from the agitated slurry

with a scoop. The sample of slurry was then analysed following the same protocol used with the dry sand: wet-washing, drying, dry-sieving. Last, mass fractions in each size class for the two samples (dry and slurried sands) were compared. Emphasis should be made on the fact that for a given sieve, the mass fraction of slurried sand was compared to that of dry sand. The relative error representing the difference in mass fractions between the two samples of 'sands' to the mass fraction of dry sand was calculated. No more than 7 % discrepancy was recorded between retained fractions; this basically represents a 1.1 % error relative to the whole sample considered.

Though the method was tested on silica sand, it is believed that particles actually used were small enough (-850 microns) and therefore experienced low settling velocity. Besides, the difference in density between silica sand and the UG2 ore used might not have had a great impact on the settling behaviour of the two species that the sampling method could still be applied to the UG2 ore.

3.4.5 Programme of batch test work

Once the necessary feed samples were prepared, the batch grinding tests were started. In this regard, powder and water were stirred and mixed in a container. The slurry was poured into the mill initially loaded with 17.8 kg of grinding media (J = 20 %). Then, the first run was initiated for a grinding time of 1 minute. After that, the mill was emptied and cleaned. The slurry was then separated from the grinding media and collected in a bucket. Using an electric stirrer, the slurry was stirred up to create a solution with particles in suspension. Then, one sample was scooped out of the bucket for particle size analysis.

The slurry and media were loaded back into the mill and further milled for 1 minute, then, the mill emptied and the slurry sampled as previously done. This process was repeated for 4 more grinding times: 4, 8, 15, and 30 minutes. Each time, the power was recorded in real time for future analysis.

Per batch test, 6 samples stored in small bottles were obtained and recordings of power data collected. The series of batch tests continued, this time for a 30 % ball filling (i.e. 26.7 kg of grinding media). And at the end of the series, 48 bottled samples were constituted for size analysis.

The last step was to dry the 48 samples at 50°C in an oven overnight. The dry powders were weighed and in generally the mass of dry samples were somewhere between 90 and 160 g. The dry samples were then wet washed successively on sieves of size 75, 53, 45 and 25 microns. The fractions retained on each screen were dried again and weighed. Finally, the materials retained on 75 microns were screened from 850 down to 75 microns and their masses recorded. This made it possible to determine good particle size distributions that were to be used later for parameter estimation.

3.5 DEM simulations

3.5.1 Objectives of the simulations

The programme of numerical experimentation essentially consisted of the use of the DEM technique to simulate some of the milling conditions used in actual experiments. Because of the limitations that come with the numerical technique, the series of tests with the Wits pilot mill carried out earlier on a ‘dry charge’ was used for comparison. Recall that the mill was loaded with grinding media only. The load behaviour was measured for the speed range of 14 to 110 % of critical: 10 measurements were collected in this interval. Now, using the DEM simulator available, input parameters were adjusted accordingly to best approximate the measured media charge behaviour. Once the output was considered satisfactory enough for the purpose, the mill power draw was explored as a function of mill speed. The aim here was to determine the actual critical speed of the mill and to help make sense of results obtained under wet conditions.

The DEM tool was expected to give a clear picture of the in-mill behaviour. To be more precise, the DEM technique was used to provide the simulated version of the toe and shoulder positions of the 'dry mill'. The simulated power draw was compared to experimentally-measured one. This was then used as a benchmark in the interpretation of results of wet milling.

3.5.2 DEM-based experiments

The Wits pilot mill was simulated with SimView, a DEM tool available at the University of the Witwatersrand. Owing to the limitation of SimView, and the DEM technique in general, only a 'dry mill' was investigated and results of simulations compared with data collected in similar conditions. SimView also has the capability to capture frames as the simulation proceeds and compile them in an animation. This feature was utilised to determine the simulated positions of the toe and shoulder of the media charge at different speeds.

Table 3.7 DEM parameters used for simulations

Normal stiffness	400 kN/m
Shear stiffness	300 kN/m
Coefficient of friction	0.4
Coefficient of restitution Ball – ball impact Ball – wall impact	 0.6 0.3
Time step, Δt	10^{-6} s
Maximum degree of overlapping allowed	2 %
Mill diameter, D Mill length, L	552 mm 40 mm
Lifter geometry Number Shape Height Base width Face angle	 18 Trapezoidal 25 mm 25 mm 20°
Mill filling, J Mill speed, ϕ [% of critical]	20 % 24.6 – 106.1 %
Ball size, d Ball density, ρ_b	10 mm 7 800 kg/m^3

Table 3.7 gives an overview of the DEM parameters initially chosen for the simulations of the Wits pilot mill. Diverse sources were consulted when choosing the different parameter values. The normal and tangential stiffness values were taken from the paper by Mishra and Rajamani (1992) as the two authors worked on data from the Wits pilot mill to calibrate their DEM code. The choice for the coefficients of friction and restitution was motivated by the work by Dong and Moys (2002). They recommended an average friction of 0.4 and a coefficient of restitution of 0.75 for ball-ball impacts. For ball-wall impacts, coefficients of restitution ranging from 0.375 to 0.53 led to similar trajectories described by measured and simulated balls. It should be noted that values of the coefficient of restitution as low as 0.36 for ball-wall impacts have also been reported in the literature (Monama and Moys, 2002; van Nierop *et al.*, 2001; Kalala *et al.*, 2005); they are even twice as small as those of ball-ball impacts (Mishra and Rajamani, 1992).

Finally, the net power estimated with the DEM simulator was compared to measurements of the net power draw of the Wits pilot mill. As a well tested and calibrated tool (Bwalya, 2001; Moys *et al.*, 2000 – 2001; Hlungwani *et al.*, 2003), SimView was used to assist in the analysis of data by providing information of the internal load behaviour where proximity and conductivity sensors could only do so much.

3.5.3 Wits' DEM simulator

All the above listed settings (see Table 3.7) were entered into SimView in a user-friendly manner via the interface above (Figure 3.10). Appendix A.6 overviews the principal functionalities offered by SimView. Other interfaces linked to SimView such as the Design Liner and Simulator Viewer are also presented.

Note that the simulations performed were three-dimensional (3D) but on a slice of the mill one tenth the actual length of the mill inside liners. The slice was used

to reduce the computation time required to complete different simulations. In the mill slicing, end wall effects were not included in the simulation model.

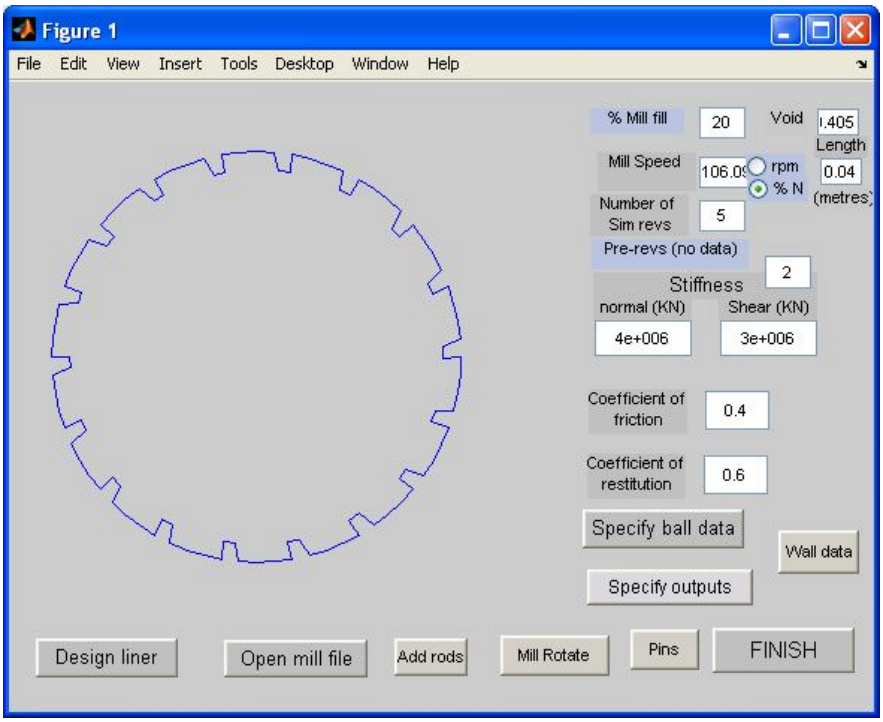

Figure 3.10 SimView interface

3.6 Difficulties encountered

The work executed with the Wits pilot mill would have been relevant to industry if larger balls and higher ball fillings were considered. However, the fragility of the sensors restricted the diameter of balls to 10 mm. There was also not enough provision for grinding balls to consider a 30 % ball filling. The other reason for choosing a 20 % ball filling was linked to the Perspex mill that could only run with such a ball filling and not more: the intention was to repeat the same tests in a pilot context. The fear of damaging the sensors was also another motivation. To build up from the information gained with the Perspex mill, a decision was taken to settle for the same ball filling even with the Wits pilot mill.

For batch testing, the main difficulty encountered was material handling. Indeed, starting from the preparation of feed samples through to the collection of

samples of slurry for particle size analysis, the problem was pertinent. During feed preparation, it was not always possible to split the ore to equal masses sensu stricto. Sample collection for particle size analysis also posed problems. A sampling method was devised and saved a tremendous amount of time; however, the volume of sample gradually collected compromise the initial milling conditions. In future, a smaller sample should be considered and the sampling technique thoroughly tested.

Lastly, the numerical capabilities at our disposal can only model ‘dry mills’; that is, grinding balls only. That is why a set of DEM experiments whereby the mill was simulated dry was initiated. The objective of the undertaking was to learn more about the in-mill dynamics of the Wits pilot mill before in conjunction with information obtained under wet milling conditions. This sought to build confidence in collected results and see inside the mill with numerical eyes rather than with the non-invasive sensors used.

3.7 Summary

The work with the Perspex mill was basically intended to elucidate the phenomenon of slurry pooling. It is expected to give more insight into the role of viscosity and slurry filling on load behaviour and on the location of the pool in particular.

The Wits pilot mill took the above work one step further by introducing the speed as another variable. In addition to this, the measured positions of the media charge and of slurry were used to ascertain the contribution of the pool in the net power draw of the mill.

In the final programme, grinding tests were carried out in the laboratory batch mill. With the information gathered in the first two series of tests, milling kinetics was studied and interpreted with a more informed knowledge of slurry pooling. The aim was to circumscribe the contribution of the pool to milling kinetics.

Chapter 4 Effects of filling degree and viscosity of slurry on mill load orientation[2]

Abstract

The presence of a pool plays a key role in governing the transport of material in wet ball mills. It also contributes in lowering the power drawn to the mill. And in the process, grinding efficiency could be altered. Understanding the pool formation in a tumbling mill and its interrelation to slurry filling is the main focus of this work.

To this end, a mixture of water and glycerol was prepared with appropriate concentrations to mimic viscosities ranging from 1 to 60 mPa.s. A transparent mill (552 × 180 mm), made of Perspex material and filled with 10 mm balls, was used for the tests. Ball filling and mill fractional speed were kept constant respectively at J = 20 % and ϕ = 60 % while slurry filling U was varied from 0 to 3.0. Using a high speed video camera, the motion of the charge was captured. The movies were then analysed frame by frame and the angular positions of the shoulder and the toe of the media charge as well as the pool of slurry were measured. The orientation of the load under different conditions was in this way determined.

Preliminary results show that there exists a definite trend between pool angle θ_{pool} and slurry filling U. A power function of the form $\theta_{pool} = C_0.U^k$ appears to be a good description of the relationship where C_0 and k are fitting parameters. It was also found that, within the range investigated, viscosity has little to no effect on the load behaviour.

Keywords: Grinding, Ball mill, Wet milling, Load behaviour, Slurry filling, Slurry viscosity, Slurry pooling

[2] The results was this chapter have been published in the Minerals Engineering Journal under the reference: Katubilwa, F.M., Moys, M.H., 2011. Effects of filling degree and viscosity of slurry on mill load orientation. Minerals Engineering, vol. 24, no. 13, pp. 1502 – 1512

4.1 Introduction

Ball milling is ubiquitous in mineral processing but yet amongst the most inefficient operations. It is done dry or wet depending on downstream processes and on the availability of water. In a wet context, two main types of product discharge exist: the overflow discharge and the grate discharge.

Overflow discharge mills generally run with a higher internal slurry level. However, they draw less power compared to grate discharge mills under similar milling conditions. The presence of a pool of slurry in overflow mills is responsible for this. It counter-balances the media charge and moves the centre of gravity of the load towards the mill axis (Morrell, 1993). A diagrammatic representation of the general load orientation of a wet mill is showed in Figure 4.1. Here the media charge defined by the toe and shoulder is clearly differentiated from the pool. Showed alongside is a simplified model of the load behaviour with the torque exerted by the pool of slurry. This torque is the reason for the reduction in mill power drawn by the media charge.

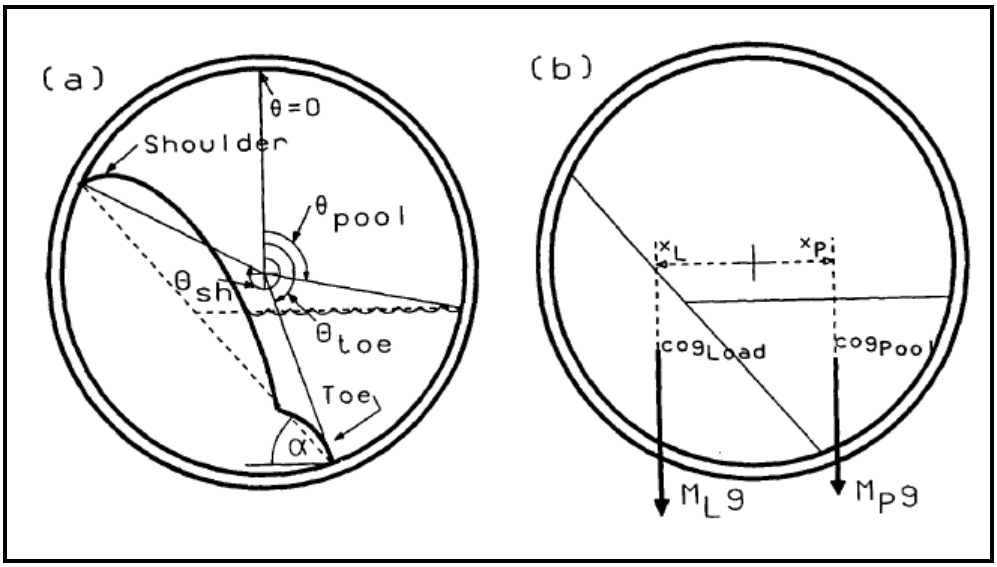

Figure 4.1 Typical behaviour of the mill load with the position of the media charge and the location of the pool represented in (a). Simplified model of the load behaviour and acting torques in a wet mill torque are shown in (b) (after Moys *et al.*, 1996a)

Recently, Clermont *et al.* (2008) introduced the use of a set of sensors called Sensomag®. It is basically a tool that allows simultaneous determination of slurry and media charge positions inside the mill. Using the Sensomag®, they investigated the effect that changing the discharge configuration of a 4.8 m diameter ball mill has on power drawn. Measurements of the media charge and slurry orientations were taken both for the grate and overflow discharge configurations. Results showed that the Sensomag® was able to pick up the presence of a pool in the overflow discharge configuration. Furthermore, the mill operated with 8 – 10 % less power as compared to the grate discharge scenario.
But, regardless of the discharge system, in-mill slurry rheology and load behaviour remain the main determinants of the mill performance. Moys (1987), for instance, investigated how slurry rheology and flowrate shape the mill load. His findings suggested that slurry position relative to media charge in the mill plays a major role in the grinding efficiency. He also argued that the key to controlling and optimising wet milling resides in the distribution of slurry within the media charge.

At this stage of knowledge, the link between load behaviour and power draw has been proved and widely accepted (Liddell and Moys, 1988; Morrell, 1993). Several online devices (Moys, 1985; Tano, 2004; De Haas, 2008) have been developed to get more insight on the internal behaviour of industrial mills. But whether the amount of invaluable data supplied by these sensors is put to effective use is the question.

In approaching the problem, attention was focused on studying the influence of viscosity and slurry filling on the orientation of the load in a laboratory mill. To achieve this, a photographic technique was employed to observe the in-mill dynamics of a transparent laboratory mill. The captured movies were uploaded on a computer, then analysed frame after frame to get an accurate measurement of the pool position and the toe and shoulder positions of the media charge. Average angles of the key positions of the load and their

respective standard deviations were also determined. A model describing the relation between the position of the pool and the filling degree of slurry for changing viscosity was proposed. It is believed that this information will be helpful in converting data supplied by online sensors into corresponding slurry filling. And lastly, the effect of slurry filling and viscosity on the position of the mill load, and specifically on the media charge, was determined.

4.2 Measurement of the Perspex mill behaviour

The backbone of the experimental work done with the Perspex mill has consisted in the measurement of the load position. To continuously do so, photographs were taken with a digital video camera (Panasonic Model NV-GS180). This camera enabled us to capture the general motion of particles inside the mill at a rate of 25 frames per second. For the 5 to 10 seconds of movies produced, approximately 125 to 250 frames were extracted. The first and last seconds were not considered. Only intermediate sequences when the mill was running at steady state conditions were retained for analysis. On average 75 to 125 frames were retrieved and corresponding still photographs produced.

For each and every frame retained for analysis, a set of axes was superimposed onto the corresponding photograph. With the help of an electronic protractor (MB-Ruler version 4.0), key angular positions of the charge were accurately measured with the 12 o'clock position being 0° (reference) while the 9 o'clock position was used as 90°. Figure 4.2 illustrates how all this was done with the location of the pool that is read off as 114.7°. This way, toe of slurry, toe and shoulder of media charge were determined frame by frame. Finally, average positions and corresponding standard deviations were calculated.

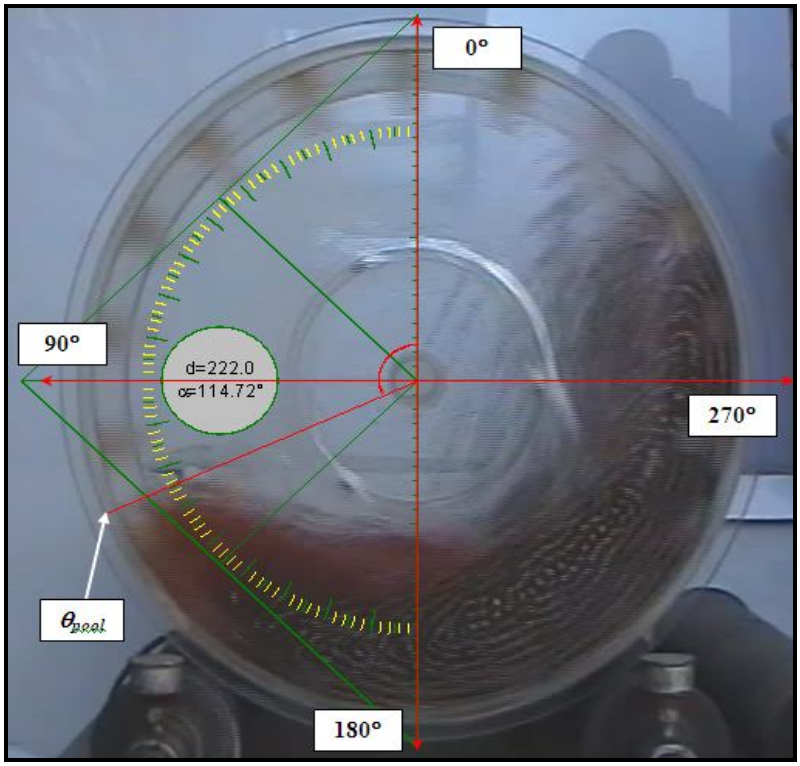

Figure 4.2 Superimposition of the protractor on a still photograph

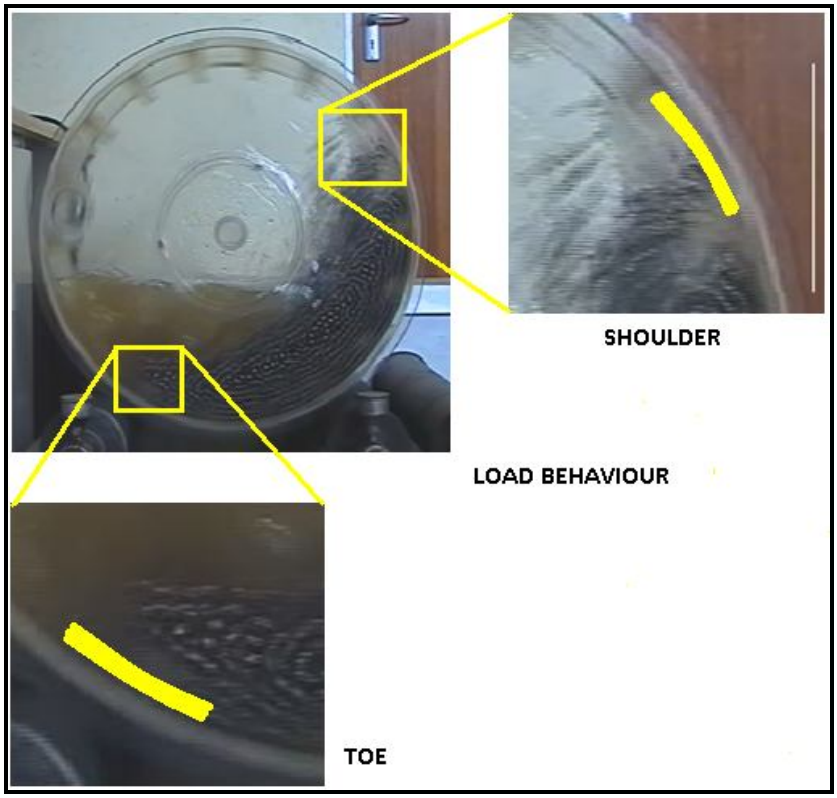

Figure 4.3 Approach taken in the determination of shoulder and toe of media charge

It should be emphasised that for every single frame considered, a region within which toe and shoulder of the media charge are respectively believed to lie are determined. For the toe (see inset in the lower left corner of Figure 4.3), this region goes from the edge of the last ball (left tip of the arc in the inset) to the point where balls are definitely in contact with the mill wall. The region defining the shoulder, on the other hand, goes from the en-masse charge to the last ball that leaves the mill wall starting its free flight motion. The centres of the two yellow curves in the zoomed-in insets (Figure 4.3) provide the average angles of the toe and shoulder respectively.

4.3 General behaviour of the Perspex mill load

Figure 4.4 presents an example of the general behaviour of the load observed as well as key angular positions. This pictorial view of the mill load behaviour has been translated into graphics as shown in Figure 4.5. It is seen here that the pool of slurry is clearly observed only after a threshold slurry filling U lies somewhere between 1.2 and 1.3 for all the viscous mixtures used. The increment in slurry filling was not refined enough to enable the detection of this crucial moment.

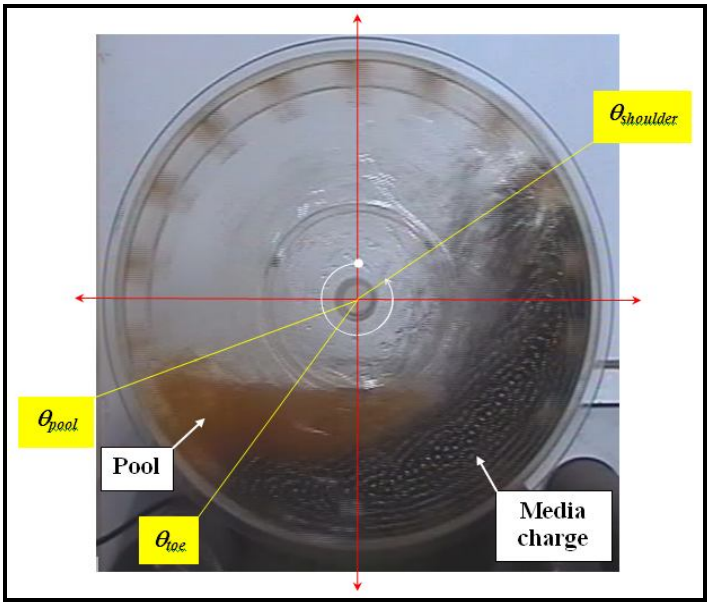

Figure 4.4 Instantaneous frame showing load behaviour and its key positions

The shoulder of the media charge varied little with the presence of slurry regardless of the level of viscosity. The toe on the contrary is initially constant, and then consistently increases right around the birth of the pool before settling at a higher angle. For all the levels of viscosity tested, the media toe angle experienced a gradual increase of no more than 20°.

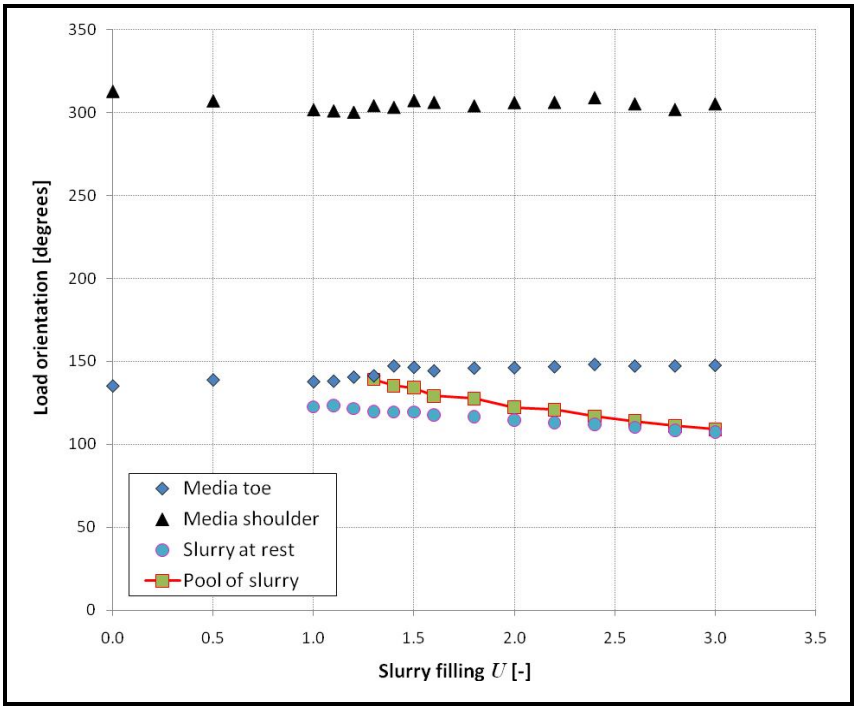

Figure 4.5 Media charge and slurry orientations in the mill at 60 mPa.s viscosity

For each slurry filling, the position of the free surface of the slurry at rest was as well measured (Figure 4.5) with the load submerged in the slurry. The pool angle decreased (i.e. the pool level increases) with slurry filling but stays between media toe and slurry-at-rest angles. This is justified by the fact that some of the slurry is dragged upwards in the rising load while the remaining defines the pool.

4.4 Data analysis methodology

The methodology adopted for model building is present below. A model describing the relationship between slurry filling and pool angle for a given viscosity is later produced.

4.4.1 Estimation of parameters

Parameter estimation generally involves nonlinear regression. Basically, the technique aims to find the best combination of fitting parameters of a model that will minimise the square of the weighted differences between the experimental values y_i and the predicted ones y_{mdl}. In other words, nonlinear regression attempts to find values for the parameters that are most likely to be correct.

With appropriate assumptions on the scatter of the data around the searched curve, such an undertaking is possible. A widely used assumption is that the data scatter follows a normal (also called Gaussian) distribution. This assumption generally works well, and is used for almost all curve fitting (Motulsky and Christopoulos, 2003).

With all the above in mind, the objective function that is to be minimised through regression can be defined as follows

$$\sum_{i=1}^{N}\left(y_i - y_{mdl}\right)^2 \qquad \textbf{(4.1)}$$

where y_i is the experimental value of y measured for a given x_i (x-value)

y_{mdl} is the predicted value of y obtained using the regression equation

N is the sample size

Equation (4.1) is also known as the uniform weighting scheme or standard weighting scheme. Motulsky and Christopoulos (2003) argue that, depending on the amount of information available on the data, other weighting schemes such as weighting by observed variability, relative weighting, Poisson weighting can be considered. Microsoft® Excel Solver, KyPlot® and Matlab® Curve Fitting Toolbox constitute a non-exhaustive list of add-in tools that can be used to numerically implement a weighted regression.

The weighting scheme by observed variability and the Curve Fitting Toolbox of Matlab® were used in the estimation of parameter. This is discussed further in Section 4.6.

4.4.2 Confidence intervals of parameters

Estimating parameters of a model is one thing, but appreciating their precision is another. In order to determine the accuracy of an estimated parameter, the notion of confidence interval is introduced.

Simply put, the best-fit parameters are usually determined using experimental data. This is subject to some degree of variability owing to the physical factors affecting the laboratory environment. Now, if one decides to repeat the same experiment, it will be argued that the new best-fit parameters will be different. It becomes therefore imperative to define the best-fit parameters not as single estimate value but rather as an estimate of the confidence interval. This will allow one to take the variability inherent to the measurements into account in the regression.

Furthermore, the notion of variability is always associated with the notion of confidence level. Triola (2001) advocates the use of a 95 % confidence level as "it provides a good balance between precision (as reflected in the width of the confidence interval) and reliability (as expressed by the confidence level)". The adoption of this confidence level signifies that we will be wrong on the model once in twenty predictions.

Motulsky and Christopoulos (2003) proposed the use of the best-fit curve and a lower and upper boundary curves and define what they call the confidence band. They interpreted the confidence band as the region within which one can be 95 % sure (level of statistical confidence) that the true best-fit curve (which can only be known if an infinite number of data points were collected) can be found. Another way of looking at it is to say that the confidence band has 95 % chance of containing the true best-fit curve.

The plotting capabilities of the Curve Fitting Toolbox of Matlab® have been used. The best-fit curve is plotted alongside with the 95 % confidence band. In doing so, one is able to tell how well we know the curve produced from experimental

data. The variability of the best-fit parameters is also assessed; this is helpful when making sense of the fitting parameters found.

4.5 Media charge position

The description of the media charge position entails the determination of its shoulder and toe angles.

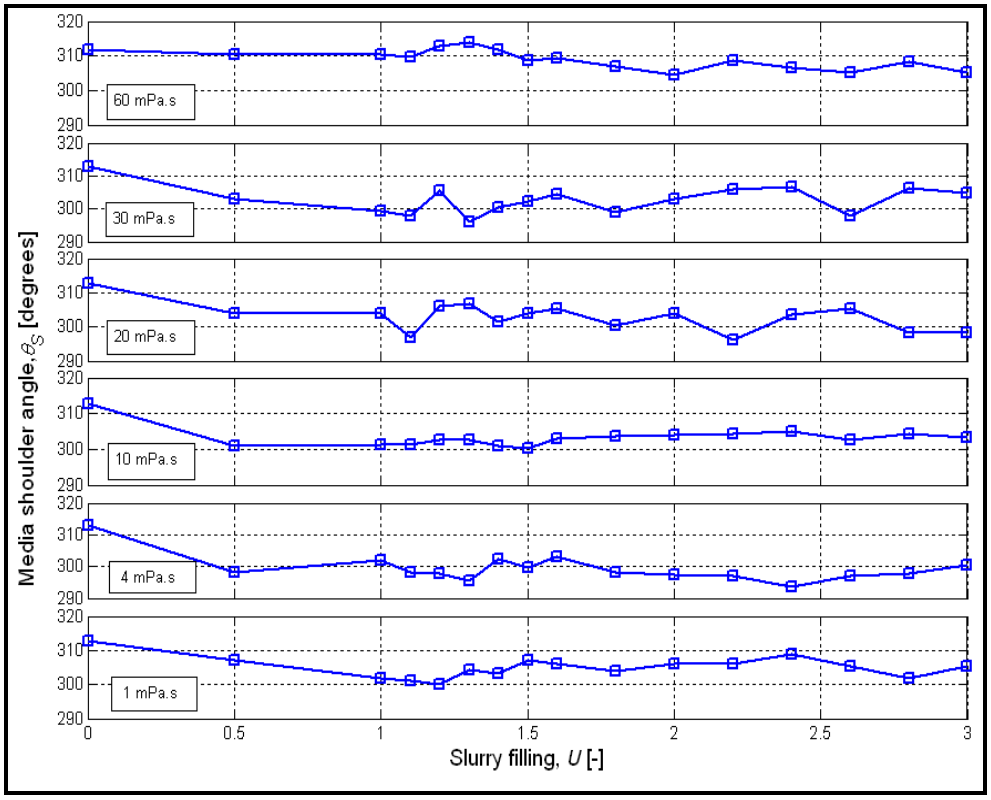

Figure 4.6 Media shoulder position as a function of slurry filling

As far as media shoulder is concerned, Figure 4.6 shows that as slurry filling increases from 0 to 3.0, the shoulder of the media charge varies within $\pm$ 6° angle. Other than that, the shoulder angle decreases by about 10 degrees as U goes from 0 to 1 except for a viscosity of 60 mPa.s.

By contrast, the toe of the media charge indicates something different. With reference to Figure 4.7, one would argue that, to a large extent, the general pattern of the different curves is about similar to a positive step function.

Indeed, an increase of approximately 20° is observed when slurry filling is varied from 0 to 3.0. Also observed is a steady increase in the media toe angle about the moment a small pool slowly appears. This is graphically supported by Figure 4.5 in which the pool was clearly measured around the rising edge of the step function. Again, this shape is consistently the same irrespective of the level of viscosity investigated in this work. In other words, a lower value is recorded for an under-filled media charge. Then a noticeable ramp appears for $1.0 < U < 1.5$, and later on, the position stabilises at a higher angle.

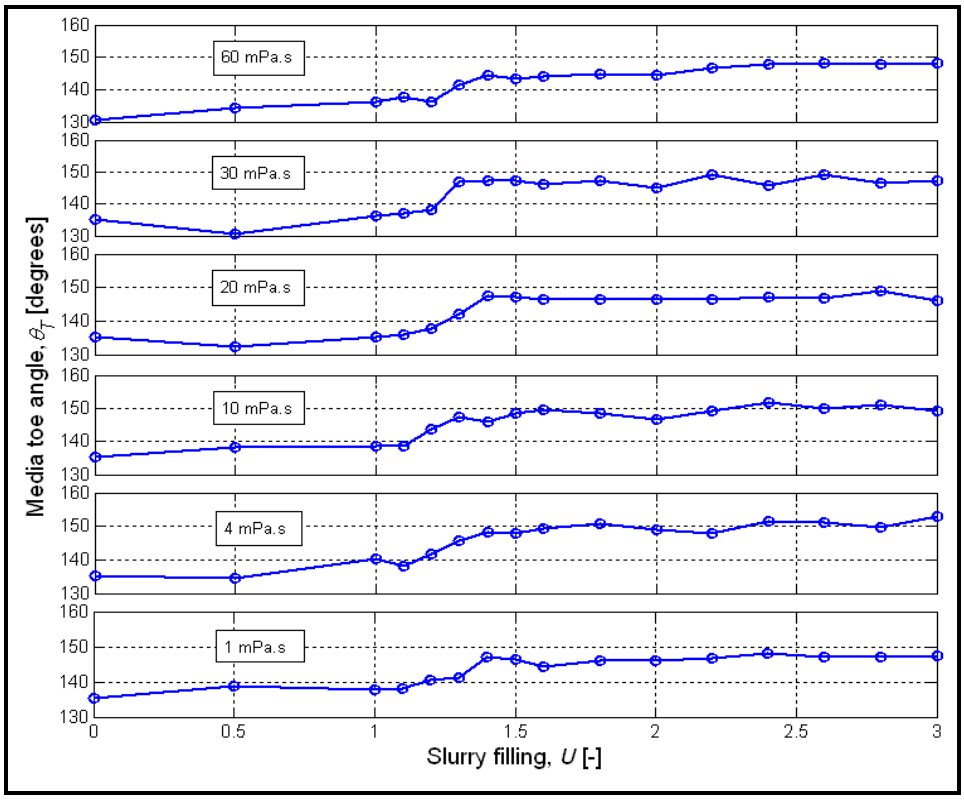

Figure 4.7 Media toe position as a function of slurry filling

It is not clear what caused this behaviour; however, it appears that the load accommodated the increasing volume of glycerol solution within the media charge. Then, the excess solution coming in afterwards that cannot find any more room in the charge drains down to form a volume of fluid above the toe of the media charge known as the pool. The expansion of the load is compensated by an increase in the media toe angle which stabilises at a higher angle. The step increase observed from U = 1.0 to U = 1.3 translates into the contraction of the

angle subtending the arc of the mill shell in contact with the media charge. The media charge bunches up and forces the concentric layers of grinding media within the charge to pile up towards the centre of the mill.

4.6 Effects of slurry filling on pool level

Visual inspection and model sense-making have allowed us to identify a good model in the description of the relationship between angular position of the pool θ_{pool} and slurry filling U. A power function was found to be a good candidate for the description of our laboratory results. The model is presented below:

$$\theta_{pool} = C_0 . U^k \qquad \textbf{(4.2)}$$

where C_0 and k are fitting parameters.

Now, with the instantaneous values of the pool angle $\theta_{i,j}$ corresponding to slurry filling U_i and photographic frame j, the average pool angle $\theta_{pool,i}$ and the standard deviation σ_i were calculated. After that, the weighed sum of squared errors was set as follows:

$$SSE = \sum_{i=1}^{N} \left(\frac{\theta_{pool,i} - \theta_{mdl}}{\sigma_i} \right)^2 \qquad \textbf{(4.3)}$$

where $\theta_{pool,i}$ is the average pool angle measured for a slurry filling U_i

θ_{mdl} is the predicted pool angle obtained using Equation (4.2)

σ_i is the standard deviation on $\theta_{pool,i}$

N is the number of slurry fillings considered in the pool model, that is, 12.

Using the Curve Fitting Toolbox provided by Matlab® version 7.1, a parameter search on Equation (4.2) was done. The best fit was obtained with a minimum for Equation (4.3) being the objective function. Figure 4.8 illustrates the pool model as fitted to the data for solution of 30 mPa.s viscosity. As would be expected, the angle of the pool decreases with an increase in slurry volume for a constant ball filling. Figure 4.8 also reports the corresponding confidence band at 95 %

confidence level. The confidence band was generated by the Curve Fitting Toolbox mentioned earlier.

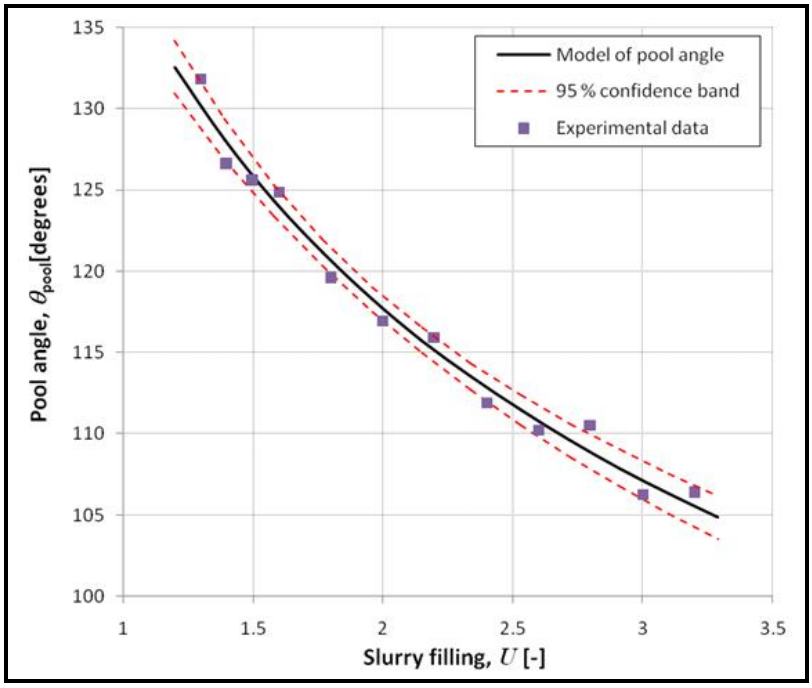

Figure 4.8 Angular position of the pool of slurry for a 30 mPa.s viscosity

Following comments by Triola (2001), one can conclude that if this test were to be repeated 20 times, at least 19 out of 20 models (i.e. 95 %) would be expected to fall within the confidence band. This implies that the confidence band represents the boundaries that are most likely to contain the 'true' curve. It therefore becomes clear that from the confidence band, a good idea of the quality of the test is obtained. In this instance, the experimental data enabled us to obtain a model accurate within $\pm$ 2° at 95 % confidence level.

Table 4.1 Confidence Intervals C.I. and Coefficients of determination

Viscosity [mPa.s]	C values			k values			
	$\overline{C}_0$	95% C.I.		$\overline{k}$	95% C.I.		R^2
1	*149.6*	147.5	151.5	*-0.2853*	-0.3039	-0.2662	*0.9988*
4	*138.2*	136.1	140.4	*-0.2324*	-0.2517	-0.2109	*0.9934*
10	*135.9*	134.9	136.8	*-0.2175*	-0.2282	-0.2068	*0.9899*
20	*139.9*	138.2	140.9	*-0.2696*	-0.2891	-0.2501	*0.9952*
30	*141.0*	139.6	142.4	*-0.2687*	-0.2843	-0.2542	*0.9836*
60	*147.8*	147.0	148.6	*-0.2992*	-0.3068	-0.2915	*0.9931*

Table 4.1 lists the values of the two fitting parameters as per Equation (4.2) as well as the goodness of the fit (R^2). The confidence intervals at 95 % confidence level are also reported.

In general, the confidence intervals give a measure of the adequacy of the model. Regarding C_0-values, their variability is seen to be within $\pm$ 2° at 95 % confidence level. This represents a relative error of approximately $\pm$ 1.5 % at 95 % confidence level which is very good for a preliminary work. As for k-values, their variability is $\pm$ 0.02 at 95 % confidence level or $\pm$ 9.5 % error.

It is to be emphasised that the confidence interval used in this work is the Confidence Interval (C.I.) on the mean (i.e. the line) that was calculated using the Curve Fitting Toolbox of Matlab®. This type of confidence interval is referred to as the 'Prediction Bounds for the fitted curve' in Matlab®. It is calculated using the coefficients produced by the fit, the confidence level, the inverse of the Student's cumulative distribution function and the diagonal elements from the estimated covariance matrix of the coefficient estimates. Details of the calculation of the confidence interval can be reviewed in Mathworks (2011) online documentation library.

The same Matlab® Add-in tool was used to calculate the standard errors of the regression termed Root Mean Squared Errors (RMSE, in degrees). They are presented in Table 4.2 along with the Sum of Squares of Errors (SSE).

Table 4.2 Standard errors of the regressions

Viscosity [mPa.s]	RMSE [°]	SSE
1	0.3740	1.259
4	0.8322	6.926
10	1.0640	11.310
20	0.6156	3.410
30	1.1520	13.270
60	0.9381	7.920

Table 4.2 also shows that the random component in the data reflected during the fitting exercise does not exceed 1.2° (RMSE) which is small compared to a full revolution (that is, 360°). And owing to the experimental setup and the adopted analysis of the photographs, Equation 4.2 can be considered entirely adequate.

4.7 Effects of slurry viscosity on load behaviour

The photographic work was intended to study the orientation of the load. The analysis of the effect of slurry viscosity is limited to a visual analysis of the general picture of the load. That is to say, an attempt has been made to see whether there would be some change in the subjective level of cataracting and in the position of the media charge with viscosity.

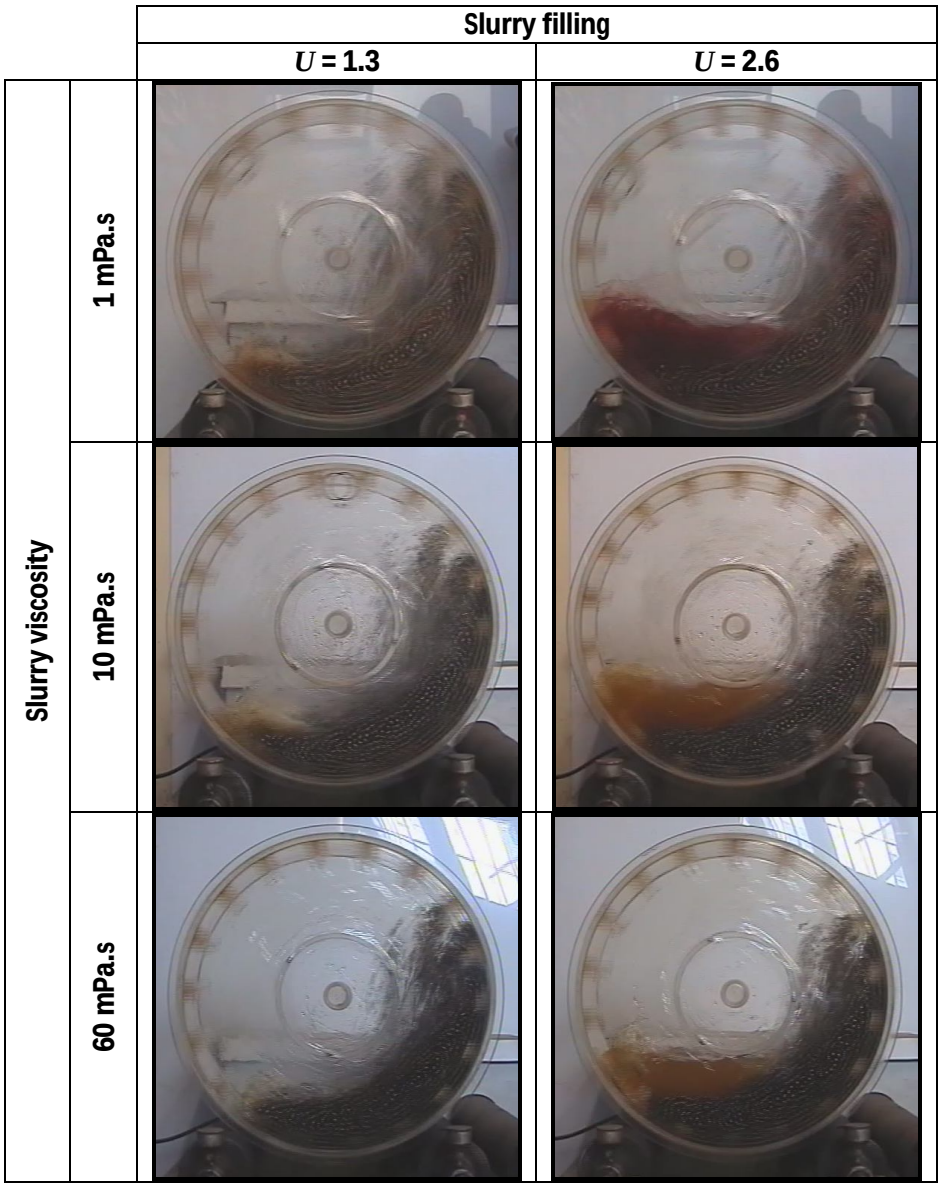

Figure 4.9 Change in load orientation with viscosity and filling degree of slurry

A visual comparison of load orientation for changes in viscosity and degree of filling of the solution used is presented in Figure 4.9. Apart from the substantial

change in pool level with slurry filling, the shape of the media charge position remains almost unchanged throughout the test. More cataracting is consistently observed for low viscosity as compared to higher viscosity. And for the same filling degree of slurry, viscosity appears to have a limited effect on the position of the pool. Within the range studied, the in-mill dynamics seems not to be affected by the viscosity of the liquid.

Table 4.1 also gives some idea about the dependence of the model upon slurry viscosity. In general, parameters C_0 and k are both insensitive to viscosity.

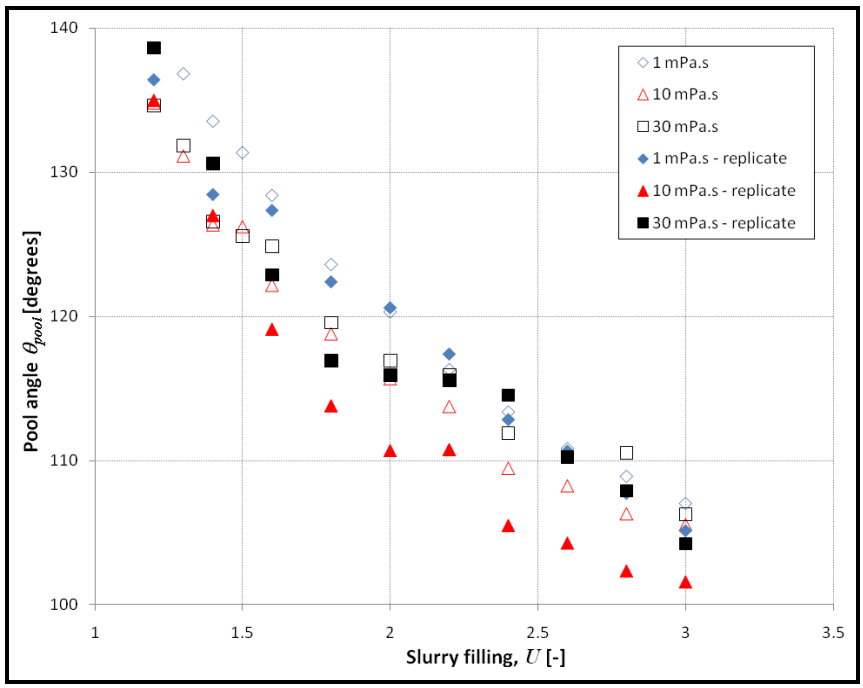

Figure 4.10 Pool position curves – Replicates

To confirm this observation, it was decided to repeat some of the tests; namely, 1, 10, and 30 mPa.s in viscosity. The results of these replicates are reported in Figure 4.10 with filled markers. Unfilled data points, on the contrary, represent results of the original tests. A look at these graphs indicates that discrepancies stay below approximately $\pm$ 10° which represent a relative error of 2.78 % with respect to one full revolution of the mill. In addition, no systematic variation of θ_{pool} is observed. It is concluded, within the accuracy of the experiment, that the

pool angle remains constant at a given slurry filling over the range of viscosity investigated.

4.8 Discussion

The pool of slurry contributes significantly to governing the transport of material in the mill (Hogg and Rogovin, 1982; Songfack and Rajamani, 1995). In this chapter, the general behaviour of the mill has been explored with a specific focus on slurry pooling. It was found that the volume of the pool increases consistently with the volume of slurry present in the mill. In addition, media charge orientation is not substantially affected by the presence of slurry even though a change of 20° has been recorded on the toe of the media charge. Simulations by Cleary *et al.* (2006) and experimental works by Latchireddi and Morrell (2003) show similar trends. And Morrell (1993) reported that indeed load profile is mainly affected by mill speed and ball filling.

To talk about the mill load, three key positions were analysed separately; namely, the media shoulder, the media charge toe and the slurry toe.

For a constant viscosity, the media shoulder angle was found to vary by no more than $\pm$ 6° at 95 % confidence level. On top of that, no compelling evidence was found that links the media shoulder to slurry viscosity or slurry filling. More cataracting is consistently observed for low viscosities as compared to higher ones. This agrees with findings by Inoue and Okaya (1995). Based on numerical simulations, they were able to show that for a twenty-fold increase in slurry viscosity, the load behaviour shifts from cataracting to cascading mode.

As for the toe of the media charge, the general pattern shows that the toe angle is constant for low level of slurry filling, i.e. U < 1.1. The toe angle then steadily increases for slurry fillings roughly between 1.1 – 1.4 and stabilises afterwards at an angle 20° greater than before. To explain this phenomenon, the results of a group of researchers will be cited.

To this end, Songfack and Rajamani (1995) simulated the radial velocity profile of slurry of an overflow mill. In their description, they reported that the velocity of the slurry approaches the mill rotational speed near the shell. But, as one moves farther away from the shell towards the centre of the mill, the slurry velocity decreases. It is understood that for a low slurry volume the velocity field shrinks and becomes thinner. As a result, a small amount of slurry flows in the direction of rotation of the mill. This causes only few layers to undergo the effect of the mill shell; consequently, the toe of the media charge rises which translates into a decrease in the media toe angle. For a rise in slurry volume, the number of layers is much larger. And intuitively, the media toe will increase due to the presence of more slurry influenced by the mill rotation. Of course, gravity will limit the indefinite rise of the toe around an equilibrium value greater than previously. We also think that the stickiness of balls brought by more liquid in the load combined with the velocity profile translates into the way media toe position changes with slurry volume (see Figure 4.7). The coating of balls makes them less free to move and more subject to mill rotation. Nonetheless, the same coating provides some lubrication which prevents the media toe from going any higher. It is possible that all these complex phenomena contribute towards positioning the media toe as observed in this preliminary work.

On the effects of volume and viscosity of slurry, the pool of slurry has been seen not to appear right after a filling equal to unity. The retardation in the appearance of the pool can be attributed to the expansion of the load. That is, the porosity of the bed in a dynamic environment seems to have exceeded 0.4, the value generally assumed in steady state conditions (Austin *et al.*, 1984).

In the discussion of the slurry pool model, it is argued that the proposed power function correlated the experimental results very well. It offers discrepancies not exceeding $\pm$ 2° at 95 % confidence level. Besides, if one assumes the possibility of gradually overfilling the mill with slurry, the pool angle would decrease and tend to zero. Mathematically, this statement would be written as follows

$$\lim_{U \to +\infty} \theta_{pool} = \lim_{U \to +\infty} C_0 . U^k$$

And because $k < 0$ (see Table 4.1), it follows that $\lim_{U \to +\infty} U^k = 0$. This reduces the pool angle to zero, as expected. The above demonstrates to some extent the ability of the model to make sense of extreme conditions.

On the other hand, the model predicts that the pool angle will become infinitely large if there is no slurry in the mill. In this particular case, this simply signifies that the slurry angle cannot even be defined in this case.

Subsequent chapters are used to study load behaviour on a pilot level. A natural mineral ore under close to industrial conditions will be used. The slurry and media charge will be measured using separate sensors. The power as affected by pool level will also be measured and modelled. In so doing, the contribution of the pool will be established. Then, based on this information, real slurry of known composition will be ground to relate milling kinetics to the general behaviour of the load. The pool volume did not cause any noticeable change in load behaviour pattern that could be used to anticipate about the implications of the pool on milling.

4.9 Conclusion

The main objective of the preliminary work was to explore load behaviour in a tumbling mill in order to determine its relation to volume and viscosity of slurry.

Within the scope of study, attempts to characterise the effect of viscosity on the load have shown that media charge orientation remains unaffected. The angles of the media toe and shoulder were found to lie respectively between 130 – 152° and 297 – 315°. The variability of the shoulder was randomly distributed about the average whereas the toe was initially low, and steadily increases to stabilise 20° higher in a quite similar fashion to a positive step function.

Through modelling, slurry pooling has been shown to be uninfluenced by the viscosity of slurry. The pool angle decreased with filling degree of slurry following a two-parameter power model (Equation 4.2) irrespective of the level of viscosity. Variations remained below $\pm$ 10° which represent 2.78 % of one full revolution of the mill. Nonetheless, videos showed more cataracting of the load when viscosity was increased.

A model relating pool angle to slurry volume has been proposed. Statistically speaking, a two-parameter power function has proved to be a good descriptor of the pool formation. The two parameters C_0 and k responded very well to fitting with their respective values of 142.1° $\pm$ 4.4° and – 0.262 $\pm$ 0.025 on the whole range of viscosities. More importantly, it was found that the pool starts to form after a threshold slurry filling situated somewhere around U = 1.2 – 1.3 is reached. This simply means that the proposed pool model (Equation 4.2) can only apply to slurry filling U > 1.2.

It appears that the delay in the appearance of the pool could be due to the load expansion that makes the porosity of the dynamic media charge exceed the value of 40 % bed porosity at rest. It is also possible that the amount of viscous slurry stuck to the wall and liners of the mill could be significant and would contribute to this late emergence of the pool.

The final point to make here is that from Table 4.1 and Figure 4.10, it has been shown that the model of the pool angle is independent of viscosity. However, it should be noted that glycerol was used to mimic slurry; as such, it may not reflect it well. Unlike glycerol, industrial slurries are non-Newtonian fluids, and the friction between balls may be substantially increased by the presence of slurry particles. That is why a real ore was used to validate these findings.

Chapter 5 Effects of slurry filling and mill speed on load behaviour[3]

Abstract

Slurry pool is known to lower the power drawn to the mill. An attempt to ascertain the observation by relating media charge and pool positions to mill power for a wide range of speeds and slurry fillings is undertaken.

In line with this, a PGM ore (-850 microns) was used to carry out several tests. The slurry was prepared at 65 % solids concentration by mass. The Wits pilot mill (552 × 400 mm), filled with 10 mm balls, was first used for testing. Ball filling was kept constant at J = 20 % while mill speed ϕ was varied between 24.6 and 106.1 % of critical. Then, in the second series of tests, slurry was added to the media charge. Slurry filling U was varied from 0 to 3.0. Using the proximity sensor and the conductivity probe mounted on the mill shell, both the motion of the media charge and slurry were measured. All the data for the load behaviour was stored on a computer via a data acquisition board. The signals were later analysed in order to determine the angular positions of the media charge and of the slurry.

The angular position of the pool was found to be well described by the pool model proposed in the previous chapter. Mill speed had no significant effect on the position of the free surface of the slurry pool. Modelling and discussions of net power data measured showed that Morrell's model could not satisfactorily explain the effect of slurry filling on net power draw for an under-filled media charge; that is, for U < 1.0. That is why an empirical model of power allowing for the slurry filling effect was proposed to deal with the inconsistencies.

Keywords: Wet milling, Load behaviour, Slurry filling, Mill speed, Slurry pooling

[3] Sections of the chapter dealing with mill power modelling using Morrell's model have been submitted for presentation and publication under the reference:
Mulenga, F.K., Moys, M.H., 2012. Effects of slurry filling and mill speed on load behaviour. The Southern African Journal of Mining and Metallurgy, Abstracts submitted for the Southern African Mineral Beneficiation and Metallurgy Conference, MINPROC 2012

5.1 Introduction

A model of the angular position of the free surface of the slurry pool as affected by slurry filling in a laboratory mill was presented in chapter 4. A transparent mill and solutions of glycerol with different viscosities were used in the test work. Beside the fact that the proposed pool model was a power function, it was found that the general load orientation was not substantially affected by viscosity.

The investigation is taken one step further by testing a Platinum ore in lieu of an artificial solution on the scale down version of a wet industrial. While taking advantage of the flexibility of the Wits pilot mill, two milling parameters were investigated: slurry filling U and mill fractional speed ϕ. A proximity sensor and a conductivity probe were simultaneously used to measure load behaviour. The net power drawn by the mill was also measured in order to better understand the contribution of the pool of slurry in ball milling.

The effects of viscosity due to changes in solids concentration in slurry (Shi and Napier-Munn, 1996) for instance or particle size distribution were not considered. The reason is that in the previous chapter, slurry viscosity was found to have no effect on the load behaviour in general and on media charge orientation in particular.

Using chapter 4 as the reference, the pool model was tested on a real ore and for different speeds. An attempt was also made to describe measured net power using four models; namely Bond (1962), Moys (1993), Morrell (1993) and the Discrete Element Method (DEM). The choice is dictated by the fact that Bond's model has been the basis for the development of the currently established empirical power models produced in the past century. Moys' model has the merit of allowing for the geometry of the lifters. Morrell, on his side, has proved his model to work with remarkable accuracy; the model has been validated using an important database of industrial mills. In addition, it has the ability to relate mill power to key positions of the load such as the position of the pool, which is impressive. The Discrete Element Method, on the other hand, offers a different

approach to power modelling altogether. And as quoted by Morrell (1993): The work on DEM by Mishra and Rajamani (1990) “should be applauded in that it represents a truly original approach to the modelling of mill power draw” even though at this point a large amount of computing time is still needed to implement it.

5.2 Empirical models of mill power draw

An overview of two models of mill power is presented below: power models by Bond (1962) and by Moys (1990). They are used together with Morrell’s model and the DEM technique discussed earlier in chapter 2.

5.2.1 Bond’s power model

The empirical formula of mill power by Bond (1962) is arguably one of the first models for mill power. Bond collated data on different mills to produce his well-known equation.

One of the forms under which Bond’s model can be found is given below:

$$P = K_1.L.D^{2.3}.(\sin\alpha_d).\rho_L.J(1-\beta_0.J).\phi.\left(1-\frac{0.1}{2^{\eta-\zeta.\phi}}\right) \qquad \textbf{(5.1)}$$

where K_1 is a constant allowing for liner design and slurry properties. It is given the value of 12.262 by Bond

ρ_L is the bulk density of the mill load [kg/m^3]

α_d is the dynamic angle of repose of the load

J is the fraction of mill volume occupied by media charge

β_0 is a parameter given a value of 0.937 by Bond

D is the diameter of the mill inside liners [m]

L is the length of the mill inside liners [m]

ϕ is mill speed as a fraction of the critical speed

η and ζ are parameters given a value of 9 and 10 respectively by Bond. These two parameters determine the position of the maximum

power. They also reflect the tendency of the mill charge to centrifuge at speeds nearing the critical speed.

Bond's model of mill power is arguably a very attractive formula because of the limited number of parameters involved. This renders the model easy to use despite some weaknesses; amongst others, slurry rheology, lifter configuration, and ball diameters are not allowed for.

The next model addresses some of these issues and is in particular well suited for the description of the effects of liner profile.

5.2.2 Moys' power model

One major problem that comes with Bond's model is its inability to clearly define the dynamic angle of repose at higher speeds. Indeed, the model has been found to work reasonably well at low speeds where the load is predominantly cascading or even to some extent cataracting. It fails to describe centrifuging loads. This situation prompted Moys (1993) to propose a semi-phenomenological model to mill power. He assumed that a reasonable model of mill power should, on the one hand, reduce to Bond's model at low speeds; and on the other hand, allow for progressive centrifuging of the charge at higher speeds.

It is therefore not surprising that Moys' model resembles Bond's with several parameters being the same. His real contribution however resides in the centrifuging fraction that he assumes draws no power but is affected by lifter design and slurry viscosity. In addition, depending on the aggressiveness of the lifters, early centrifuging can be observed: this hypothesis has been confirmed in practice with actual centrifuging starting in some cases earlier than the critical speed (King, 2001). The premature centrifuging increases the layer of centrifuged charge with speed; thereby, reducing the fraction of load effectively drawing power. That is why Moys (1993) defined the effective filling of the non-centrifuging fraction (J_{eff}) using the following equation:

$$J_{eff} = \frac{J - 4\delta_c(1-\delta_c)}{(1-2\delta_c)^2} \quad \textbf{(5.2)}$$

where δ_c is the thickness of the prematurely centrifuging layer as a fraction of the mill diameter (D). He empirically modelled it as follows:

$$\delta_c = J^{\Delta_J} \exp\left(-\frac{\phi^* - \phi_{100}}{\Delta_N}\right) \quad \textbf{(5.3)}$$

with J is the total fractional ball filling

ϕ_{100} is the speed of the mill [percent of critical speed]

Δ_J governs the strength of the dependence of δ_c on J and is a strong function of liner profile. Moys (1993) showed that lifters dramatically reduced the effect of J on δ_c.

Δ_N is a parameter that is a strong function of liner profile and slurry viscosity. Moys (1993) proposed the following empirical equation to relate the number of lifters n_L to Δ_N: $\Delta_N = 20.3 - 2.4\ln(n_L)$

ϕ^* was found to be approximately constant at a value of 136 but could vary between 134 and 138 (Moys, 1993). This parameter is virtually independent of liner design.

Moys (1993) analysed the effect of mill speed (from 10 % to 135 % of critical speed) on mill power and showed that it was a strong non-linear function of liner design, load volume and mill speed. For the model to come about, Moys assumed that the charge comprises two parts: a centrifuging layer and a non-centrifuging fraction. The non-centrifuging fraction is assumed to behave in a manner which Bond's equation adequately described, without its speed correction function. The centrifuging fraction, on the other hand, is posited to be affected by lifter design and slurry viscosity, such that it would tend to centrifuge earlier than the remainder of the charge as the mill speed increases. The relative magnitude of this fraction was modelled empirically and considered existent even at low speed; that is why, the term 'premature centrifuging' (Moys, 1993)

was coined to describe this phenomenon. Note that cataracting does not play a role in the model.

On the whole, the non-centrifuging fraction of the charge was considered to be solely responsible for the power delivered by the motor drive while the centrifuging fraction drew no power. This provided a simple but effective way of incorporating the effect of changes in speed, liner design and viscosity on power draw, by relating them to the thickness of the prematurely centrifuging layer. Thus, as the centrifuging layer increased the tendency to reduce the mill power draw would be accentuated. It becomes evident that the power drawn by the non-centrifuging charge is basically the mill power draw.

Ultimately, the power of a ball mill as proposed by Moys (1993) was given by:

$$P = K_2.L.D_{eff}^{2.3}\left(\sin\alpha_d\right).\rho_L J_{eff}\left(1-\beta_0.J_{eff}\right).N_{eff} \qquad \textbf{(5.4)}$$

where L is the mill length

D_{eff} is the effective diameter due to the centrifuged layer, given by

$$D_{eff} = \left(1-2\delta_c\right).D$$

α_d is the dynamic angle of repose of the load. An average value of 37° was found from the conductivity probe data from the first experimental program during the variation of the load mass. There was no indication that α_d was a function of load volume.

ρ_L is the bulk density of the load [kg/m^3]. The basic definition of load density can be written as follows:

$$\rho_L = \frac{M_L}{V_{mill}.J}$$ with M_L load mass [kg] and V_{mill} mill volume [m^3]

N_{eff} is the effective speed (percent of critical speed) calculated from:

$$N_{eff} = \sqrt{\frac{D_{eff}}{D}}.\phi$$ (van Nierop and Moys, 2001)

β_0 is a Bond model parameter determining at which load volume maximum power occurs.

K_2 is a constant that is a function of liner design and slurry properties.

In summary, Moys' model (Equation 5.4) is in substance similar to Bond's (Equation 5.1). The fundamental difference is that Moys empirically modelled the effects of lifters and slurry properties using a semi-phenomenological description of load behaviour. However, Equation 5.4 suffers from a lack of precise measurements of the actual behaviour of the load in the mill and so, remains essentially empirical (van Nierop and Moys, 2001). On top of that, Morrell (1993) pointed out that Moys' model has not yet been validated against industrial data.

5.3 Raw data manipulation

5.3.1 Signals collected from the Wits pilot mill

From the Wits pilot mill, four signals were collected: marker signal, torque signal, proximity probe signal, and conductivity probe signal. Waveview® was used as the system for data acquisition of the above signals. The software supplied the data in a text file format that was then exported to Microsoft Excel. In this format, the data came as a 10001-by-5 matrix containing the sampling times and all four signals.

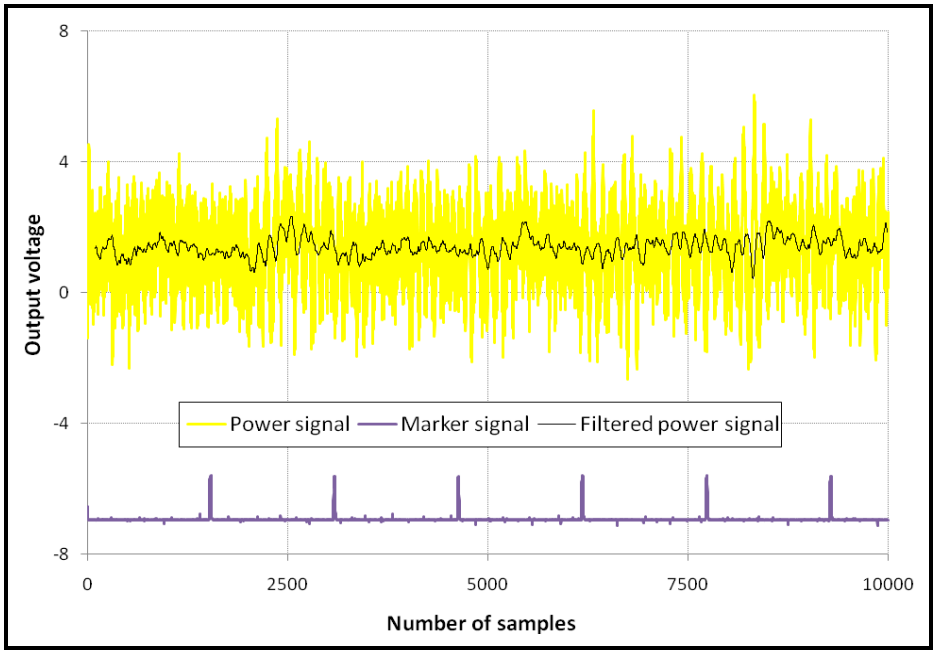

Figure 5.1 Typical outputs recorded with Waveview®

The marker signal was used to identify the beginning and the end of a full revolution. This way, the speed of the mill and a clear zero reference were accurately determined. Figure 5.1 shows an example of the marker and mill torque signals for 5 revolutions of the mill. Note the level of noise typical of the aggressive milling environment; the moving average technique was used to filter the signal and extract the necessary information for the determination of the net power. The filtered torque signal is graphed alongside side its corresponding raw power data.

The next step was to sort the data into conductivity probe signal, proximity sensor signal, and mill power signal per revolution. Signals were rescaled and plotted from 0 to 360 degrees rotational angle. In doing so, successive revolutions could be compared on the same set of axes to assess their reproducibility; Figure 5.2 gives a typical example of the proximity signals.

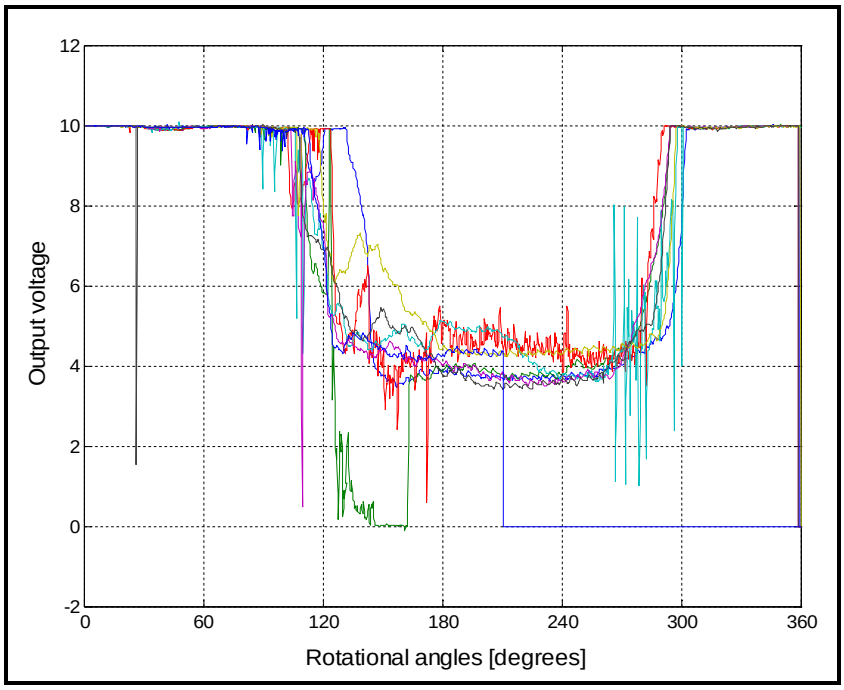

Figure 5.2 Example of output produced by the **MillSignals.m** script (see Appendix A.2.2)

The last thing left to do was the selection of useful signals and the manual determination of key positions, i.e. toe and shoulder for the media charge and pool level. This is discussed in the next section.

5.3.2 Determination of the load behaviour

Concordant works have demonstrated that the full characterisation of the load behaviour in wet milling implies accurate measurement of the relative positions of the media charge and slurry. The 12 o'clock position as shown in Figure 5.3 was chosen as the reference in the definition of the abovementioned key positions of the mill load.

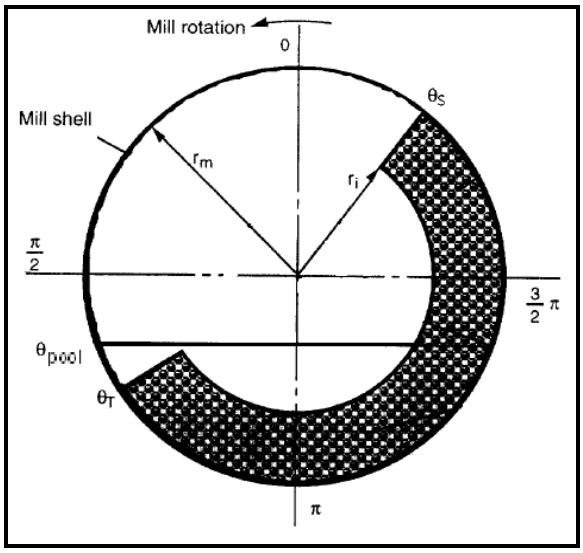

Figure 5.3 Key positions of the load in the Wits pilot mill: Angular locations of the pool of slurry θ_{pool}, the toe θ_T and shoulder θ_s of the media charge (redrawn after Shi and Napier-Munn, 1999)

Two graphs (Figures 5.4 and 5.5) giving insight into the signals collected from the proximity probe for five revolutions are presented.

As far as the proximity probe is concerned, an example of the output for 5 consecutive revolutions of the mill is shown in Figure 5.4. One can clearly see that as the probe does not sense the presence of the load, the voltage output remains at about 10 Volts. But, once the sensor enters the active load (at 120° approximately), there is a sudden drop in voltage corresponding to the toe of the media charge. The signal stabilises around 3 – 5 Volts, then later returns to 10 Volts around 300°. This point is identified as the shoulder of the media charge.

Note that before the start of the media charge toe, spikes appear every now and again, indicative of cataracting balls landing on the mill shell. In addition, the toe proves to be more difficult to define unambiguously owing to the level of noise in the region. The shoulder, on the other hand, is more reproducible and quite straightforward to determine.

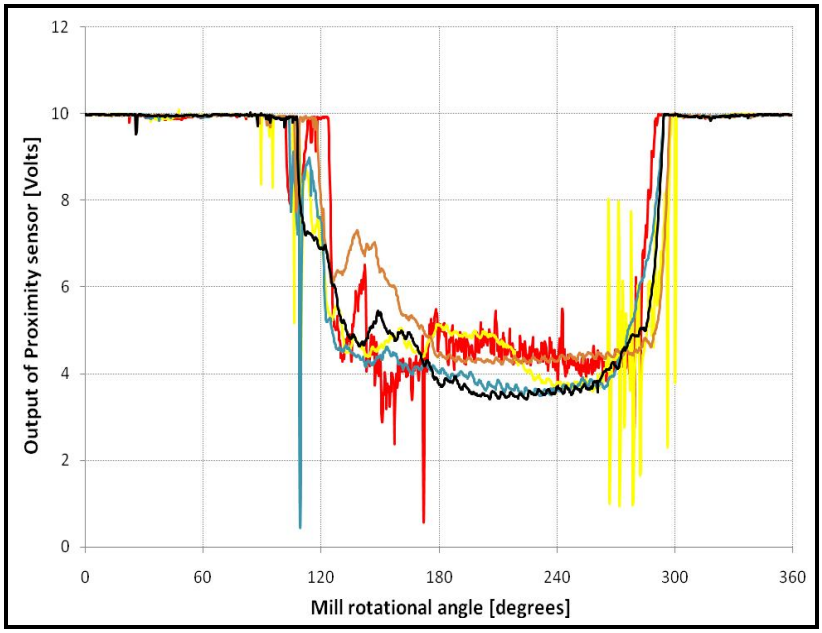

Figure 5.4 Example of proximity probe signals. Conditions: 65 % N_c and U = 2.4

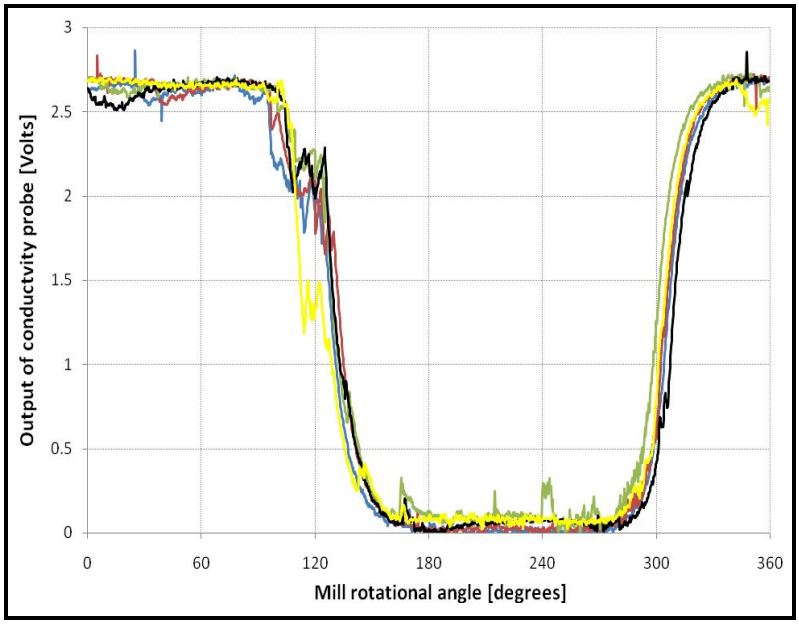

Figure 5.5 Example of conductivity probe signals. Conditions: 65 % N_c and U = 2.4

As for the conductivity probe, Figure 5.5 shows the typical signal output for the same 5 revolutions as above. This signal was simultaneously measured with the proximity sensor one. The reproducibility of the signals compares well to that found with the proximity sensor. However, the slurry toe (that is, the position of the free horizontal surface of the pool) is much easier to locate.

In order to get a clear picture of the load behaviour, the two signals have been plotted on the same set of axes as shown in Figure 5.6. This way, it was possible to identify the presence of the pool of slurry as well as the relative positions of the media charge and the slurry.

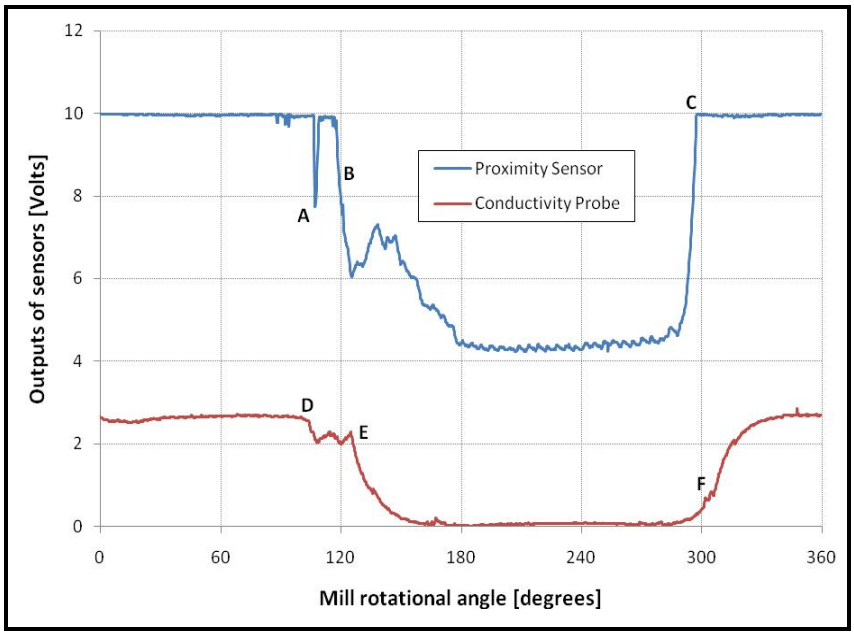

Figure 5.6 Comprehensive interpretation of load orientation.
Operating conditions: 65 % N_c and U = 2.4

Regarding the proximity sensor, one can see that as the mill rotates, the signal is at 10 Volts telling us that the sensor is still outside the active load. At about 100° (Point A in Figure 5.6), a brief negative spike appears, witness of some cataracting balls landing on the mill shell. Afterwards, the signal goes back to 10 Volts; it then drops noticeably, signalling the presence of the media charge. This is where the toe (Point B) of the media charge lies: Between 120° and 180° where the random behaviour of the proximity signals is observed. The signal

then settles around 4 Volts signalling a locked-in charge on the proximity probe. Later on, it shoots up indicating that the sensor is leaving the media charge. Point C can be positively identified as the shoulder of the media charge.

Now, as far as the conductivity probe is concerned, not only does it give as good evidence of the position of the slurry, but it also reveals some interaction between media charge and slurry. To elaborate, point D is an indication of the beginning of the pool of slurry whereas point E, which is a further increase in conductivity, corresponds to a definite presence of grinding media. In a way, this is indicative of a very rough position of the media charge toe. Towards 300° rotational angle, the signal starts to increase in an exponential fashion due to the delay in slurry to drain away from the probe. That is the reason why the slurry shoulder is located at point F where 10 % of the maximum voltage (approximately 2.65 Volts) is reached, that is, 0.265 Volts in this case.

The last comment is that the magnitude of the interval DE is a reflection of the level of slurry present in the mill. A more accurate estimate of the pool volume is found by working out the difference in angular positions between the toe of the media charge (that is, point B) and the location of the free surface of the slurry pool (that is, point D).

Table 5.1 Toe and shoulder positions of the 'dry mill' and their standard deviations

Mill Speed [% of critical]	Toe position [degrees]		Shoulder position [degrees]	
	Toe angle	σ_T	Shoulder angle	σ_S
24.6	137.9	4.33	261.8	4.49
35.5	142.1	3.05	268.8	6.05
46.9	147.0	2.57	269.4	4.03
57.2	148.0	2.81	283.4	5.44
62.7	146.8	3.22	289.6	5.50
67.4	140.1	5.64	297.9	5.91
71.9	120.8	7.76	316.7	15.08
77.5	98.1	12.33	324.5	12.36
89.9	31.8	13.40	346.7	11.51
106.1	0		360	

Recall that experiments were carried out with a dry mill first, then later with the wet mill. Table 5.1 shows angular positions of the toe and shoulder of the media

charge for the 'dry mill'. In this case, only the proximity probe provided the useful information.

Table 5.2 Angular positions of the pool for the wet mill

	% N_c	65	70	75	80	85
	rpm	**37.3**	**40.5**	**43.3**	**45.9**	**48.5**
Slurry filling U [-]	**1.0**	143.0	146.9	148.9	144.2	140.3
	1.1	138.3	143.5	143.1	141.5	135.3
	1.2	131.9	136.5	134.5	136.3	134.0
	1.3	129.5	131.1	132.0	134.5	130.1
	1.4	125.2	128.2	129.9	132.0	128.1
	1.5	120.6	126.7	125.5	129.9	125.5
	1.6	117.3	122.3	124.9	126.9	122.7
	1.8	115.8	117.4	117.5	122.4	118.3
	2.0	108.9	114.7	110.8	116.7	114.9
	2.2	106.8	110.9	110.1	113.0	111.7
	2.4	104.6	107.4	105.8	111.9	105.9
	2.6	102.5	105.4	100.2	110.8	103.9
	2.8	99.0	102.7	99.3	106.2	101.8
	3.0	98.6	97.8	96.0	105.8	100.2

Similar analysis was performed for the wet mill to determine the position of the pool for the range of speeds and slurry fillings considered. Results are presented in Table 5.2 above.

5.3.3 Data analysis methodology

In the methodology adopted for model validation and comparison, the following should be emphasised: First, the dry mill was studied in terms of load orientation; then net mill power was curve-fitted with Bond's and Moys' models. Net power was also compared to predictions given by Morrell and the DEM. Second, the wet mill was studied in the same way, but this time the pool was compared against the pool model proposed in chapter 4. Net power draw measured under different conditions was then studied using Morrell's power model (Equation 2.18). An empirical model was also proposed and assessed based on the work by Moys and Smit (1998).

To do all this, visual inspection was used extensively throughout the modelling exercise. Nonetheless, if large discrepancies were found, some parameters were adjusted following their definition in the literature to force a match.

Where the estimation of parameters was necessary, nonlinear regression was used. And in that case, a simple sum of squared deviations between measured and predicted data was used as the objective function:

$$\sum_{i=1}^{N}\left(\frac{y_i - y_{mdl}}{\sigma_i}\right)^2 \qquad \textbf{(5.5)}$$

where y_i is the experimental value of y measured for a given x_i (x-value)

y_{mdl} is the predicted value of y obtained using the regression equation

σ_i is the standard deviation calculated on the N replicates for a given series of measurements corresponding to a given value of x_i

N is the sample size

5.4 Effects of mill speed on load orientation

5.4.1 Variation of the toe and shoulder positions

On average, the load behaviour was measured for 5 revolutions. For each revolution, the toe and shoulder angles were determined; their average angles and the margin of error were then calculated.

The margin of error E_m, also called the maximum error of the estimate (Triola, 2001), was used to obtain the confidence interval. For a critical value $z_{\alpha/2}$, it is given by

$$E_m = z_{\alpha/2}.\frac{\sigma}{\sqrt{N}} \qquad \textbf{(5.6)}$$

where $z_{\alpha/2} = 1.96$ as found in Statistics tables for the most commonly used 95 % confidence level

σ is the standard deviation for the N values of the toe or shoulder positions collected for the N revolutions considered in the series of test.

A careful look at Figure 5.7 reveals that the two solid lines, representing the models of the toe and shoulder positions respectively, cross all the error bars. This is an indication that the fitted curves stay within the margin of error associated with each measurement of the toe and shoulder.

Note that the two curves have a discontinuity at approximately 90 % of critical speed suggesting the beginning of centrifuging.

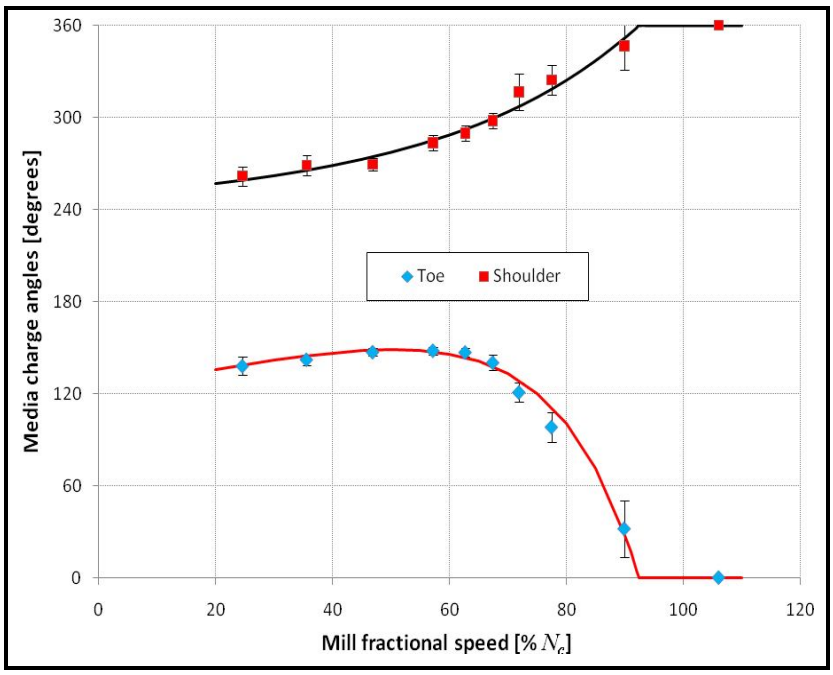

Figure 5.7 Variations of the toe and shoulder positions of the media charge with the percent fractional speed of the mill

The data points were curve fitted using Equations (2.13) and (2.14) with A, B, E, and ϕ_c as fitting parameters. The optimised values found were compared to those in Equations (2.19) and (2.20) and are given in Table 5.3.

Table 5.3 Fitted parameters for the model of load behaviour (Equations 2.13 and 2.14)

Parameter	Morrell's value	Fitted value
A [degrees]	156.54	123.09 + 69.63 ϕ
B	19.42	6.65
E	0.3386 + 0.1041 ϕ	0.5855 – 0.1597 ϕ
F	1.54 – 2.5673 ϕ	1.54 – 2.5673 ϕ
ϕ_c	ϕ for ϕ > 1.1074 1.1074 for $\phi \leq$ 1.1074	ϕ for ϕ > 0.9243 0.9243 for $\phi \leq$ 0.9243

In the fitting process, fixing F did not affect the quality of the fit in any way. Parameter ϕ_c, which defines the actual critical speed, is different from the theoretically calculated one. According to Morrell (1993), his experimental tests resulted in ϕ_c = 110.74 % of critical. In the present case, centrifuging rather starts at a lower speed, that is, at ϕ_c = 92.43 % of critical. For some reason, a low B value (that is, B = 6.65) produces a good fit to the experimental data. Parameter A has been found to increase with mill speed and does not remain constant as proposed by Morrell. It was discovered that trying to keep it constant impacts negatively on the quality of the fit.

5.4.2 Variation of the angular position of the pool

The influence of mill speed on the position of the slurry with respect to media charge is assessed in this section. It should be noted that the position of the slurry shoulder was slightly lower than that of the media charge throughout (see Appendix A.2.2; Tables A.16 and A.18). That is why it is argued that to a large extent the two shoulders are similar, and therefore, only the angular location of the free surface of the pool was discussed.

In this regard, five slurry fillings have arbitrarily been selected to show how the pool location changes with mill speed. There is little evidence to suggest that there is a particular trend between pool angle and mill speed. However, if one ignores data points at 75 % of critical speed in Figure 5.8, especially those corresponding to high slurry fillings (i.e. U = 2.6 and 3.0), there seems to be a pattern. An increase of 5 – 7° between 65 and 80 of critical speed is present probably caused by an increased take-up of slurry by the media charge, then follows a decrease that could be the result of cataracting media. By and large, it is reasonable to assume that the pool is not affected by mill speed within the range investigated. However, variations of the order of $\pm$ 5° in magnitude were recorded.

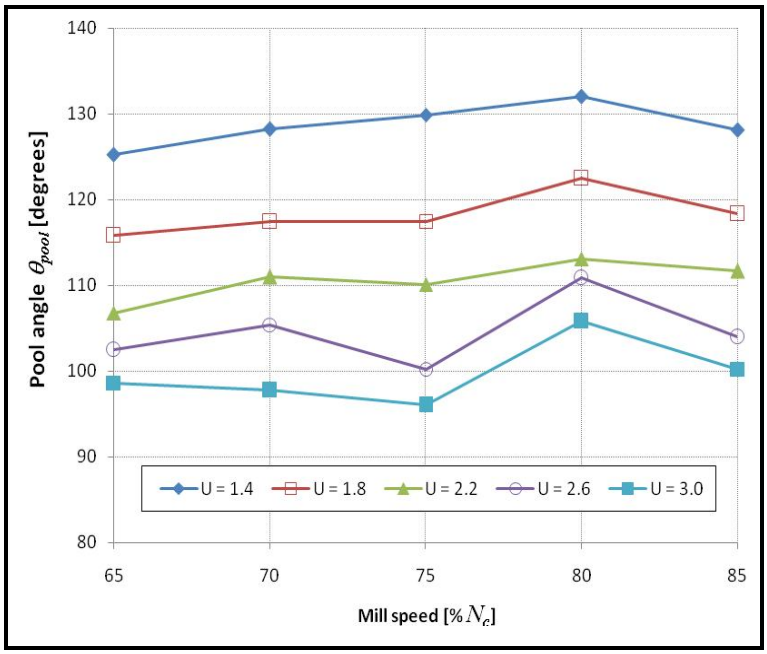

Figure 5.8 Pool angle as a function of mill speed for constant slurry filling

5.5 Effects of slurry filling on load orientation

5.5.1 Orientation of the charge of media balls

It was demonstrated in the previous chapter that the presence of slurry did not substantially affect the position of the media charge. Similar types of tests were used here with a natural ore to further validate this finding.

Figure 5.9 presents a graph of the measured shoulder and toe position for different degrees of slurry filling and for 75 % critical speed of the mill. It shows that the two positions of the media charge are not altered by slurry, further confirming the results reported in the previous chapter. Table 5.4 summarises the calculated average toe and shoulder angular positions and their standard deviations for the five mill speeds considered.

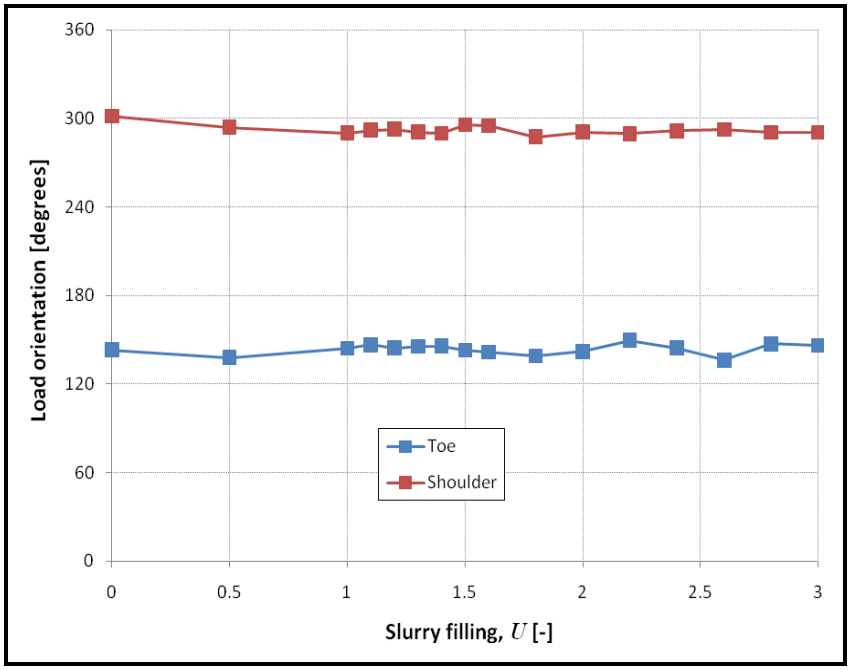

Figure 5.9 Example of variation of media charge orientation with slurry filling at 75 percents of critical speed of the mill

Table 5.4 Average angles [in degrees] and corresponding standard deviations

Mill speed % of critical	Toe position		Shoulder position	
	Average	σ_{toe}	Average	$\sigma_{shoulder}$
65	144.19	2.43	278.37	4.24
70	145.69	2.14	281.59	2.32
75	146.63	3.51	286.66	3.67
80	143.43	3.54	292.11	3.28
85	125.27	8.82	296.81	5.09

Added to this, it was observed that as mill speed increases from 65 to 75 % critical, the toe angle increases, and then decreases afterwards. The trend is consistent with the load behaviour and suggests that at speeds below 75 % critical, balls are pulled into the rising media charge. This carries on, but the lowering toe angle is due to cataracting balls landing on the mill shell. These are being detected and interpreted as the toe. This is further confirmed by the increasing standard deviation indicating the erratic behaviour of the cataracting fraction of the media charge. Conversely, the shoulder angle monotonically increases with mill speed indicating a tendency to centrifuge at higher speeds.

5.5.2 Angular position of the pool of slurry

To complete the analysis initiated in previous section, the pool model (see Equation 4.2) was validated. The intention, this time, was to validate the model with the UG2 ore and to further investigate the effects of mill speed on the pool.

The position of the pool was curve-fitted using the same methodology described in Section 4.6. Figure 5.10 is an illustration of how well the pool model worked on the pilot mill data.

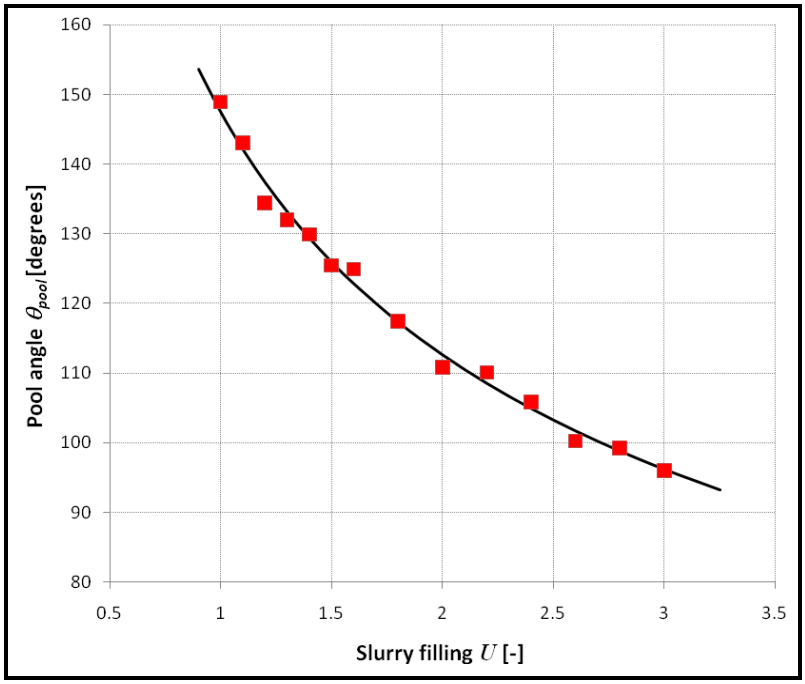

Figure 5.10 Comparison of the measured and modelled angles of the pool of slurry at 75 percents of critical speed and 65 % solids content by mass

Table 5.5 Regressed parameters obtained using the pool model (Equation 4.2)

Mill Speed [% Critical]	Model parameters		
	C_0	k	R^2
65	140.85	-0.3422	0.9889
70	145.82	-0.3515	0.9934
75	147.49	-0.3892	0.9931
80	144.92	-0.2937	0.9930
85	125.37	-0.3132	0.9942

Here once more, the two parameters C_0 and k as well as the coefficient of determination were calculated. Similarly to Table 4.1, the model was found still

to be valid even for a naturally occurring ore (Table 5.5). It can also be stated that, within the investigated speeds (i.e. 65 – 85 % critical), the pool occupies the same position. The concluding comment is that the pool model is an adequate mathematical description of slurry pooling inside the Wits pilot ball mill.

5.6 Determination of the net power drawn by the dry mill

The net power drawn by the Wits pilot mill loaded with ball media was analysed using the following models: Bond, Moys, Morrell, and the DEM. Findings are presented below.

5.6.1 Dynamic angle of repose of the media charge

The proximity and conductivity probe signals were used to determine the times of occurrence of the two dynamic events characterising the toe and shoulder positions. Equation 5.7 was then used to get an estimate of the dynamic angle of repose (Herbst *et al.*, 1990; Tano, 2005):

$$\alpha_d = \pi.(T_{toe} + T_{shoulder}).N_m - \frac{\pi}{2} \qquad \textbf{(5.7)}$$

where α_d is the dynamic angle of repose in radians

T_{toe} is the time of entry in seconds of the proximity probe when the toe is detected with the 3 o'clock position being the starting point

$T_{shoulder}$ is the exit time in seconds corresponding to the shoulder position

N_m is the mill speed in revolutions per second.

The dynamic angle can also be calculated using geometrical considerations applied to a circle. The slope defined by the chord joining the positions of the toe and shoulder is indeed the dynamic angle of repose of the load.

Lower speeds provide better estimates of the dynamic angle of repose because of the cascading nature of the load. A shift of the load behaviour towards cataracting or centrifuging makes it difficult to have a good identification of the

toe and shoulder positions. As a result, estimated angles of repose after about 80 % of the critical speed become physically meaningless (see Figure 5.11).

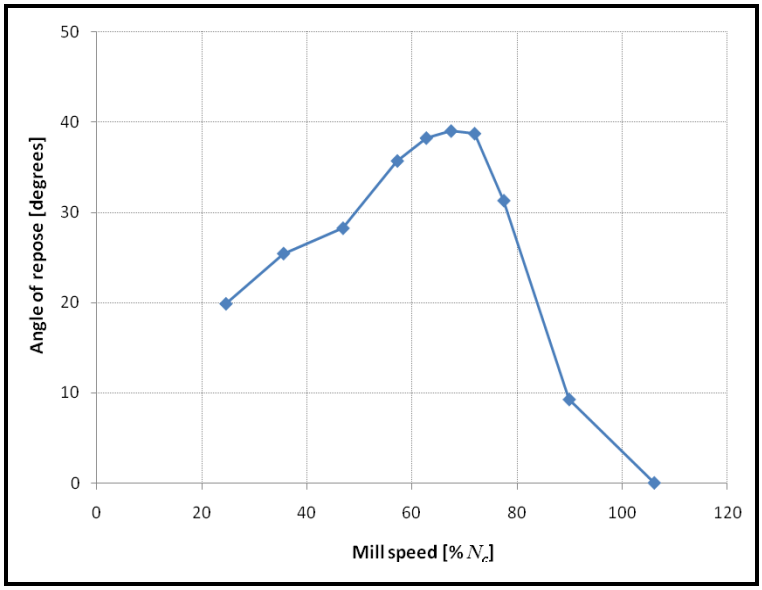

Figure 5.11 Dynamic angle of repose versus mill speed

The most important point to make is that the maximum angle is found to be 39° which corresponds to 67.4 % critical speed.

5.6.2 Regression of dry mill power using Bond's model

The adequacy of Bond's model to describe data collected from the Wits pilot mill under the conditions given in Table 3.4 is assessed. With appropriate adjustments to some parameters listed in Table 5.6, Bond's model is seen to follow the data points pretty well (Figure 5.12). Nevertheless, after 80 % critical speed, the power quickly plunges down to zero at approximately 98.2 % critical. And thereafter, the power becomes negative.

In general, Bond's model was found insensitive to parameters β_0 and ζ. That is the reason why they were kept constant. An average value of the dynamic angle of repose α_d of 37° is proposed in the literature (van Nierop and Moys, 2001); the value of 39° was found to be more appropriate for the current data.

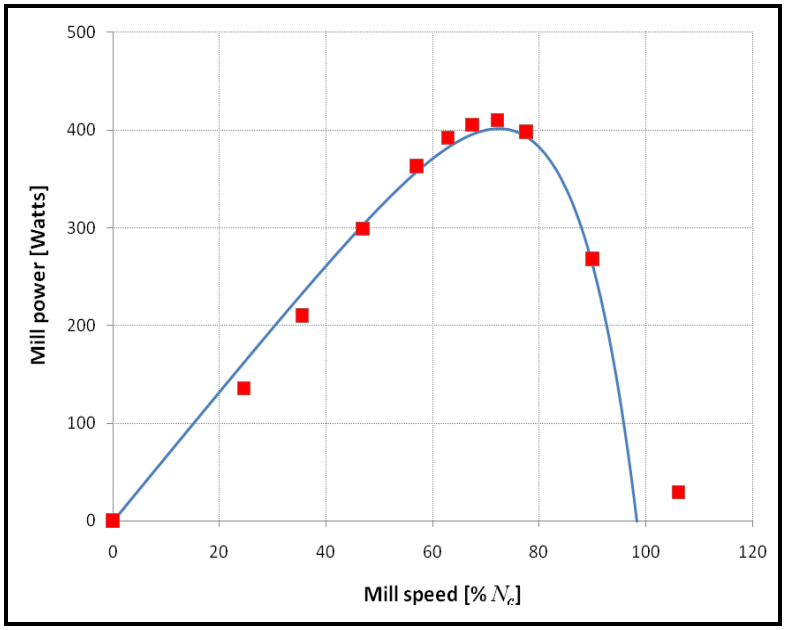

Figure 5.12 Bond's regression of net power draw as a function of mill speed

Adjustments made on three parameters to force-fit Bond's model to the data suggest that ball size and lifter height may have something to do with the drastic change in K_1 and η.

Table 5.6 Bond's and adjusted parameter values in Equation (5.1)

Parameter	Bond's value	Adjusted value
K_1	12.262	13.650
α_d	37*	39
β_0	0.937	0.937
η	9	6.5
ζ	10	10

*Reference: van Nierop and Moys (2001)

Note that Bond's model is unable to account for the power measured at speed 106.2 % critical where the whole charge was observed to be centrifuging.

5.6.3 Regression of dry mill power using Moys' model

The possibility of a more differentiated behaviour of the mill due to the aggressive nature of the lifters (25 mm high) and the size of balls used (10 mm) has been raised as one among many explanations of the low η-value (Table 5.6).

Moys' model, known for its capability to empirically model lifter design, was tested as a result.

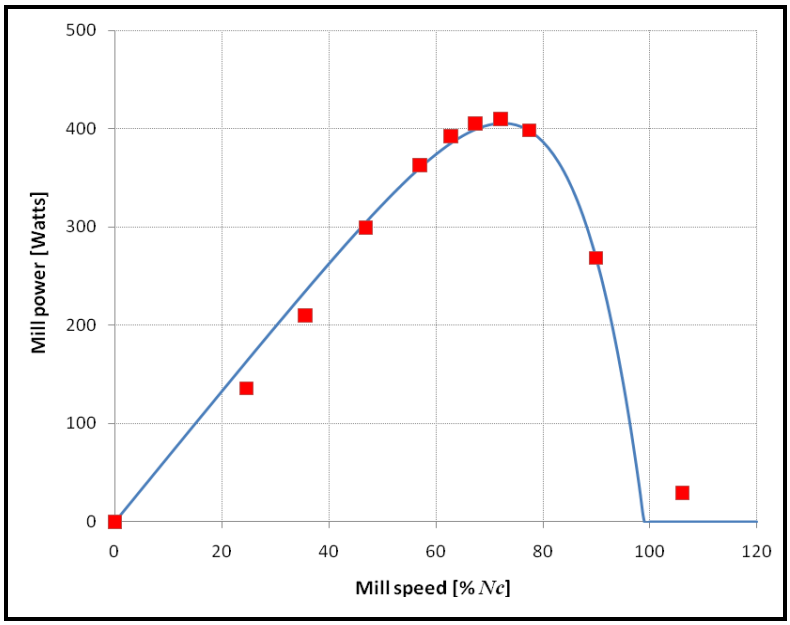

Figure 5.13 Moys' regression of net power draw as a function of mill speed

For the purpose of comparison, the adjusted parameters along with Moys' are tabulated below. The latter values are those reported on a quite identical mill fitted with 18 square lifters having the same height as the trapezoidal lifters that were used for pilot testing.

Table 5.7 Moys' and adjusted parameter values in Equation (5.4)

Parameter	Moys' value	Adjusted value
K_2	12.0	13.9
β_0	0.99	0.99
Δ_J	0.16	0.17
Δ_N	14.2	13.9

The noticeable change happens with K_2: It is possible that the face angle difference between the two lifters influences the effective angle of the bed. By so doing, parameter K_2 follows with an increased estimate (Tangsathitkulchai, 2003). The effect of lifter profile is also characterised by parameter Δ_N that has varied little. This is believed to be an indication of the ability of Moys' model to detect changes in lifter design.

5.6.4 Prediction of dry mill power using Morrell's model

Next, Morrell's power model was tested against the pilot data. The goal was to compare predicted power and data reported for the 'dry mill'. Since, the model provides a comprehensive description of the load behaviour, the large volume of data collected using the Wits pilot mill represented a good opportunity to make sense of the relationship between load behaviour and net power draw.

The first observation is that net power as calculated with Morrell's model is an under-prediction of the measured power for speed below 80 % critical (see Figure 5.14). The other observation is that experimental and predicted powers peak at different speeds: 72 % and 95 % of critical respectively. It is important to mention that net power measured from the pilot mill (see Appendix A.2.3) has been compared to the theoretical net power calculated using Equation 2.18.

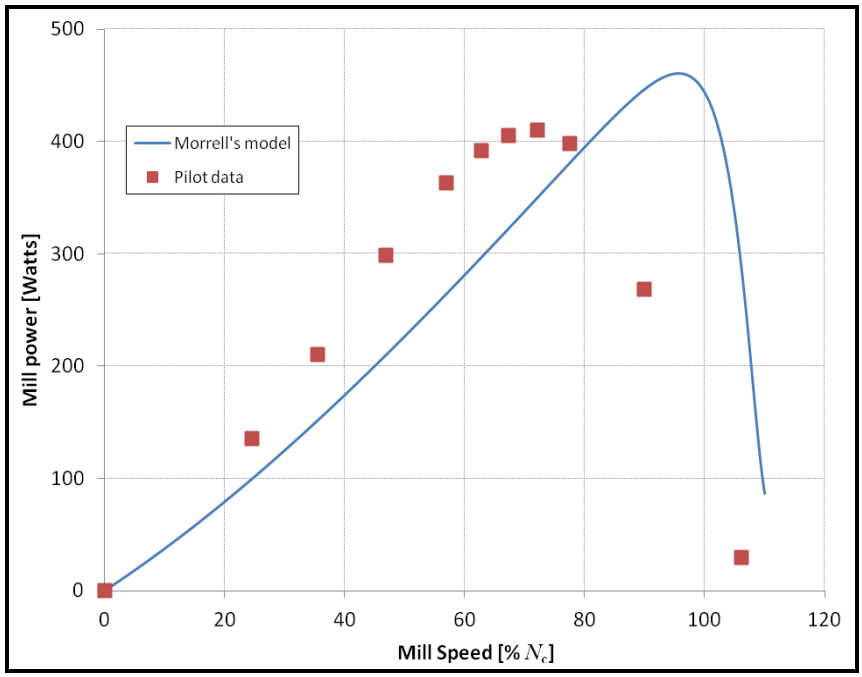

Figure 5.14 Morrell's model of net power draw as a function of mill speed

It is believed that the huge discrepancies are the result of the size of lifter (25 mm) used relative to ball diameter (10 mm). The lifters have indeed the tendency to lift two layers of media higher and further than expected while forcing the grinding balls to stick against the mill wall. The effective charge of the

mill (Moys, 1993) reduces and provokes a decrease in the net power draw. It is therefore possible that the shift in load behaviour is the reason for deviance of the Wits pilot mill from Morrell's model. Changes in load behaviour are analysed with the DEM technique in the next section.

5.6.5 DEM prediction of dry mill power

Finally, SimView was used to run some simulations of the Wits pilot mill. Amongst the outputs, the net power draw of the mill was calculated; screenshots of the mill load behaviour were also created in order to later measure load orientation. Comparison between DEM and measured powers yielded a reasonable match for speeds below approximately 65 % of critical (Figure 5.15). Peaks were recorded at 72.1 % and 78.3 % of critical speed respectively for the pilot data and the DEM simulator. Moreover, the two graphs diverged significantly at high speeds with the DEM overestimating the actual net power.

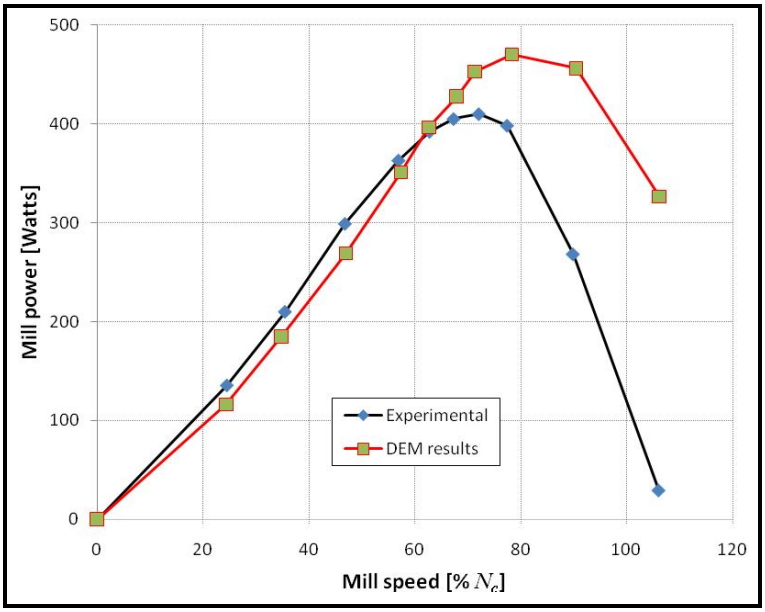

Figure 5.15 Comparison of net power measured to DEM predictions for the following initial parameters: (a) Stiffness: 400 kN/m (normal) and 300 kN/m (shear); (b) Coefficient of friction: 0.4; (c) Coefficient of restitution: 0.6 (ball-ball impact) and 0.3 (ball-wall impact)

On average, the observed discrepancies were in less than 15 % up until 77.5 % critical was reached. After that, the differences became unrealistically large. This may be due to the inability of SimView to model supercritical speeds; and as a result, to reproduce cataracting and centrifuging accurately.

To some extent, the SimView has been able to predict the net power measured in the laboratory reliably for speeds below 65 % of critical. After this, simulated power is very high. Several reasons can be attributed to over-predicted power at super-critical speeds. But at this point, suffice it to say that comparison between measured and simulated power suggest an early shift in the internal behaviour of the load presumably due to the aggressive nature of the lifters used.

A new programme was therefore tried, where key DEM parameters were varied and simulations carried out until simulated and measured load orientations were similar. For this reason, values were changed as shown in Table 5.8.

Table 5.8 Adjustment of DEM parameters: best values are in brackets

Normal stiffness	400 kN/m
Shear stiffness	300 kN/m
Coefficient of friction	**(0.2)**, 04, 0.8
Coefficient of restitution	
Ball – ball impact	0.6, 0.65, 0.7, **(0.75)**, 0.8
Ball – wall impact	0.3, 0.4, **(0.5)**, 0.6

The outcome of the endeavour proved to be encouraging as shown in Figure 5.16 below. The following DEM parameters produced an acceptable fit: A coefficient of friction of 0.2, and coefficients of restitution of 0.75 and 0.5 for ball-ball and ball-wall impacts respectively as reported in brackets and boldface in Table 5.8. Time step was kept constant at 10^{-6} s (see Table 3.7).

It should be mentioned that the position of the load was measured with the help of the same electronic protractor (MB-Ruler version 4.0) used in chapter 4; the difference is that DEM frames extracted from the animations were now involved.

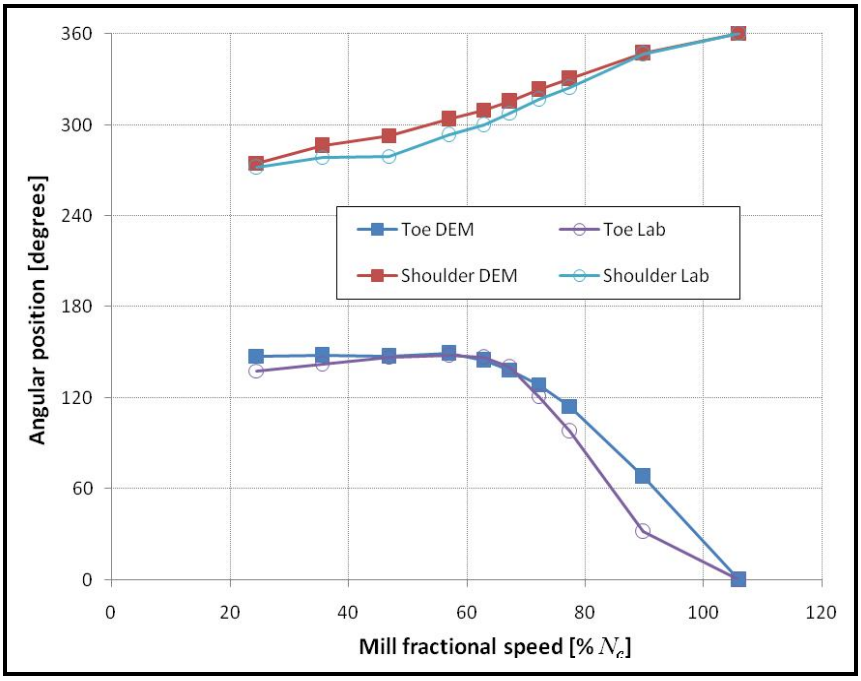

Figure 5.16 Comparison of DEM and measured load orientations for the following DEM input parameters: (a) Stiffness: 400 kN/m (normal) and 300 kN/m (shear); (b) Coefficient of friction: 0.2; (c) Coefficient of restitution: 0.75 (ball-ball impact) and 0.5 (ball-wall impact)

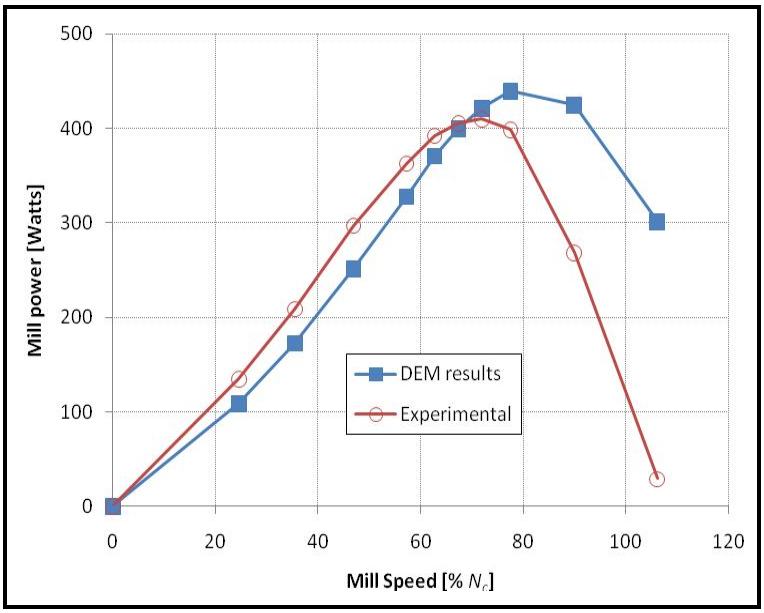

Figure 5.17 DEM-simulated and measured net mill powers for the following DEM input parameters: (a) Stiffness: 400 kN/m (normal) and 300 kN/m (shear); (b) Coefficient of friction: 0.2; (c) Coefficient of restitution: 0.75 (ball-ball impact) and 0.5 (ball-wall impact)

The consequence incurred thereafter was that measured and DEM-determined powers were still not comparable as shown in Figure 5.17, especially towards centrifuging (that is, after 80 % critical). This is consistent with Figure 5.16 in which poor prediction of the angular position of the toe was recorded in the centrifuging region. It is possible that SimView is coded in such a way, the impact energy of cataracting and nearly centrifuging balls landing on the mill shell is not transferred back to the mill. If this is the case, DEM power would be the result of the load being lifted, thereby justifying high values in the centrifuging region.

Other than this, the DEM simulations showed that centrifuging begins around 89.9 % of the theoretical critical speed. It is possible that the proximity probe is somehow not an appropriate sensor for centrifuging loads; however, the argument is to be validated with photographic evidence of the load. But because Figure 5.16 shows a good match between DEM and measurements, the DEM snapshots were used to gain more insight on the internal behaviour of the load, thereby informed interpretation of the data followed.

5.7 Effects of slurry pool on mill power

5.7.1 Measured net power draw of the Wits pilot mill

Recall that the presence of a pool reduces the net power draw (Moys and Smit, 1988). An attempt was made to determine the impact of the pool volume on mill power. The aim was to lay a solid foundation for chapter 6. Indeed, this is needed in order to relate slurry pool and mill power to milling kinetics.

As far as slurry pooling is concerned, Figure 5.18 depicts the drop in power experienced by the Wits pilot mill. Initially, power increased smoothly from around 400 Watts to a peak at $U \cong 1$, which is a function of mill speed. After a slurry filling $U = 1 – 1.2$, the power slowly drops.

For speeds below 75 % critical, the peak in power was observed at $U = 1.2$ approximately. By the same token, this threshold filling was also found in

Chapter 4, Section 4.5. In contrast to this, the two higher speeds reach the maximum at U = 1 which is the generally expected value after which the pool starts to form. It appears that the Wits pilot mill tends to exhibit similar behaviour to the Perspex mill at low speeds. This clearly shows that the operating conditions are close to the 60 % critical speed used (see Table 3.1) with the Perspex mill. As to why the same does not happen at high speeds is not clear.

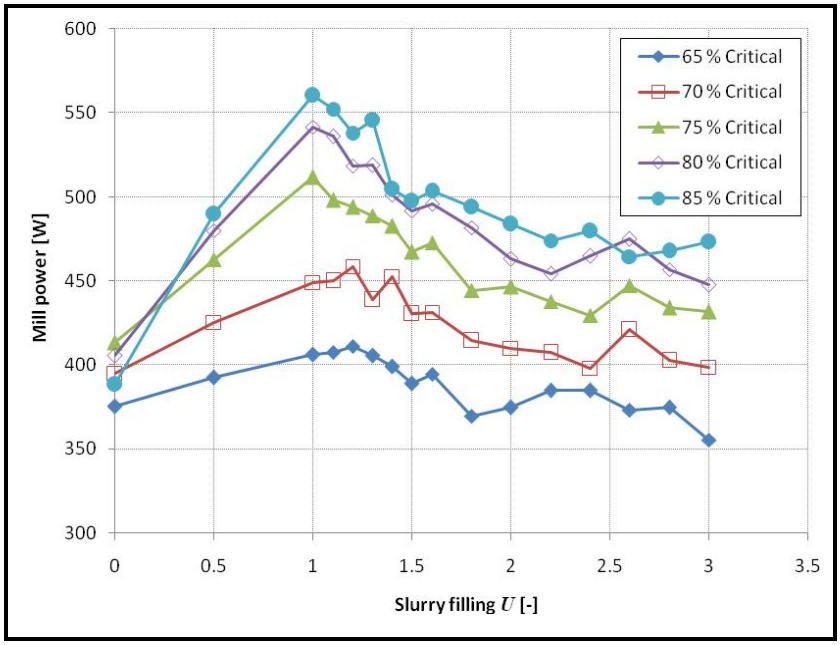

Figure 5.18 Effects of slurry filling on net mill power for constant fractional speed

5.7.2 Morrell's model of slurry pooling effect

Morrell (1993) equated the effect of the slurry pool on the net power draw of a mill (see Equation 2.18). As an example data, four speeds (65 %, 70 %, 75 % and 80 % of critical) were compared to Morrell's power model to evaluate its adequacy for predicting the effect of slurry pooling.

First, the net power is under-predicted for all four speeds at slurry filling U = 0; this changes for 85 % of critical speed not shown in Figure 5.23. On the other hand, the influence of slurry pooling is correctly modelled because the decrease in power measured is mimicked reasonably well. Indeed, the modelled effect of

slurry pooling follows the decreasing trend of power for 1.0 < U ≤ 3.0. For all four speeds, solid lines stay approximately parallel to their corresponding scatter points when the slurry pool is present.

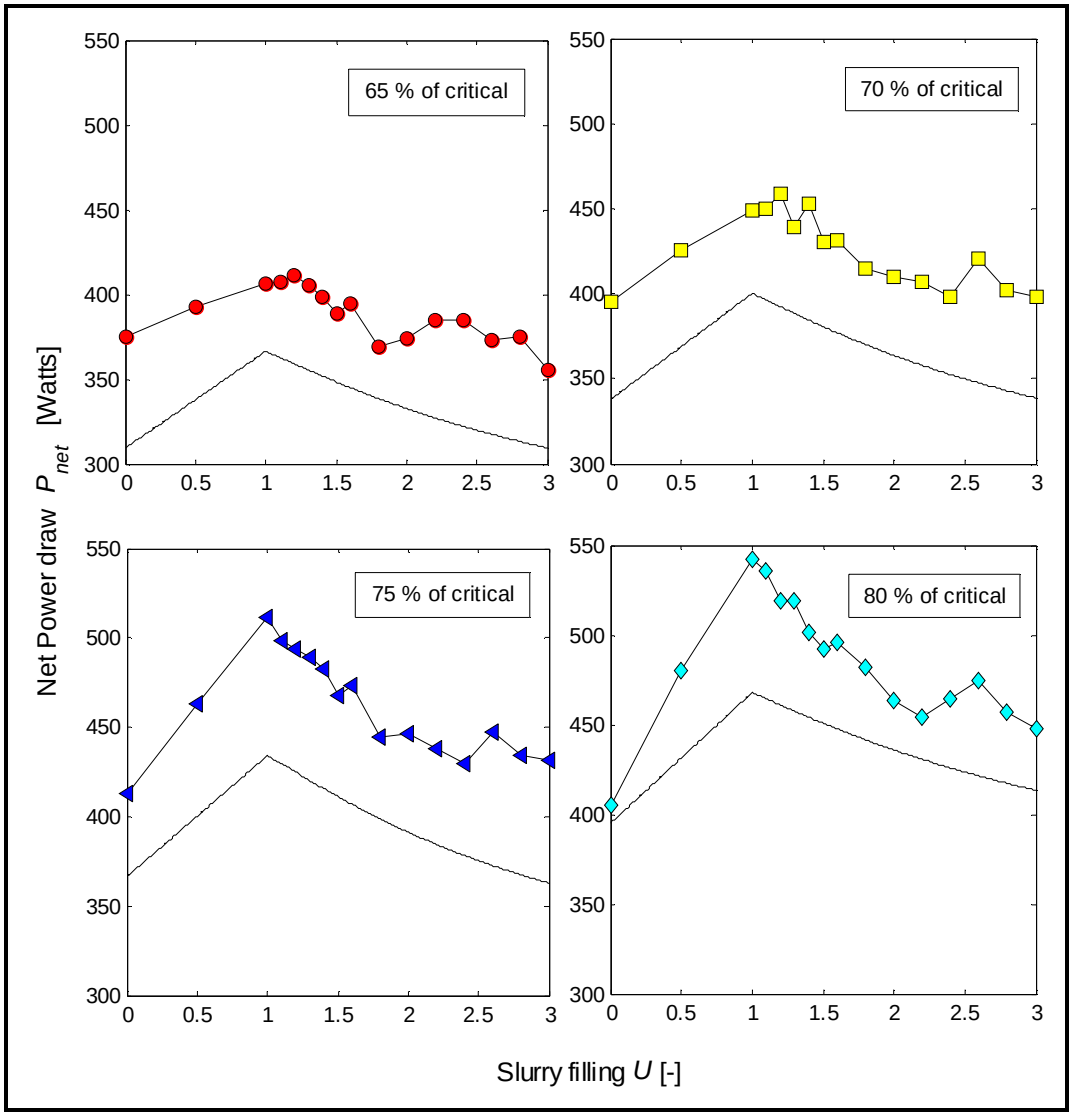

Figure 5.19 Morrell's slurry pooling effects on net power for four mill speeds

Second, except for a 70 % critical speed, the slope of the straight line for 0 ≤ U ≤ 1.0 is not reproduced by Morrell's model. Measured slopes are higher than modelled ones for speeds above 70 % critical; the slope is low for 65 % critical.

It is definitely clear that Morrell's model is sensitive to slurry pool but fails to model the under-filled media charge (i.e. 0 ≤ U ≤ 1.0) of the Wits pilot mill. In addition, discrepancies of about 13.6 % in magnitude have been recorded

between model and measurement; a detailed discussion is done later in the chapter. At this point, it appears that Morrell's prediction and measured net power diverge noticeably from each other. Perhaps this is due to the choice of grinding ball size (10 mm) and lifter geometry (25 mm high) used.

5.7.3 Tangsathitkulchai's model of slurry pooling effect

In the study of the effects of slurry filling on mill power, Tangsathitkulchai (2003) proposed an equation based on his laboratory data. It is envisaged to see whether the pilot data agrees with the empirical equation or not. In this regard, the confidence interval of the fitted parameters was determined to have a quantitative description of the quality of the fit.

To suit the purpose, Tangsathitkulchai's model of slurry pooling (see Equation 2.21) has been rearranged as follows:

$$P_{net} = a_1 . U^{a_2} \exp\left(-a_3 U\right) \qquad \textbf{(5.13)}$$

where a_1 is a fitting parameter allowing for the mass of balls M_b in the mill

a_2 and a_3 are fitting parameters that were found to be strong functions of the volumetric concentration of powder in the slurry in the range $0.3 \le C_v \le 0.55$

U and C_v are the slurry filling and slurry concentration respectively.

One thing transpires from Equation (5.13): The net power P_{net} reduces to zero when there is no slurry, that is, U = 0. This simply means that the mill draws power only when slurry is present, which completely contradicts the norm.

Now, in order to accommodate this violating case, Equation 5.13 has been modified by adding one parameter P_0 to represent the net power at U = 0:

$$P_{net} = a_1 . U^{a_2} \exp\left(-a_3 U\right) + P_0 \qquad \textbf{(5.14)}$$

Figure 5.20 illustrates the outcome of curve-fitting Equation (5.14) to the measured net power P_{net} as a function of slurry filling U for a 75 % critical speed.

The confidence band at 95 % confidence level is plotted along to have a good idea about the quality of the fit. It appears that though the fit seems to follow the trend given by the scatter plot, all data points do not fall within the 95 % confidence band.

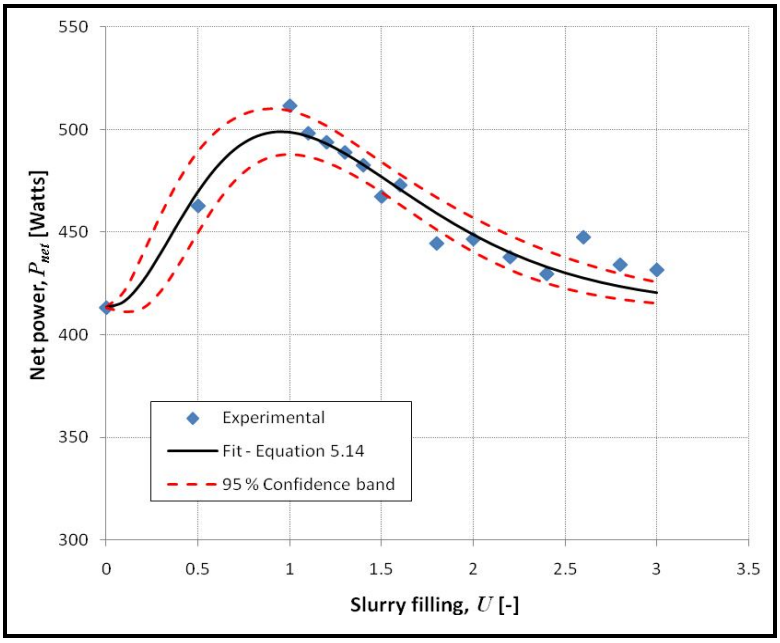

Figure 5.20 Curve fitting of modified power model – Equation (5.14)

Further confirmation of the poor quality of the model comes with the variabilities associated with the three parameters involved: a_0, a_1, and a_2. Indeed, the quality of a fit is dictated by two elements (Motulsky and Christopoulos, 2003): First, a visual inspection of the graph to determine whether all data points are within the confidence band at an appropriate confidence level (generally 95 %); and second, the variability of every fitting parameter present in the model to assess whether they are lower than the average error margin E_m of the model.

Table 5.9 Report generated with the Curve Fitting Toolbox of Matlab®

Parameter	Fitted value	Confidence band
a_1	1143.06	34.44 – 2251
a_2	2.475	1.404 – 3.546
a_3	2.592	1.678 – 3.505
P_0	413.1	fixed at bound

In line with this, Equation (5.14) that is used to describe the pilot results yields an average error margin of about 6.5 %. And generated confidence bands on all three parameters are way above the error margin (see Table 5.9 above).

Regression with the Curve Fitting Toolbox of Matlab® reveals that the variability of all the parameters is so wide that the model is considered inadequate. Parameter a_1 exemplifies it with a staggering 96.9 % variability at 95 % confidence level; in other words, (2251 – 1143.06)/1143.06 = 96.9 %. Using the same approach on a_2 and a_3, we find a variability of 43.3 % and 35.2 % respectively. P_0 was fixed as it was shown in Equation 5.14 to represent the net power of the mill at slurry filling U = 0.

5.7.4 Piece-wise function model of slurry pooling effect

Previous attempts to model the effect of slurry pooling on net power draw to the Wits mill have been to a large extent limited. That is why empirical modelling is now used to identify the trends present in the pilot data graphed in Figure 5.18 above. In order to achieve this, the following piece-wise function was conveniently used to model the measured net power (see Appendix A.2.3):

$$y = f(x) = \begin{cases} A_1 + A_2.x & \text{for } 0 \le x \le 1 \\ (A_1 + A_2).x^{-b} & \text{for } 1 \le x \le 3 \end{cases} \qquad \textbf{(5.15)}$$

where A_1, A_2, b are the curve fitting parameters

y and x representing respectively the net power draw P_{net} and the slurry filling U while f is the Matlab function '**powerdraw.m**' listed in Appendix A.5.5.

It is worth mentioning that f is a linear function for an under-filled media charge (that is, for $0 \le x \le 1$). The piece-wise function f becomes a power function based on the slurry pool model (Equation 4.2) proposed in this thesis for an over-filled media charge (that is, for $1 < x \le 3$).

Afterwards, the parameter search was performed on the whole series of data pertaining to the mill power. Figure 5.21 illustrates how well Equation 5.15 worked for the two extreme mill speeds; namely, 65 and 85 % of critical.

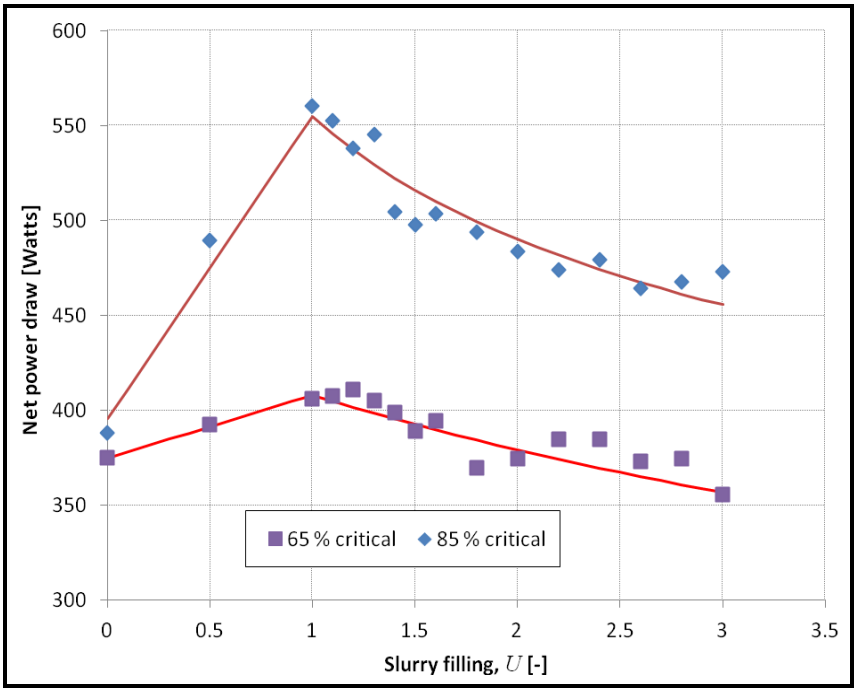

Figure 5.21 Empirical modelling of the slurry pooling effects on net mill power

To have an idea of the quality of the fit, the fitting parameters as well as relevant statistics associated with the fitted curves are also reported in Table 5.10. Relevant statistics that were calculated are: the coefficient of determination R^2, the standard error of estimate s_e and the margin of error E_m at 95 % confidence level (Triola, 2001).

Table 5.10 Parameters and statistics of the empirical Equation (5.15)

	65 %	**70 %**	**75 %**	**80 %**	**85 %**
A_1	374.9	394.9	414.3	408.8	395.5
A_2	36.5	61.6	92.1	128.5	159.5
b	0.1076	0.1271	0.1624	0.1715	0.1794
R^2	79.95	85.01	93.88	94.66	93.86
s_e	6.98	8.05	7.27	8.41	10.63
E_m	3.42	3.94	3.56	4.12	5.21

Parameter A_1 represents the y-intercept of the model which is in fact the power drawn by a 'dry mill'. In Section 5.6.3, Moys' power equation was shown to satisfactorily model the dry mill power.

Contrary to the general belief, the gradient of the net power increases with slurry filling in the range $0 \leq U \leq 1$. Figure 5.21 depicts this well, so does parameter A_2 in Table 5.10. This unexpected behaviour became the prompting point in trying to correlate parameter A_2 to mill speed.

Figure 5.22 shows a clear linear correlation between parameter A_2 and mill speed. It becomes apparent that parameter A_2 represents the gradient of the power draw with respect to mill speed for a mill under-filled with slurry. In a quite similar fashion, parameter b shows some correlation with mill speed. However, it is believed that parameter b is somehow related to the angular position of the pool presented in Section 5.5.2.

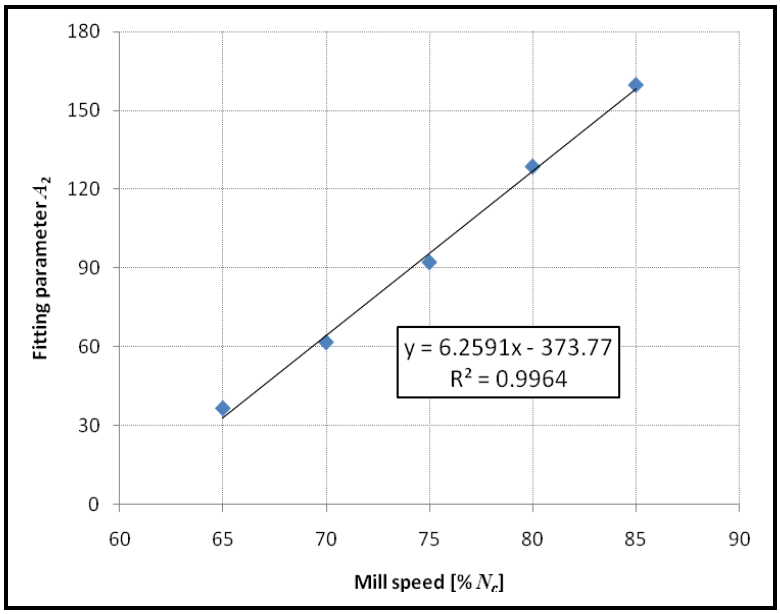

Figure 5.22 Dependency of parameter A_2 in Equation (5.15) with mill speed

The next section proposes a model of power that uses the empirical findings above in a torque-arm framework to allow for the contribution of slurry pooling.

5.7.5 Torque-arm model of slurry pooling effect

Lastly, a simplified analysis of the effects of the pool of slurry on mill power, proposed by Moys and Smit (1998), was tested. Here the load is divided into two components: the media charge with interstices completely filled with slurry and a pool of slurry made up with the remainder (Figure 5.23).

The two components exert two forces ($M_L.g$ and $M_p.g$) acting on their respective centre of mass x_L and x_p. Then, following the torque-arm principle, the resulting torque about the centre of the mill can be calculated.

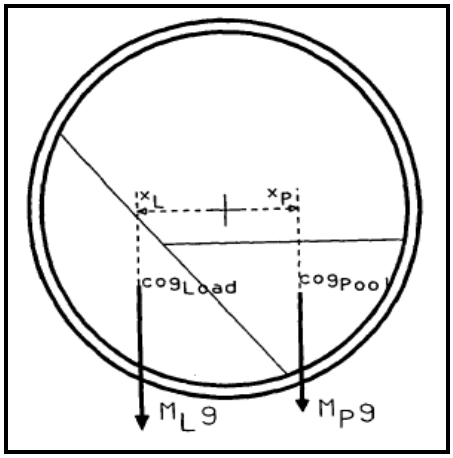

Figure 5.23 Torque-arm model applied to a wet mill
(after Moys and Smit, 1998)

With this end in view, a Matlab® script (see Appendix A.5.3) was prepared to calculate the contribution of both the pool and the media charge. The power was deduced with the mill speed known a priori. Figure 5.24 below shows the graphical comparison.

Note that the load behaviour has been here modelled with the following considerations:

1. The media charge was assumed to follow Equation 5.15 between U = 0 and 1.0; that is, power increases with slurry filling under the aforementioned conditions as demonstrated in Figure 5.22.

2. The dynamic angle of repose of the load was assumed to remain constant at 39° (see Table 5.6). In doing so, the pool could be geometrically determined as its angular position is known (see Section 5.5.2).

The general picture (Figure 5.25) shows that power increases with slurry filling until U = 1.0 is reached, thereafter power monotonically decreases. It is also noted that for 1.0 < U ≤ 3.0, power experiences a decreasing regime that is quite similar for all five speeds (from 65 % to 85 % critical). Indeed, line charts in this section of the graph (i.e. for 1.0 < U ≤ 3.0) are almost parallel to one another. This could be attributed to the fact that pool angles were almost similar within the range of viscosity studied in the previous chapter (refer also to Table 3.2). The same slurry pooling model, when applied to data of the present chapter, proves to still hold for the speeds tested (see Table 3.4). It is only for 85 % of critical speed that a significant departure from the average parameters C_0 and k was observed. By and large, the slurry pool volume is identical in the remaining four speeds and under similar operating conditions; hence, the trend observed could be justified.

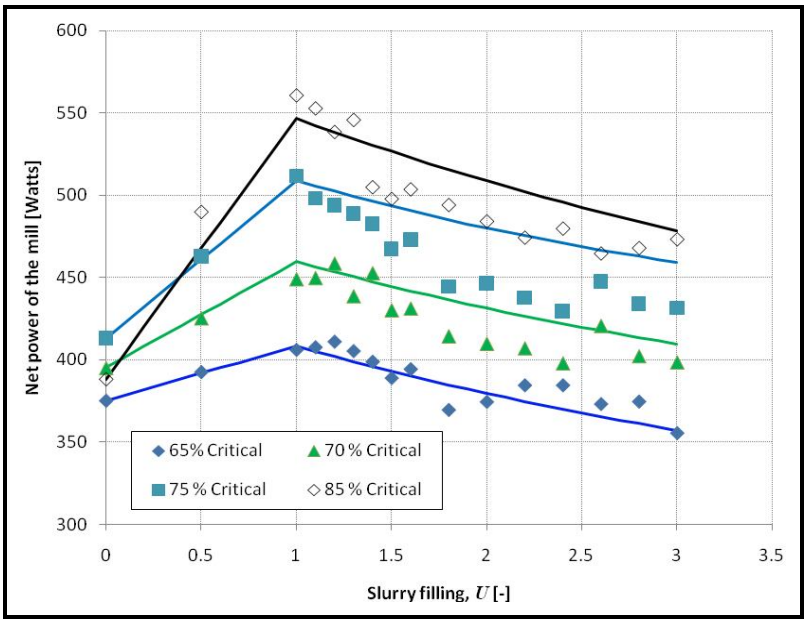

Figure 5.24 Modelling net power draw using the torque-arm paradigm

Lastly, at lower speeds, the torque-arm model agrees reasonably well with measurements. But, as speed increases, the model exhibits a systematic departure from the data and consistently overpredicts net power. The worst case is observed at 75 % critical speed (Figure 5.25).

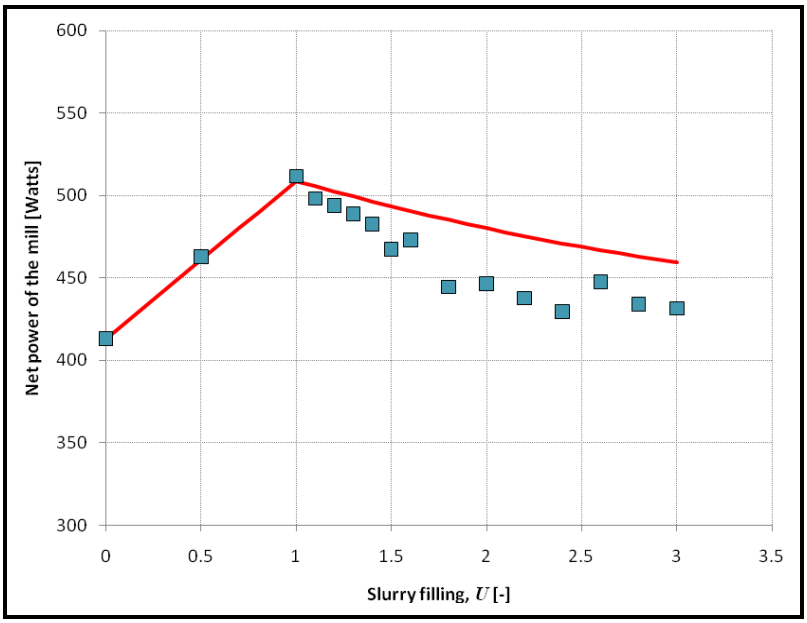

Figure 5.25 Comparison of predicted powers with the torque-arm model and measured net powers at 75 % of critical speed

Possible reasons for this are identified later and qualitatively assessed. The implications of the underlying assumptions used in the development of the torque-arm model are also discussed.

5.8 Discussion

5.8.1 Load behaviour of the Wits pilot mill

The role that load behaviour plays in power modelling was appreciated. First, the influence of mill speed on media charge and slurry was evaluated. At low speeds, toe and shoulder angles of the media charge were found to increase with mill speed. This expected behaviour is attributed to the lifters that are 'scraping' the media balls towards the rising load. The trend carries on for the shoulder until

centrifuging. The toe, on the other hand, initially increased with mill speed and as one approaches centrifuging, it suddenly dipped down. It is believed that balls are landing on the mill shell making the conductivity probe detect their presence earlier than the actual toe of the cascading load. In fact, it becomes very difficult to even define the toe itself. The combination of all these contributes towards lower angular values of the toe. Another note to make is that the measured critical speed was found to be 92.43 % of the theoretical critical. This much lower value is believed to have a connection with the lifter height and ball diameter.

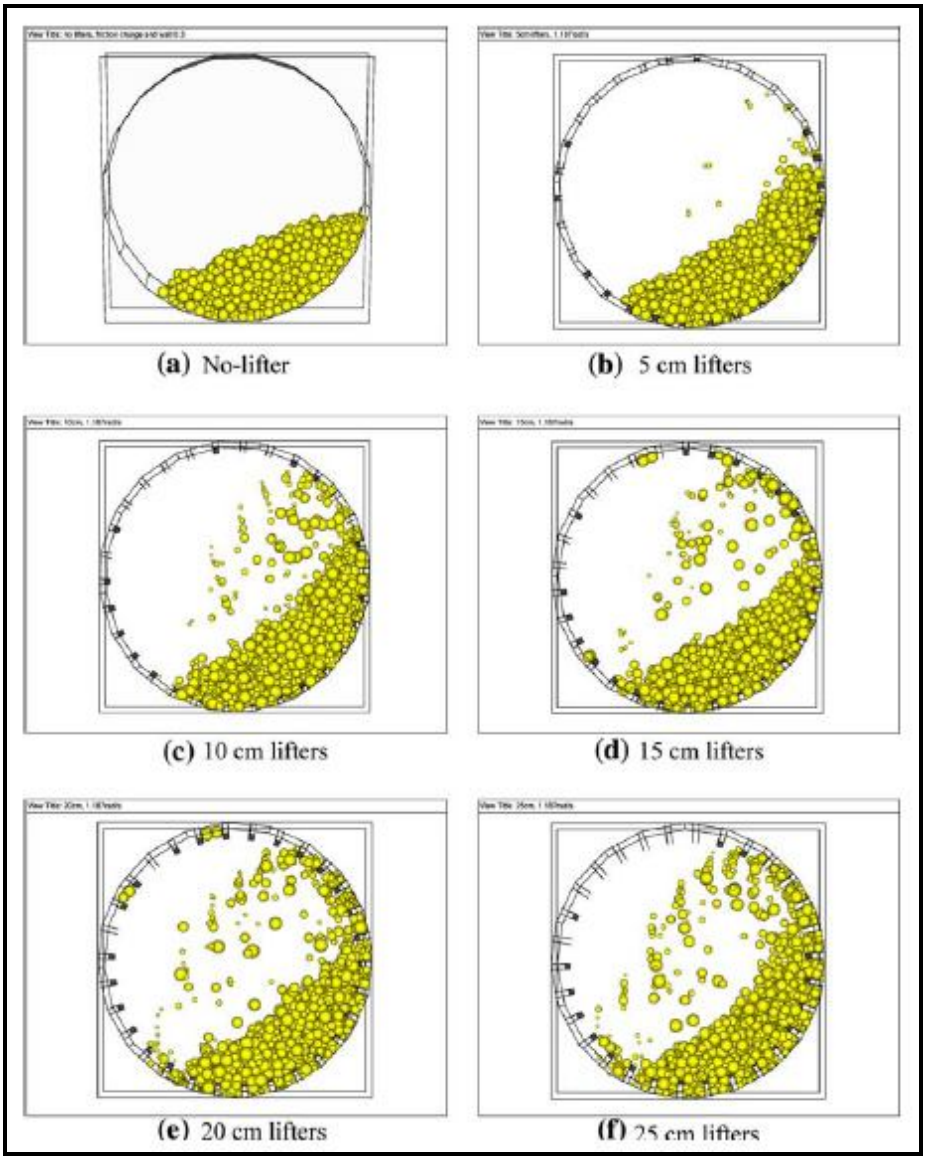

Figure 5.26 Effects of lifter height on load behaviour for a SAG mill. Simulated lifter heights range from 0 (no lifter) to 25 cm (after Djordjevic *et al.*, 2004)

Simulations carried out by Djordjevic *et al.* (2004) on a SAG mill have been used to support the argument. Their reported snapshots (Figure 5.26) clearly indicate a tendency of the load to prematurely centrifuge once the height of lifters exceeds 15 cm even with particles as large as 150 cm. It is possible that this is what happened in the pilot mill as grinding balls (10 mm) were small compared to lifter height (25 mm). The pool angle remained relatively unchanged for a constant slurry filling. Probably, the hydrodynamics of the slurry is responsible of such behaviour. The fluidity of slurry makes it difficult for the lifters to entrain it.

Second, the effect of slurry filling on load orientation was analysed. Typically, the position of the media charge did not change with slurry filling. This finding was explained in chapter 4. Now, the new observation just confirms that the statement is also true for a naturally occurring ore. The difference comes with the media charge for which the toe is fairly constant throughout. To expand on this, one can compare Figure 5.9 to Figures 4.5 and 4.7 to see that the toe does not jump with the natural ore. It is unclear why there is a kink with the glycerol solution, but perhaps balls stick against each other differently for the two solutions. At this point, there seems to be no hard evidence that negates beyond any doubt the idea of stickiness. In fact, if the UG2 slurry does not make balls to stick more than glycerol, grinding balls are more free to move around. The en-masse load becomes subjected to less entrainment by the ascending lifters in the toe region than when glycerol is involved. As a result, even if slurry completely fills the voids within the media charge (i.e. at U = 1.0 – 1.2), the toe position will not substantially increase as was observed with glycerol (refer to Figure 4.7).

On another note, Figure 5.27 presents snapshots of the mill generated by Wits SimView. The first column shows frames of the mill for identical speeds to those actually used during pilot testing. The next column traces individual particles on two consecutive frames and plots their corresponding trajectories. The last column, however, is a more statistical representation of the simulated load behaviour. It is known as the Position Density Plot (or PDP for short). Basically,

Dong and Moys (2003) define a PDP as ‘a digital, visual and statistical representation of the charge distribution in a mill’. It is constructed by superimposing a number of independent digitised still images or simulated screenshots of a mill load at steady state. The occupancy of each pixel over the entire time period the mill or the simulation is run is represented in greyscale or in a different colour-coded scale. By doing so, the average load orientation can be appreciated. In the case of Figure 5.27, darker regions of PDP plots simply signify larger occupancy or in statistically terms higher frequency of particles passing through the picture element.

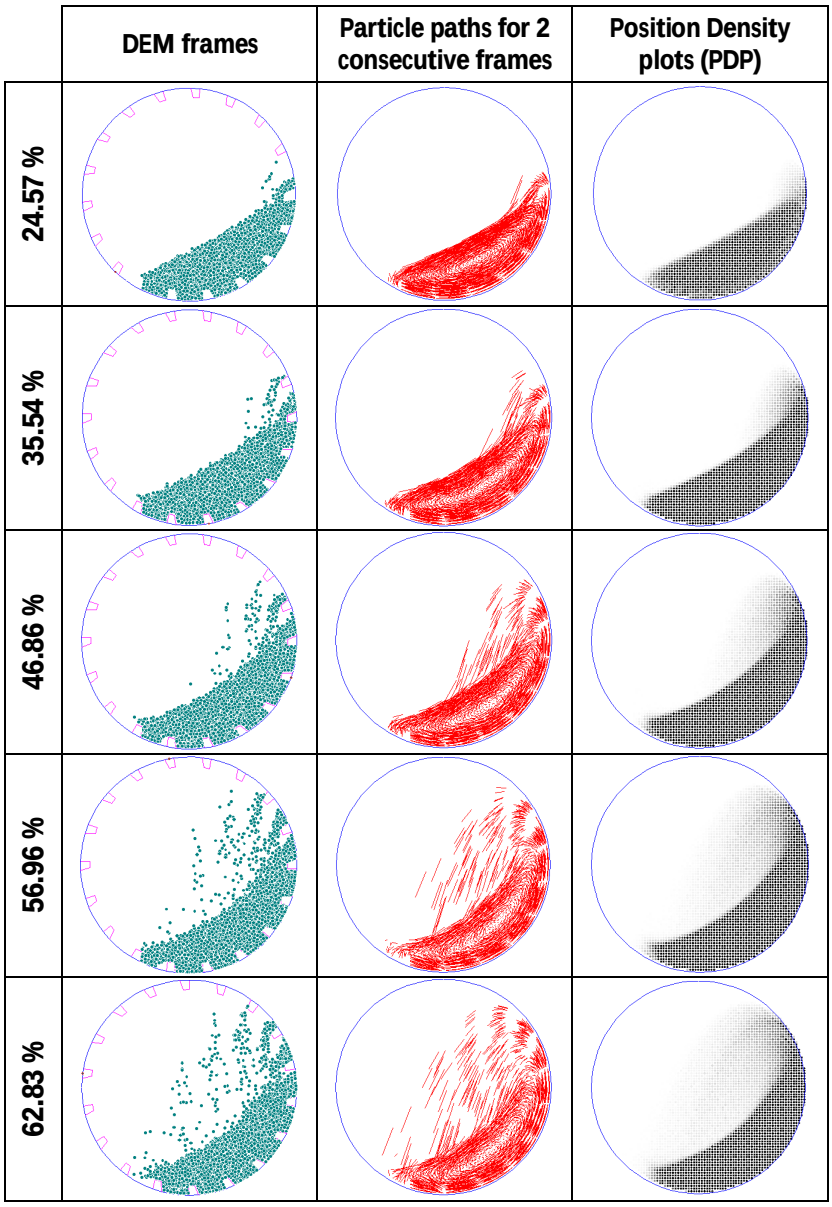

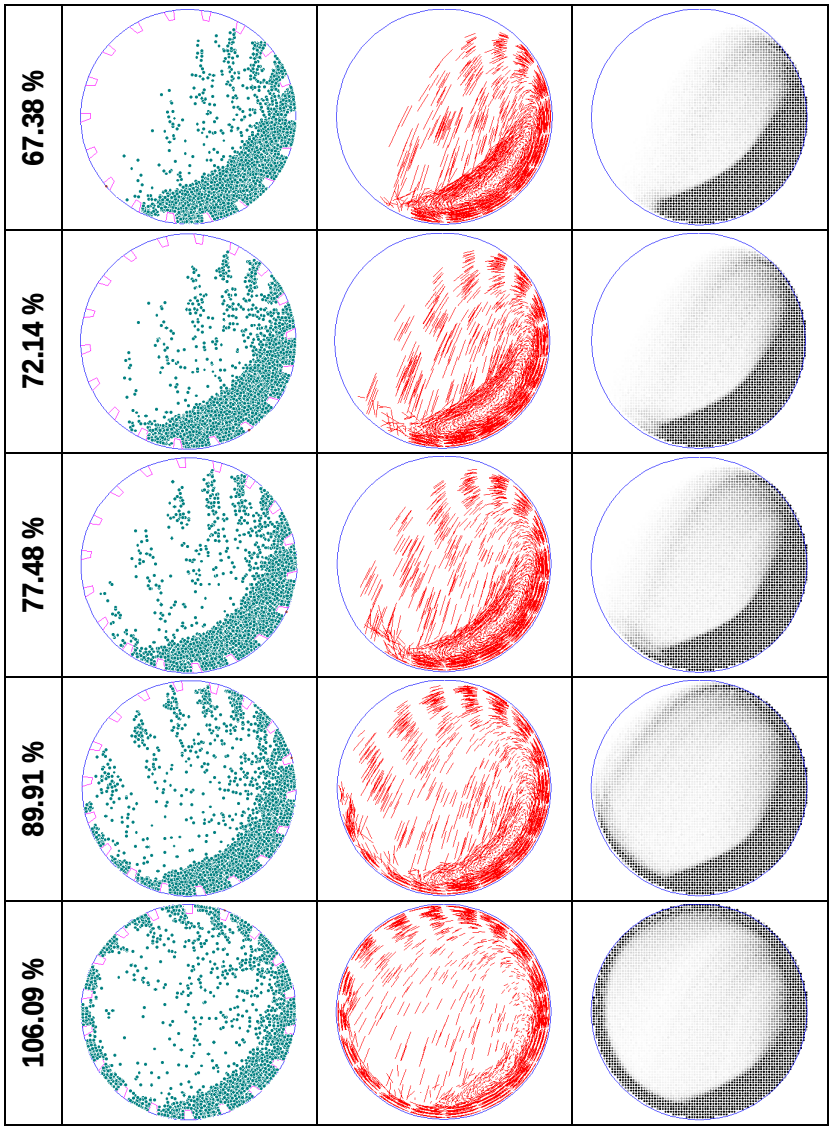

Figure 5.27 DEM results for the simulations of the dry mill as modelled using parameters in Table 5.8

A closer look at the PDP plots indicated that within the load, an inclined surface the angle of which lies between 20° and 40° exists; this range is close to that found at low speeds in Figure 5.11. At 89.91 and 106.09 % critical, the incline is barely visible as almost the whole media charge is centrifuging. The same conclusion can be drawn from the outputs presented in column one. The next observation confirms that centrifuging starts somewhere between the last two speeds tested. This is consistent with previous findings that showed that centrifuging speed is lower than the theoretical one at 92.43 % critical.

Trajectories given in column two show that the load cascades at very low speeds only. Beyond the speed of 35.54 % critical, a significant fraction of grinding balls cataract; media then begin to land into the toe region starting from approximately 62.83 % critical. DEM simulations confirm that the lifters used were very aggressive relative to ball diameter; as a result, cataracting and even centrifuging start much earlier than usual. Furthermore, the large fraction of balls landing on the mill shell triggers an early detection of the toe by the proximity probe which consequently makes the actual toe very difficult to determine. The loss of this information impacts negatively on the analysis of the load using the on-the-shell sensor.

Last, column two gives a qualitative idea on the occupancy profile of the active charge of the mill.

5.8.2 Calculations of the net power draw

Attempts to model power drawn by the dry mill shall first be discussed. Recall that 'dry mill' as defined in this thesis simply refers to the media charge with no slurry or powder.

Moys' model has the merit to empirically account for lifter profile. This, on its own, predisposed the model to pass the curve fitting test as demonstrated in Figure 5.13. Morrell's model, on the other hand, does not explicitly incorporate the effect of lifter design and its interaction with mill speed and mill filling. As such, it shall not come as a surprise if the pilot power data did not follow the predicted behaviour using Morrell's power model (see Figure 5.14). But even so, Morrell's model has been so impressively applied to a large database (Erdem *et al.*, 2004; Morrell *et al.*, 1992; Morrell, 1993; Morrell, 2003; Napier-Munn *et al.*, 1996) that one question persists: What went wrong with the current experiments?

It is believed that the answer could be found in the choice of lifter geometry and grinding ball size. To consolidate this view, Figure 5.26 is re-examined with the crescent shape proposed by Morrell (1993) in mind. It can be seen that as lifter height is increased, the two outermost layers of the charge experience most of the lifting effect resulting in premature centrifuging. The en-masse charge that is receiving less lifting can be approximated to the inclined load orientation. DEM evidence provided in Figure 5.27 suggests that the load inside the Wits pilot mill was shaped to some extent the afore-described way. It is then appropriate to consider the charge as comprising two contiguous crescent shapes as advocated by Morrell (2003): the outermost with low toe angle and high shoulder angle, and the inner one with high toe angle and low shoulder angle (see Figure 5.30 below). Equations 2.13 and 2.14 are to be revisited accordingly (as was done in Table 5.3) and the respective velocity profile of the two 'strips' accurately modelled (see Figure 2.32).

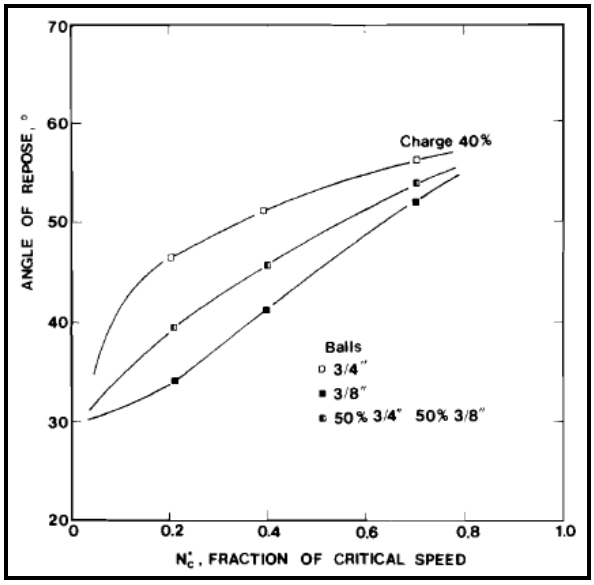

Figure 5.28 Variation of the dynamic angle of repose with mill speed for three different ball size distributions at 40 % ball filling (Lo *et al.*, 1987)

With all the above said, the dynamic angle of the charge can be discussed next. Previous findings reported that the angle of repose varied with mill speed. Here as well, the argument is supported with a similar trend observed by Lo *et al.*,

(1987) as shown in Figure 5.28. Using a Perspex laboratory mill, they were able to show that the dynamic angle of repose increases with increasing mill speeds until about 80 % critical. Similar patterns were reported in Figure 5.11; above 75 – 80 % critical speed, the angle of repose calculated becomes probably meaningless with no geometric significance. The important statement to make is that despite the presence of the angle of repose in most of the widely used models, its unambiguous definition is subject to some form of subjectivity and empiricism. That is where Morrell's model presents its full strength: the milling conditions and the dimensions of the mill are all that are needed. Furthermore, the expected accuracy of the predicted net power draw was argued to be $\pm$ 9.5 % at 95 % confidence level (Morrell, 1993). As far as the Wits pilot mill is concerned, the net power draw calculated with slurry present in the load did not match the measurement satisfactorily (see Figure 5.19). Prediction of the net power draw yielded more than 13 % error for 70 and 75 % of critical speed for instance. This clearly indicates the particularity of the pilot mill data compared to the widely accepted power model by Morrell (1993). The other thing is the increase in net power with mill speed observed in Figure 5.22 instead of constant slope as predicted by Morrell's model (Figure 5.19). It is apparent that this mysterious phenomenon has everything to do with slurry alone. This is supported by the fact that media charge orientation was not substantially altered by the presence of slurry. Hence, the change in gradient observed in the measured power with respect to mill speed should logically be the result of the changing distribution of slurry within the media charge.

Turning the attention to the torque-arm model proposed in Section 5.7.5, one can see an improved model of the slurry pooling effects. Simply put, the parity plot in Figure 5.29 shows reasonably good agreement to within $\pm$ 10 % error in spite of the systematic discrepancy observed. Indeed the torque-arm model consistently over-predicts the data, but follows the same slope throughout with all the data points falling within the confidence band. It is believed that the overpredictions are due to the geometry of the pool that changes with mill

speed; thereby, departing more and more from the idealised curved triangular shape shown in Figure 5.23 which forms the basis of the model (refer to Appendix A.5.3).

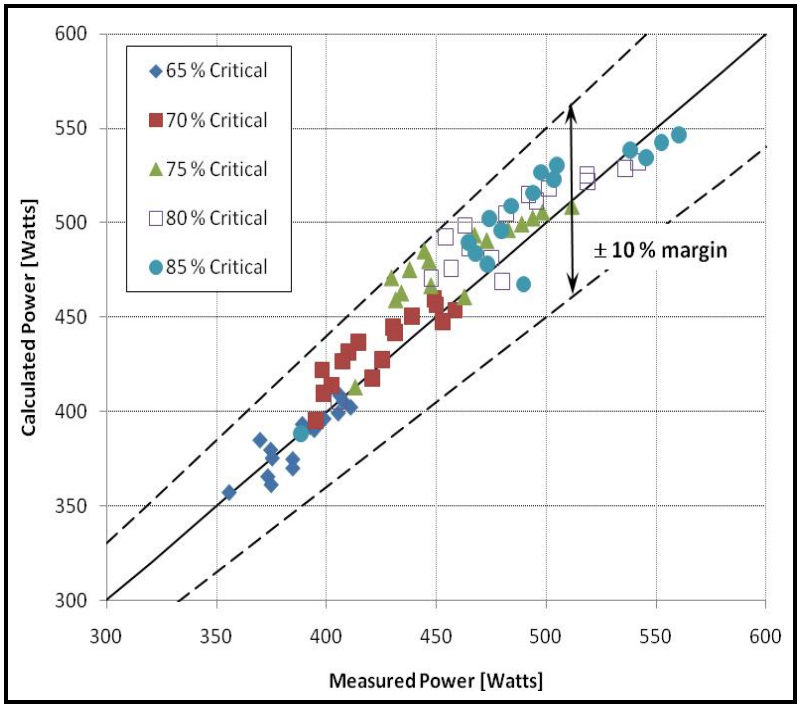

Figure 5.29 Adequacy of the torque-arm model

Th next topic in the discussion is the attempt to model power drawn by the dry mill. Power models by Bond, Moys, and Morrell were examined. On the other hand, DEM-based results were used to complement the analysis of the power data by the precedent three models and, where necessary, they were discussed.

First, power models by Bond and Moys yielded similar results. Understandably, Bond's model is empirical and therefore describes the most encountered operating speeds (60 – 85 % critical as argued by King, 2001). This explains why power is predicted to be negative in the centrifuging region and simply points out the inadequacy of Bond's model to describe centrifuging media charges. Moys' model, on the contrary, forces the net power to reduce to zero beyond centrifuging, which is physically reasonable. Combined with its ability to take lifter design into account, this aspect secures the position of Moys' model over Bond's. However, unresolved issues such as the dynamic angle of repose are still

pending. Discussions held around Figures 5.11 and 5.28 consolidate the argument as to why it should be seen as a fitting parameter rather than a physical property of the media charge when either Bond's or Moys' model is used. This is further supported a realistic value of 39° (see Table 5.6).

Second, the more recent power model by Morrell is equally a good candidate for modelling mill power. The real problem is the difference between measured and predicted power (see Figure 5.14). The argument to this strange finding is believed to reside in the adopted geometry of the pilot mill itself.

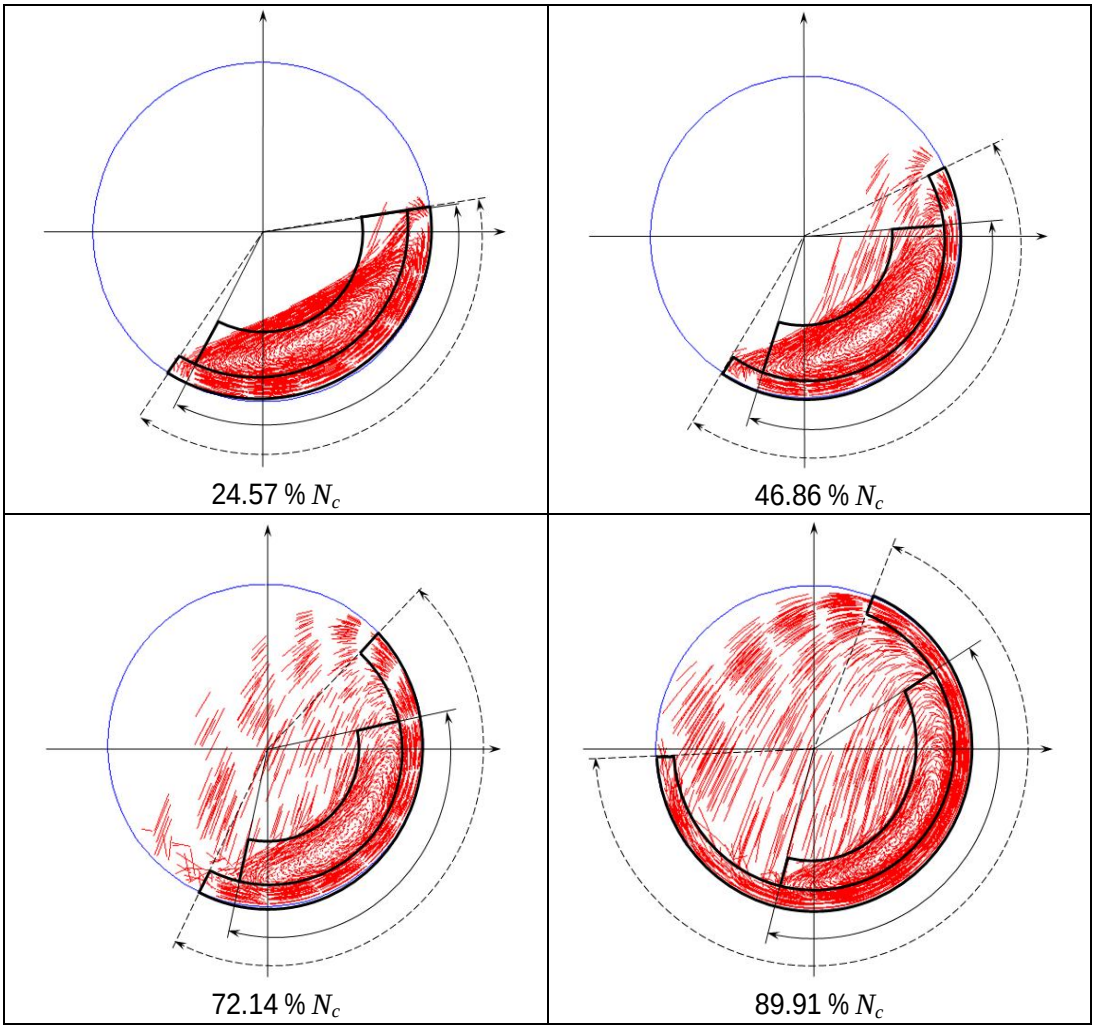

Figure 5.30 DEM shapes of the load following Morrell's paradigm

Expanding on this, Morrell expounded a crescent-shaped profile of the load to develop his model. DEM screenshots of the mill reveal that because of the

aggressive lifters (25 mm high) and the diameter of grinding balls used (10 mm), the dynamic media charge could be better approximated using two contiguous crescent shapes each with its own relationship between media charge position (shoulder θ_S and toe θ_T) on the one hand, and mill filling J and speed N_m on the other. Morrell (2003) proposed this as one of the avenues to explore in order to improve his model. This has been graphically done in Figure 5.30 and the qualitative analysis demonstrates that the outermost layer elongates more as speed increases while the inner one remains more or less invariant. Difficulties linked to the description of the inner layer and the limited information available were the main reasons for providing only a qualitative description of the media charge shape. Laboratory tests with a glass-ended mill would have been more invaluable here, but unfortunately the fixed speed of the Perspex mill was a technological limitation for such an undertaking.

To sum up, the inadequate choice of lifters and ball diameter used in the test work has been identified to be the plausible explanation for pilot data to disagree with Morrell's prediction of net power draw. Because Morrell's model has been tested, validated and calibrated on a large database, it is more likely that data collected from the Wits pilot mill represents an unusual response for mill power.

5.8.3 Slurry pooling

In order to discuss the slurry pooling phenomenon, consider a mill running at low speed. The charge of grinding media is lifted and takes a shape close to the simplistic behaviour. The slurry, on the other hand, remains more or less horizontal as schematically shown in Figure 5.31 provided it has zero viscosity. The fraction of slurry in the media charge occupies the voids and therefore represents a lower volume fraction than the fraction of slurry in the pool. But as a simplifying assumption, slurry is assumed to be evenly distributed in the two aforementioned fractions. By symmetry, no power is drawn by slurry; and

therefore, media charge is the only determinant of mill power draw. In this situation, it is reasonable to consider that there is no sensible difference between dry and wet mill loads. In addition, the fraction of slurry found inside the media charge is not uniformly distributed within it and is mainly found in the lower part of the media charge. This case in itself negates the assumption that slurry is uniformly distributed within the load. To put it another way, the load in this case cannot be considered well mixed.

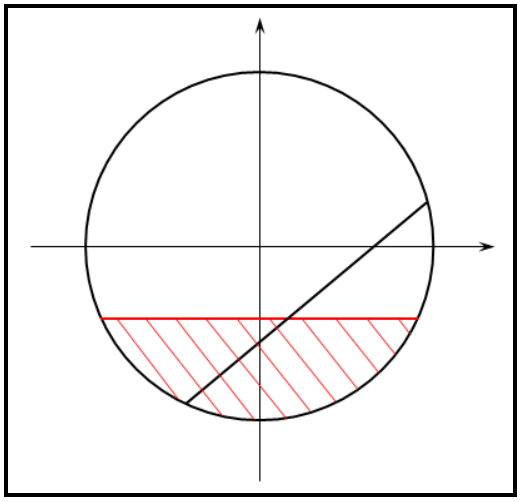

Figure 5.31 Orientation of the mill load at low speed with the idealised media charge and the horizontal slurry shaded in red

Along these lines, it is intuitively valid to assume that as speed gradually increases, the slurry adopts more and more the shape of the media charge. It is also adequate to say at this point that the load tends to become well-mixed. However, the general profile of the load becomes more crescent-shaped as advocated by Morrell (2003). Alternatively, a more simplistic proposal ascribed to Dong and Moys (2003) could be to consider that the free rolling surface of the en-masse load evolves first from linear to bilinear and finally becomes trilinear-saddle (see Figure 5.32).

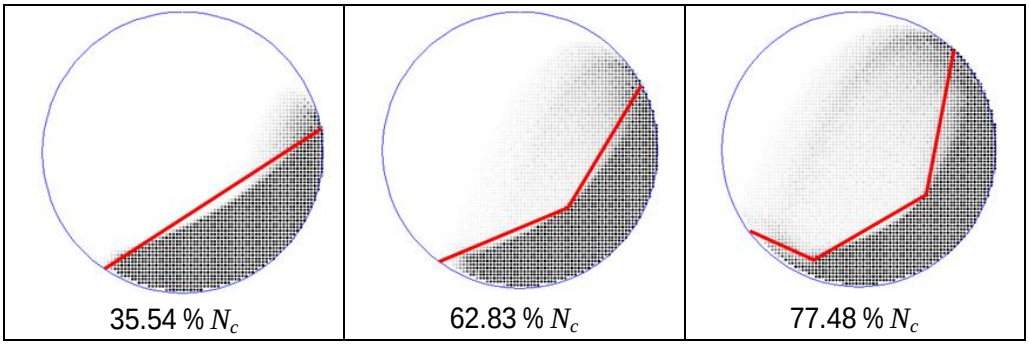

Figure 5.32 Changing profile of free rolling surface of en-masse load with mill speed

With these simplified profiles, it is understood that the volume of the slurry pool would be slightly larger than assumed with the torque-arm model in Figure 5.23. This effect combined with the change in the gravity centre of the pool should result in an over-predicted net power; which is what happened in Figure 5.24.

In an attempt to explain what happens to the load as slurry filling increases at normal speed, the slurry pooling phenomenon was discussed first; then hypotheses on slurry distribution inside the load were made.

From the observations made with the Perspex mill and the Wits pilot mill, it was concluded that slurry viscosity and mill speed have no significant effect on slurry pooling. To put this into perspective, the data from the Perspex mill has shown that the pool of slurry starts to form approximately after U = 1.2; a similar pattern was observed with the Wits pilot mill. Moreover, the pool model proposed (Equation 4.2) does not present any conclusive dependency upon viscosity or mill speed. It is therefore true to say that the pool of slurry forms and grows the same way irrespective of the level of viscosity and the volume of slurry present inside the mill. Accordingly, the same mass of slurry is held up in the media charge at all times provided U > 1.2; the remainder forms the pool.

The other observation, also important, is that the position of media charge (shoulder and toe angles) is invariably the same. This suggests to a great extent that the general motion of the media charge is not influenced by the presence of

slurry. The distribution of slurry within the media charge could presumably be the reason why power varies with speed for $0 < U \leq 1.0$ (see Figure 5.22).

Finally, the last point to be discussed is the slurry distribution within the load. There is definitely an interrelation between voids and slurry distribution within the media charge. The widely accepted assumption is to equate the static porosity to the dynamic porosity of the media charge. The reality is far complex from this to be described in simple terms. Using the technique called Positron Emission Particle Tracking (PEPT), Sichalwe *et al.* (2011) were able to reconstruct the history of a radioactively induced particle for a long period of time. In doing so, they studied the average porosity of the load under different conditions. One of their findings was that the average porosity inside the mill increases with speed. Even though the PEPT technique has a low statistical significance (one particle used), at least there is a clear evidence that seems to suggest a wide variability in porosity distribution and therefore in slurry distribution (see Figure 5.33). And based on this result, one can clearly identify a more porous region circumscribing the boundaries of the load (in red). This band becomes larger at high speed probably because of cataracting. The highly packed region is located between the eye and the ascending fraction of the load (colour-coded in blue).

Flow dynamics in this region determines somehow the percolation and flow pattern of slurry through the porous bed. Because of the high packing, it is possible that as the speed of the mill increases, the chance that all of the slurry in the core (eye) of the mill load has to reach the periphery of the mill is reduced. As a result, the time spent to percolate to the mill shell is increased. Less slurry then reaches the mill periphery; the interstices within the media charge are less occupied by slurry, resulting in reduced density along the mill shell. In addition, the turnover rate of the central region of the load (particles not cataracting, but also not being lifted by the lifters) increases. The fraction of slurry that should be percolating to the mill shell is now quickly swept up and redistributed on top of the particles in and around the eye of the load.

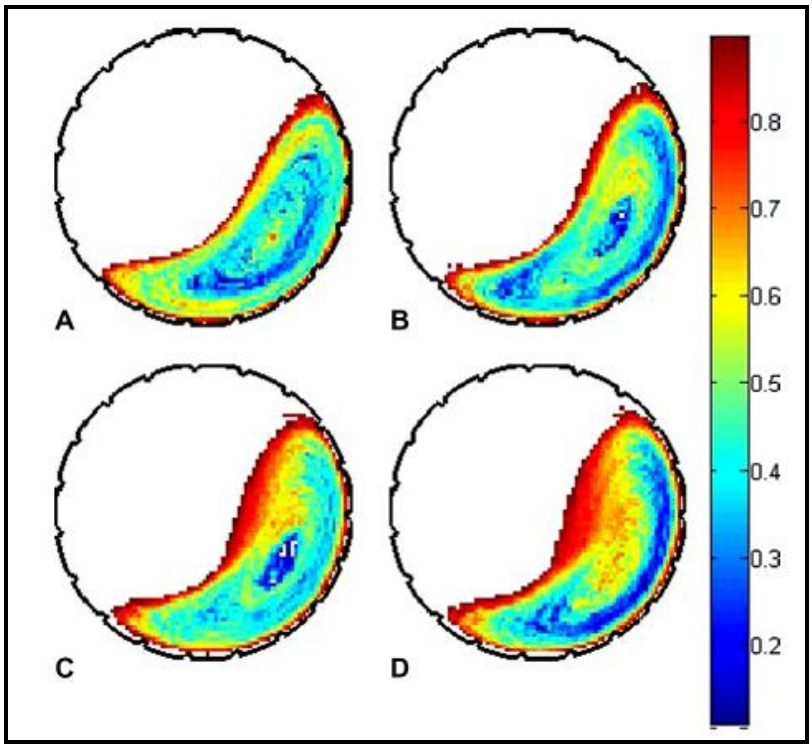

Figure 5.33 Rendered distribution of porosity inside the load using the PEPT technique at (A) 60 %, (B) 70 %, (C) 75 %, and (D) 80 % critical (after Sichalwe *et al.*, 2011)

There are of course other parameters playing a role in the milling reactor: drag forces, buoyancy, slippage between concentric layers, and lubrication are amongst the most important ones. Suffice it to say that the combination of all these complex phenomena has an impact on power usage. One possible route would be to revisit the velocity field inside the mill under a wider range of milling conditions to assert that its dynamics is governed by $z = (1 - J)^{0.4532}$ as proposed by Morrell (1993). This appears to be worthwhile because z and r_i are the only parameters varying with mill conditions in Equation 2.18. Therefore, they have a connection with the in-mill flow pattern and behaviour of the load (i.e. particles and grinding media).

5.9 Summarised findings

A non-invasive set of sensors was utilised to characterise the load behaviour of a wet ball mill under a range of speeds and slurry fillings. The first sensor which is

the proximity probe enabled an accurate determination of the position of the media charge whereas the second, that is the conductivity probe, was used to detect the position of slurry. With these two sensing devices, the mill load was comprehensively studied in terms of angular positions of the shoulder and toe for both the media charge and the slurry. The net power drawn by the mill was also recorded throughout the survey.

First, the interaction between media charge and slurry was found to be weak. To be more precise, the set of sensors used revealed that the position of the media charge is not substantially affected by the volume of slurry present. Consequently, any variation in power that could be observed in the mill should in principle be the result of slurry or anything else and not the media charge.

Motivated by this finding, a DEM simulation of the mill was initiated and results compared to those of a 'dry mill', that is, a mill loaded with grinding media only. This was aimed at obtaining a visual behaviour of the media charge that the set of on-the-shell sensors could not provide. Because the mill internal behaviour was found to be insensitive to the presence of slurry, it is understood that DEM could somehow give an idea of what was actually happening inside the mill.

A comparison of measured and simulated net power provided an indication of a match between the two set of data. This did not work out well – specifically at super-critical speeds; that is why, DEM input parameters were adjusted systematically until the shoulder and toe positions obtained from the DEM screenshots were reasonably close to the experiment ones (determined from the proximity probe). By the same token, a recent article by Pérez-Alonso and Delgadillo (2012) does not recommend a strategy whereby DEM parameters be tuned to match measured mill power. The best option force a match in load behaviour, that is, shoulder and toe of the media charge: this is what was done.

After successfully calibrating the Wits DEM simulator, an attempt to characterise load behaviour, as proposed by Dong and Moys (2003) was made. It was found

that the free-rolling surface of the media charge shifted slowly from a linear profile to a bilinear profile, as speed was increased. As a result, more cascading was observed. When the mode changed to more cataracting and centrifuging, the profile became a trilinear saddle. No trilinear-chair profiles were observed in any simulations.

As far as Morrell's description of the shape of the load is concerned, the observed pattern indicated that the crescent-shaped profile works reasonably well at low speed. But, as speed increases, the shape becomes more like two concentric and contiguous crescent layers; the outermost being longer and thinner whilst the inner one is shorter and thicker. It is believed that this departure from the initial shape proposed by Morrell *et al.* (1992) is due to the height of lifters used (25 mm) relative to ball diameter (10 mm). One of the consequences of all this was that the dynamic angle of repose of the media charge was difficult to determine. As a result, modelling the power of the dry mill suffered. Nonetheless, models by Moys (1993) and Morrell (1993) proved to be good candidates for the regression of mill power.

Second, the net power drawn by the wet mill as a function of mill speed and slurry filling was evaluated. In this instance, measurements did not agree with predictions by Morrell's model. However, there appeared to be a trend relating slurry filling to mill speed and net power, specifically for slurry filling less than unity. It is argued that slurry is responsible for this because media charge remained 'stationary' under all the conditions investigated.

Prior to this study, slurry has been acceptably assumed uniformly distributed inside the media charge and the mill load well mixed. The present findings have demonstrated that the assumption does not hold. That is why more laboratory tests need to be carried out in order to relate slurry distribution and slurry pooling to mill power.

Lastly, the slurry pooling phenomenon was studied and a testing programme to validate the pool model proposed in Chapter 4 initiated. The pool model (i.e. $\theta_{pool} = C_0.U^k$; see Equation 4.2) proved to work well even with the slurried platinum ore used here. Added to this, the pool of slurry was found to grow starting from approximately U = 1.2 and in a similar fashion irrespective of mill speed.

5.10 Conclusion

The main objective of the chapter has been to understand the phenomenon of slurry pooling in a ball mill better and the associated implication on mill power. It was found that the torque-arm model was more adequate for the analysis of the net power draw, as altered by pool volume, than any other model investigated.

Morrell's model, on the other hand, has got sufficient parameters to study slurry pooling inside the Wits pilot mill. However, a detailed analysis of results proved that the geometry of lifters used both with respect to mill diameter and ball size was very aggressive. A proper choice of mill design and operating conditions should be done in future to complete the study.

It is concluded that a programme of work should be initiated whereby mill parameters are varied within the window of applicability of Morrell's power model to elucidate the discrepancies recorded. This includes the case of media charges under-filled with slurry.

Chapter 6 Modelling the effects of pool volume on the kinetics and efficiency of milling

Abstract

In wet milling, the presence of a pool is generally the result of mill overfill. The effects of overfilling on milling kinetics have been examined. Assessment of milling efficiency has also been made.

To this end, batch grinding tests were carried out at 75 % of critical speed. A laboratory mill, filled with 20 mm balls, was used for the tests. Two levels of ball volumetric filling were considered: J = 20 and 30 %. Slurry filling U was varied from 1.5 to 3.0 with reference to 20 % ball filling. Equal masses of slurry were also used for a 30 % ball filling which made slurry filling U change accordingly. Power draw was measured throughout the experimentation.

It was found that product size distribution is a definite function of slurry filling U. Graphical analysis of the results suggests that the voids within the media charge of the mill should be completely filled with slurry without allowing the formation of the pool. This way, optimal output shall be expected.

Keywords: Batch grinding tests, Wet milling, Slurry filling, Pool volume, Milling efficiency

6.1 Introduction

Complete description of milling necessitates an accurate determination of parameters involved in the Population Balance Model (PBM). The best way of doing this is to run well planned batch tests on mono-sized feed samples using the methods known as the 'one-size-fraction method'. The problem is that the method is laborious even though good estimates are obtained.

To get around this difficulty, researchers have resorted to back-calculation methods. Although less reliable owing to the number of parameters involved, the method is preferred over its counterpart. Indeed, one has to use a feed size distribution for batch tests, then with appropriate assumptions on the milling kinetics, work out all the breakage parameters.

Due to the limited scope for the modelling aspect of this research, it was decided that the back-calculation approach assisted by N. Chimwani's laboratory work be used. In other words, some of the breakage parameters Chimwani (2012) measured for the very same ore as part of his Masters project currently underway were used as the starting point. Then, the remaining parameters were back-calculated from batch test results. This way, information on the breakage characteristics of the Platinum ore under the current experimental conditions was compiled.

To do the analysis, two industrial descriptions of milling have been employed: the size reduction curves and the grinding index. They basically consist in a quantification of the degree of size reduction and are discussed later in the chapter.

The final analysis is an attempt to apply the population balance framework to the milling operation. The adequacy of the first-order kinetics model is evaluated and further recommendations made.

6.2 Models and characterisation of ball milling

An overview of several techniques used to describe milling as a size reduction process is presented. Two sets of techniques are reviewed: graphical techniques and phenomenological techniques. The significance of the associated outputs is also succinctly discussed.

6.2.1 Graphical assessment of grinding

Bazin and Hodouin (2004) conceived a graphical method for the evaluation of size reduction by grinding that is applicable to both laboratory and industrial data. The method is easy to apply and was claimed to provide a flexible way of comparing mill performances under different conditions. It can also be used to simultaneously compare different ores.

Basically, the technique is a spatial transformation of milling from the space used to plot cumulative passing curves into what is called a 'size reduction space', i.e. a space in which product undersize is expressed as a function of feed undersize.

To grasp the essence of this graphical technique, consider Figure 6.1:

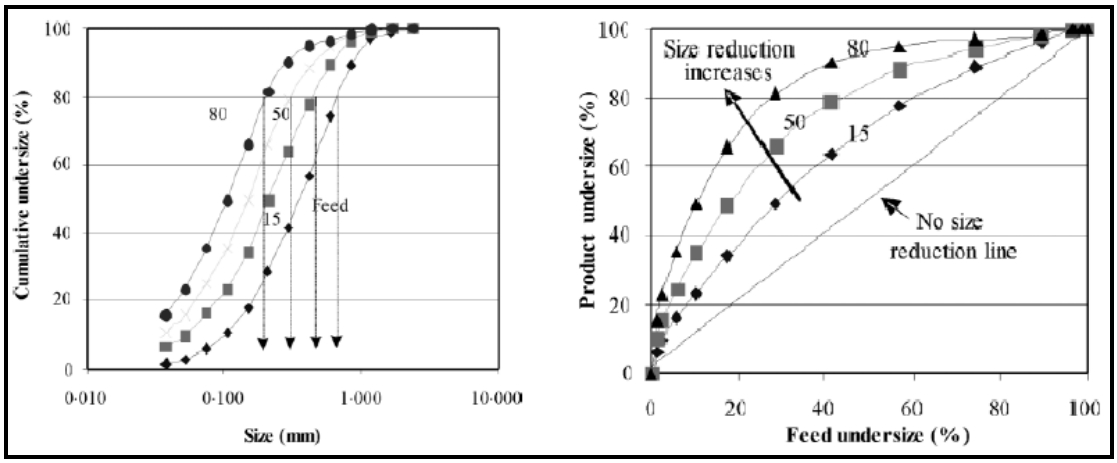

Figure 6.1 Rationale of the generation of the size reduction curves (after Bazin and Hodouin, 2004)

In order to construct the size reduction curves, several cut-off sizes are defined from the finest to the coarsest particle size. Next, fractions passing the predefined cut-off sizes are determined for different grinding times. Hence, plots

of product size passing against feed size passing and the corresponding size reduction curves are generated. As seen in Figure 6.1, it is understood that as the curve moves far away from the bisect line, so does size reduction increase.

This idea prompted the definition of a single point estimate for the size reduction process. That is why, the two researchers (Bazin and Hodouin, 2004) went on to quantifying the degree of size reduction (SR) using the area (see area in yellow in Figure 6.2) between the size reduction curve and the no-size reduction line (i.e. the bisect line):

$$SR = \left(\frac{A_0}{5000} \right) \times 100\% \qquad \textbf{(6.1)}$$

where A_0 is the area between the bisect line and the product distribution line estimated using numerical integration methods

5000 $\%^2$ represents the maximum area that can be reached.

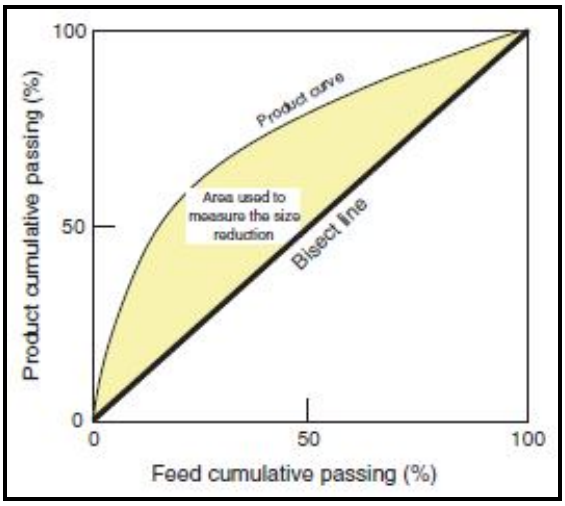

Figure 6.2 Estimation of the size reduction index
(after Bazin and Obiang, 2007)

An important concept to remember is that the size reduction curve and the size reduction index (SR) should only be used to compare the degree of milling for materials having similar feed size distributions (Bazin and Hodouin, 2004; Bazin and Obiang, 2007). In addition, data for milling can be from laboratory or industrial tests.

6.2.2 Grinding index: Definition

Many ways of describing mill performance are available. Some are different ways of expressing the same thing (Moys, 1989; Klimpel, 1982), and therefore they overlap with each other. At times, they are ambiguous from one plant to another. But, the most commonly used definition of mill performance in recent times is the Grinding Index (GI). The criterion was symbolically defined by (Shi and Napier-Munn, 2002) as:

$$GI = \left(\frac{S_D - S_F}{100 - S_F} \right) \times 100\% \qquad \textbf{(6.2)}$$

where S_D and S_F represent the percent passing a specified size respectively in the mill discharge and in the mill feed.

The interpretation of the Grinding Index should be done as follows: GI = 0 % simply signifies that there has been no size reduction whereas 100 % represents a feed 100 % coarser than the specified size that has completely been reduced to below the specified size. Bazin and Chapleau (2005) is a good example of the successful use of the GI index to describe laboratory grinding tests.

Take note: Klimpel (1982) used ‘Net production rate to less than specified size’, whilst Moys (1989) used ‘Grinding rate’, and Shi and Napier-Munn (2002) use ‘Grinding Index’ to describe the same thing.

6.2.3 Specific energy consumption and capacity of milling

An efficient milling operation is the result of good distribution of slurry within the load. Moys (1987) was able to show that viscosity is the most important factor of the in-mill dynamics of slurry. Because of the difficulty associated with the measurement of slurry distribution either in a laboratory scale or industrially, researchers have proposed alternative ways of inferring the efficiency of the milling process. The specific energy consumption has been chosen in the present thesis.

The ‘specific energy consumption’ has been defined as the amount of energy consumed per unit mass of material produced below a certain size, expressed in kWh/ton or any other equivalent units.

Sichalwe *et al.* (2011) have produced some promising results on slurry distribution. Their findings provided more insight on the link between slurry distribution and specific energy consumption. Surely, this new development will be matured as the future of more efficient milling depends on this type of endeavour.

Finally, it shall be noted that grinding is more efficient when its specific energy consumption, as defined, is low. As a result, less energy is utilised for breakage and more material of specified fineness is being produced. This has implications on the ability of the ball mill to process more feed as the capacity of the mill will increase accordingly.

6.2.4 Population balance framework

The application of the Population Balance Model (PBM) to milling is generally subject to an accurate knowledge of the selection and breakage functions. The selection function is correctly modelled when four parameters are unambiguously known. They can all be measured in the laboratory, and if this is not possible, some of them could be inferred by means of back-calculation or even looked up in peer-reviewed works. Back-calculation is discussed in the next section of the chapter.

The breakage function also contains four parameters. Likewise, their determination requires a similar treatment as the selection function. Here, at least a reasonable assumption about the normalisation of the material is used to reduce the number of parameters to three.

In short, the number of parameters needed for the application of the linear framework of the PBM to normalisable materials is seven (Equations 2.16 and

2.20); namely, a, α, μ, Λ, β, γ and Φ_j. Under special circumstances, and particularly if the material is fine enough, one might find that Λ and μ are not needed, further dropping the number of parameters to five. The nonlinear framework (Bilgili *et al.*, 2006; Capece *et al.*, 2011) is a different story altogether that has not be touched upon in the thesis.

6.2.5 Back-calculation of breakage parameters

Austin *et al.* (1984) described a comprehensive way for the determination of breakage parameters from laboratory and industrial data. The underlying principle behind the so-called 'back-calculation method' is to use initial guesses of breakage parameters for the PBM model; thereby generating several size distributions for known grinding times. After this, one after the other, the differences between measured and predicted particle size distributions for a particular grinding time are calculated. These differences are reduced by minimising the objective function or the sum of squared errors. Finally, parameters are adjusted iteratively until the sum of squared errors is minimal. The set of parameters obtained corresponding to the minimum sum of squared errors will constitute the back-calculated parameters.

As mentioned earlier, the problem with this approach is that milling kinetics has to be assumed beforehand with all the implications. To put this into perspective, the discussion has been limited to the selection function only.

It is generally assumed that milling kinetics follows the first-order model. It has been mentioned in the literature review (Chapter 2) that this is not always the case especially when a mixture of particles of different sizes is involved (Bilgili and Scarlett, 2005). Capece *et al.* (2011) offered the most elaborate back-calculation method currently available. Not only does it cover all the aspects of modelling nonlinear breakage, but it also reduces to linear breakage, advocated by Austin *et al.* (1984), should the material behave linearly.

6.3 Batch grinding results

6.3.1 Particle size distributions

Upon constitution of data of measured mass per sieve size, particle size distributions were plotted. Figure 6.3 illustrates an example of grinding kinetics obtained for a slurry filling U_0 = 1.5 and a ball filling J = 20 %.

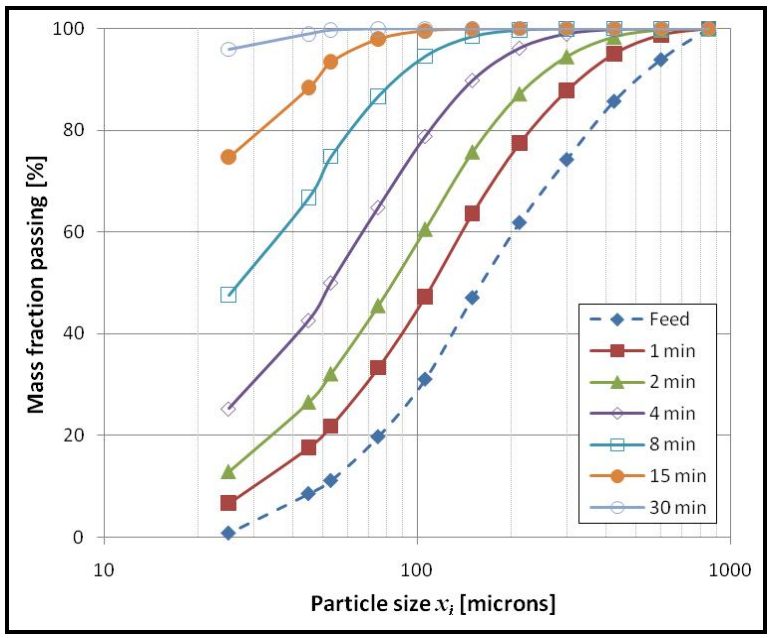

Figure 6.3 Particle size distribution obtained for 6 different grinding times: Initial slurry filling U = 1.5 and ball filling J = 20 %

Similar graphs were obtained for other grinding conditions and their data are reported in Appendix A.3.2. Note that the initial feed disappears into less than 60 microns after 30 minutes of milling; this of course varies with milling conditions as is showed later in the chapter.

6.3.2 Breakage characteristics of the UG2 ore used

As explained in Section 6.2.4, some of the selection function and breakage function parameters measured by Chimwani (2012) have been used. The decision to use his partial results was based on the fact that he used the same UG2 ore from the same batch sample supplied by the concentrator. In addition,

some of his milling conditions are close to those used in this work. The difference is he prepared mono-sized feeds and not continuous feeds. This is the main reason why the B-II method proposed by Austin *et al.* (1984) was best suited to his data. Consequently, his measured parameters are in principle more reliable.

The breakage parameters listed in Table 6.1 are those widely accepted to be material-dependent (Yekeler, 2007; Austin *et al.*, 1984); therefore, they remain constant regardless of milling conditions. These parameters were estimated using the B-II method (Austin *et al.*, 1984) that was applied on particle size distributions produced by Chimwani (2012).

***Table 6.1 UG2 ore – Breakage parameters* (after Chimwani, 2012)**

Selection function		Breakage function	
α	0.81	β	6.2
		Φ_j	0.60

The values in Table 6.1 were used to do a constrained nonlinear optimisation of the parameters remaining as variables. Computer scripts (see Appendix A.3.4) were written to regress model parameters.

6.3.3 Modelling of the sampling procedure for mill product

The modelling of the milling kinetics required size reduction information over a range of time intervals. In the present work, six time intervals were considered: 1, 2, 4, 8, 15, and 30 min. Hence, if all experiments were conducted separately for 6 time intervals and two ball levels, a total of 234 kg of ore would be required. For easy feed sample preparation, it was decided that a relatively small ore sample be used. After cone and quartering, the feed sample to the mill went through a cycle comprising batch milling for a certain time, emptying of the mill, separation of grinding media from slurry, collection of representative slurry sample for size analysis, reloading of the mill, batch milling for next time interval, and so on. Throughout the handling process, no additional water was added; only a scoop, a brush and a bucket were used.

Following the sampling procedure described in Section 3.4.4, it was evident that the collection of samples for size analysis resulted in a gradual reduction of the initial slurry filling. Table 6.2 (taken from Appendix A.3.3) exemplifies the effects of the sampling methodology used on the actual slurry filling and net power for an initial slurry filling U_0 = 2.0 and ball filling J = 20 %.

Table 6.2 Progressive reduction of slurry filling due to sampling

Time interval in min		Actual slurry filling U_i [-]	Net power draw P_{net} [Watts]
From	To		
0	1	2.000	119.4
1	2	1.964	117.7
2	4	1.937	119.1
4	8	1.907	119.3
8	15	1.866	120.7
15	30	1.830	121.7

To address the effects that the unconventional sampling method had on the data, the calculations of kinetics parameters had to accommodate the progressive reduction in mass of the solids in the mill. The PBM framework for batch milling (Equation 2.8) was revisited to include Equation 2.9 or 2.10. It was decided to use Equation 2.9 as it applies to a wider range of slurry filling (U = 0 to 2.0); in this work, slurry fillings tested ranged from 0 to 3.0.

In a sense, the approach models the sampling method by subtracting the mass of slurry collected from the total mass of slurry present in the mill at the end of each run. This way, the PBM model coincides exactly with the experiment in which the initial slurry filling is updated to the actual slurry filling after each time interval. Three Matlab® scripts (see Appendix A.3.4) were used to back-calculate the milling parameters while taking the above adjustments into account. Below is the correction factor that catered for the progressive decrease in slurry filling:

$$S_i = S_i(U_0, U_t) = a.x^{\alpha}.\left(\frac{2.80e^{-4.1U_t} + e^{-0.8U_t}}{2.80e^{-4.1U_0} + e^{-0.8U_0}}\right) \qquad \textbf{(6.3)}$$

where U_0 and U_t are the initial slurry filling and the actual slurry filling at a given grinding time t respectively.

6.4 Determination of milling efficiency

The implications of slurry pooling on the size reduction process are discussed below. Three evaluation indices have been used; namely, the specific energy consumption, the Size Reduction index (SR ratio) and the Grinding index (GI). The analysis is expected to lay the foundation for milling optimisation with slurry volume (or equally slurry filling U) as the control parameter. However, it should be noted that the progressive collection of small samples from the mill made the calculation of indices not strictly true, but consistent for comparing efficiency at given times and under different conditions.

6.4.1 Effects of pool volume on the specific energy consumption

There is apparently no clear and unanimous definition of the specific energy efficiency. Depending on the ore and the industry the meaning of the specific energy efficiency will differ. The energy in kWh required to produce a ton of fine material less than 75 microns was the adopted definition. It is understood that if the initial feed contains a certain fraction of -75 microns, then the difference in proportion between the final product and the feed should be used to calculate the kWh/ton of new -75 micron material produced. This calculation took the progressive reduction in mass of solids into account.

Table 6.3 Specific energy [kWh/t of -75 microns] for varying ball and slurry fillings

	Initial slurry filling U_0							
	J = 20 %				**J = 30 %**			
	U = 1.5	**U = 2.0**	**U = 2.5**	**U = 3.0**	**U = 1.0**	**U = 1.3**	**U = 1.7**	**U = 2.0**
1 min	4.4	3.8	3.1	2.6	4.9	4.3	3.5	3.4
2 min	4.7	4.0	3.2	2.8	5.3	4.5	3.7	3.7
4 min	5.6	4.4	3.6	3.0	6.7	5.3	4.2	4.0
8 min	7.6	5.8	4.5	3.8	10.2	7.6	5.9	5.3
15 min	12.0	8.8	7.0	5.7	17.7	12.8	10.1	8.3
30 min	22.6	17.2	13.6	10.6	33.8	25.8	20.3	15.8

Having said this, Table 6.3 summarises the specific energy found for different milling conditions. In general, for the same mass of slurry in the mill, a lower

level of balls indicates more efficient milling as less energy is required to produce a ton of fine material. And as far as slurry pooling is concerned, for any particular grinding time, the process is more energy efficient if slurry filling is high. In fact, the presence of the slurry pool reduces mill power draw, and thereby energy usage. The product size distributions were not very different and hence specific energy consumptions are expected to be low for high slurry fillings. This explains therefore the lower values observed specifically for U_0 = 3.0 and J = 20 %.

6.4.2 Effects of pool volume on the size reduction index

A similar analysis as previously performed is presented here; the difference is that Size Reduction index (see Equation 6.1) has been used.

Table 6.4 Size reduction indices for varying ball and slurry fillings

	Initial slurry filling U_0							
	J = 20 %				**J = 30 %**			
	U = 1.5	**U = 2.0**	**U = 2.5**	**U = 3.0**	**U = 1.0**	**U = 1.3**	**U = 1.7**	**U = 2.0**
1 min	24.69	22.36	21.26	20.25	29.78	27.21	26.13	22.27
2 min	41.77	38.06	36.58	34.81	49.65	45.90	43.95	37.79
4 min	62.99	59.07	57.25	55.25	72.38	68.89	66.83	59.49
8 min	81.71	79.14	77.76	75.99	88.64	86.80	85.69	80.39
15 min	91.24	90.13	89.49	88.53	94.04	93.60	93.34	91.13
30 min	94.48	94.27	94.17	93.97	94.84	94.84	94.81	94.57

The SR index does not change: small reductions in the index are observed as the size of the pool increases, but not in proportion to the increase in mass of solids in the mill. Nonetheless, SR indices are higher J = 30 %. This simply signifies that more grinding is realised at high level of media filling.

6.4.3 Effects of pool volume on the grinding index

Lastly, the grinding indix (GI) was used to assess the effects of the pool of slurry on milling. By applying Equation 6.2 to the experimental particle size distributions, it was possible to draw up Table 6.5 below.

It is understood that high GI index implies more grinding achieved. In the light of this, a 30 % media filling produces more grinding at any grinding time (see Table 6.5). In addition, the ore essentially results in total grinding after about 30 min; that is to say, the product obtained after this grinding time is less than 75 microns. A 20 % ball filling, on the other hand, will require a little bit more grinding time to achieve this. Now, for the same ball filling, if one compares slurry fillings, it is apparent that GI indices are high for lower slurry fillings. This suggests that the production of fines (that is, less than 75 microns) is accelerated for lower slurry filling irrespective of the volume of media considered.

Table 6.5 Grinding indices for varying ball and slurry fillings

	Initial slurry filling U_0							
	J = 20 %				**J = 30 %**			
	U = 1.5	**U = 2.0**	**U = 2.5**	**U = 3.0**	**U = 1.0**	**U = 1.3**	**U = 1.7**	**U = 2.0**
1 min	17.01	15.29	14.46	13.71	22.65	20.47	19.44	15.85
2 min	32.18	28.94	27.42	26.01	42.14	38.28	36.23	29.80
4 min	56.25	51.66	49.30	47.09	69.93	65.16	62.62	53.11
8 min	83.46	79.41	77.10	74.67	93.31	90.62	88.99	81.23
15 min	97.48	96.01	95.03	93.86	99.65	99.30	99.02	96.81
30 min	99.96	99.91	99.85	99.76	100	100	100	99.95

To sum up, it appears that it is desirable to consider a high level of ball filling and a reasonably low level of slurry filling in order to expect fast production of fines. The latter statement is motivated by the fact that under the following conditions, J = 30 % and U_0 = 1.0, the GI index has recorded the higher values compared to all other grinding times considered.

6.5 Effects of pool volume on milling kinetics

In order to evaluate the effects of slurry filling and pool volume on milling kinetics, results of the particle size analysis were used to calculate the outstanding breakage parameters; namely, a and γ. These are later compared to one another to see if there is any detectable trend in their variation.

The application of the hypothesis of 'normalisable ore' for the breakage function must be considered. Recall that the hypothesis does not always hold true for every ore but presents the advantage of reducing the number of parameters to be back-calculated.

6.5.1 Normalisation of breakage function

The data produced by Chimwani (2012) was used to assess the adequacy of normalisation of the breakage function. In section 2.3.3, the definition of the breakage function as well as the notion of normalisation of breakage function were presented. Recall that a material is said to be 'normalisable' if the breakage function parameter Φ_j (see Equation 2.7) is not a function of the parent size j but a constant. This explicitly implies that plots of cumulative breakage functions ($B_{i,j}$) for a reduced particle size should fall on top of each other regardless of their corresponding milling conditions. This should be true because the material breaks the same way when normalisable.

As far as the UG2 ore is concerned, Chimwani (2012) found that his results presented a wide variation in breakage function ($B_{i,j}$) values. But, because there were no discernable pattern between $B_{i,j}$ values and experimental conditions, he was forced to assume the ore to be normalisable. He then calculated the average breakage parameters for the ore (see Table 6.1) using the 'normalisable ore' assumption.

Following Chimwani's argument, the UG2 ore was considered normalisable. And because of the limited scope of the present analysis, it was further chosen to model the Selection function using Equation (6.3). Consequently, two parameters were to be search in the PBM framework: a and γ. The first is a Selection function parameter whereas the second is a Breakage function one.

6.5.2 Population balance analysis

As highlighted in Section 6.2.5, the different particle size distributions were used to back-calculate the selection function parameters on a case basis. The underlying assumptions were as follows:

- Milling follows a first-order kinetics model (see Equation 2.2)
- The ore is normalisable so that the breakage model proposed by Chimwani (2012) can be used (see Table 6.1)
- The ore is fine enough not to experience abnormal breakage; as a result, Equation (2.4) applies
- The progressive loss of slurry during sampling is accommodated using the correction factor in Equation (6.3).

The parameter search was therefore reduced to finding two parameters; namely, a and γ. To solve the multi-variable problem subject to constraints, the approach was to find a and γ for known α, β and Φ_j, by minimising the objective function $\sum\left[P_{expt}(t) - P_{model}(t)\right]^2$. The measured and predicted particle size distributions $P_{expt}(t)$ and $P_{model}(t)$ were in fact compared in an iterative process until the sum of their squared differences was the lowest. The Matlab® scripts in Appendix A.3.4 were used to perform in a structured way the numerical search of the PBM parameters.

The optimised parameters found are presented in Table 6.6 below. One can clearly see that a-values for both 20 and 30 % ball filling decrease with increasing slurry filling U and pool volume. They are significantly higher for 20 % ball filling; it is possibly due to larger values of slurry filling U.

Table 6.6 PBM parameters found

J = 20 %			J = 30 %		
U_0	a	γ	U_0	a	γ
1.5	1.71	0.97	**1.0**	2.32	0.81
2.0	1.51	0.96	**1.3**	2.09	0.80
2.5	1.42	0.96	**1.7**	1.97	0.79
3.0	1.34	0.94	**2.0**	1.58	0.85

Values of γ, on the one hand, seem to remain fairly constant at 1.00 for 20 % ball filling with a slight variation. And on the other hand, they initially decrease before increasing for U_0 = 3.0 and 30 % ball filling.

Curve-fitted and measured size distributions were also compared to assess the adequacy of the proposed linear breakage model. Visual inspection indicates that the linear PBM framework works well especially at short grinding times (1 and 2 min), but predicts slightly coarser products at times longer than 2 min. It is understood that because of the progressive collection of slurry samples, the actual slurry filling was gradually decreasing (see Table 6.2). Therefore, curve-fitted distributions should be seen merely as what particle size distributions were supposed to be if there was no loss of slurry as a result of sampling. From this point of view, Figure 6.4 actually suggests that the product should be finer at low slurry filling. This view is also supported by Figure 6.5 in which low slurry filling (i.e. U_0 = 1.5) yields finer product. Other than that, the curve fitting exercise has been successfully implemented on the laboratory results.

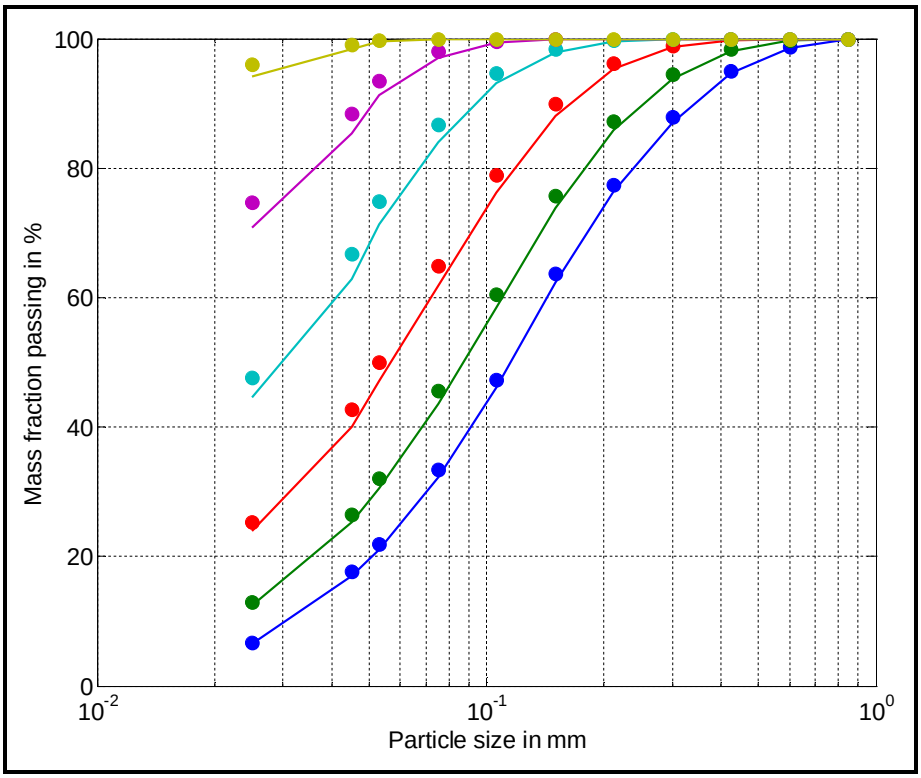

Figure 6.4 Model fit obtained through back-calculation for J = 20 % and U_0 = 1.5

The physical meaning of the milling parameters in Table 6.6 is illustrated in Figure 6.5. The graph shows the effect of slurry volume on particle size distribution for 3 selected grinding times: 2, 8, and 30 min. Starting off with the same feed, a finer product is seen for low slurry filling where the pool is either absent or small. In the process, a-value has gone from 1.71 and 1.34; in other words, the grinding rate has decreased with the presence of the pool. Recall that parameter a represents the grinding rate of the ore of size 1 mm.

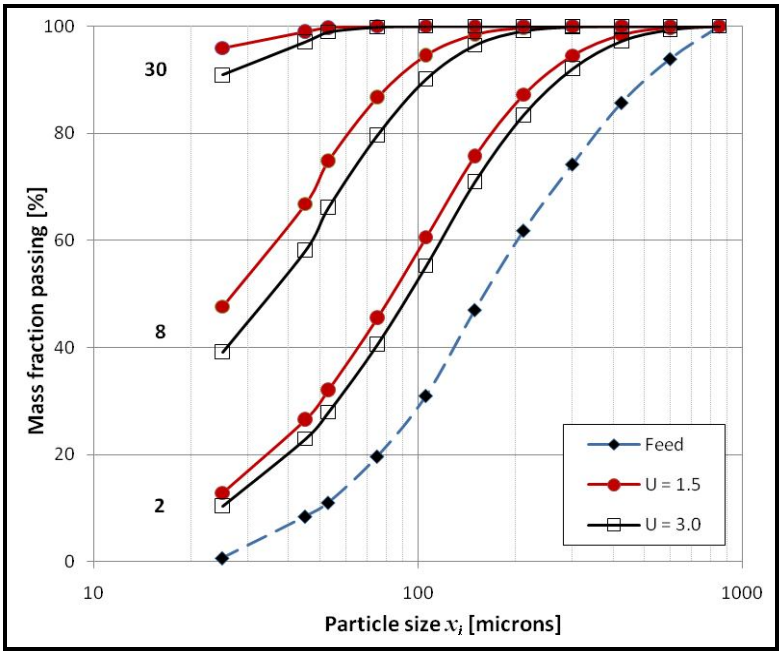

Figure 6.5 Effects of slurry filling on particle size distribution.
Milling conditions: J = 20 % and 75 % N_c

With reference to the definition of milling parameter a, one can state that an increase in ball filling results in an increase of milling rate. That is to say, loading the mill with more grinding media accelerates the rate of disappearance of particles in classes close to 1 mm (in this case 850 microns). This however does not necessarily translate into more fines being produced. On the contrary, parameter γ regulates the production of fines. Again, Table 6.6 indicates a clear decrease in γ-values for an increase in ball filling. Austin *et al.* (1984) argued that product size distribution is sensitive to the value of γ. They also added that in general, softer materials would have lower values of γ as compared to harder

materials. The low value found (i.e. γ = 0.81) would therefore imply that more effective breakage action is experienced in the case of J = 30 % which results in high production of fines. The physical interpretation agrees well with Figure 6.5.

6.6 Optimisation of the milling process

6.6.1 Influence of slurry filling on net power draw of the mill

Before attempting to optimise milling with slurry volume as the optimisation variable, the variation of mill power with slurry filling has been considered. To this end, the mill was run under the conditions listed in Table 3.5; only a 20 % ball filling was tested. Furthermore, water and a 65 % mass solids concentration of UG2 slurried ore were used. The key objective of this set of tests was to see whether the laboratory batch mill was sensitive to the presence of a pool and to what extent.

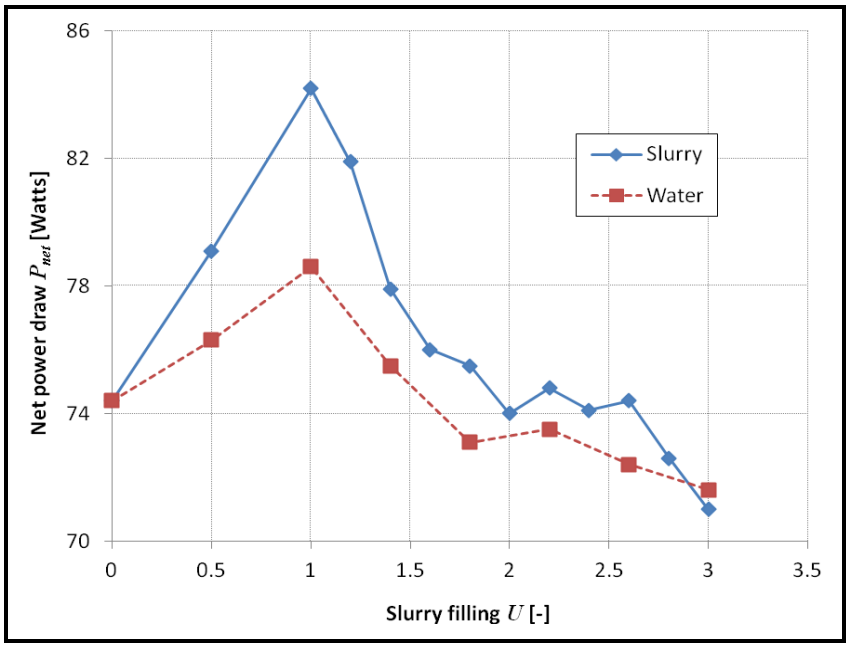

Figure 6.6 Effects of slurry filling on mill power for slurry and water (see Appendix A.4)

What came out of the initiative (i.e. Figure 6.6) is a trend consistent with Figure 5.18 on page 166: net power draw initially increases with slurry filling, and then gradually drops as the pool forms for slurry fillings greater than unity. On top of

that, the maximum and minimum powers recorded are approximately 84 and 71 Watts for the ore. When only water was used, the net power changed these figures to 79 and 72 Watts and in both cases, maximum power roughly represents an increase of about 10 % in power relative to their respective minimum powers recorded.

The last observation was that net power draw with water as the fluid is lower compared to what is recorded with slurry. This can be attributed to the difference in density between the two solutions. But the gap almost disappears at higher slurry filling owing to the much higher weight that the pool of UG2 slurry exerts to counterbalance the load.

6.6.2 Process optimisation: The way forward

The optimisation of the milling process should be seen as a trade-off that needs to be made between throughput and energy utilisation. To be more precise, the best combination of milling conditions should enable a fast production of fine materials (less than 75 microns) while ensuring a reasonably low power draw.

It then becomes apparent that the solution is to look for high SR and GI indices and low specific energy consumption (kWh/t). From Tables 6.3 through 6.5, one can deduce the following:

- SR index indicates that the optimal mill should be highly loaded with media (that is, high J)
- GI index also supports a high ball filling but with a low level of slurry (low U)
- The Specific energy consumption advocates a high slurry filling U.

With all the above, it appears that a high volume of balls with just enough slurry to fill the interstices (that is, U = 1.0) is the way forward. This has been clearly recommended by Latchireddi and Morrell (2003) who found that “the condition required for the best grinding efficiency corresponds to the maximum slurry hold-up that can be held in grinding media without a pool”. As to whether this

should be close to U = 1.0, only an accurate knowledge of the dynamic porosity and the associated porosity distribution of the media charge can be used to solve the problem. That is why the work by Sichalwe *et al.* (2011) becomes more relevant in moving towards more efficient mills.

6.7 Significance of results

The aim of the chapter was to model milling within the Population Balance framework and to evaluate the implications of slurry pooling on the kinetics and efficiency of milling.

To start off, the modelling side of milling was discussed. In general, the assumptions made in the definition of the PBM framework (see Section 6.5.1) worked reasonably well. As a result, PBM parameters involved were successfully back-calculated and possible trends identified.

First of all, back-calculated parameters reported in Table 6.7 indicate a decrease in *a*-values with slurry filling, but also consistently low values of a for low ball filling. If one remembers that parameter a could be interpreted as the rate of disappearance of particles of size 1 mm, it becomes clear that size reduction is more pronounced at high ball volumetric fillings and low pool volume. That is to say, the absence of a pool of slurry encourages fast grinding. Secondly, parameter γ lies around 0.96 and 0.80 respectively for J = 20 and 30 %. Physically speaking, parameter γ characterises the relative amount of fines produced from the breakage of the top size class. It therefore directly relates to the efficiency of the grinding process. A higher value of γ implies coarser progeny fragments the size of which is close to that of the parent material broken in this case at a slow rate. By contrast, a lower value of γ would imply more effective breakage action with high production of fines (Makokha and Moys, 2006). It follows that high ball and slurry fillings tend to produce a finer material except for J = 30 % and U_0 = 3.0 where the behaviour seems to indicate that an excess of slurry is undesirable.

If this is truly the case and not an outlier, one would say that a high ball filling combined with a slurry filling leading to a very small pool will give rise to a finer product as shown in Figure 6.7.

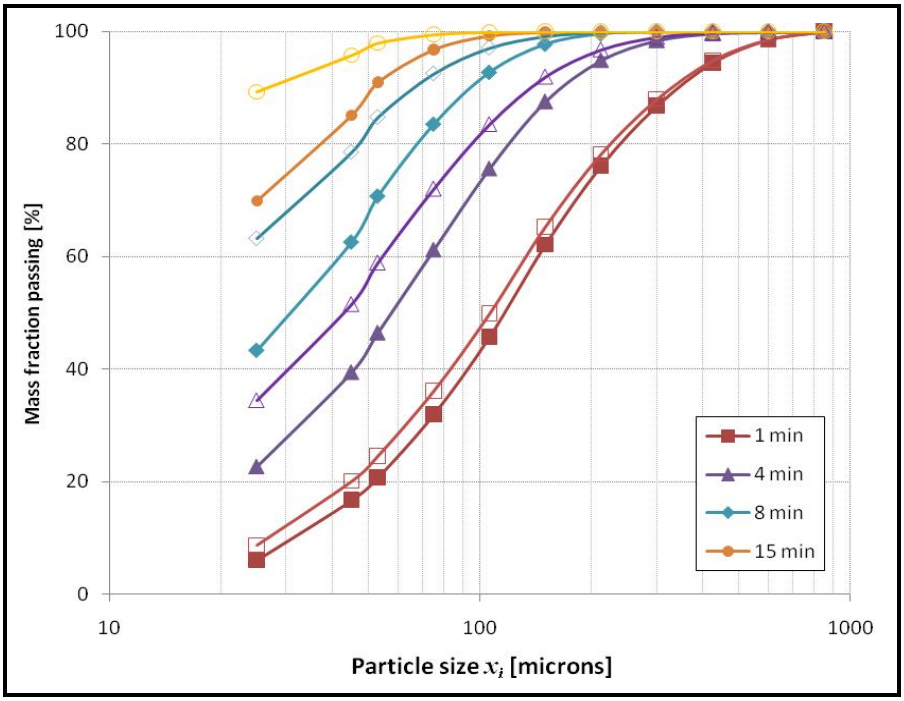

Figure 6.7 Effects of ball volumetric filling on particle size distribution. The mass of slurry corresponds to U_0 = 2.0 for J = 20 %. Filled and open data points represent J = 20 % and 30 % respectively

This is further confirmed by Figure 6.8 in which the difference in the effects of ball filling is reduced for a slurry filling U_0 = 3.0. Moreover, this observation is consistent with the value of γ = 0.85 listed in Table 6.7. It is therefore possible that the increase in γ is ascribed to the large pool volume resulting from the high slurry volumetric filling U.

These findings have paved the way for optimising the milling process. Three indicators have been utilised in this regard; namely, the Size Reduction ratio (SR), the Grinding Index (GI), and the Specific energy consumption.

The first two indicators (SR and GI) led to the same conclusion, that is, higher ball filling produces a high production of fines. However, SR indices in Table 6.4

are inconclusive for the optimal level of slurry because the difference in SR values becomes smaller and smaller as grinding progresses.

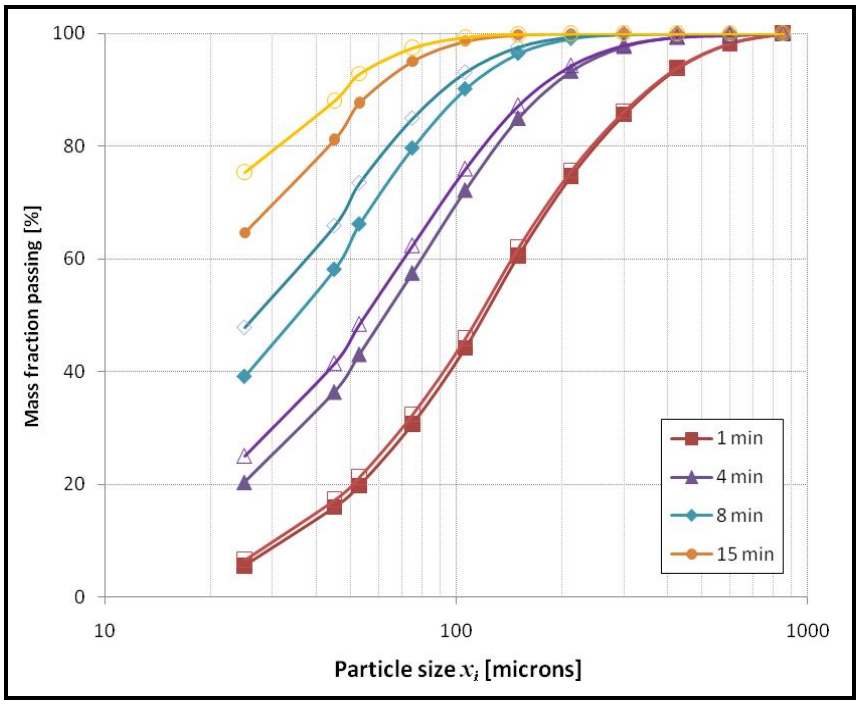

Figure 6.8 Reduction in the production of fines due to the ball filling effect at U_0 = 3.0: Filled data points (J = 20 %) and open data points (J = 30 %)

By contrast, besides supporting a highly loaded mill with grinding media, the GI index indicates that a low level of slurry incurs a high production of fines; and thereby, more grinding. It is clear that GI index does not only advise on the optimal level of grinding media, but also has a say on slurry filling unlike the SR ratio.

Finally, the specific energy consumption indicates high volumes of slurry and low volumes of grinding balls. Though surprising at first, one has to understand that the adopted definition of the specific energy consumption is all about energy necessary for the production of fines. In chapter 5, it has been demonstrated that power drawn – and therefore energy consumed – decreases with slurry filling for U > 1.0. The laboratory mill is no different to this observation (see Figure 6.6). As such, the larger the pool of slurry the better it is for energy consumption. By the same token, mill power is low for a small mass of grinding

media (see Figure 2.5). However, the production of fines suffers as a result of all the above.

The problem arises with the fact that the specific energy consumption should be seen as a ratio between energy consumed and mass of fines produced. So, in order to expect efficient milling, either the energy consumed is to be low or a large amount of fines is to be produced. Now based on the fracture mechanics of rocks, it is accepted that more energy is needed for more breakage. It is therefore possible that the drop in energy consumption due to the pool does not translate into a proportionate reduction of fine material produced; thus, the seemingly contradictory findings. That is why one can use either a combination of low ball filling and high slurry filling to expect a more efficient usage of the input energy (that is a high production of fines for a given amount of energy) or a combination of high ball filling and low slurry filling for more rapid grinding regardless of the amount of energy used. In the first case a pool of slurry will be present with less grinding but good usage of energy available. In the second case, however, there will be no pool of slurry, but conversely more grinding will be recorded for a poor usage of energy.

6.8 Conclusion

Modelling milling has been successfully implemented for the past few decades using the population balance framework. It has fundamentally witnessed little improvements. The latest development has been the addition of nonlinear effects of breakage. There is no evident indication that the present case study was nonlinear, because the linear Population Balance Model worked well for the ball and slurry fillings investigated. The back-calculation method was successfully used to characterise and interpret milling as a function of ball and slurry fillings.

To turn to milling optimisation, it has been explained that there was a difficulty in reconciling results found with the three indicators: SR ratio, GI, and specific

energy consumption. In fact, from concordant results obtained using SR and GI, it would be argued that high ball filling tends to guarantee more optimal milling. The dynamics of slurry filling, on the other hand, seems to be not well understood, especially when the specific energy consumption is involved. The most important point to make is that the specific energy consumption should rather be seen as an indicator of the performance of milling and not as a criterion for optimisation. In this regard, orientations given by SR and GI should weigh more in the decision-making process. Needless to say that SR can only be used when similar feed sizes are compared for different milling conditions.

It becomes evident that depending on the objectives fixed by the Process Engineer and the indicator used, different conclusions could be reached. The complexity of the objectives may be impossible to handle with these indices. And the real issue is that Size Reduction index, Grinding Index, and Specific Energy Consumption are all based on the definition of a cut-off size, in this case 75 microns. Where a product is required to be within a specified size window, -75 +10 microns for instance, these indicators are not so readily applicable and lose any physical meaning. Because of this limitation, a novel optimisation approach is presented in the next chapter.

Chapter 7 Attainable region analysis of the effects of pool volume on milling

Abstract

The first-order milling kinetics can be regarded as the basis for the analogy between milling and chemical reactions. The hypothesis has worked reasonably well over the years with significant consequences. Amongst the most important ones is the introduction of the Attainable Region method in the analysis of milling. Admittedly, the technique brings nothing more than a different, and yet more flexible, tool for the graphical analysis of data. Most interesting is the fact that the analysis makes it possible to determine whether mixing is required to achieve concentrations unobtainable by milling alone.

With the aforementioned, the data from the previous chapter has been revisited using the Attainable Region technique. Initially, the technique needed to be modified in order to be used also for feed size distributions. After satisfactory manipulation, the graphical analysis was initiated.

It was found that the rate of production of fines tends to remain unchanged for constant slurry-to-ball filling ratio. Over-filling the mill with slurry did result in a less efficient operation. In fact, results suggested that for a more efficient operation it is imperative to fill the voids between media with slurry without producing a pool. But it is equally important to consider higher ball fillings.

Keywords: Attainable region, Energy consumption, Wet milling, Process optimisation

7.1 Introduction

Comminution is the term used to describe processes that reduce particle size. It is found in a wide range of applications including the minerals, pharmaceutical and chemical industries. As far as minerals industry is concerned, comminution is reckoned to be one of the pivotal processes. In particular, milling is the option of choice despite being a significant consumer of energy. Considerable focus has therefore been placed upon improving its energy efficiency.

In chapter 6, wet milling was studied through extensive modelling. A framework describing the process was built. Several metrics were used to assess the impact that slurry filling and pool volume have on milling efficiency. As result, more insight on the relevance of a pool of slurry was gained and the way forward for future work proposed.

In 1997, Glasser and Hilderbrandt proposed a new way of analysing chemical engineering reactor systems. The proposed analysis has been tested successfully on both laboratory and pilot scale. The method known as the Attainable Region (AR) analysis looks at reactor synthesis holistically. Chemical reactions are described using graphs, while looking at the fundamental processes that take place in the system, rather than the pieces of equipment themselves. The plotted graphs are interpreted in terms of both optimised operations required and a flowsheet. To put it simply, it is possible to tell from the results graphically produced with the AR method how to synthesize the process and the reactors. The advantage of the method resides in that it is model-free; that is to say, no model is required to do the analysis but only knowledge of how the fundamental processes transform the feed to product.

Attempts to extend the method to comminution have been satisfactorily undertaken. And even if the method has still got a long way to go and has not yet found large acceptance in the minerals industry, encouraging results have been produced. For instance, the comminution path required to efficiently achieve a given product size distribution has been deduced. Laboratory batch grinding

tests have validated the predictions with interesting insights on the process than any other analysis technique has been able to describe so far (Khumalo, 2007).

The method looks at comminution operations, and ball milling in particular, as chemical reactions. Consequently, milling parameters such as mill geometry, mill speed, liner profile, ball size, ball size distribution were not considered. With this in mind, the novel technique has been considered with the objective of further weighing options that can unlock the full potential of ball milling. This could open doorways to better control and optimisation of milling through the pool volume.
To this end, the AR technique has been succinctly reviewed and a way of extending its capabilities to natural feeds proposed. Then, the strategy resented by Metzger *et al.* (2009) was used to study the effect of the slurry filling and pool volume on milling for given product size and energy constraint. It was expected from the AR method to provide complementary findings to corroborate conclusions reached in chapter 6.

7.2 The attainable region method and ball milling

The Attainable Region (AR) methodology was primarily intended for chemical process optimisation. In this environment, variables used to characterise processes are, in general but not always, concentrations of both reactants and products of interest. In milling, however, one has to deal with particles breaking into different sizes. The analogy between chemical reactions and milling has naturally enabled researchers to treat size classes as chemical species. In doing so, the feed size class is considered as the reactant and the undersized classes as the products of the breakage reaction.

In the following sections, the major steps necessary to the optimisation of ball milling in particular and the problems that arise with the analogy chemical reaction – milling are presented.

7.2.1 State variables in comminution

In reaction engineering, state variables can be defined as the variables which characterise the output of the system and that are sufficient to completely describe its kinetics as well as the objective function at hand (Khumalo *et al.*, 2006). It is therefore understood that the concentrations of both the reactants and the target products constitute the state variables. But, the choice of reactants and products to be considered is dictated by the optimisation problem.

As far as ball milling is concerned, the span of particle sizes is generally divided into size classes following a $\sqrt{2}$ sequence. It follows that the mass fraction in each size class or in a combination of several consecutive size classes can be a state variable. The source of unbroken material, i.e. the feed class, is always a state variable because without it there is no broken product. This is easy to appreciate when the feed is mono-sized. Natural feeds, unfortunately, come as a size distribution and not as a single sized material. As such, the definition of the feed class poses a problem. The AR tool that has been used on one-fraction feeds (Khumalo, 2007; Khumalo *et al.*, 2006 – 2008; Metzger *et al.*, 2009) so far. Adjustments are to be made accordingly to accommodate natural feeds. Section 7.3.2 proposes one amongst many ways of dealing with this issue; that is, the definition of size classes for a feed size distribution in an AR context.

7.2.2 Mass fraction space

On an AR point of view, there can in principle be as many mass fractions one wishes for the size classes. But because the AR method is essentially a graphical exercise, it is easier to plot and interpret systems limited to two or three state variables. If there is no other choice, the analysis can be extended to higher dimensional spaces: this is probably true for some complex chemical reactions requiring detailed investigation. In milling, however, it generally seems

convenient enough to only use the feed class (if easy to define) and the desired product size (dictated by downstream processes).

7.2.3 Process optimisation

The aim of any comminution circuit is to produce material of a desired particle size distribution at a minimum operational cost. This consideration can vary with the industry under consideration. In the pharmaceutical industry, cost is not regarded as an issue owing to the fact that human life cannot be priced. As for the diamond industry, even though the milling process is governed by cost, the final product is such a well rated commodity that cost can at times be overlooked.

The truth is that downstream processes and expected final products generally determine what the objective function imbedded in the process optimisation should be.

7.3 Attainable region plots

Metzger *et al.* (2007) argued that the application of the attainable region technique entails four principal steps:

1. Choice of the fundamental processes
2. Choice of the state variables
3. Construction of the Region
4. Finding the optimum

Khumalo *et al.* (2006) identified three fundamental processes that take place in comminution systems: breakage, mixing and separation. The programme of experimentation adopted in the present thesis involved a simple batch reactor. However, depending on the state variables adopted, the attainable region

analysis might show that the addition of mixing to breakage using a ball mill could be beneficial to the entire comminution arrangement.

With this, the next logical step should be to choose the state variables which describe the breakage process and characterise the objective function that we are trying to optimise. The choice of these state variables is discussed in the next section.

7.3.1 Definition of size classes

The system investigated encompasses a Platinum ore that is to be ground to less than 75 microns for further downstream processes involving flotation. The first step in this process is to focus on the key variables for optimisation referred to as the state variables. Since the general goal of mineral processing operations is to maximise the production of the finely sized species, the combined mass fraction in size classes below 75 microns is the first variable to include in the analysis. The other obvious one is the source of material that becomes fine, that is, the feed size class. And depending on the practical interest, one can include some of the intermediate size classes. But it should be clearly emphasised that each situation will be addressed differently before moving forward.

A situation whereby the product size class of interest is defined between 75 and 25 microns can be considered. The reason for the lower limit is that in the processing plant of interest the milled product is sent to a bank of flotation cells. With this in mind, it is understood that the production of particles less than 10 microns (both material of value and gangue) should be limited to a strict minimum as they may be mechanically entrained in the froth phase. As a result, the flotation process becomes inefficient. However, the minimum of size in the stack of sieves used for particle size analysis was 25 microns. That is the reason why it was decided to use a product size class spanning from 75 to 25 microns.

7.3.2 Choice of state variables

As mentioned earlier, it has been difficult to define in a simple manner the feed size class. This is because a feed size distribution is statistically speaking a cumulative frequency distribution. Consequently, a good descriptor of the size distribution would be either the arithmetic average or the mode.

Feed size distributions have traditionally been described in terms of mass fraction passing a certain size. This way of defining the feed statistically signifies the 50th or 80th percentile of the feed size distribution is used as a representative of the feed size. They are termed d_{50} and d_{80} respectively.

To apply the AR methodology to natural feed size distributions, consider a feed given by $F(x_i)$ with F the cumulative distribution function of the feed and the sieve sizes $1 \leq i \leq 11$. The number 11 reported in the definition of i caters for the 11 data points making up the feed size distribution shown in Figure 7.1 below. After this, state variables are intuitively chosen as follows:

(i) Size class m_1 defined as the mass fraction of material of size x retained by screen of size d_{80}.

(ii) Size class m_2 is the mass fraction of particles of size x falling between d_{80} and d_{50}.

(iii) Size class m_3 is the mass fraction of particles of size x between d_{50} and x_8.

(iv) The fines size class m_4 is defined as the mass fraction of material passing screen size x_8; that is to say, passing 75 microns.

An important remark is that in view of the changing mass of solids, mass of size fraction (i.e. mass fraction multiplied by mass of solids) could be used as the state variables. The problem is that different slurry fillings cannot be compared; that is why, the analysis has been simplified by assuming no loss of slurry during sampling (see Section 6.3.3).

From the above, it is clear that the mass fraction space to use in the AR analysis will be three-dimensional, that is, $\boldsymbol{(m_1, m_2, m_4)}$.

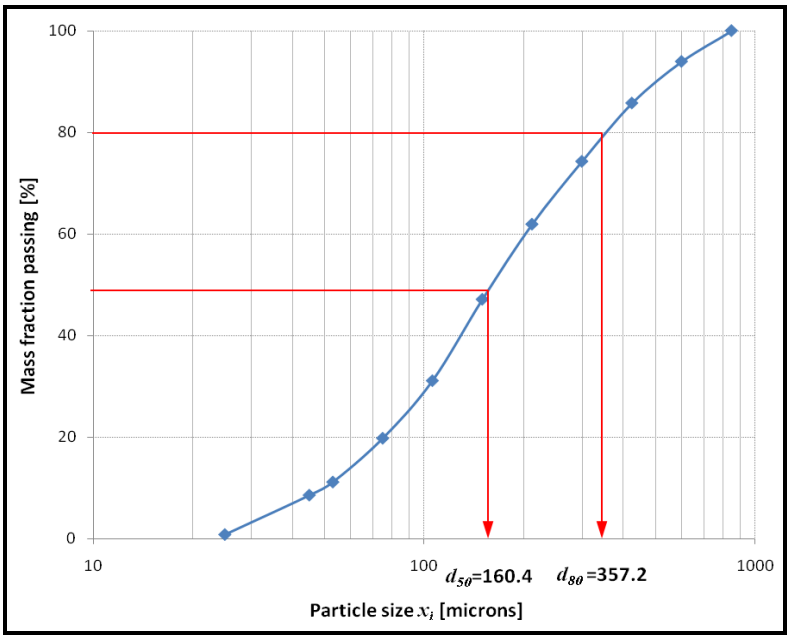

Figure 7.1 Size distribution of the feed used

With the feed size distribution used (see Figure 7.1), the cut-off sizes were found to be 357.2; 160.4 and 75 microns. And based on this, the four size classes that have been been used are defined below:

m_1: x < 357.2 microns

m_2: 357.2 ≤ x < 160.4 microns

m_3: 160.4 ≤ x < 75 microns

m_4: x < 75 microns

It is worth mentioning that the mass fractions in class m_3 can be determined by mass balance once the three other classes are unambiguously known.

The other case study considered was to combine all the mass fractions above 75 microns into M_1; then M_2 contained materials between 75 and 25 microns; and finally M_3, the sink fraction, was the mass fraction of material less than 25 microns. This arrangement is interesting because it takes the downstream process into account. Consequently, the analysis looks at milling more holistically by incorporating constraints proper to flotation. Here, unlike in the first case, M_1 was plotted against M_2 only with M_3 that can be calculated through mass balance.

7.3.3 Construction of the 3D attainable region plot

In order to construct the AR paths, the kinetics of the state variables (i.e. m_1, m_2 and m_4) were first plotted. Then, their respective mass fractions were read off for successive grinding times.

Once the data was represented in this way, the construction of the Attainable Region path could start. With the state variables defined a priori, the three mass fractions corresponding to the state variables were located in a three dimensional space (Figure 7.2). After that, the different data points are connected successively following the order of precedence given by the batch grinding time. The line chart obtained stands for the AR path.

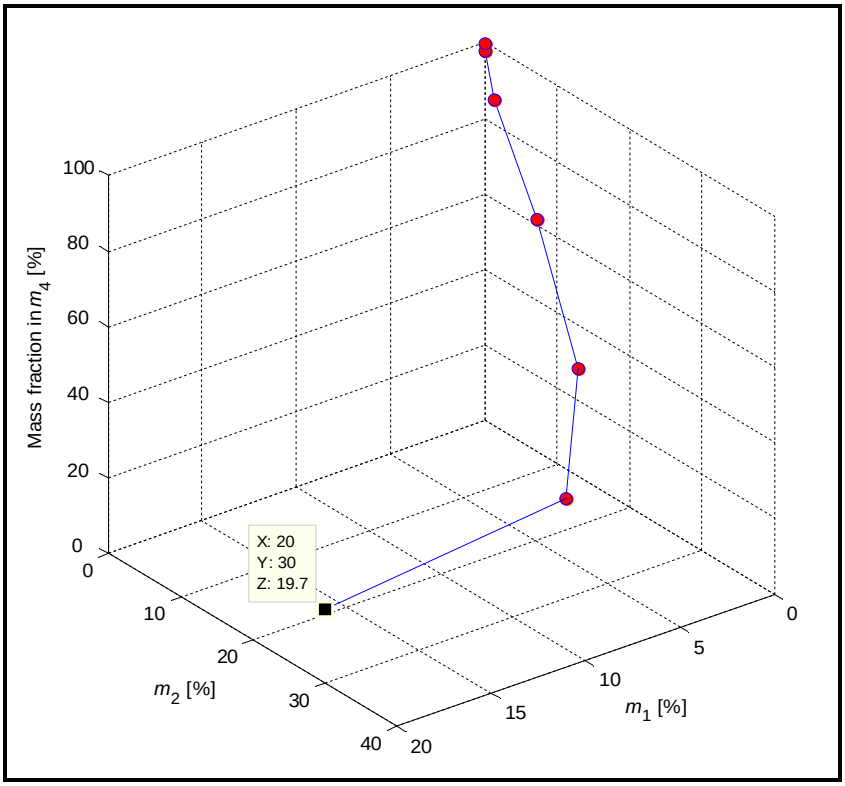

Figure 7.2 Illustration of a 3D attainable region path

In Figure 7.2, note the datatip pinned to the feed the coordinates of which read as m_1 = 20; m_2 = 30 and m_4 = 19.7 %. Despite the difficulty associated with interpreting 3D space, one can see that grinding proceeds from the datatip to the upper corner of the 3D cube.

The last step is to reduce the 3D cube to a 2D representation using Monge's transformation that forms the basis of descriptive geometry. The manner in which the transformation was done is epitomised in Figure 7.3 below.

To put it in simple terms, the AR path is projected respectively onto the three planes making up the trihedron (see Figure 7.3). Next, the base and the right-hand planes are rotated downwards and towards the right respectively. During these rotations, their intersections with the left-hand plane are used as hinges. The rotations are complete when the two planes coincide with the left-hand plane. Finally, the spatial exercise is done; it has in the process enabled the transformation of the three dimensional AR path into a two-dimensional one.

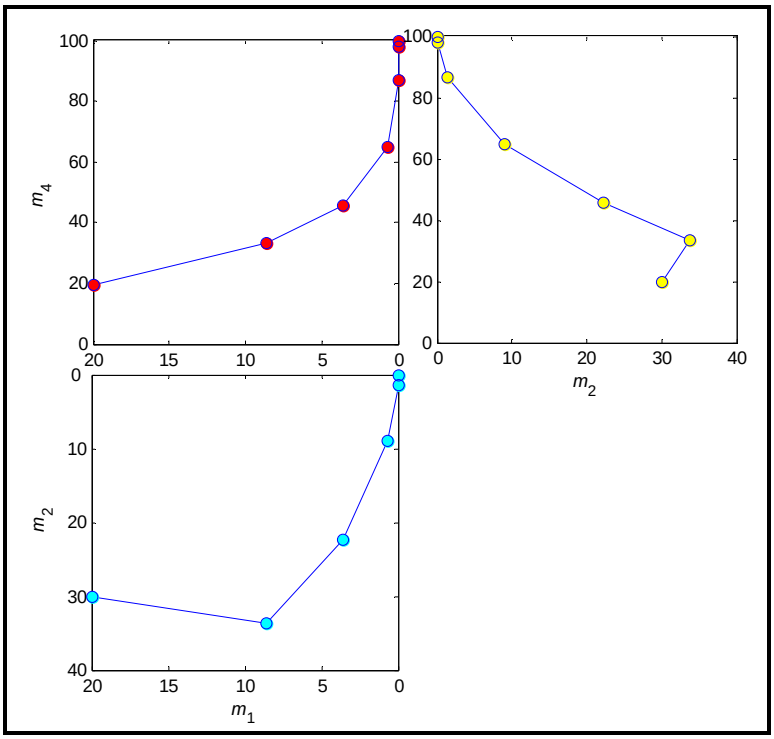

Figure 7.3 Spatial mapping of the AR path showed in Figure 7.2 using Monge's transformation

Monge's transformation has simplified the understanding of the AR path and, at the same time, made it possible to take advantage of the power of the Attainable Region technique. For one, it becomes easier to compare several runs carried out under different conditions. And two, with limited effort one can tell whether the optimisation conditions will be met or not.

7.3.4 Attainable region plots of milling under flotation constraints

Attention is now turned to the AR path following the second setup where M_1 and M_2 are used as state variables. Recall that M_1 is the mass fraction of material retained on a 75 microns sieve whereas M_2 is the mass fraction passing 75 microns but retained on 25 microns.

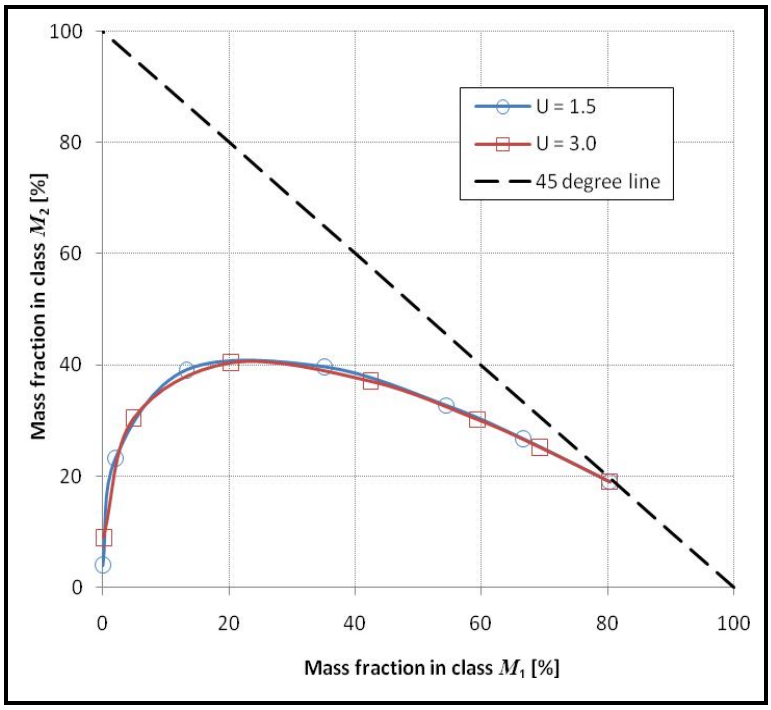

Figure 7.4 Attainable region paths under flotation constraints.
Effects of slurry filling: Ball filling J = 20 % and 75 % N_c

Figure 7.4 illustrates the type of AR profile that is produced with these new state variables. Reading the graph from right to left, one can see that milling starts off with 80.30 % M_1 and 18.97 % M_2; then, as the process proceeds, M_1 quickly decreases while the production of M_2 slowly increases until about 40 % before sharply dropping down to null. At this point, the product becomes finer than 25 microns. Another thing is the convexity of the AR paths, which signifies that there will be no benefit in including some form of mixing around the mill. As a result, an open circuit should in principle be considered as the best option when configuring the flowsheet. However, it is still possible to try and produce more M_2 by recycling the unbroken M_1 in the product back into the feed. In this case,

only a simulation of the closed milling circuit or a full sampling campaign at pilot level can tell how far this would be valid. The final comment is that slurry filling does not change the grinding path significantly, but it would be interesting to see whether energy consumption will show any difference. This is what the next section deals with: doing an in-depth analysis of milling with the help of the AR technique in order to ultimately optimise the process.

7.4 Results

7.4.1 Definition of the objective function

As mentioned earlier, the AR approach is novel in that it is a graphical technique the focus of which is to plot the desired size fraction against the feed. It has been successfully used to solve optimisation and process synthesis problems for reactor systems and has been extended to processes incorporating breakage, mixing and separation.

The backbone of the AR method is a clear definition of the classes to be considered, especially if a feed size distribution is concerned. Immediately after this is done (refer to Section 7.3.2), the objective function that sustains the essence of the optimisation process can be tackled. In our case, two things are to be borne in mind: the energy consumption and the production of fine particles (that is, class m_4 or M_2).

With the above, the objective function can be formulated as follows: “What would be the best (and perhaps the ultimate) milling conditions that will produce as much material in class m_4 (or class M_2) as possible from a feed size distribution while maintaining the input energy at a minimum”.

One comment though, the production of fines is dictated by the milling process itself whilst the input energy is controlled by the pool volume as shown in chapter 5. The only thing the AR analysis does is to provide orientations as to

how best should this objective be achieved. That is why, besides the (m_1, m_2, m_4) space, the (M_1, M_2) space presented in Section 7.3.2 above has also been studied.

7.4.2 Effects of slurry filling and pool volume

It has been demonstrated in chapters 4 and 5 that there is a definite relationship between slurry filling and pool volume. That is the reason why the two denominations are used interchangeably in the presentation of results.

In the next paragraph, it is shown how slurry filling shapes the AR paths for a 20 % ball filling. For ease of interpretation, only the two extreme slurry filling (namely, U_0 = 1.5 and U_0 = 3.0) are reported in Figure 7.5.

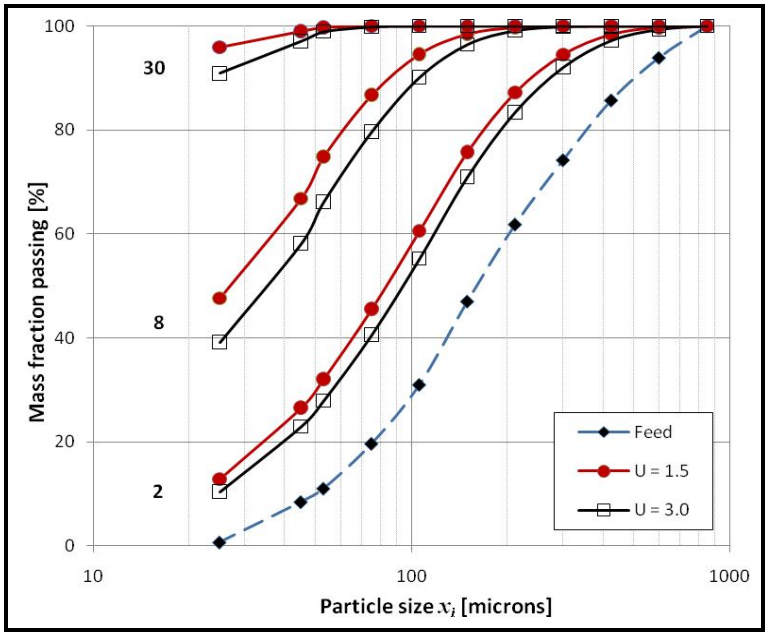

Figure 7.5 Effects of slurry filling on particle size distributions for a 20 % ball filling and two slurry fillings: U_0 = 1.5 and U_0 = 3.0

The general comment that can be made here is that Figure 7.5 indicates a finer product for an under-filled media charge, that is U_0 = 1.5; but as demonstrated in chapter 5, this comes with an increase in mill power and energy consumption.

The above set of data has also been plotted in a 3D mass fraction space. One can clearly see that there is a slightly differentiated behaviour between the two profiles considered (U_0 = 1.5 and U_0 = 3.0). However, the difficulty in visualising such as plot has led to using the mapped version of the AR paths.

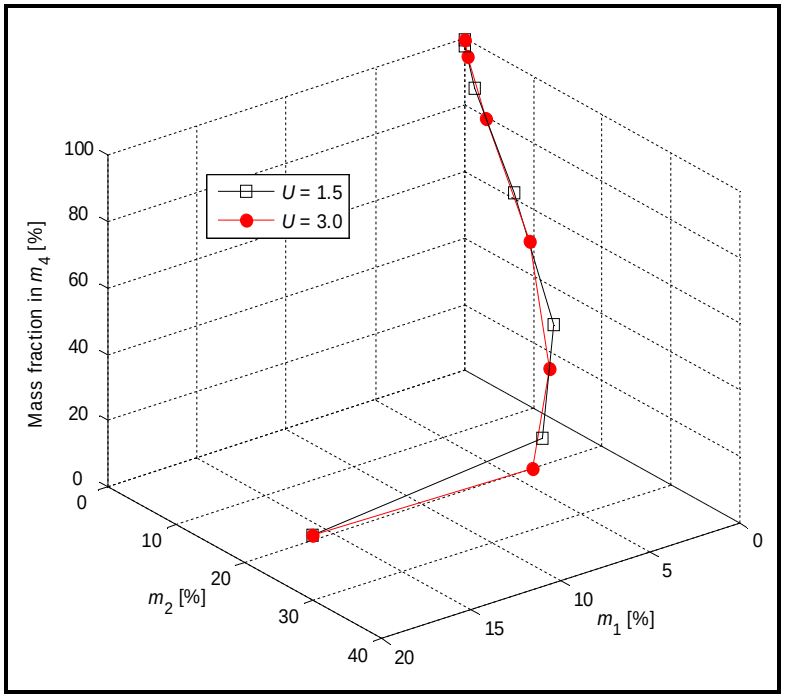

Figure 7.6 AR paths plotted for a 20 % ball filling and two different levels of slurry filling: U_0 = 1.5 and U_0 = 3.0

The next paragraphs report what has been learned from the mapped AR paths as far as the effect of slurry filling is concerned.

Owing to improved interpretation the two dimensional system offers, one can confidently say that class m_1 is the main source of material reporting to class m_4. The reason behind this statement is that a decrease in m_1 leads to a quite proportionate increase in m_4 (see subplot 1 in the upper left region of Figure 7.7). Subplots 2 (upper right) and 3 (lower left) initially increase then drop with a monotonic increase in m_4. This suggests that the initial increase in m_2 is due to the formation and accumulation of m_2 broken from m_1.

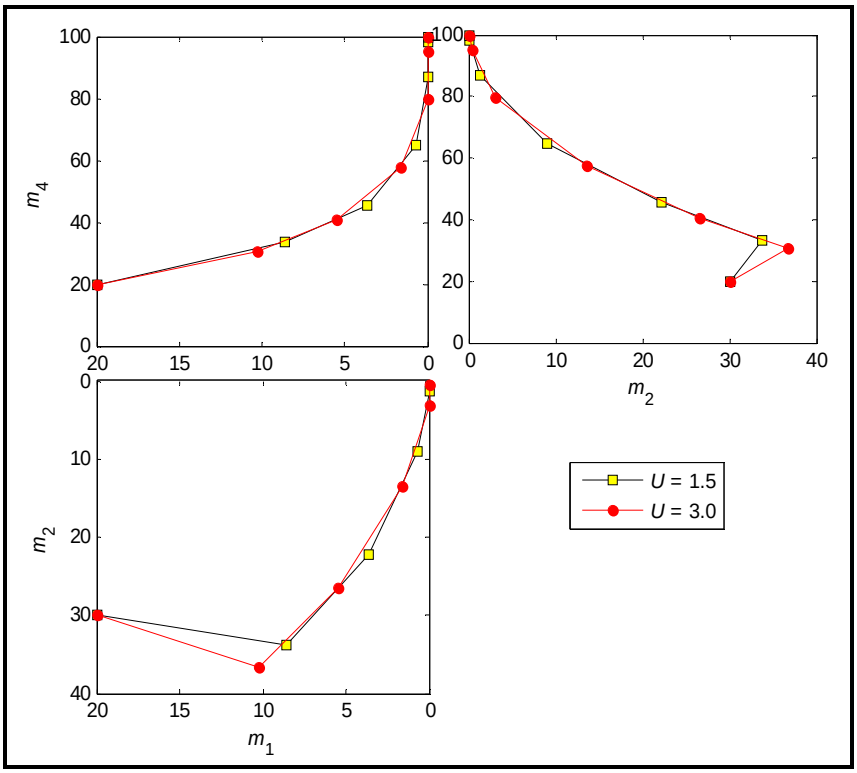

Figure 7.7 Effects of slurry filling – Mapped AR paths

Overall, the mapped AR plots seem to indicate that despite the different kinetics, the grinding paths are similar irrespective of the level of slurry U. Nonetheless, a further increase in slurry volume makes the material in class m_1 to report more rapidly to class m_4 with a temporary build-up in class m_2 observed (see subplot 3) at short grinding times. In other words, an increase in slurry filling causes an important accumulation of material in m_2 before its disappearance into m_4 after further grinding. This implies that higher levels of slurry volume would necessitate longer grinding times.

Interestingly, the very same set of data graphed in the (M_1, M_2) space shows that the AR paths are somehow superimposed, and therefore similar (see Figure 7.4 above). The noticeable difference is that the data points do not coincide; implying different regimes of energy consumption. This aspect is where it is believed that the optimisation strategy should be looked for.

7.4.3 Effects of ball filling

The partial conclusion reached from the previous analysis is that slurry filling and pool volume have only affected the AR paths at shorter grinding times. Using the same procedure as before, the effects of ball filling J on the AR paths has been examined. From a laboratory point of view, only two ball fillings were considered and consequently the two are reported; namely, J = 20 % and 30 %.

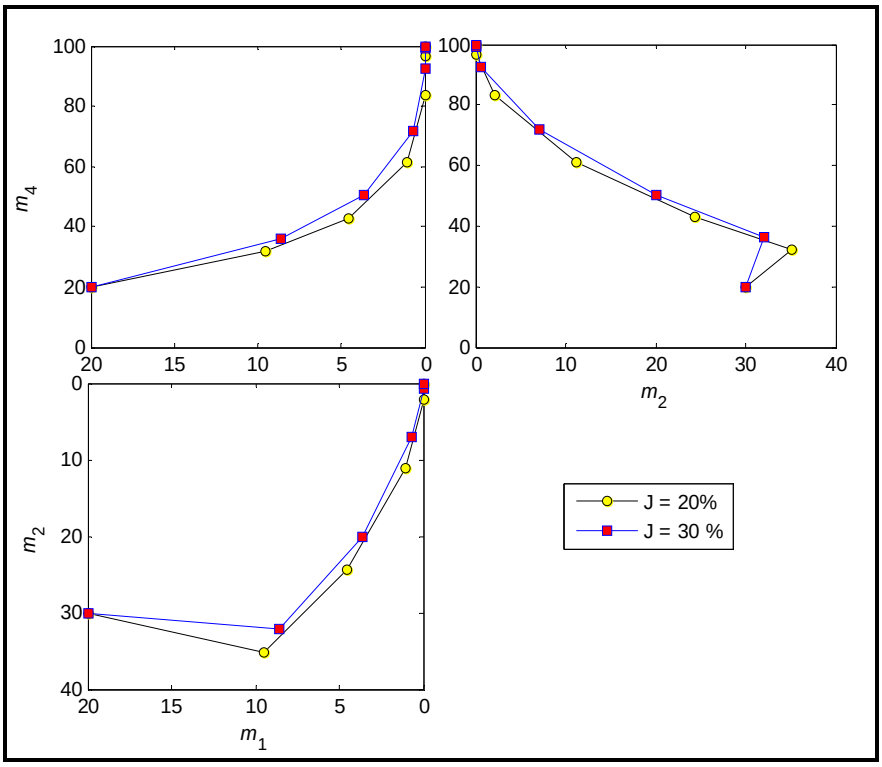

Figure 7.8 Effects of ball filling on mapped AR paths for the same mass of slurry, that is, U_0 = 2.0 with respect to J = 20 %

Here again, similar comments can be made as in the previous section. In addition, a larger media filling accelerates the production of fine material m_4. This is seen in Figure 7.8, subplot 1, where one AR path (J = 30 %) is consistently above the other.

It can also be seen that subplot 1 contains more information than the other two. With AR paths generated using only classes m_1 and m_4, it is still possible to do a reasonable analysis of milling, compare different scenarios, and reach similar conclusions as with mapped AR paths.

The second space, that is (M_1, M_2), on the other hand, gives more valuable information compared to its counterpart. Figure 7.9 readily suggests that a 20 % ball filling favours a relatively high production of M_2. It appears that a less loaded mill could be the way forward. This observation is consistent with findings published by Metzger (2011) showing that at high speeds, the optimum of class M_2 is generally experienced at low ball fillings.

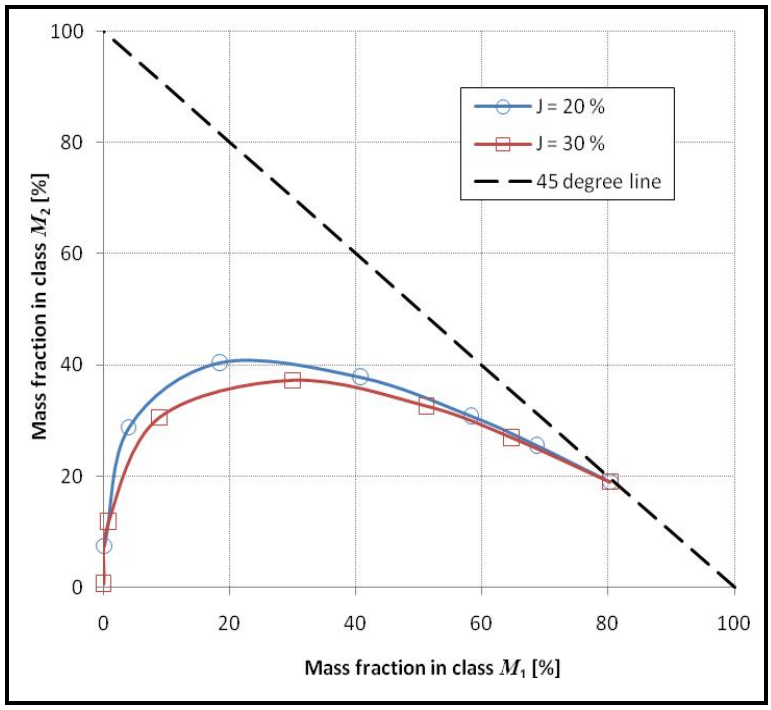

Figure 7.9 Attainable region paths under flotation constraints.
Effects of ball filling: Slurry filling U_0 = 2.5 and 75 % N_c

Lastly, it is valid to say that the ideal AR path that guarantees full optimisation should follow the 45 degree line from the low right end to the high left end before plunging down along the M_2 axis. Any path close to this is desirable: a 20 % ball filling does just that!

7.4.4 Energy consumption of milling

In mineral processing, the general problem of efficient and effective milling includes the prevention of under- or over-grinding, the minimisation of energy

consumption and the control of grinding (in this thesis, through the pool volume).

An important aspect of the AR analysis is that besides the AR paths, one can also look at the milling kinetics profiles. These are graphs showing the evolution of mass fractions in each class with the energy consumed.

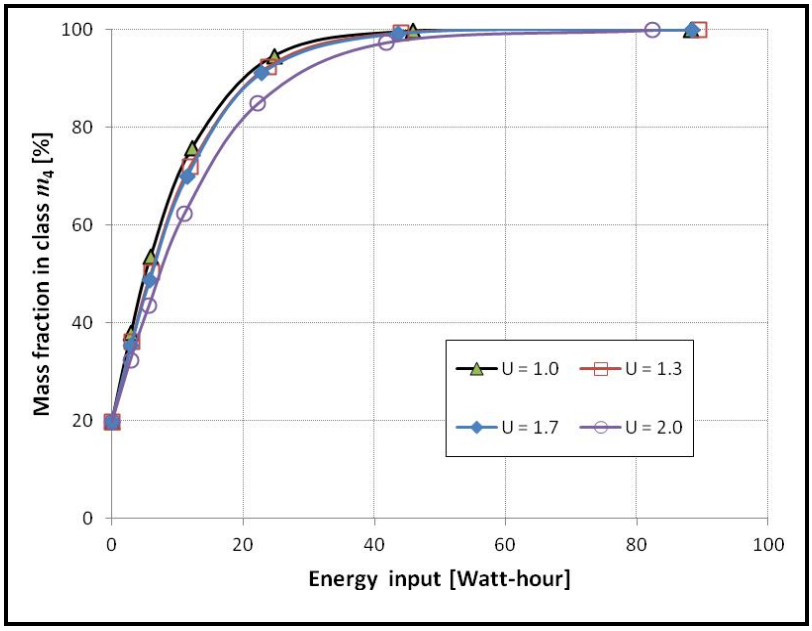

Figure 7.10 Production of fines for different slurry volumes and J = 30 %

Investigating the effects of pool volume on energy consumed reveals that the same energy transferred to the mill is not effectively used in a similar fashion. Simply put, for a 20 Watt-hours of energy input, the production of fines drops from approximately 90 to 80 % when slurry filling U jumps progressively from 1.5 to 3.0 (see Figure 7.10). Note here that slurry filling U is reported with reference to J = 20 %; as a result, the actual fillings U corresponding to J = 30 % increase from 1.0 to 2.0.

In general, energy usage for the production of fines is reasonably the same when $U \leq 2.5$ with a more differentiated trend for U_0 = 3.0 (see Figure 7.10). Varying ball filling essentially exhibits similar trends as shown in Figure 7.11.

Furthermore, the data in Figure 7.11 implies that grinding is done in a similar way regardless of the volume of media loaded in the mill.

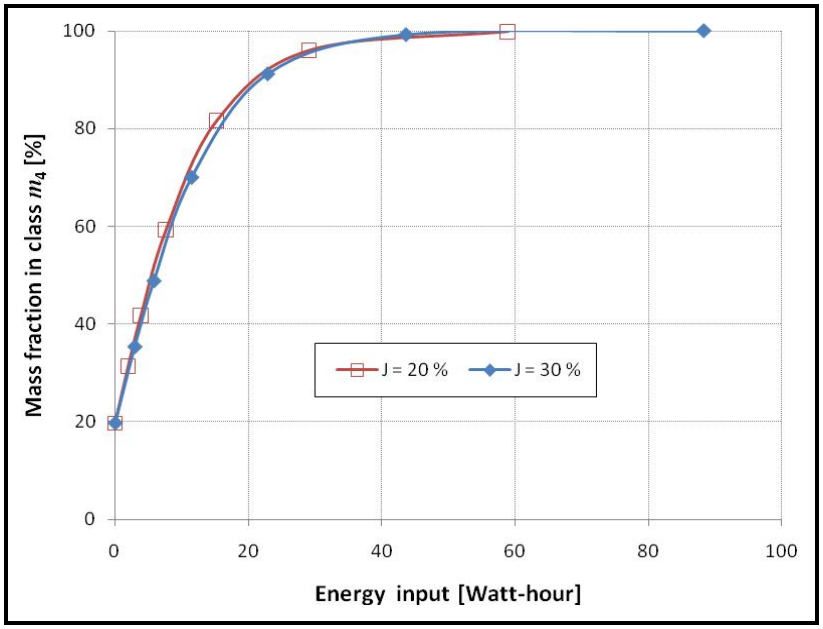

Figure 7.11 Production of fines for two different ball fillings and a slurry filling U_0 = 2.5 with J = 20 % as the basis

In the next figure, the same data as in Figure 7.10 was plotted with M_2 as the state variable. The addition of flotation constraints in view of downstream operations led to identical energy consumption for the range of slurry fillings investigated until maximum production of M_2 ($\cong$ 40 %) is reached.

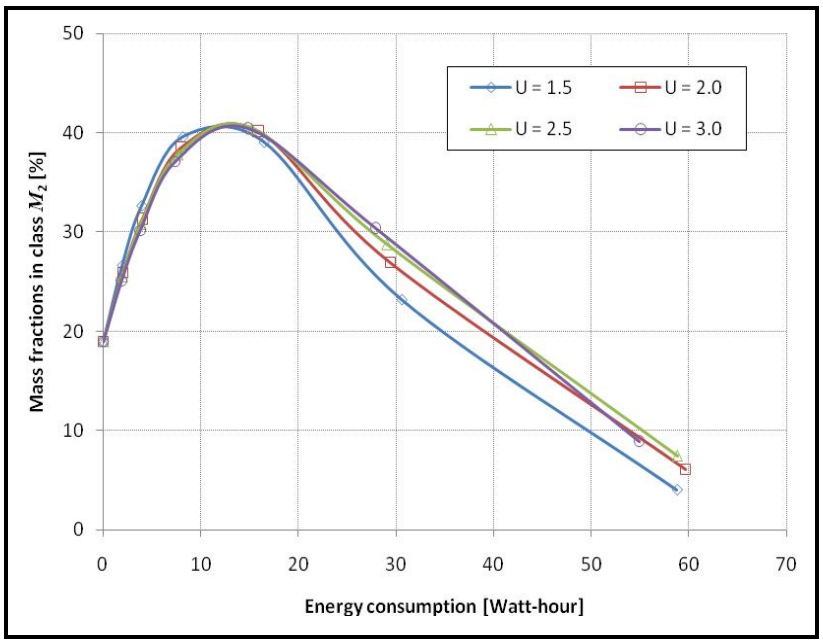

Figure 7.12 Effects of slurry filling on energy consumption. Grinding conditions: J = 20 % and 75 % N_c

Even if Figure 7.13 has limited value, a slurry filling U_0 = 1.5 seems to be the best reaching the optimal the fastest with a little bit more that 10 Watt-hours.

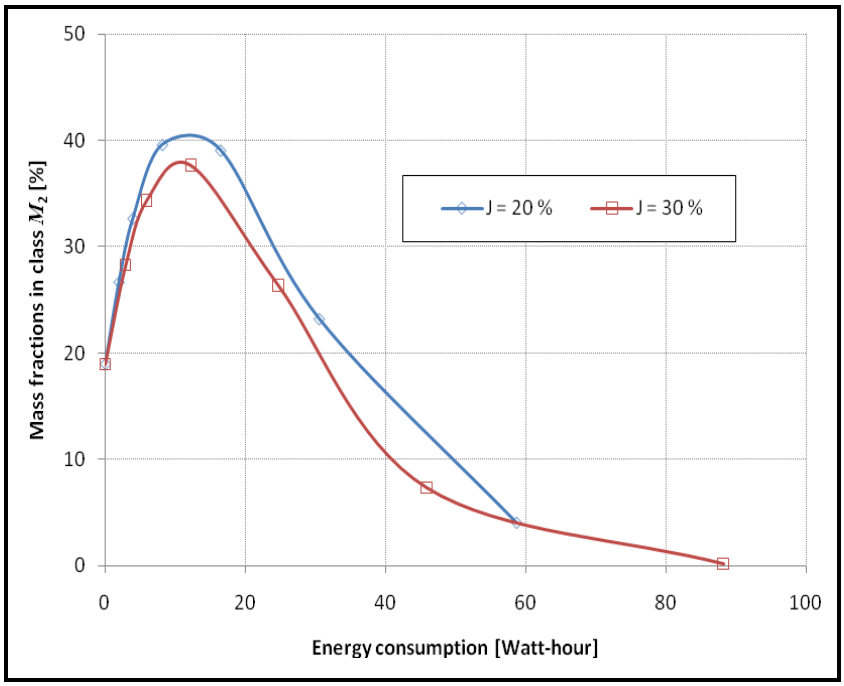

Figure 7.13 Effects of ball filling on energy consumption.
Grinding conditions: U_0 = 1.5 and 75 % N_c

The effect of ball filling, unlike what Figure 7.11 suggested, indicates that for the same amount of energy expended, a 20 % ball filling is marginally more efficient that a ball filling J = 30 %. This finding complements well Figure 7.9 discussed above.

7.5 Interpretation of results and discussion

Interpreting AR plots in a 2D system is generally straightforward and pleasant providing the physics of the process and its graphical representation are well understood. In the present chapter, however, it has been necessary to rethink the generation and interpretation of AR plots.

To put this into perspective and in an attempt to clarify what is happening, consider Figure 7.7. Subplot 1 (upper left graph) presents the AR paths plotted

between the upper feed size class m_1 and the desired product m_4. The general upwards concavity in AR paths suggests that mixing is to be considered as the production of fines is one of the objectives. In other words, the flowsheet should be configured in such a way that some fraction of the feed is ground finer than required, then mixed to the remaining fraction of fresh feed to constitute a product of specified fineness. However, care should be taken to separate out the material in class m_1 from the rest before bypassing the feed.

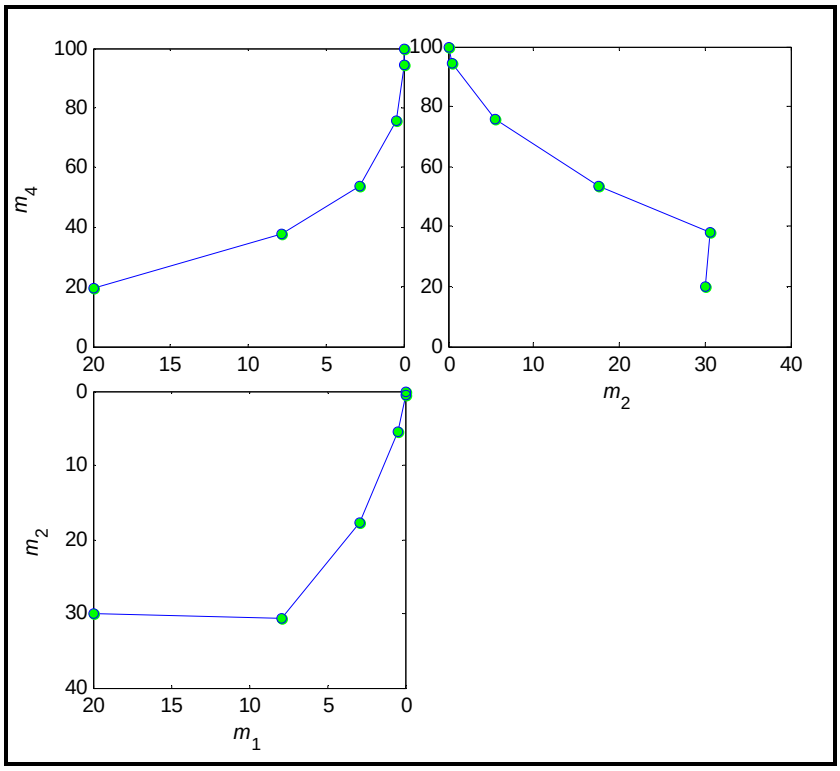

Figure 7.14 Improved AR path for U_0 = 1.0 and J = 30 %

In terms of efficiency, one would say that the most efficient path is achieved when the AR path is a straight line joining the feed (lower data point in subplot 1) to the finely ground product (upper data point in subplot 1). Having said that, one realises that there is a possibility to extend the AR region above the AR paths in Figure 7.7, subplot 1. Be that as it may, subplot 3 indicates that before reporting to class m_4, particles in class m_1 break down and build up into class m_2. The reason for this accumulation could be a lower disappearance of particles in class m_2. The process should rather run in such a way that materials in classes m_1,

m_2 and m_3 are converted into m_4 with less to no transition in intermediate classes. It follows that the closer to unity slurry filling is ($U \cong 1.0$), the better the process becomes. This is supported by Figure 7.14 in which slurry filling U_0 = 1.0 for a 30 % ball filling.

Indeed, Figure 7.14, subplot 2 shows that by just filling the interstices between media (U_0 = 1.0), the AR path comes much closer to becoming a straight line. At the same time, in subplot 3, the starting mass fraction (i.e. 30 % m_1) remains slightly unchanged before decreasing and eventually disappearing. The consequence of all the above would ultimately be a more efficient milling and a linear AR path in subplot 1.

The real question though would be: What is the optimal slurry level U that the mill has to carry? This investigation has shown that a slurry level close to U_0 = 1.0 is the answer. It appears as if the presence of a pool is not to be desired to ensure efficient milling. Concordant works (Latchireddi and Morrell, 2003; Tangsathitkulchai, 2003) also reached the same conclusion.

As far as ball filling is concerned, Figure 7.7 shows that for the same mass of slurry, a higher ball filling is more efficient. Certainly, if one considers similar slurry filling and not mass of slurry, that is, U_0 = 2.0 and 3.0 respectively for J = 20 % and 30 %, grinding follows surprisingly the same AR paths (see Figure 7.15). This thus suggests that it is not all about ball filling or slurry filling; it is rather a combination of the two that will guarantee efficient milling.

The last point on the agenda can now be discussed, that is, the issue of energy consumption. With reference to Figures 7.8 and 7.9, one can deduce that for a given ball filling, there exists an optimum slurry filling close to unity that guarantees low energy usage. Added to this, for different ball fillings, milling will follow the same trajectory provided slurry filling U, calculated in each case using the actual ball filling, is similar (see Figure 7.15).

All in all, the AR methodology has demonstrated its ability to guide the Process Engineer in the choice, not only of the optimum milling conditions, but also of the flowsheet configuration. In addition, the presence of the pool impinges on milling efficiency, and therefore is not desirable. Perhaps this behaviour is linked to the breakage mechanisms that changes from impact to abrasion and attrition.

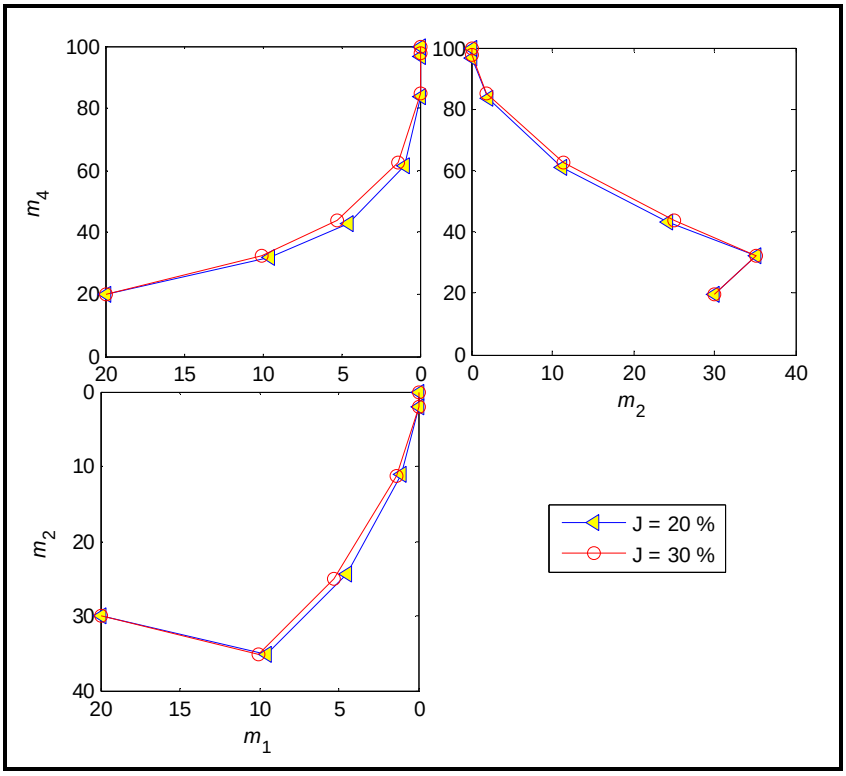

Figure 7.15 Comparison of AR plots for a similar slurry filling (i.e. U_0 = 2.0)

The optimum conditions should be that of a preferential breakage into a fine product. Due to the distribution of the initial feed, this can only be achieved through some combination of the three breakage mechanisms. Breakage by impact should deal with coarse feed predominantly in class m_1 and m_2 whereas material in m_3 will be reduced by abrasion and attrition.

To sum up, our graphical analysis of laboratory batch results has revealed that ball mills should be operated around slurry fillings of unity. This should in fact correspond to the birth of the pool. In chapter 4, for instance, the critical commencement was found to be somewhere around 1.2 < U < 1.3 depending on

the dynamic porosity of the bed of media charge. This information has been reported to be crucial in the efficient operation of ball mills as porosity can easily range from 0.4 to 0.75 within the load (Sichalwe *et al.*, 2011). It is believed that every attempt to optimise milling should not overlook this parameter.

Redefining the state variables in the (M_1, M_2) space has brought to the surface some aspects of the AR technique that are worth exploring in future. In the following paragraphs, the discussion has been limited to showing the implications of the change in state variables.

Figures 7.16 and 7.17 illustrate the maximum production of M_2 as well as the associed energy usage for all the combinations of ball fillings J and slurry fillings U tested.

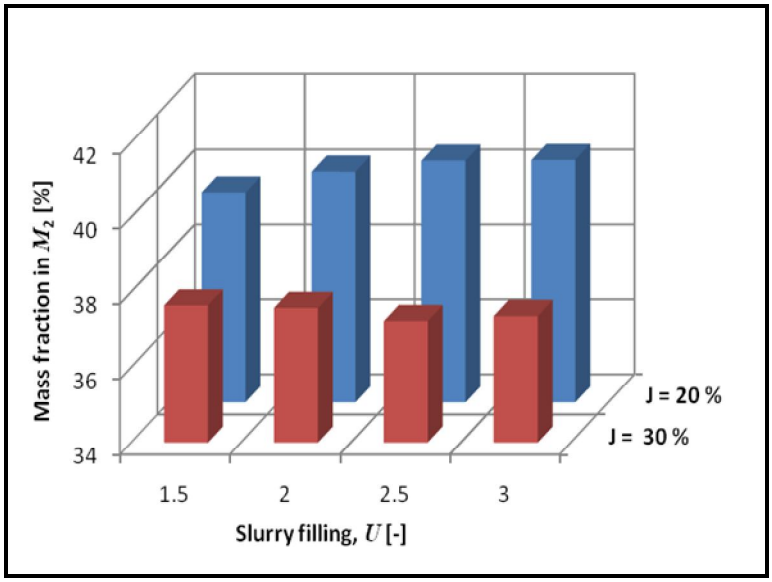

Figure 7.16 Maximum production of material in class M_2 for different combinations of ball and slurry fillings

Note that slurry fillings for the two ball fillings were compared on the basis of similar corresponding masses of slurry. In order words, the following slurry fillings were considered for J = 20 %: U_0 = 1.5, 2.0, 2.5, and 3.0. The same masses when then used for J = 30 % forcing the actual slurry fillings to be adjusted down

to U_0 = 1.0, 1.3, 1.7, and 2.0. But for the purpose of comparison, it has been chosen to collectively refer to all of them as U_0 = 1.5, 2.0, 2.5, and 3.0.

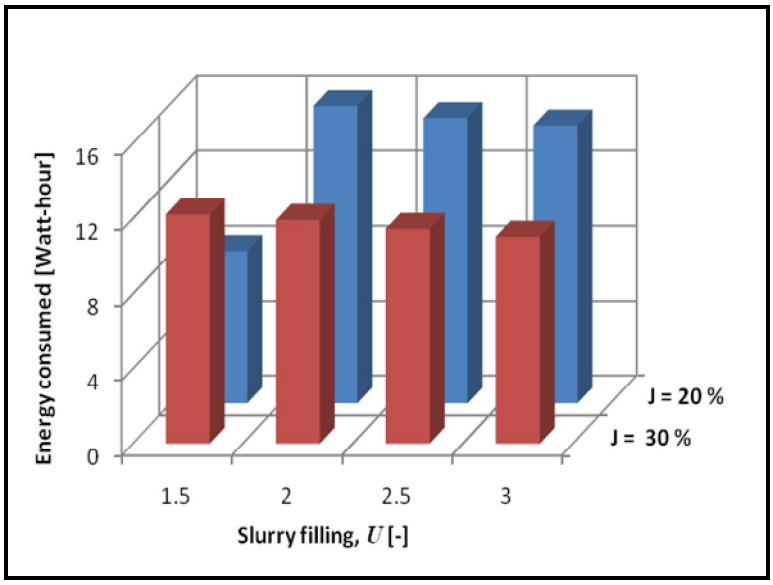

Figure 7.17 Energy consumption corresponding to maximum production of material in class M_2 for different combinations of ball and slurry ball fillings

To come back to milling optimisation, it is clear that depending on the motivation behind the milling process, one would go for one combination over the others. To clarify the matter, consider that the objective is to maximise the production of M_2. The obvious choice would be J = 20 % and U_0 = 3.0; in other words, a low ball loading with over-filled slurry as the optimum. However, Figure 7.17 indicates that energy consumption in this case is high. Also note that the energy consumed with a low ball filling (J = 20 %) surpasses that with a ball loading J = 30 % irrespective of slurry filling except for U_0 = 1.5.

The other objective could be to limit the use of energy while ensuring acceptable production of M_2. If this is the case, operating at J = 20 % and U_0 = 1.5 will represent the optimal milling conditions.

The most important statement to make after this analysis is that the choice of state variables has great implications. As described in the literature review (Section 2.8.2), the class of interest is to have upper and lower size boundaries to

expect successful optimisation. Space (M_1, M_2) is proof of this because M_2 is a definite class – 75 + 25 microns. Space (m_1, m_2, m_4), on the other hand, failed to give results of sensible value because m_4 is a semi-infinite class.

Moreover, the new AR space (M_1, M_2) has demonstrated that in the case whereby flotation was the next operation, milling is better performed in an open-circuit; that is, with no feed by-pass. A seemingly low volume of grinding media J with no pool of slurry but enough slurry to occupy the interstices (that is, $U \cong 1.0$) could be the optimal operating condition.

A final note: the AR analysis applied under flotation constraints has shown that efficient milling should be expected at low ball filling and slurry filling of unity with the mill in an open-circuit configuration. This finding contrasts with commonly accepted practice, especially in the platinum industry. That is why a proper industrial testing campaign and a detailed AR analysis of results will clarify views.

7.6 Conclusion

An attainable region analysis has been performed to assess the effect of pool volume on both milling and energy consumption.

As a starting point, the AR methodology has been generalised in order to accommodate natural feeds. The old concepts of 50 % and 80 % passing sizes were brought back with satisfactory and meaningful results.

After close examination of the AR paths produced, it is concluded that there should be a trade-off to consider in the control of milling. Firstly, the media charge is to be filled in such a way that the interstices are completely occupied by slurry. This implies that a pool of slurry is not desirable for efficient operation. Secondly, both media filling J and slurry filling U were found to contribute significantly to milling optimisation. In fact, the amount of slurry relative to

grinding media is the key to optimal milling. And lastly, a better knowledge of the distribution of porosity within the media charge is necessary for an efficient size reduction.

In conclusion, it seems that low ball fillings with tuned-to-optimal slurry fillings are likely to be more efficient.

Chapter 8 Conclusions and Recommendations

Successive laboratory tests have made it possible to show that slurry has minor effects on load behaviour. In the first set of experiments, slurry viscosity was varied systematically to see how it affects mill charge orientation. After that, slurry filling and mill speed were investigated on a pilot scale to determine their contribution to net power draw. Finally, batch grinding tests on a Platinum ore were conducted to assess the effects of the pool of slurry on milling kinetics.

The main findings as well as the answers to the key research questions are summarised. The research work has also raised some questions; these are formulated here for future work.

8.1 Development of a model of load behaviour

Load behaviour is comprehensively described when the orientations of the media charge and slurry respectively are known under given operating conditions. And to complete the full description, mill power is also measured. That is why, the results from the Perspex mill together with those from the Wits pilot mill are summarised in the following sections.

8.1.1 Media charge position

Initial tests with the Perspex mill under well controlled conditions showed that media charge position did not change much within the operating ranges investigated. The transparent nature of this mill was taken advantage of and videos were captured. The shoulder of the media charge remained reasonably constant with a reported angle lying between 297 – 315°. The variability associated with each case was no more than $\pm$ 6° at 95 % confidence level.

The position of the toe changed significantly after the slurry filling U = 1.2 but then stabilised. It stayed between 130 – 152° for all the conditions tested. It is believed that this sudden increase could be associated with a change in load behaviour before the pool of slurry starts to form. Perhaps, the distribution of slurry within the media charge changed dramatically at this point due to dilation of the bed of grinding media. More work is needed to elucidate this phenomenon.

The abrupt change in the toe angular position before the appearance of the pool (that is, for U > 1.1) was absent when the Wits pilot mill was used with real ore. Here, the toe angle remained fairly constant in all the cases investigated (between 125 – 147°) with variability not exceeding 4° on average at 95 % confidence level. The shoulder presented no inadequacy compared to the preliminary tests: reported angles stayed between 278 – 297° for both mills.
Viscosity did not affect either the shoulder or the toe of the media charge over the range tested. And slurry filling was found to have no influence on the load orientation.

The load behaviour was also measured and modelled as function of mill speed. The actual critical speed was found to be 92.43 % of the theoretical critical speed. It appeared that the premature centrifuging was due to the diameter of balls used (10 mm) relative to the height of the lifters (25 mm). The ball diameter and the lifter height considered for pilot testing were the geometric scale-down of those used in an industrial mill: 40 mm balls and 100 mm lifters. Furthermore, Morrell's equations describing the variations of shoulder and toe with mill speed were modified to match the measured angles. A better choice of grinding media, lifters, ball size distribution and ball filling would be sensible in future to closely mimic industrial mills and make the work more relevant.

The DEM technique was finally used in the study of the media charge. Insight was gained regarding the influence of lifters and grinding balls on load behaviour. It

was found that media charge position was fairly well simulated and that load behaviour had departed significantly from the crescent shape.

8.1.2 Slurry position

Tests in the Perspex mill, using a solution of glycerol showed that the position of the free horizontal surface of the pool was not affected by the changes in viscosity. A model expressing the variation in the angular position of the pool θ_{pool} with slurry filling U was proposed:

$\theta_{pool} = C_0 . U^k$ where C_0 and k are fitting parameters.

The order of magnitude of the two parameters was found to fall within the following ranges: $135.9 \leq C_0 \leq 149.6$ and $-0.2175 \leq k \leq -0.2992$ for viscosities between 1 and 60 mPa.s. Note that the viscosity of real slurries will normally be as high as 150 mPa.s (Shi and Napier-Munn, 2002); that is why, high viscosity and larger balls should be considered in future.

The above pool model was tested on a pilot scale for speeds ranging from 65 % to 85 % critical using a slurry of ore at 65 % mass solids concentration. Results were in good agreement with the model for the whole range of speeds investigated. The two fitting parameters of the pool model were found to vary within $125.37 \leq C_0 \leq 147.49$ and $-0.2937 \leq k \leq -0.3892$ for the range of speeds tested. Moreover, results led to the conclusion that not only does slurry pooling occur the same way irrespective of the level of slurry viscosity, but this is also true for different mill speeds.

The pool did not appear at the theoretical slurry filling U = 1.0. The laboratory and pilot tests showed that the pool starts to form at least after U = 1.1 or higher. One explanation to this is that the porosity of the dynamic bed had increased relative to the static bed, thereby enhancing the ability of the media charge to hold more slurry before the pool appears.

It is proposed that a detailed investigation on the variation of bed porosity and porosity distribution in a wide range of milling conditions be initiated. Because slurry distribution inside the media charge dictates mill performance, understanding the way slurry builds up inside the media charge is undeniably of paramount importance. It is expected that improvements of daily running of mills in mineral processing plants will follow.

8.1.3 Mill power draw

Prior to now, the widely accepted theory of slurry pooling and mill power was that slurry builds up inside the media charge first before the pool forms. This phenomenon implied an increase in net power draw with slurry filling only. The experiments with the pilot mill showed that not only mill power drawn increased with slurry filling, but it also linearly increased with mill speed. This finding definitely negates the assumption of a well-mixed load and rather suggests that the distribution of slurry inside the media charge is a function of mill speed and slurry filling. A direct consequence of this is that the optimisation of wet milling should include mill speed as an additional parameter. Most industrial mills have a fixed speed, which can be changed in principle; this however has not widely been the case.

Notwithstanding the above comments, attempts to empirically model the slurry pooling phenomenon have provided more insight on its effects on the net power. A mechanistic approach based on the torque-arm principle also offered a simple alternative to the determination of power in a wet mill under slurry pooling conditions. It has also been demonstrated that the relationship between shoulder and toe positions of the media charge and mill speed can be adjusted for a particular geometry of the lifters. Similar analysis can be done in an attempt to incorporate lifter design into Morrell's model of power.

8.1.4 Numerical model of a wet ball mill

The increasing need for a better understanding of the slurry distribution inside the media charge requires more sophisticated measurement techniques and highly instrumented mills. The alternative route is the introduction of more powerful simulators that can reliably model the multi-physics involved in wet milling. To put it another way, the interaction between grinding balls, water, particulate solids forming with water the slurry is to be reproduced, calibrated and validated against experiments before confidently using the computer codes and search engines behind the simulators. This need has been recently expressed by researchers such as Naidoo (2012). Until either of the above is satisfactorily done, the multiple phase systems characterising wet milling will still be a challenge to model for some time to come.

8.2 Model of milling kinetics

8.2.1 Population balance model

The PBM framework has been successfully utilised on laboratory grinding data with the following assumptions:

1. The milling kinetics was assumed to follow the first-order-kinetics model (see Equation 2.2).
2. The ore was assumed normalisable; in other words, the breakage function parameters remained constant leading to similar breakage patterns irrespective of the initial particle sizes or milling conditions considered.
3. The selection function was assumed to fall in the normal breakage region such that it could be expressed using Equation (2.4):

   $S_i = a.x_i^{\alpha}$ where a and α are selection function parameters dependent on milling conditions and feed material respectively.
4. Furthermore, a correction factor was added to the selection function to take into account the progressive loss of slurry during sampling. The selection function model became (see Equation 6.3):

$S_i = S_i(U_0, U_t) = a.x^{\alpha}.\left(\frac{2.80e^{-4.1U_t} + e^{-0.8U_t}}{2.80e^{-4.1U_0} + e^{-0.8U_0}}\right)$ where U_0 and U_t are the initial slurry filling and the actual slurry filling at a given grinding time t respectively.

Because of the nature of the feed used, direct parameter estimation was not possible. But with the aforementioned assumptions, the milling parameters were back-calculated and the effects of slurry volume on milling were evaluated.

Data analysis showed that, within the PBM context, milling conditions incurring a high production of fines (i.e. material less than 75 microns) would correspond to a high ball filling (that is, J = 30 % considering the two cases investigated) and a slurry filling U situated somewhere between 1.3 and 1.7.

In a scenario whereby the mill was loaded at 20 % of its volume capacity, optimum slurry filling occurred at U = 1.5 consistent with conclusions drawn when J = 30 %.

8.2.2 Grinding performance

A graphical assessment of milling performance was done as a complementary tool to formal modelling. The easy use in the generation and interpretation of results especially when comparing two or more operating conditions are two of its main advantages. In this regard, size reduction ratio and grinding index were calculated under the various milling conditions investigated. The general comment is that these metrics were quick to produce and provided good description of the size reduction process. By and large, laboratory tests showed that better grinding was achieved with high ball filling and slurry volumetric filling close to unity, that is, U = 1.0.

The last point is that, granted that the methodology is used correctly within the relevant context, meaningful conclusions can be reached.

8.2.3 Attainable region method

The attainable region is an elegant and powerful analysis technique; its application to milling is only beginning to be explored. However, the AR method should be regarded merely as a simple description of what the data is. To put it another way, the AR technique offers a different way of looking at the data at hand; yet complementary to existing techniques. Hidden information that could not be picked up otherwise is revealed. In addition to this, the AR method enables the optimisation of ball milling as a single unit process in a more complex flowsheet or as a section in a series of unit processes in an integrated fashion. The method, though useful, cannot be used in a situation where what-if analysis is expected. It is only a visualisation tool that provides a flexible analysis of and an in-depth insight into minerals processing data in general, and milling data in particular. That is the reason why the combination of the Population Balance Model with the Attainable Region technique has the potential to become an invaluable tool of analysis and optimisation of minerals engineering processes.

8.3 Overall conclusion

The key research question was to determine how much the pool of slurry contributes to milling efficiency and to the whole load behaviour of the mill. In order to answer the question, two hypotheses were formulated for testing. The first was related to the formation of the pool of slurry and the second proposed a dependency between net power draw under slurry pooling conditions and the production of a fine grind.

As far as milling efficiency is concerned, it has been shown that depending on the initial feed size distribution, batch grinding yields a finer product when slurry filling U is low and/or ball filling J is high. This however did not necessarily translate into a more efficient size reduction process. To determine whether the operating conditions led to efficient milling, three indicators were used; namely, the degree of Size Reduction (SR), the Grinding Index (GI) and the Specific

energy consumption. It was found that the reduction in net power draw due to slurry pooling did not result in a proportionately coarser grind. However, with the objective of generating as much fine material (i.e., less than 75 microns) as possible, high ball fillings with a slurry filling of unity tend to guarantee efficient milling. Indeed, findings suggested that the presence of a slurry pool has a negative impact on the production of fines while milling efficiency is increased.

The Attainable Region (AR) technique has also been used as an alternative to the three milling indicators, i.e. SR, GI, and Specific Energy Consumption. From an AR point of view, it appeared that low ball filling with tuned-to-optimal slurry filling (that is, $U \cong 1.0$) is likely to be more efficient. In other words, high production of fines should be expected primarily from milling conditions that promote breakage by abrasion and attrition rather than from high power draw.

In the second part of the research question, the interrelation between slurry and media charge behaviour was determined. The present work supported the fact that slurry pooling always leads to reduced mill power. Furthermore, the position of the media charge was found to remain unchanged with the volumetric filling U and the level of viscosity of slurry. On the other hand, the angular position of free horizontal surface of the slurry pool was related to slurry filling. That is why it is believed that slurry distribution plays an important role in the net power.

In summary, the use of the cinematographic technique, the proximity probe and the conductivity sensor in the measurement of load behaviour has been informative. With the gained knowledge, it has been possible to underscore the contribution of slurry to milling. But, if every other milling parameter remains identical except slurry filling, grate discharge mills offer more room to efficient milling because they are more likely to have no slurry pool. Nonetheless, a lot needs to be done, especially in the study of slurry distribution inside the load. To be relevant to industry, the work also has to be extended to a continuous pilot or industrial mill. In the end, a thorough assessment of the contribution of slurry pooling can be made.

8.4 Recommendations for future work

The present study has evolved entirely around laboratory and pilot work. Milling was investigated by means of batch grinding tests. In accordance to this, conclusions reached suffered some limitations. That is why avenues that could be explored to finalise the work are proposed in the next lines.

First and foremost, intensive research should be invested in developing ways of measuring the distribution of slurry within the media charge for changing slurry fillings. In this regard, Makokha (2011) is to be commended for exploring the use of a gamma-ray video camera to study the flow and mixing behaviour of slurry inside a laboratory mill. Though, his findings were only qualitative and inconclusive as far as slurry distribution is concerned, they paved the way to sophisticated measurement techniques of the mill load behaviour. This could be one way in the quest for a better understanding of slurry pooling.

Second, the shape of the load is subject to many milling parameters. For example, it has been underpinned throughout the thesis that significant changes in load profile can be expected owing to lifter design and ball diameter. That is the reason why it is believed that improvements on mill power models are needed to accommodate slurry distribution, lifter geometry, ball size distribution, and super-critical speeds.

Last, the current decade is witnessing the development of numerical analysis techniques that attempt to couple the Discrete Element Method (DEM) and Computational Fluid Dynamics packages (CFD). DEM Solutions is one such example (DEM Solutions, 2012). The approach has the potential to surpass physical measurement techniques once well calibrated. The end product would offer flexibility and easy study of wet milling. However, the validation of these tools has been the main limiting factor to their growth. The present work provides a good database against which simulations can be compared. It is expected that the development of numerical modelling of wet milling will be promoted.

References

Abd El-Rahman, M.K., Mishra, B.K., Rajamani, R.K., 2001. Industrial tumbling mill power prediction using the discrete element method. Minerals Engineering, vol. 14, no. 10, pp. 1321 – 1328

Arbiter, N., Harris, C.C., 1982. Scale-up and dynamics of large grinding mills – a case study. Design and installation of comminution circuits, Mular. A.L. and Jergensen II.G.V. (eds) AIME, New York, Chap. 26, pp. 491 – 505

Austin, L.G., Bhatia, V.K., 1971/72. Experimental methods for grinding studies in laboratory mills. Powder Technology, vol. 5, no. 5, pp 261 – 266

Austin, L.G., Brame, K., 1983. A comparison of Bond method for sizing wet tumbling ball mills with a size-mass balance simulation model. Powder Technology, vol. 34, no. 2, pp. 261 – 274

Austin, L.G., Klimpel, R.R., Luckie, P.T., 1984. Process Engineering of Size Reduction: Ball Milling. Society of Mining Engineers of the AIME, New York

Austin, L.G., Shoji, K., Everett, M.D., 1973. An explanation of abnormal breakage of large particle sizes in laboratory mills. Powder Technology, vol. 7, no. 1, pp. 3 – 7

Austin, L.G., Shoji, K., Luckie, P.T., 1976. The effect of ball size on mill performance. Powder Technology, vol. 14, no. 1, pp. 71 – 79

Austin, L.G., Trimarchi, T., Weymont, N.P., 1977. An analysis of some cases of non-first-order breakage rates. Powder Technology, vol. 17, no. 1, pp. 109 – 113

Bazin, C., Chapleau, C.B., 2005. The difficulty associated with measuring slurry rheological properties and linking them to grinding mill performance. International Journal of Mineral Processing, vol. 76, no. 1 – 2, pp. 93 – 99

Bazin, C., Hodouin, D., 2004. A graphical method to assess size reduction by grinding. Mineral Processing and Extractive Metallurgy (Trans. Inst. Min. Metall. C), vol. 113, pp. C96 – C102

Bazin, C., Obiang, P., 2007. Should the slurry density in a grinding mill be adjusted as a function of grinding size?. Minerals Engineering, vol. 20, no. 8, pp. 810 – 815

Bilgili, E., 2007. On the consequences of non-first-order breakage kinetics in comminution processes: Absence of self-similar size spectra. Particle and Particle System Characterization, vol. 24, no. 1, pp. 12 – 17

Bilgili, E., Scarlett, B., 2005. Population balance modeling of non-linear effects in milling processes. Powder Technology, vol. 153, no. 1, pp. 59 – 71

Bilgili, E., Yepes, J., Scarlett, B., 2006. Formulation of a non-linear framework for population balance modeling of batch grinding: Beyond first-order kinetics. Chemical Engineering Science, vol. 61, no. 1, pp. 33 – 44

Bond, F.C., 1962. Additions and revision to “Crushing and grinding calculations” (Bond, 1961). in Morrell, S., 1993. Prediction of power draw in wet tumbling mills, PhD Thesis, University of Queensland (JKMRC), Australia

Bwalya, M.M., Moys, M.H., Hinde, A.L., 2001. The use of the discrete element method and fracture mechanics to improve grinding rate prediction. Minerals Engineering, vol. 14, no. 6, pp. 565 – 573

Capece, M. Bilgili, E., Dave, R., 2011. Identification of the breakage rate and distribution parameters in a non-linear population balance model for batch milling. Powder Technology, vol. 208, no. 1, pp. 195 – 204

Chhabra, R.P., Richardson, J.F., 2008. Non-Newtonian flow and applied rheology, Second Edition. Engineering Applications, Elsevier, ISBN 978-0-7506-8532-0

Chimwani, N., 2012. An attainable region approach to optimising product size distribution for flotation purposes. Masters dissertation, University of the Witwatersrand, Johannesburg, in progress

Chimwani, N., Glasser, D., Hildebrandt, D., Metzger, M.J., Mulenga, F.K., 2012. Determination of the milling parameters of a platinum group minerals ore to optimize product size distribution for flotation purposes. Minerals Engineering, http://dx.doi.org/10.1016/j.mineng.2012.09.013

Cleary, P.W., 1998. Predicting charge motion, power draw, segregation and wear in ball mills using discrete element methods. Minerals Engineering, vol. 11, no. 11, pp. 1061 – 1080

Cleary, P.W., 2001. Charge behaviour and power consumption in ball mills: sensitivity to mill operating conditions, liner geometry and charge composition. International Journal of Mineral Processing, vol. 63, no. 2, pp. 79 – 114

Cleary, P.W., 2006. Axial transport in dry ball mills. Applied Mathematical Modelling, vol. 30, no. 11, pp. 1343 – 1355

Cleary, P.W., 2009. Ball motion, axial segregation and power consumption in a full scale two chamber cement mill. Minerals Engineering, vol. 22, no. 9 – 10, pp. 809 – 820

Cleary, P.W., Morrison, R.D., 2012. Prediction of 3D slurry flow within the grinding chamber and discharge from a pilot scale SAG mill. Minerals Engineering, vol. 39, pp. 184 – 195

Cleary, P.W., Sinnott, M., Morrison, R., 2006. Prediction of slurry transport in SAG mills using SPH fluid flow in a dynamic DEM based porous media. Minerals Engineering, vol. 19, no. 15, pp. 1517 – 1527

Clermont, B., de Haas, B., Hancotte, O., 2008. Real time management tools stabilizing your milling process. Third International Platinum Conference

'Platinum in Transformation', The Southern African Institute of Mining and Metallurgy

Datta, A., Mishra, B.K., Rajamani, R.K., 1999. Analysis of power draw in ball mills by the discrete element method. Canadian Metallurgical Quarterly, vol. 38, no. 2, pp. 133 – 140

De Haas, B., 2008. Method for evaluating the filling rate of a tubular rotary ball mill and device thereof. United States Patent, US 7 347 113 B2, Mar. 25, 2008

DEM Solutions, 2012. New CFD Coupling Interface for EDEM Enables Particle-Fluid Simulation with Any CFD Software. Available from: www.dem-solutions.com/, [Accessed on November 06, 2012]

Djordjevic, N., Shi, F.N., Morrison, R., 2004. Determination of lifter design, speed, and filling effects in AG mills by 3D DEM. Minerals Engineering, vol. 17, no. 11 – 12, pp. 1135 – 1142

Dong, H., Moys, M.H., 2002. Assessment of discrete element method for one ball bouncing in a grinding mill. International Journal of Mineral Processing, vol. 65, no. 3 – 4, pp. 213 – 226

Dong, H., Moys, M.H., 2003. Load behavior and mill power. International Journal of Mineral Processing, vol. 69, no. 1 – 4, pp. 11 – 28

Epstein, B., 1947. The mathematical description of certain breakage mechanisms leading to the logarithmico-normal distribution. Journal of the Franklin Institute, vol. 244, no. 6, pp. 471 – 477

Epstein, B., 1948. Logarithmico-normal distribution in breakage of solids. Industrial and Engineering Chemistry, vol. 40, no. 12, pp. 2289 – 2291

Erdem, A.S., Ergüm, Ş.L., Benzer, A.H., 2004. Calculation of the power draw of dry multi-compartment ball mills. Physicochemical Problems of Mineral Processing, vol. 38, pp. 221 – 230

Fuerstenau, D.W., Kapur, P.C., Velamakanni, B., 1990. A multi-torque model for the effects of dispersants and slurry viscosity on ball milling. International Journal of Mineral Processing, vol. 28, no. 1 – 2, pp. 81 – 98

Glasser, D., Hildebrandt, D., 1997. Reactor and process synthesis. Computers in Chemical Engineering, vol. 21, Suppl. 1, pp. S775 – S783

Gudin, D., Kano, J., Saito, F., 2007. Correlation between the grinding rate constant and the impact energy of beads during wet bead milling. Journal of Chemical Engineering of Japan, vol. 40, no. 11, pp. 980 – 985

Gupta, A., Yan, D.S., 2006. Mineral Processing Design and Operation: An introduction. Elsevier, Perth

He, M., Wang, Y., Forssberg, E., 2004. Slurry rheology in wet ultrafine grinding of industrial minerals: a review. Powder Technology, vol. 147, no. 1 – 3, pp. 94 – 112

Herbst, J.A., Hales, L.B., Gabardi, T.L., 1990. Continuous measurement and control of charge volume in tumbling mills. Control 90, pp. 163 – 171

Hlongwani, O, Rikhotso, J., Dong, H., Moys, M.H., 2003. Further validation of DEM modelling of milling: effects of liner profile and mill speed. Minerals Engineering, vol. 16, no. 10, pp. 993 – 998

Hogg, R., Fuerstenau, D.W., 1972. Power relationships for tumbling mills. SME – AIME Transactions, vol. 252, pp. 418 – 423

Hogg, R., Rogovin, Z., 1982. Mass transport in wet, overflow ball mills. Proceedings of the XIV International Mineral Processing Congress, Toronto, Canada

Hosseini, P., Martins, S., Martin, T., Radziszewski, P., Boyer, F.R., 2011. Acoustic emissions simulation of tumbling mills using charge dynamics. Minerals Engineering, vol. 24, no. 13, pp. 1440 – 1447

Huang, P., Jia, M., Zhong, B., 2009. Investigation on measuring the fill level of an industrial ball mill based on the vibration characteristics of the mill shell. Minerals Engineering, vol. 22, no. 14, pp. 1200 – 1208

Hukki, R.T., 1954. Correlation between principal parameters affecting mechanical ball wear. Mining Engineering, pp. 642 – 644

Inoue, T., Okaya, K., 1995. Analysis of grinding actions of ball mills by discrete element method. Proceedings of the XIX International Mineral Processing Congress – Comminution, Simulation and Control, vol. 1, pp. 191 – 196

Kalala, J.T., Bwalya, M.M., Moys, M.H., 2005. Discrete element method (DEM) modelling of evolving mill liner profiles due to wear. Part I: DEM validation. Minerals Engineering, vol. 18, no. 15, pp. 1386 – 1391

Katubilwa, F.M., Moys, M.H., Glasser, D., Hildebrandt, D., 2011. An attainable region analysis of the effect of ball size on milling. Powder Technology, vol. 210, no. 1, pp. 36 – 46

Kawatra, S.K., Eisele, T.C., 1988. Rheological effects in grinding circuits. International Journal of Mineral Processing, vol. 22, no. 1 – 4, pp. 251 – 259

Kelly, E.G., Spottiswood, D.J., 1982. Introduction to Mineral Processing. John Wiley & Sons, New York

Kelly, E.G., Spottiswood, D.J., 1990. The breakage function; What is it really?. Minerals Engineering, vol. 3, no. 5, pp. 405 – 414

Kelsall, D.F., Reid, K.J., Restarick, C.J., 1968. Continuous grinding in a small wet ball mill – Part I. A study of the influence of ball diameter. Powder Technology, vol. 1, no. 5, pp. 291 – 300

Kelsall, D.F., Reid, K.J., Restarick, C.J., 1969. Continuous grinding in a small wet ball mill – Part II. A study of the influence of hold-up weight. Powder Technology, vol. 2, no. 3, pp 162 – 168

Kelsall, D.F., Reid, K.J., Restarick, C.J., 1969/1970. Continuous grinding in a small wet ball mill – Part III. A study of distribution of residence time. Powder Technology, vol. 3, no. 1, pp. 170 – 178

Kelsall, D.F., Stewart, P.S.B., Weller, K.R., 1973. Continuous grinding in a small wet ball mill – Part IV. A study of the influence of grinding media load and density. Powder Technology, vol. 7, no. 5, pp. 293 – 301

Kelsall, D.F., Stewart, P.S.B., Weller, K.R., 1973. Continuous grinding in a small wet ball mill – Part V. A study of the influence of media shape. Powder Technology, vol. 8, no. 1 – 2, pp. 77 – 83

Khumalo, N., 2007. The application of the attainable region analysis in comminution. PhD Thesis, University of the Witwatersrand, Johannesburg

Khumalo, N., Glasser, D., Hildebrandt, D., Hausberger, B., 2008. Improving comminution efficiency using classification: an attainable region approach. Powder Technology, vol. 187, no. 3, pp. 252 – 259

Khumalo, N., Glasser, D., Hildebrandt, D., Hausberger, B., Kauchali, S., 2006. The application of the attainable region analysis to comminution. Chemical Engineering Science, vol. 61, no. 18, pp. 5969 – 5980

Khumalo, N., Glasser, D., Hildebrandt, D., Hausberger, B., Kauchali, S., 2007. An experimental validation of a specified energy-based approach for comminution. Chemical Engineering Science, vol. 62, no. 10, pp. 2765 – 2776

Kiangi, K.K., 2011. Effect of particle filling and size on the behaviour of the ball load and power in a dry mill. PhD Thesis, University of the Witwatersrand, Johannesburg

Kiangi, K.K., Moys, M.H., 2006. Measurement of the load behaviour in a dry pilot mill using an inductive proximity probe. Minerals Engineering, vol. 19, no. 13, pp. 1348 – 1356

Kiangi, K.K., Moys, M.H., 2008. Particle filling and size effects on the ball load behaviour and power in a dry pilot mill: Experimental study. Powder Technology, vol. 187, no. 1, pp. 79 – 87

King, R.P., 2001. Modeling and simulation of mineral processing systems. Butterworth-Heinemann, Oxford

Klimpel, R.R., 1982. Slurry rheology influence on the performance of mineral/coal grinding circuit – Part 1. Mining Engineering, vol. 34, no. 12, pp. 1665 – 1668

Kolacz, J., 1997. Measurement system of the mill charge in grinding ball mill circuits. Minerals Engineering, vol. 10, no. 12, pp. 1329 – 1338

Latchireddi, S., Morrell, S., 2003. Slurry flow in mills: grate-only discharge mechanism (Part 1). Minerals Engineering, vol. 16, no. 7, pp. 625 – 633

Latchireddi, S., Morrell, S., 2006. Slurry flow in mills with TCPL – An efficient pulp lifter for AG/SAG mills. International Journal of Mineral Processing, vol. 79, no. 3, pp. 174 – 187

Liddell, K.S., 1986. The effect of mill speed, filling and pulp rheology on the dynamic behaviour of the load in a rotary grinding mill. Master of Science Dissertation, University of the Witwatersrand, Johannesburg

Liddell, K.S., Moys, M.H., 1988. The effects of mill speed and filling on the behaviour of the load in a rotary grinding mill. Journal of the South African Institute of Mining and Metallurgy, vol. 88, no. 2, pp. 49 – 57

Lo, Y.C., Rogovin, Z., Herbst, J.A., Lee, K., 1987. Detection and prediction of overload conditions in ball mill grinding. Minerals and Metallurgical Processing, pp. 214 – 217

Lux, J., Clermont, B., 2003. The influence of grate versus overflow discharge in open circuit milling open versus closed circuit milling with an overflow mill. Abstracts of the XXIII International Mineral Processing Congress – Cape Town, South Africa, pp. 321

Lux, J., Clermont, B., 2004. The influence of mill speed and pulp density on the grinding efficiency for secondary stage grinding. International Platinum Conference 'Platinum Adding Value', The South African Institute of Mining and Metallurgy, Sun City, South Africa

Makokha, A.B., 2011. Measuring, characterisation and modelling of load dynamic behaviour in a wet overflow-discharge ball mill. PhD Thesis, University of the Witwatersrand, Johannesburg

Makokha, A.B., Moys, M.H., 2006. Towards optimising ball-milling capacity: Effect of lifter design. Minerals Engineering, vol. 19, no. 14, pp. 1439 – 1445

Makokha, A.B., Moys, M.H., 2012. Multivariable approach to on-line prediction of in-mill slurry density and ball load volume based on direct ball and slurry sensor data. Minerals Engineering, vol. 26, pp. 13 – 23

Mathworks, 2011. Online documentation on the Curve Fitting Toolbox, Available from: http://www.mathworks.com/help, [Accessed on May 19, 2011]

Metzger, M.J., 2011. Numerical and experimental analysis of breakage in a mill using the attainable region approach. PhD Thesis, New Brunswick, The State University of New Jersey

Metzger, M. J., Desai, S. P., Glasser, D., Hildebrandt, D. and Glasser, B. J., 2012. Using the attainable region analysis to determine the effect of process parameters on breakage in a ball mill. American Institute of Chemical Engineers Journal, vol. 58, no. 9, pp. 2665 – 2673

Metzger, M.J., Glasser, B.J., Glasser, D., Hausberger, B., Hildebrandt, D., 2007. Teaching reaction engineering using the attainable region. Chemical Engineering Education, vol. 41, no. 4, pp. 258 – 264

Metzger, M.J., Glasser, D., Hausberger, B., Hildebrandt, D., Glasser, B.J., 2009. Use of the attainable region analysis to optimize particle breakage in a ball mill. Chemical Engineering Science, vol. 64, no. 17, pp. 3766 – 3777

Mishra, B.K., 2003. A review of computer simulation of tumbling mills by the discrete element method, Part II – Practical applications. International Journal of Mineral Processing, vol. 71, no. 1 – 4, pp. 95 – 112

Mishra, B.K., Rajamani, R.K., 1990. Motion analysis in tumbling mills by the discrete element method. Kona Powder and Particle, no. 8, pp. 92 – 98

Mishra, B.K., Rajamani, R.K., 1992. The discrete element method for the simulation of ball mills. Applied Mathematical Modelling, vol. 16, no. 11, pp. 598 – 604

Monama, G.M., Moys, M.H., 2002. DEM modelling of the dynamics of mill startup. Minerals Engineering, vol. 15, no. 7, pp. 487 – 492

Montini, A., Moys, M.H., 1988. The measurement of rheological properties inside a grinding mill. Journal of the South African Institute of Mining and Metallurgy, vol. 88, no. 6, pp. 199 – 206

Mori, H., Mio, H., Kano, J., Saito, F., 2004. Ball mill simulation in wet grinding using a tumbling mill and its correlation to grinding rate. Powder Technology, vol. 143 – 144, pp. 230 – 239

Morrell, S., 1993. The prediction of power draw in wet tumbling mills. PhD Thesis, University of Queensland (JKMRC), Australia

Morrell, S., 2003. Grinding mills: How to accurately predict their power draw. Proceedings of the XXII International Mineral Processing Congress, Cape Town, South Africa, pp. 49 – 58

Morrell, S., Napier-Munn, T.J., Andersen, J., 1992. The prediction of power draw in comminution machines (Chapter 17). in Comminution – Theory and Pratice, Society of Mining Engineers of the AIME, ISBN 0-87335-112-6

Morrell, S., Stephenson, I., 1996. Slurry discharge capacity of autogenous and semi-autogenous mills and the effect of grate design. International Journal of Mineral Processing, vol. 46, no. 1 – 2, pp. 53 – 72

Motulsky, H.J., Christopoulos, A., 2003. Fitting models to biological data using linear and nonlinear regression: A practical guide to curve fitting. GraphPad Software Inc., San Diego, www.graphpad.com

Moys, M.H., 1985. The measurement of parameters describing the dynamic behaviour of the load in a grinding mill. MINTEK 50 – International Conference on recent advances in mineral sciences and technology, Sandton, South Africa

Moys, M.H., 1986. The effect of grate design on the behaviour of grate-discharge grinding mills. International Journal of Mineral Processing, vol. 18, pp. 85 – 105

Moys, M.H., 1987. The dynamic behaviour of the load in a wet high-speed grinding mill. South African Institute of Mining and Metallurgy, Colloquium on "Milling", Randburg

Moys, M.H., 1989. Slurry rheology – the key to further advance in grinding mill control. SAG '89, The University of British Columbia (UBC), Vancouver Press et al., 1986, Press Syndicate of the University of Cambridge, New York, pp. 713 – 727

Moys, M.H., 1990. A model for mill power as affected by mill speed, load volume and liner design. in Schonert, K. (Ed.), Preprints of the 7th European Symposium on Comminution, University of Yugoslavia, Ljubljana, pp. 595 – 607

Moys, M.H., 1993. A model of mill power as affected by mill speed, load volume, and liner design. Journal of the South African Institute of Mining and Metallurgy, vol. 93, no. 6, pp. 135 – 141

Moys, M.H., Smit, I., 1998. The effect of discharge arrangement, load volume, slurry rheology and mill speed on power and slurry hold-up in rotary mills. Chemical Engineering in the Mines, Chemical Technology, November/December '98, pp. 27 – 30

Moys, M.H., Smit, I., Stange, W., 1996a. The measurement of forces exerted by the load on liners in rotary mills (wet and dry). International Journal Mineral of Processing, vol. 44 – 45, pp. 383 – 393

Moys, M.H., van Nierop, M.A., Smit, I., 1996b. Progress in measuring and modelling load behaviour in pilot and industrial mills. Minerals Engineering, vol. 9, no. 12, pp. 1201 – 1214

Moys, M.H., van Nierop, M.A., Glover, G., Hinde, A.L., 2001. A discrete element method investigation of the charge motion and power draw of an experimental two-dimensional mill. International Journal of Mineral Processing, vol. 61, no. 2, pp. 77 – 92

Moys, M.H., van Nierop, M.A., van Tonder, J.C., Glover, G., 2000. Validation of the discrete element method (DEM) by comparing predicted load behaviour of a grinding mill with measured data. in: Massacci, P. (Ed.), Proceedings of the International Mineral Processing Congress, C3. Elsevier Science B.V., Rome, Italy, pp. 39 – 44

Naidoo, G., 2012. Tactical mill management using next generation DEM tools. Minerals Engineering, Proceedings of the VIII International Comminution Symposium – Comminution '12, Cape Town, South Africa

Napier-Munn, T.J., Lynch, A.J., 1992. The modelling and computer simulation of mineral treatment processes – Current status and future trends. Minerals Engineering, vol. 3, no. 2, pp. 143 – 167

Napier-Munn, T.J., Morrell, S., Morrison, R.D., Kojovic, T., 1996. Mineral comminution circuits – Their operation and optimization. JKMRC Monograph Series, University of Queensland

Ozkan, A., Yekeler, M., 2003. Fine dry grinding of zeolite in a laboratory ball mill. Particle and Particle Systems Characterization, vol. 20, no. 4, pp. 276 – 282

Pérez-Alonso, C., Delgadillo, J. A., 2012. Experimental validation of 2D DEM code by digital image analysis in tumbling mills. Minerals Engineering, vol. 25, no. 1, pp. 20 – 27

Powell, M.S., Morrell, S., Latchireddi, S., 2001. Developments in the understanding of South African SAG mills. Minerals Engineering, vol. 14, no. 10, pp. 1143 – 1153

Powell, M.S., Weerasekara, N.S., Cole, S., LaRoche, R.D., Favier, J., 2011. DEM modelling of liner evolution and its influence on grinding rate in ball mills. Minerals Engineering, vol. 24, no. 3 – 4, pp. 341 – 351

Radziszewski, P., 1999. Comparing three DEM charge motion models. Minerals Engineering, vol. 12, no. 12, pp. 1501 – 1520

Reid, K.J., 1965. A solution to the batch grinding equation. Chemical Engineering Science, vol. 20, no. 11, pp. 953 – 963

Rogovin, Z., 1983. The Transport and grinding of material in a continuous, wet, overflow ball mill. PhD Thesis, The Pennsylvania State University

Rogovin, Z., Hogg, R., 1988. Internal classification in tumbling grinding mills. Powder Technology, vol. 56, no. 3, pp. 179 – 189

Shi, F.N., Napier-Munn, T.J., 1996. A model for slurry rheology. International Journal of Mineral Processing, vol. 47, no. 1 – 2, pp. 103 – 123

Shi, F.N., Napier-Munn, T.J., 1999. Estimation of shear rates inside a ball mill. International Journal of Mineral Processing, vol. 57, no. , pp. 167 – 183

Shi, F.N., Napier-Munn, T.J., 2002. Effects of slurry rheology on industrial grinding performance. International Journal of Mineral Processing, vol. 65, no. 3 – 4, pp. 125 – 140

Shoji, K., Lohrasb, S., Austin, L.G., 1980. The variation of breakage parameters with ball and powder loading in dry ball milling. Powder Technology, vol. 25, no. 1, pp. 109 – 114

Shoji, K., Austin, L.G., Smaila, F., Brame, K., Luckie, P.T., 1982. Further studies of ball and powder filling effects in ball milling. Powder Technology, vol. 31, no. 1, pp. 121 – 126

Sichalwe, K., Govender, I., Mainza, A.N., 2011. Characterising porosity of multi-component mixtures in rotary mills. Minerals Engineering, vol. 24, no. 3 – 4, pp. 276 – 281

Songfack, P.K., Rajamani, R.K., 1995. Fluid mechanics of slurry flow through the grinding media in ball mills, Proceedings of the XIX International Mineral Processing Congress – Comminution, Simulation and Control, vol. 1, pp. 172 – 175

Tangsathitkulchai, C., 2002. Acceleration of particle breakage rates in wet batch ball milling. Powder Technology, vol. 124, no. 1 – 2, pp. 67 – 75

Tangsathitkulchai, C., 2003. Effects of slurry concentration and powder filling on the net power of a laboratory ball mill. Powder Technology, vol. 137, no. 3, pp. 131 – 138

Tano, K., 2005. Continuous monitoring of mineral processes with special focus on tumbling mills – A multivariate approach. Doctoral Thesis, Lulea University of Technology, Sweden

Triola, M.F., 2001. Essentials of Statistics. Second Edition, Pearson Addison-Wesley, Boston

van Nierop, M.A., Glover, G., Hinde, A.L., Moys, M.H., 2001. A discrete element method investigation of the charge motion and power draw of an experimental two-dimensional mill. International Journal of Mineral Processing, vol. 61, no. 2, pp. 77 – 92

van Nierop, M.A., Moys, M.H., 2001. Exploration of mill power modelled as function of load behaviour. Minerals Engineering, vol. 14, no. 10, pp. 1267 – 1276

Vermeulen, L.A., Ohlson de Fine, M.J., Schakowski, F., 1984. Physical information from the inside of a rotary mill. Journal of the South African Institute of Mining and Metallurgy, vol. 84, no. 8, pp. 247 – 253

Watson, J.L., 1985. An analysis of mill grinding noise. Powder Technology, vol. 41, no. 1, pp. 83 – 89

Wills, B.A., Napier-Munn, T.J., 2005. Wills' mineral processing technology: An introduction to the practical aspects of ore treatment and mineral recovery. Seventh Edition, Elsevier, London, ISBN: 0750644508

Yekeler, M., 2007. Breakage and morphological parameters determined by laboratory tests (Chapter 9). in Handbook of Powder Technology, vol. 12, pp. 437 – 486, ISSN 0167-3785

Zhi-gang Su, Z., Wang, P., Yu, X., Lv, Z., 2008. Experimental investigation of vibration signal of an industrial tubular ball mill: Monitoring and diagnosing. Minerals Engineering, vol. 21, no. 10, pp. 699 – 710

Appendices

A.1 Data for Perspex mill

This section contains data relative to the Perspex mill (Tables A.1 through A.13). Tables A.1, A.3, A.5, A.7, A.9, and A.11 present the toe and shoulder angles of the media charge as well as the location of the pool for the mill at rest and in motion. Measured angles are reported as the lowest, the highest and the average for 30 successive frames. That is why, for every slurry level, numerical figures are given in threes. Tables A.2, A.4, A.6, A.8, A.10, and A.12, on the other hand, are averaged values for approximately 125 – 250 successive frames.

Table A.1 Load orientation for viscosity of the solution 1 mPa.s

U [-]	Media		Slurry		U [-]	Media		Slurry	
	Toe	Shoulder	At rest	Toe		Toe	Shoulder	At rest	Toe
0.0	126.82	318.09			**1.6**	139.76	303.49		128.17
	132.71	307.62				149.38	311.31		129.31
	130.41	311.89				144.24	309.19	117.16	128.42
0.5	129.96	308.51			**1.8**	140.66	302.16		122.69
	136.66	313.32				145.62	308.47		127.76
	134.47	310.44				144.92	307.06	115.62	123.62
1.0	130.70	307.21			**2.0**	141.90	300.07		118.25
	138.54	314.65				148.36	307.20		122.09
	136.32	310.29	122.98			144.40	304.65	114.34	120.33
1.1	133.62	305.92			**2.2**	143.86	302.19		112.24
	139.50	313.07				150.32	311.12		117.99
	137.51	309.77	122.24			146.81	308.80	111.55	116.33
1.2	131.29	305.48			**2.4**	144.07	301.91		110.05
	139.09	316.31				148.27	311.08		114.62
	136.12	312.75	120.60			147.83	306.69	110.40	113.38

1.3	135.00	310.95		133.33	**2.6**	144.38	303.20		107.51
	147.45	314.30		139.74		150.07	310.85		111.90
	141.56	313.84	119.78	136.86		148.10	305.26	108.61	110.84
1.4	143.96	304.92		131.81	**2.8**	142.99	304.52		105.35
	147.51	313.09		135.16		151.53	308.62		110.64
	144.60	311.92	118.98	133.57		147.66	308.37	106.93	108.91
1.5	139.91	307.65		128.72	**3.0**	144.81	299.03		101.36
	144.82	312.84		133.67		155.10	307.08		109.08
	143.42	308.59	117.56	131.39		148.19	305.03	105.39	107.03

Table A.2 Average angles of the load – Viscosity 1 mPa.s

U [-]	θ_T	θ_S	At rest	θ_{Pool}
0.0	130.41	311.89		
0.5	134.47	310.44		
1.0	136.32	310.29	122.98	
1.1	137.51	309.77	122.24	
1.2	136.12	312.75	120.60	
1.3	141.56	313.84	119.78	136.86
1.4	144.60	311.92	118.98	133.57
1.5	143.42	308.59	117.56	131.39
1.6	144.24	309.19	117.16	128.42
1.8	144.92	307.06	115.62	123.62
2.0	144.40	304.65	114.34	120.33
2.2	146.81	308.80	111.55	116.33
2.4	147.83	306.69	110.40	113.38
2.6	148.10	305.26	108.61	110.84
2.8	147.66	308.37	106.93	108.91
3.0	148.19	305.03	105.39	107.03

Table A.3 Load orientation for viscosity of the solution 4 mPa.s

U [-]	Media		Slurry		U [-]	Media		Slurry	
	Toe	Shoulder	At rest	Toe		Toe	Shoulder	At rest	Toe
0.0	126.01	305.65			**1.6**	140.26	298.87		118.72
	137.56	313.48				148.51	308.29		128.20
	135.30	312.86				146.17	304.58	116.99	124.28
0.5	124.68	298.10			**1.8**	142.93	296.93		114.85
	135.53	310.21				150.07	300.83		120.55
	130.60	302.99				147.39	298.90	115.22	119.24
1.0	131.14	295.14			**2.0**	142.01	299.38		113.30
	144.03	305.63				147.45	304.48		119.00
	136.32	299.16	123.69			144.97	303.02	112.77	116.32
1.1	132.57	294.06			**2.2**	144.76	304.06		111.39
	140.16	301.87				150.00	312.46		114.60
	137.16	297.78	122.13			149.30	305.77	111.80	113.45

1.2	130.01	297.17		133.33	**2.4**	142.87	300.26		111.45
	140.46	306.03		146.02		148.99	307.24		116.68
	138.09	305.57	121.62	135.43		145.80	306.57	109.35	112.70
1.3	142.01	293.58		129.84	**2.6**	144.70	295.03		105.28
	150.43	302.72		134.81		150.44	304.54		113.16
	147.03	295.88	120.77	131.59		149.25	297.95	108.43	109.64
1.4	142.45	297.16		123.16	**2.8**	144.61	304.76		104.37
	150.61	307.85		133.88		151.04	310.86		109.22
	147.11	300.43	118.80	128.37		146.52	306.34	107.00	106.17
1.5	141.81	301.01		123.32	**3.0**	144.70	299.42		103.10
	148.74	306.21		128.78		149.24	311.28		108.52
	147.30	302.24	118.19	126.07		147.17	304.86	105.30	105.64

Table A.4 Average angles of the load – Viscosity 4 mPa.s

U [-]	θ_T	θ_S	At rest	θ_{Pool}
0.0	135.30	312.86		
0.5	130.60	302.99		
1.0	136.32	299.16	123.69	
1.1	137.16	297.78	122.13	
1.2	138.09	305.57	121.62	135.43
1.3	147.03	295.88	120.77	131.59
1.4	147.11	300.43	118.80	128.37
1.5	147.30	302.24	118.19	126.07
1.6	146.17	304.58	116.99	124.28
1.8	147.39	298.90	115.22	119.24
2.0	144.97	303.02	112.77	116.32
2.2	149.30	305.77	111.80	113.45
2.4	145.80	306.57	109.35	112.70
2.6	149.25	297.95	108.43	109.64
2.8	146.52	306.34	107.00	106.17
3.0	147.17	304.86	105.30	105.64

Table A.5 Load orientation for viscosity of the solution 10 mPa.s

U [-]	Media		Slurry		U [-]	Media		Slurry	
	Toe	Shoulder	At rest	Toe		Toe	Shoulder	At rest	Toe
0.0	126.01	305.65			**1.6**	144.46	301.15		117.63
	137.56	313.48				150.35	307.53		125.66
	135.30	312.86				146.49	305.36	116.31	122.18
0.5	128.92	298.92			**1.8**	144.58	295.58		117.97
	133.71	306.35				149.81	303.28		124.02
	132.29	303.82				146.58	300.31	113.86	118.81
1.0	132.83	300.32			**2.0**	141.42	299.54		113.66
	137.11	306.15				148.87	312.21		120.69
	135.16	303.82	123.09			146.45	304.08	113.20	115.70

1.1	132.70	294.54			**2.2**	144.41	294.61		111.40
	138.29	301.51				151.99	300.22		115.71
	136.11	296.84	122.26			146.56	296.17	111.08	113.77
1.2	131.22	296.26		133.68	**2.4**	141.93	298.90		108.87
	140.09	307.14		138.31		149.29	304.74		110.72
	137.71	305.89	120.08	134.83		147.26	303.63	109.37	109.49
1.3	133.91	300.36		129.43	**2.6**	145.40	301.59		105.72
	145.98	308.18		134.57		149.53	305.37		109.13
	142.22	306.82	119.78	131.15		146.81	305.34	108.10	108.27
1.4	143.33	300.44		124.72	**2.8**	145.75	295.56		101.85
	152.09	305.59		128.66		148.91	299.65		108.35
	147.55	301.55	118.58	126.37		148.83	298.45	106.88	106.33
1.5	142.88	303.43		122.64	**3.0**	143.69	294.64		101.47
	151.34	310.97		127.46		150.22	303.62		107.12
	147.14	303.97	117.70	126.24		145.95	298.12	105.02	105.57

Table A.6 Average angles of the load – Viscosity 10 mPa.s

U [-]	θ_T	θ_S	At rest	θ_{Pool}
0.0	135.30	312.86		
0.5	132.29	303.82		
1.0	135.16	303.82	123.09	
1.1	136.11	296.84	122.26	
1.2	137.71	305.89	120.08	134.83
1.3	142.22	306.82	119.78	131.15
1.4	147.55	301.55	118.58	126.37
1.5	147.14	303.97	117.70	126.24
1.6	146.49	305.36	116.31	122.18
1.8	146.58	300.31	113.86	118.81
2.0	146.45	304.08	113.20	115.70
2.2	146.56	296.17	111.08	113.77
2.4	147.26	303.63	109.37	109.49
2.6	146.81	305.34	108.10	108.27
2.8	148.83	298.45	106.88	106.33
3.0	145.95	298.12	105.02	105.57

Table A.7 Load orientation for viscosity of the solution 20 mPa.s

U [-]	Media		Slurry		U [-]	Media		Slurry	
	Toe	Shoulder	At rest	Toe		Toe	Shoulder	At rest	Toe
0.0	126.01	305.65			**1.6**	146.20	300.45		120.96
	137.56	313.48				152.34	308.69		126.98
	135.30	312.86				149.53	303.06	116.32	122.09
0.5	132.26	299.48			**1.8**	144.61	299.86		115.94
	141.27	302.03				151.03	308.66		122.06
	138.33	300.81				148.57	303.69	113.96	119.74

1.0	131.26	295.67			**2.0**	144.07	299.41		113.93
	140.26	301.84				150.37	306.05		122.75
	138.59	301.13	122.12			146.74	304.00	113.93	117.94
1.1	131.87	296.90			**2.2**	146.96	299.48		111.85
	139.17	302.84				152.27	308.24		118.06
	138.76	301.44	121.75			149.38	304.19	112.79	114.63
1.2	143.32	300.34		130.46	**2.4**	144.43	298.41		111.43
	148.38	304.82		135.55		152.44	309.81		114.52
	143.54	302.62	119.48	135.00		151.72	305.01	112.32	112.79
1.3	144.43	298.73		128.37	**2.6**	146.11	299.19		107.98
	152.17	304.94		133.72		151.11	308.25		111.80
	147.49	302.55	118.23	128.41		150.01	302.75	110.35	109.82
1.4	140.09	299.03		126.17	**2.8**	147.13	299.03		105.66
	148.55	307.95		128.91		152.67	308.17		109.07
	146.09	301.05	117.65	126.76		151.15	304.17	108.80	108.70
1.5	142.26	294.44		120.35	**3.0**	144.97	298.21		102.72
	148.90	303.76		126.36		152.23	309.57		108.79
	148.38	300.37	116.81	123.54		149.31	303.46	106.70	106.42

Table A.8 Average angles of the load – Viscosity 20 mPa.s

U [-]	θ_T	θ_S	At rest	θ_{Pool}
0.0	135.30	312.86		
0.5	138.33	300.81		
1.0	138.59	301.13	122.12	
1.1	138.76	301.44	121.75	
1.2	143.54	302.62	119.48	135.00
1.3	147.49	302.55	118.23	128.41
1.4	146.09	301.05	117.65	126.76
1.5	148.38	300.37	116.81	123.54
1.6	149.53	303.06	116.32	122.09
1.8	148.57	303.69	113.96	119.74
2.0	146.74	304.00	113.93	117.94
2.2	149.38	304.19	112.79	114.63
2.4	151.72	305.01	112.32	112.79
2.6	150.01	302.75	110.35	109.82
2.8	151.15	304.17	108.80	108.70
3.0	149.31	303.46	106.70	106.42

Table A.9 Load orientation for viscosity of the solution 30 mPa.s

U [-]	Media		Slurry		*U* [-]	Media		Slurry	
	Toe	Shoulder	At rest	Toe		Toe	Shoulder	At rest	Toe
0.0	126.01	305.65			**1.6**	141.38	300.19		119.85
	137.56	313.48				151.02	307.86		128.32
	135.30	312.86				149.22	303.14	117.46	124.88

0.5	130.68	294.06			**1.8**	147.91	293.23		115.40
	136.94	303.49				157.36	302.26		120.13
	134.46	298.21				150.82	298.09	115.55	119.57
1.0	132.97	299.86			**2.0**	143.51	295.53		116.31
	142.69	305.40				152.13	303.49		117.57
	140.26	301.98	124.59			148.81	297.33	113.88	116.94
1.1	135.49	296.46			**2.2**	143.73	295.89		113.86
	138.96	301.44				150.90	299.00		117.59
	138.20	298.07	122.78			147.75	296.86	112.44	115.93
1.2	138.01	294.21		133.88	**2.4**	146.24	297.57		107.27
	143.95	302.19		136.12		151.70	302.40		112.71
	141.77	297.62	120.92	134.62		151.63	293.71	110.79	111.91
1.3	140.97	293.26		129.99	**2.6**	147.19	293.14		108.52
	148.21	299.20		132.33		151.41	301.70		114.44
	145.74	295.50	120.45	131.85		151.20	296.90	109.54	110.22
1.4	144.19	299.65		124.39	**2.8**	147.34	292.62		108.62
	152.01	306.08		130.45		151.05	300.44		112.38
	148.28	302.19	118.97	126.59		149.64	297.92	108.53	110.52
1.5	141.74	299.52		121.64	**3.0**	146.43	295.78		103.19
	148.21	304.26		127.50		155.07	304.84		109.34
	147.91	299.87	117.71	125.57		152.97	300.36	107.78	106.27
					3.2	149.19	297.62		103.52
						156.36	303.48		108.06
						153.65	303.41	105.54	106.36

Table A.10 Average angles of the load – Viscosity 30 mPa.s

U [-]	θ_T	θ_S	At rest	θ_{Pool}
0.0	135.30	312.86		
0.5	134.46	298.21		
1.0	140.26	301.98	124.59	
1.1	138.20	298.07	122.78	
1.2	141.77	297.62	120.92	134.62
1.3	145.74	295.50	120.45	131.85
1.4	148.28	302.19	118.97	126.59
1.5	147.91	299.87	117.71	125.57
1.6	149.22	303.14	117.46	124.88
1.8	150.82	298.09	115.55	119.57
2.0	148.81	297.33	113.88	116.94
2.2	147.75	296.86	112.44	115.93
2.4	151.63	293.71	110.79	111.91
2.6	151.20	296.90	109.54	110.22
2.8	149.64	297.92	108.53	110.52
3.0	152.97	300.36	107.78	106.27
3.2	153.65	303.41	105.54	106.36

Table A.11 Load orientation for viscosity of the solution 60 mPa.s

U [-]	Media		Slurry		U [-]	Media		Slurry	
	Toe	Shoulder	At rest	Toe		Toe	Shoulder	At rest	Toe
0.0	126.01	305.65			**1.6**	142.47	304.51		125.85
	137.56	313.48				148.02	307.14		130.52
	135.30	312.86				144.28	306.16	117.65	129.09
0.5	128.35	302.49			**1.8**	141.49	299.34		123.09
	139.27	308.80				146.92	307.06		129.43
	138.91	307.05				145.90	304.11	116.57	127.63
1.0	129.51	298.65			**2.0**	142.42	303.96		122.10
	140.33	305.01				147.99	310.76		124.10
	137.85	301.77	122.66			146.10	306.06	114.59	122.26
1.1	135.00	297.97			**2.2**	141.87	303.42		117.98
	140.79	305.62				149.65	308.62		122.91
	138.15	301.04	123.47			146.71	306.22	113.02	120.78
1.2	135.61	296.67			**2.4**	143.43	305.37		114.02
	146.01	303.56				150.29	311.60		119.71
	140.56	300.17	121.56			148.08	309.01	111.90	116.81
1.3	139.68	302.51		136.68	**2.6**	142.61	302.42		109.73
	148.19	308.22		139.68		150.82	309.21		118.25
	141.34	304.20	119.60	139.06		147.14	305.27	110.24	114.02
1.4	145.60	299.72		134.26	**2.8**	145.72	298.69		107.06
	149.81	308.08		137.69		149.17	304.57		114.13
	147.17	303.20	119.45	135.33		147.17	301.88	108.43	110.98
1.5	143.61	303.94		127.94	**3.0**	143.49	300.07		104.90
	147.77	308.18		136.28		149.73	306.25		109.71
	146.37	307.29	119.58	134.11		147.53	305.26	107.30	108.95

Table A.12 Average angles of the load – Viscosity 60 mPa.s

U [-]	θ_T	θ_S	At rest	θ_{Pool}
0.0	135.30	312.86		
0.5	138.91	307.05		
1.0	137.85	301.77	122.66	
1.1	138.15	301.04	123.47	
1.2	140.56	300.17	121.56	
1.3	141.34	304.20	119.60	139.06
1.4	147.17	303.20	119.45	135.33
1.5	146.37	307.29	119.58	134.11
1.6	144.28	306.16	117.65	129.09
1.8	145.90	304.11	116.57	127.63
2.0	146.10	306.06	114.59	122.26
2.2	146.71	306.22	113.02	120.78
2.4	148.08	309.01	111.90	116.81

2.6	147.14	305.27	110.24	114.02
2.8	147.17	301.88	108.43	110.98
3.0	147.53	305.26	107.30	108.95

Table A.13 Summary of data for duplicates tests

	1 mPa.s			**10 mPa.s**			**30 mPa.s**		
***U* [-]**	θ_T	θ_S	θ_{Pool}	θ_T	θ_S	θ_{Pool}	θ_T	θ_S	θ_{Pool}
0	133.11	306.23		135.30	312.86		135.30	312.86	
0.5	135.55	303.50		132.29	303.82		134.46	298.21	
1.0	137.98	303.08		135.16	303.82		140.26	301.98	
1.1							138.20	298.07	
1.2	136.12	304.97	136.45	137.71	305.89	135.03	141.77	297.62	138.62
1.4	144.22	300.87	128.49	147.55	301.55	127.03	148.28	302.19	130.59
1.6	147.83	287.63	127.39	146.49	305.36	119.13	149.22	303.14	122.88
1.8	145.09	302.06	122.43	146.58	300.31	113.81	150.82	298.09	116.94
2.0	147.23	297.41	120.63	146.45	304.08	110.70	148.81	297.33	115.93
2.2	142.73	297.16	117.42	146.56	296.17	110.77	147.75	296.86	115.57
2.4	144.70	297.91	112.87	147.26	303.63	105.49	151.63	293.71	114.52
2.6	148.99	298.87	110.68	146.81	305.34	104.27	151.20	296.90	110.27
2.8	146.74	298.48	107.75	148.83	298.45	102.33	149.64	297.92	107.91
3.0	147.30	298.48	105.16	145.95	298.12	101.57	152.97	300.36	104.22

A.2 Data for Wits pilot mill

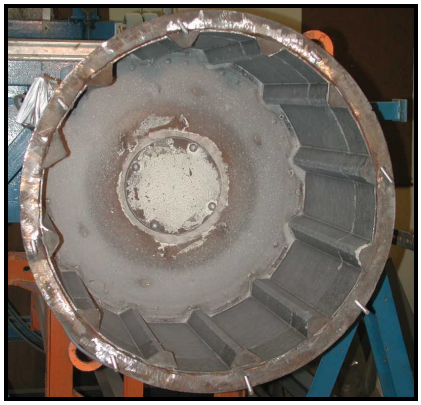

A.2.1 Calibration charts

The proper use of the Wits pilot mill necessitates the calibration of the load cell beam and of the speed. The reason for this is that the load beam cell supposed to measure mill power in fact transmits a voltage to the computerised data acquisition system. It is therefore for the post-processing stage to convert the output voltage into adequate torque, and eventually power. For this to be done, the load beam cell needs to be calibrated.

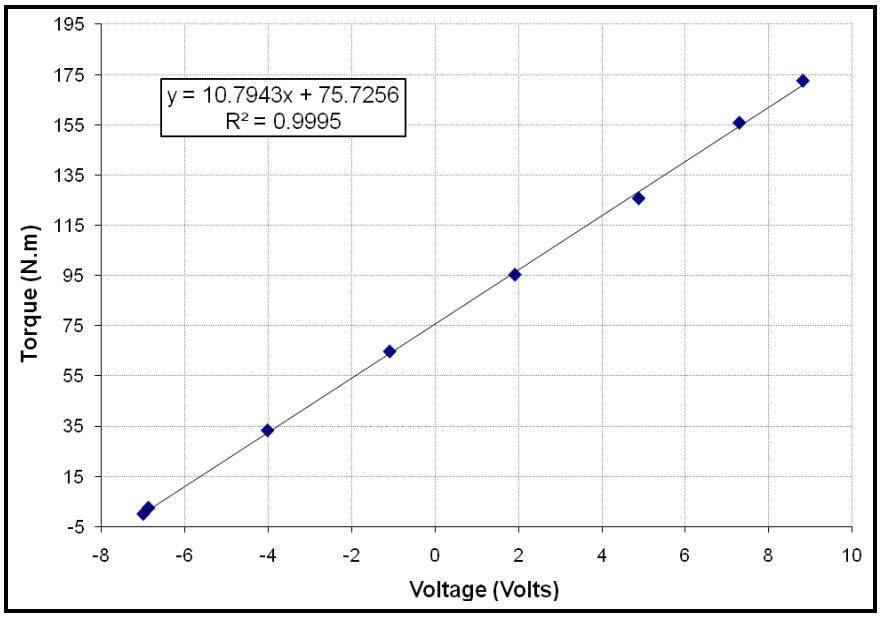

Figure A.1 Calibration chart of the load beam cell

Similarly, the speed of the mill is set up by means of a button connected to a control box. The analogue reader on the control box provides a means to

visualise the speed rate but does not indicate the actual speed. It becomes clear that the speed is to be calibrated to enable one the easy conversion between settings (readings) and speeds.

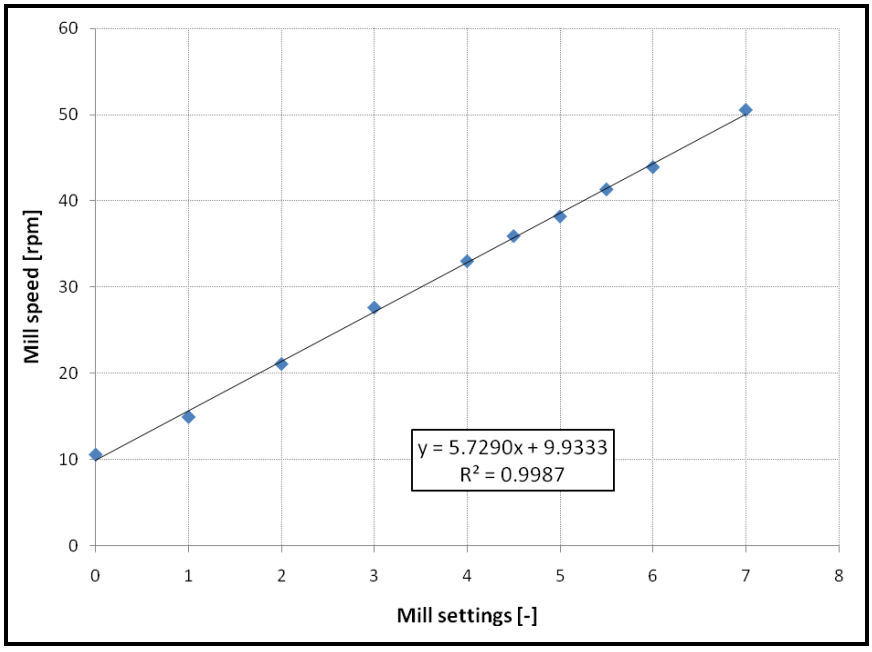

Figure A.2 Calibration of the speed

A.2.2 Signal processing for media charge and slurry positions

Waveview® provides the data in a text file that will then be exported to Excel. Under this format, the data will come as 10001-by-5 matrix containing the sampling times, the marker signal, the conductivity probe signal, the proximity sensor signal, and the mill power signal.

The Marker signal identifies the beginning and the end on a full revolution. This way, the speed of the mill and a clear zero reference can be accurately determined. In the example below is illustrated the marker and mill power signals for 5 revolutions. The level of noise typical of the aggressive milling environment forced us to resort to signal filtering to draw the necessary information on power. The filtered signal is graphed alongside side the raw data.

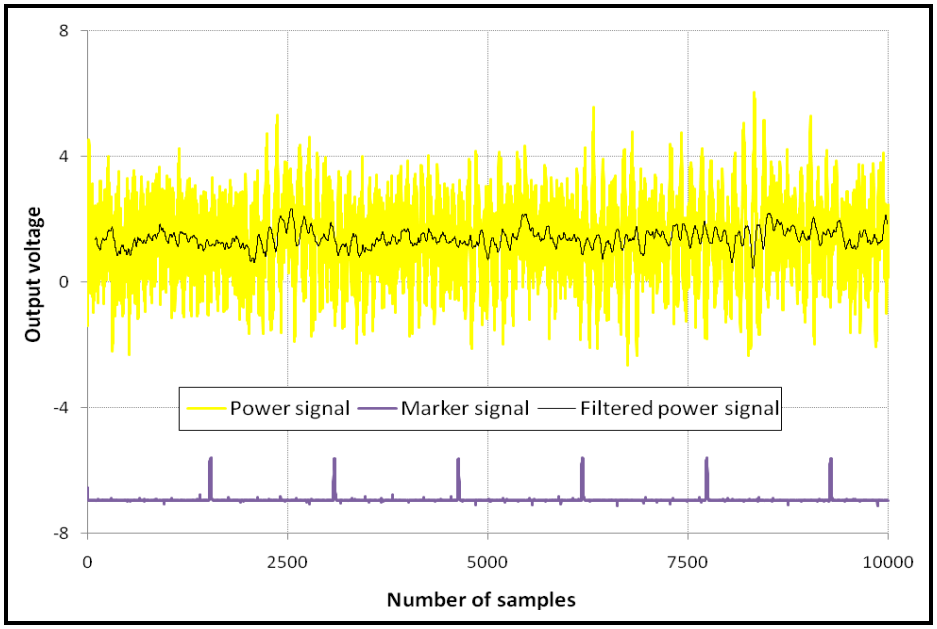

Figure A.3 Typical outputs recorded with Waveview®

The next step was to sort the data into conductivity probe signal, proximity sensor signal, and mill power signal per revolution. In order words, signals are to be rescaled and plotted from 0 to 360 degrees rotational angle. In doing so, successive revolutions can be compared on the same set of axes to assess their reproducibility. To this end, the following Matlab code was used:

```
%% Description of the Code
% ------------------------------------------------------------------
% This piece of code determines the period of rotation and the
% fractional speed of the mill used.
% It also extracts the following information from sampled signals:
% 1. Mill Power draw, Media Charge position, Slurry position.
% 2. Load behaviour as a function of rotation angle.
% ------------------------------------------------------------------
%% Clearing the workspace
clear
%
%% Definition of initial inputs
% Time base used with the Waveview Software in the laboratory
% Default value = 0.001
delta = 0.001;
%
%% Processing the Pilot Mill signals
% Read Excel file containing the mill signals
signals = xlsread('PilotMill.xls');
% Extract relevant signals from the PilotMill.xls file
MillTorque = signals(:, 2);
Proximity = signals(:, 3);
Conductivity = signals(:, 4);
Marker = signals(:, 5);
```

```
%
%% Processing the Marker signal
% Definition of a threshold on the marker signal
MarkerSignal = (Marker > -6.5);
% Preallocation of a marker signal matrix
MarkerMatrix = zeros(1, length(MarkerSignal));
% Detection of the upwards edges of the marker signal
for i = 1:length(MarkerSignal) - 1
    if MarkerSignal(i+1) > MarkerSignal(i)
        MarkerMatrix(i+1) = 1;
    else
        MarkerMatrix(i+1) = 0;
    end
end
%
% Identification of sample indices corresponding to upward edges
SampleIndices = find(MarkerMatrix==1);
% Period of the signal
period = mean(delta*(SampleIndices(2:length(SampleIndices)) - ...
    SampleIndices(1:length(SampleIndices) - 1)));
% Rotational speed of the mill in rpm
MillSpeed = 60/period;
% Fractional speed of the mill in percent
%
%% Processing the Torque signal
% Calculation of Mill power draw
% First determine the Average Voltage measured
% Then convert it to Torque using the Torque calibration equation
PowerAverage = (10.7943*mean(MillTorque)) + 75.7256;
%
%% Packing the summarized signals in a three-dimensional array
% Determine the number of samples per revolution
SamplesRev = SampleIndices(2:length(SampleIndices)) ...
    - SampleIndices(1:length(SampleIndices) - 1);
% Adjustment on the position of the switch for the Marker signal
% -----------------------------------------------------------------
SampleIndices = SampleIndices +
ceil(max(SamplesRev*108/(pi*560))/2);
% -----------------------------------------------------------------
% Define the number of pages of the three-dimensional array first
% Then preallocate the three-dimensional array 'AllSignals'
AllSignals = zeros(max(SamplesRev), 4, length(SampleIndices));
% Sort signals in the three-dimensional array 'AllSignals'
for i = 1:length(SampleIndices)
    if SampleIndices(i) < (10000 - max(SamplesRev))
        AllSignals(1:SamplesRev(i), :, i) = ...
            signals(SampleIndices(i):SampleIndices(i+1)-1, 2:5);
    else
        AllSignals(1:10001-SampleIndices(i), :, i) = ...
            signals(SampleIndices(i):10000, 2:5);
    end
end
%
%% Definition of the x-axis in degrees
angle = linspace(0, 360, max(SamplesRev));
%
%% Processing Proximity signal
% ----------------------------------------------------------------
% Filtering the Proximity signal with a digital filter of order 20
```

```
% ProximitySignal = filter(1/20*ones(1, 20), 1, Proximity);
% ------------------------------------------------------------------
% Plotting the filtered signal
% plot(Proximity, '.')
% hold on
% plot(ProximitySignal, 'r')
% hold off
% ------------------------------------------------------------------
% Matrix of all the Proximity probe signals recorded per
revolution
AllProximity(:, 1:length(SampleIndices)) = ...
                  AllSignals(:, 2, 1:length(SampleIndices));
%
% Calculating the average proximity probe signal
AverProxy = mean(AllProximity(:, 1:length(SamplesRev)), 2);
% plot(angle, AverProxy, '.')
% ------------------------------------------------------------------
%% Processing Conductivity signal
% Matrix of all the Conductivity probe signals recorded per
revolution
AllConductivity(:, 1:length(SampleIndices)) = ...
                  AllSignals(:, 3, 1:length(SampleIndices));
% figure(2), plot(angle, AllConductivity, '.')
%
% Calculating the average conductivity probe signal
% AverConduct = mean(AllConductivity(:, 1:length(SamplesRev)), 2);
% plot(angle, AverConduct, '.')
% ------------------------------------------------------------------
%
MillSpeed
%
```

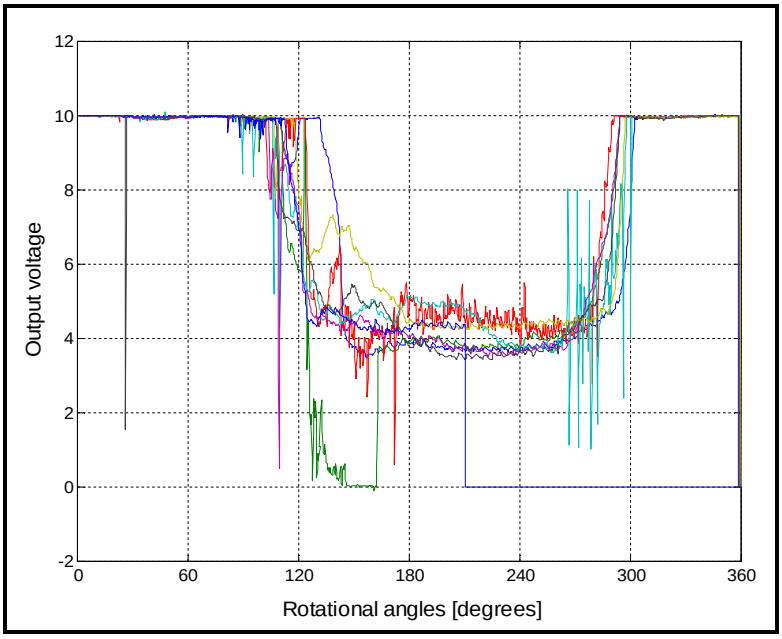

Figure A.4 Example of output produced by the MillSignals.m script

The last thing left to now do is the selection of useful signals and the manual determination of key positions, i.e. toe and shoulder for both the media charge and slurry. Tables A.14 through A.18 below report the results pertaining to the orientations of the media charge and slurry.

Table A.14 Angular positions and standard deviations of toe and shoulder of the media charge for the dry mill

Mill speed		**Toe angle**		**Shoulder angle**	
rpm	**%** N_c	θ_T	$\Delta\theta_T$	θ_S	$\Delta\theta_S$
14.12	24.6	137.9	4.3	261.8	4.4
20.42	35.5	142.1	3.1	268.8	6.1
26.93	46.9	147.0	2.6	269.4	4.0
32.86	57.2	148.0	2.8	283.4	5.4
36.02	62.8	146.8	3.2	289.6	5.5
38.74	67.4	140.1	5.6	297.9	5.9
41.31	72.1	120.8	7.8	316.7	15.1
44.51	77.5	98.1	12.3	324.4	12.4
51.66	89.9	31.8	13.4	346.7	11.5
60.96	106.1	0		360	

Table A.15 Angular positions of the slurry pool for the wet mill

	% N_c	**65**	**70**	**75**	**80**	**85**
	rpm	**37.3**	**40.5**	**43.3**	**45.9**	**48.5**
Slurry filling U **[-]**	**1.0**	143.0	146.9	148.9	144.2	140.3
	1.1	138.3	143.5	143.1	141.5	135.3
	1.2	131.9	136.5	134.5	136.3	134.0
	1.3	129.5	131.1	132.0	134.5	130.1
	1.4	125.2	128.2	129.9	132.0	128.1
	1.5	120.6	126.7	125.5	129.9	125.5
	1.6	117.3	122.3	124.9	126.9	122.7
	1.8	115.8	117.4	117.5	122.4	118.3
	2.0	108.9	114.7	110.8	116.7	114.9
	2.2	106.8	110.9	110.1	113.0	111.7
	2.4	104.6	107.4	105.8	111.9	105.9
	2.6	102.5	105.4	100.2	110.8	103.9
	2.8	99.0	102.7	99.3	106.2	101.8
	3.0	98.6	97.8	96.0	105.8	100.2

Table A.16 Angular positions of the slurry shoulder for the wet mill

	% N_c	65	70	75	80	85
	rpm	**37.3**	**40.5**	**43.3**	**45.9**	**48.5**
Slurry filling U [-]	**0.5**		267.6	274.8	281.6	297.6
	1.0	281.9	264.9	277.5	282.8	285.8
	1.1	283.7	278.7	279.9	285.4	302.5
	1.2	277.9	274.6	278.2	283.2	295.5
	1.3	285.1	277.9	280.4	281.3	298.0
	1.4	275.9	275.4	271.2	281.8	284.5
	1.5	266.9	265.3	283.3	278.8	291.2
	1.6	270.8	251.8	284.7	289.4	282.1
	1.8	276.5	268.8	279.8	279.5	284.9
	2.0	261.8	264.5	276.0	284.3	296.5
	2.2	266.9	272.8	266.5	294.4	279.4
	2.4	259.5	278.8	281.2	280.3	285.0
	2.6	268.3	282.4	284.1	294.8	273.3
	2.8	259.2	257.2	283.5	288.5	292.1
	3.0	268.1	277.9	275.3	295.2	293.8

Table A.17 Toe positions of the media charge for the wet mill

	% N_c	65	70	75	80	85
	rpm	**37.3**	**40.5**	**43.3**	**45.9**	**48.5**
Slurry filling U [-]	**0.0**	144.3	144.7	151.0	143.0	135.2
	0.5	147.9	148.3	154.2	137.9	118.2
	1.0	143.0	147.0	148.1	144.2	140.3
	1.1	144.7	145.3	144.6	146.4	133.1
	1.2	143.1	145.5	147.4	144.3	135.4
	1.3	142.2	144.6	144.1	145.5	132.4
	1.4	144.5	143.1	143.3	145.6	131.7
	1.5	143.4	144.1	145.7	142.8	125.1
	1.6	140.5	142.2	142.3	141.6	123.7
	1.8	139.8	143.2	144.2	138.9	127.7
	2.0	142.3	145.5	141.5	141.9	124.9
	2.2	146.4	145.1	146.0	149.4	116.5
	2.4	144.5	150.0	146.0	144.3	113.0
	2.6	145.6	146.6	146.7	136.1	112.9
	2.8	148.7	147.7	151.2	147.2	114.9
	3.0	146.2	148.3	149.9	145.9	119.2

Table A.18 Shoulder positions of the media charge for the wet mill

	% N_c	65	70	75	80	85
	rpm	**37.3**	**40.5**	**43.3**	**45.9**	**48.5**
Slurry filling U [-]	**0.0**	286.0	287.3	296.3	301.5	301.3
	0.5	287.9	285.5	292.4	293.9	303.8
	1.0	280.1	279.2	286.8	290.1	296.4
	1.1	273.8	281.1	286.4	291.9	298.2
	1.2	278.4	281.4	286.4	292.6	297.6
	1.3	281.8	280.6	286.2	290.8	295.5
	1.4	279.4	283.2	285.1	289.7	296.4
	1.5	279.1	282.5	286.8	295.7	297.0
	1.6	278.6	279.7	282.4	295.0	298.7
	1.8	271.3	280.4	283.9	287.4	296.9
	2.0	274.3	280.9	290.5	290.6	297.7
	2.2	277.0	280.5	285.7	289.6	300.6
	2.4	276.9	278.7	281.9	291.6	298.7
	2.6	275.3	283.3	283.9	292.3	279.8
	2.8	277.1	279.4	285.3	290.5	295.6
	3.0	277.1	281.7	286.5	290.3	295.0

A.2.3 Net power measurements

Table A.19 presents a value of net power draw [in Watts] as a function of mill speed for the dry mill charge, that is, the mill filled with grinding media only.

Table A.19 Net power draws of the dry mill charge

Mill speed		**Net power draw**
rpm	**% N_c**	P_{net}
14.12	24.6	134.9
20.42	35.5	208.8
26.93	46.9	297.2
32.86	57.2	363.0
36.02	62.8	392.2
38.74	67.4	405.2
41.31	72.1	410.1
44.51	77.5	398.5
51.66	89.9	268.4
60.96	106.1	29.3

Table A.20 Net power draws of the wet mill charge – Wits pilot mill

		Net power [Watts]				
	rpm	**37.3**	**40.5**	**43.3**	**45.9**	**48.5**
	% N_c	**65**	**70**	**75**	**80**	**85**
Slurry filling U [-]	**0**	375.2	395.2	413.1	405.4	388.2
	0.5	392.6	425.4	462.7	479.9	489.7
	1.0	406.1	449.1	511.6	541.8	560.4
	1.1	407.7	449.9	498.2	535.9	552.5
	1.2	411.1	458.6	493.8	518.6	538.2
	1.3	405.4	438.8	488.8	518.9	545.5
	1.4	398.9	452.8	482.6	501.3	504.7
	1.5	389.0	430.4	467.3	491.9	497.6
	1.6	394.4	431.3	472.9	495.6	503.4
	1.8	369.6	414.5	444.4	481.7	493.9
	2.0	374.5	410.0	446.6	463.1	484.0
	2.2	384.6	407.2	437.8	454.3	474.1
	2.4	384.6	398.1	429.6	464.8	479.6
	2.6	373.2	420.8	447.5	474.9	464.5
	2.8	374.7	402.4	434.1	456.8	467.8
	3.0	355.5	398.6	431.5	447.6	473.1

A.3 Data for Laboratory mill

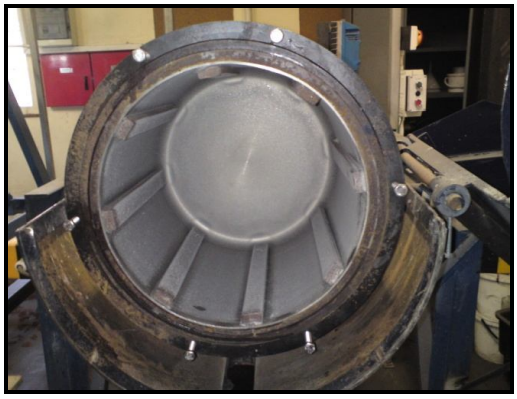

A.3.1 Power calibration chart

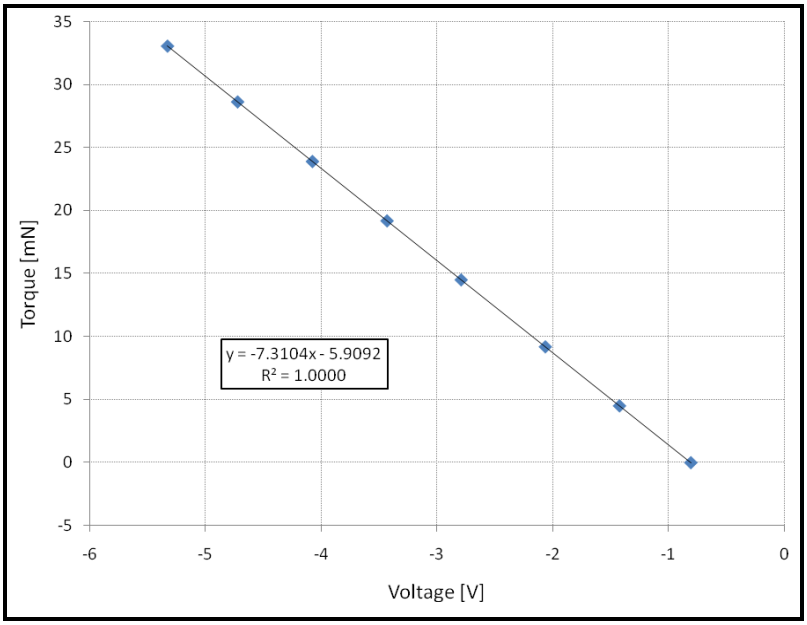

Figure A.5 Power calibration chart of the laboratory mill

A.3.2 Particle size distributions

Table A.21 Ball filling J = 20 % and initial slurry filling U = 1.5

	Percent Passing per Grinding times in %						
Size x_i [mm]	**0 min**	**1 min**	**2 min**	**4 min**	**8 min**	**15 min**	**30 min**
850	100	100	100	100	100	100	100
600	93.93	98.75	99.74	99.99	100	100	100
425	85.74	95.07	98.39	99.84	100	100	100
300	74.25	87.83	94.52	98.98	99.97	100	100
212	61.87	77.46	87.20	96.18	99.71	100	100
150	47.07	63.68	75.77	89.85	98.46	99.96	100

106	31.04	47.33	60.57	78.86	94.60	99.60	100
75	19.70	33.36	45.54	64.87	86.72	97.98	99.97
53	11.08	21.87	32.12	50.05	74.88	93.49	99.73
45	8.49	17.66	26.55	42.65	66.81	88.43	98.99
25	0.73	6.68	12.87	25.26	47.64	74.77	95.94

Table A.22 Ball filling J = 20 % and initial slurry filling U = 2.0

	Percent Passing per Grinding times in %						
Size x_i [mm]	**0 min**	**1 min**	**2 min**	**4 min**	**8 min**	**15 min**	**30 min**
850	100	100	100	100	100	100	100
600	93.93	98.51	99.49	99.85	100	100	100
425	85.74	94.46	97.79	99.60	100	100	100
300	74.25	86.77	93.31	98.38	99.94	100	100
212	61.87	76.10	85.33	94.85	99.49	99.99	100
150	47.07	62.13	73.35	87.52	97.65	99.89	100
106	31.04	45.74	57.83	75.61	92.66	99.24	100
75	19.7	31.98	42.94	61.18	83.47	96.80	99.93
53	11.08	20.77	29.98	46.47	70.69	90.96	99.45
45	8.49	16.73	24.73	39.44	62.54	85.11	98.26
25	0.73	6.07	11.59	22.69	43.31	69.88	93.83

Table A.23 Ball filling J = 20 % and initial slurry filling U = 2.5

	Percent Passing per Grinding times in %						
Size x_i [mm]	**0 min**	**1 min**	**2 min**	**4 min**	**8 min**	**15 min**	**30 min**
850	100	100	100	100	100	100	100
600	93.93	98.37	99.42	99.85	100	100	100
425	85.74	94.12	97.52	99.54	99.99	100	100
300	74.25	86.20	92.71	98.09	99.90	100	100
212	61.87	75.39	84.41	94.15	99.31	99.99	100
150	47.07	61.34	72.17	86.30	97.09	99.84	100
106	31.04	44.95	56.51	73.88	91.46	98.97	99.99
75	19.70	31.31	41.72	59.29	81.61	96.01	99.88
53	11.08	20.24	28.90	44.69	68.44	89.42	99.21
45	8.49	16.28	23.76	37.80	60.31	83.19	97.72
25	0.73	5.78	10.89	21.45	41.16	67.24	92.45

Table A.24 Ball filling J = 20 % and initial slurry filling U = 3.0

	Percent Passing per Grinding times in %						
Size x_i [mm]	**0 min**	**1 min**	**2 min**	**4 min**	**8 min**	**15 min**	**30 min**
850	100	100	100	100	100	100	100
600	93.93	98.22	99.32	99.79	100	100	100
425	85.74	93.76	97.20	99.39	99.98	100	100

300	74.25	85.63	92.05	97.68	99.85	100	100
212	61.87	74.70	83.44	93.31	99.09	99.98	100
150	47.07	60.59	70.97	84.96	96.44	99.76	100
106	31.04	44.21	55.24	72.18	90.13	98.62	99.98
75	19.70	30.71	40.59	57.51	79.66	95.07	99.81
53	11.08	19.79	27.96	43.08	66.19	87.72	98.89
45	8.49	15.92	22.97	36.41	58.15	81.17	97.06
25	0.73	5.57	10.41	20.39	39.19	64.64	90.87

Table A.25 Ball filling J = 30 % and initial slurry filling U = 1.5

	Percent Passing per Grinding times in %						
Size x_i [mm]	**0 min**	**1 min**	**2 min**	**4 min**	**8 min**	**15 min**	**30 min**
850	100	100	100	100	100	100	100
600	93.93	98.81	99.77	99.99	100	100	100
425	85.74	95.51	98.67	99.89	100	100	100
300	74.25	89.06	95.64	99.38	99.98	100	100
212	61.87	79.70	89.82	97.72	99.90	100	100
150	47.07	67.08	80.49	93.80	99.50	100	100
106	31.04	51.76	67.52	86.46	98.10	99.96	100
75	19.70	37.89	53.54	75.85	94.63	99.72	100
53	11.08	26.03	40.11	63.09	88.16	98.80	100
45	8.49	21.33	33.88	55.59	82.49	97.28	99.97
25	0.73	9.60	19.17	38.18	68.25	92.36	99.79

Table A.26 Ball filling J = 30 % and initial slurry filling U = 2.0

	Percent Passing per Grinding times in %						
Size x_i [mm]	**0 min**	**1 min**	**2 min**	**4 min**	**8 min**	**15 min**	**30 min**
850	100	100	100	100	100	100	100
600	93.93	98.58	99.57	99.91	100	100	100
425	85.74	94.89	98.16	99.74	100	100	100
300	74.25	87.96	94.55	98.97	99.98	100	100
212	61.87	78.22	88.04	96.74	99.82	100	100
150	47.07	65.31	78.01	91.92	99.13	99.99	100
106	31.04	49.84	64.50	83.48	97.05	99.90	100
75	19.70	36.14	50.44	72.02	92.47	99.44	100
53	11.08	24.57	37.27	58.89	84.72	97.93	99.98
45	8.49	20.08	31.44	51.53	78.49	95.77	99.91
25	0.73	8.73	17.29	34.44	63.16	89.23	99.52

Table A.27 Ball filling J = 30 % and initial slurry filling U = 2.5

	Percent Passing per Grinding times in %						
Size x_i [mm]	**0 min**	**1 min**	**2 min**	**4 min**	**8 min**	**15 min**	**30 min**
850	100	100	100	100	100	100	100

600	93.93	98.44	99.30	99.81	100	100	100
425	85.74	94.54	97.70	99.59	100	100	100
300	74.25	87.37	93.78	98.65	99.96	100	100
212	61.87	77.46	86.93	96.09	99.74	100	100
150	47.07	64.42	76.58	90.78	98.86	99.98	100
106	31.04	48.90	62.83	81.80	96.35	99.84	100
75	19.70	35.31	48.79	69.98	91.16	99.21	100
53	11.08	23.90	35.79	56.82	82.78	97.30	99.97
45	8.49	19.52	30.03	49.59	76.32	94.77	99.86
25	0.73	8.35	16.18	32.74	60.59	87.35	99.30

Table A.28 Ball filling J = 30 % and initial slurry filling U = 3.0

	Percent Passing per Grinding times in %						
Size x_i [mm]	**0 min**	**1 min**	**2 min**	**4 min**	**8 min**	**15 min**	**30 min**
850	100	100	100	100	100	100	100
600	93.93	98.26	98.90	99.66	100	100	100
425	85.74	93.97	96.94	99.32	99.99	100	100
300	74.25	86.19	92.24	97.91	99.90	100	100
212	61.87	75.66	84.32	94.28	99.40	99.99	100
150	47.07	61.98	72.80	87.20	97.61	99.89	100
106	31.04	45.95	57.95	75.94	93.09	99.35	100
75	19.70	32.43	43.63	62.35	84.93	97.44	99.96
53	11.08	21.33	30.94	48.40	73.46	92.86	99.69
45	8.49	17.27	25.65	41.44	65.87	88.08	99.00
25	0.73	6.61	12.66	24.98	47.84	75.36	96.31

A.3.3 Net power draw and progressive reduction of slurry filling

Table A.29 lists the different net power measured for two ball fillings and six grinding times considered.

Table A.29 Net power draw of the laboratory mill

		J = 20 %				**J = 30 %**			
Slurry filling U_0		**1.5**	**2.0**	**2.5**	**3.0**	**1.0**	**1.3**	**1.7**	**2.0**
Grinding time [min]	**1**	117.6	119.4	117.8	109.8	176.4	179.1	176.7	164.8
	2	122.3	117.7	116.3	111.6	183.5	176.5	174.5	167.4
	4	123.5	119.1	114.3	111.2	185.2	178.7	171.4	166.8
	8	122.3	119.3	114.6	110.4	183.4	179	171.9	165.7
	15	118.1	120.7	116.1	113.5	177.2	181.1	174.2	170.3
	30	116.7	121.7	117.5	113.0	175.0	182.5	176.2	169.5

Table A.30 presents the effects of the progressive sampling of slurry after each time interval throughout a full run of batch test on the actual slurry filling. Table A.31 on the other hand reports the mass of samples collected after each grinding time; this mass was used in the determination of the actual slurry filling U_i present in the mill during a particular time interval.

Table A.30 Progressive reduction of slurry filling due to sampling

Time interval in min		**Actual slurry filling U_i [-]**							
From	**To**	**J = 20 %**				**J = 30 %**			
0	**1**	1.500	2.000	2.500	3.000	1.000	1.333	1.667	2.000
1	**2**	1.473	1.964	2.472	2.973	0.981	1.306	1.649	1.981
2	**4**	1.443	1.937	2.439	2.943	0.959	1.287	1.627	1.961
4	**8**	1.411	1.907	2.404	2.909	0.932	1.266	1.604	1.932
8	**15**	1.375	1.866	2.370	2.877	0.901	1.235	1.578	1.911
15	**30**	1.342	1.830	2.323	2.840	0.872	1.207	1.547	1.886
After 30 min		1.310	1.797	2.294	2.793	0.846	1.184	1.529	1.856

Table A.31 Mass of slurry sample [in g] collected after a given grinding time

		J = 20 %				**J = 30 %**			
Slurry filling U_0		**1.5**	**2.0**	**2.5**	**3.0**	**1.0**	**1.3**	**1.7**	**2.0**
Grinding time [min]	**1**	89.6	119.6	93.8	90.2	93.6	136.6	90.2	94.8
	2	99.2	91.4	109.4	100.4	113.0	96.0	107.6	100.6
	4	107.1	99.5	115.3	113.4	131.9	102.7	114.2	144.9
	8	118.8	135.8	114.8	106.1	158.4	157.6	131.6	106.5
	15	111.3	121.3	156.0	121.3	142.0	137.1	152.4	122.3
	30	106.5	106.7	96.5	157.6	130.5	114.1	93.1	148.7

A.3.4 Back-calculation of breakage parameters: Matlab files

Listed below are three Matlab scripts that were used in the back-calculation of selection function and breakage function parameters.

The driver of the algorithm is the '**BatchTestParam.m**' script. Upon calling this code, it will first import to the Matlab workspace different particle size distributions obtained from a particular batch test. The latter are captured in an Excel spreadsheet specifically designed for the purpose. Afterwards, the code will call for '**PbmSearch.m**' which is the objective function used in the search for

curve fitting parameters. Once, the search is terminated, the optimised parameters are displayed in the Matlab command window. Finally, '**PlotResults.m**' can be used with the new selection function and breakage function parameters to visualise the outcome of the parameter search.

A.3.4.1 Driver – BatchTestParam.m

```
% Matlab script for data acquisition 'BatchTestParam.m'
% The code reads batch test results from an Excel spreadsheet
% and sorts it so as to compare them to predicted ones using
% PbmSearch.m
%% Initial treatment
% Extract data from Batch test results.xls
data = xlsread('Batch test results');
% Sort data as particle size distribtuions and size classes
Screens = data(:, 1);
MeasuredPsd = data(:, 2:length(data(1, :)));
%
%% Parameter search
% Initial guesses of PBM parameters
% Parameters are given in the following order:
% x0 = [A, alpha, beta, gamma, phi]
x0 = [1.58, 1.23, 6.2, 1.32, 0.59];
% The search domain is defined as follows:
% 0.1 < A < 3; 0.5 < alpha < 3;
% 5 < beta < 15; 0 < gamma < 5; 0 < phi < 1;
lb = [ 0.1, 0.5, 6.8, 0, 0.60];
ub = [10.0, 1.5, 6.8, 5, 0.60];
[x, fval, exitflag] = fmincon(@PbmSearch, x0,[],[],[],[], lb, ub);
%% Printing output and convergence criteria
fprintf('\nValue of Objective Function @ termination =%g\n',fval);
if exitflag
    fprintf('\nSuccess: The search converged to a solution\n');
    fprintf('\n A = %4.2f; alpha = %4.2f\n', x(1:2))
    fprintf('\nbeta = %4.2f; gamma = %4.2f; phi =%4.2f\n',x(3:5));
else
    fprintf('Error: Maximum number of iterations reached\n')
end
%
```

A.3.4.2 Objective function – PbmSearch.m

```
% Matlab function that computes particle size distributions with
% the following parameters:
% - Selection function parameters A and alpha
% - Breakage function parameters beta, gamma, and phi
% Refer to Austin, L.G., Klimpel, R.R., Luckie, P.T., 1984.
% Process Engineering of Size Reduction: Ball Milling.
% Society of Mining Engineers of the AIME, New York'
% for more on the Population Balance Model used here
% ------------------------------------------------------------------
%% Definition of the PbmSearch function
function y = PbmSearch(x)
```

```
% Extraction of variables
A = x(1); alpha = x(2); beta = x(3); gamma = x(4); phi = x(5);
%
%% Initial data
% Screen sizes used in the lab and extras for simulation purposes
x = [850; 600; 425; 300; 212; 150; 106; 75; 53; 45; 25; 19];
x = x/1000; % Sizes are converted to mm
% Input feed size distribution
f = [6.07 8.19 11.49 12.38 14.8 16.03 11.34 8.62 2.59 7.76 0.73];
f = f/100; % Mass fractions passing size class
% Input grinding times considered for batch milling test in min
t = [0 1 2 4 8 15 30];
% Input actual slurry filling due to progressive sampling
U = [1.5 1.473 1.443 1.411 1.375 1.342];
%
%% Various calculations
% Number of size classes considered
n = length(x) - 1;
% ---------------------------------------------------------------
% Correction of selection function parameter A
Acor = A*(2.80*exp(-4.1*U) + exp(-0.80*U)) ...
      /(2.80*exp(-4.1*U(1)) + exp(-0.80*U(1)));
% ---------------------------------------------------------------
% Selection function values for all sizes x and grinding times t
S = repmat(Acor, n, 1).*(repmat(x(1:n), 1, length(Acor)).^alpha);
% ---------------------------------------------------------------
% Cumulative breakage function matrix B(i, j)
B = [diag(diag(ones(n))); zeros(1, n)];
for i = 2:n
    for j = 1:n-1
        if (i <= n) && (i > j)
            B(i, j) = phi*(x(i)/x(j+1))^gamma ...
                + (1 - phi)*(x(i)/x(j+1))^beta;
        end
    end
end
% ---------------------------------------------------------------
% Primary breakage function matrix b(i, j)
b = tril(B(1:n, :) - B(2:n+1, :));
% ---------------------------------------------------------------
% Three-dimensional array a(i, j, k)
% Populate array a(i, j, k) with zeros
a = zeros(n, n, length(t) - 1);
% Case (i == j) && (j == 1)
a(1, 1, :) = f(1);
% Other cases
for k = 1:length(t) - 1
    for i = 1:n
        for j = 1:n
            if (i < j)
                a(i, j, k) = 0;
            elseif (i == j) && (i ~= 1)
                a(i, j, k) = f(i) - sum(a(i, 1:j-1, k));
            elseif (i > j)
                a(i, j, k) = 1/(S(i, k) - S(j, k)) ...
                    *sum(S(j:i-1, k).*(b(i, j:i-1))'.* ...
                    a(j:i-1, j, k));
            end
        end
```

```
    end
end
% ------------------------------------------------------------------
% Mass fraction in each size interval for different grinding times
% Retained mass fractions
m = zeros(n, length(t));
for k = 1:length(t) - 1
    m(:, k) = a(:, :, k)*exp(-S(:,k)*t(k));
end
%
% Correction of the retained mass in the sink fraction
% Mass in sink fraction obtained by mass balance because Sn = 0
m(n, :) = m(n, :) + (1 - sum(m));
% ------------------------------------------------------------------
% Percent passing particle size
Predicted = 100*flipud(cumsum(flipud(m)));
% ------------------------------------------------------------------
%% Definition of the objective function
% Capture of 'MeasuredPsd' from the Matlab base workspace
Measured = evalin('base', 'MeasuredPsd');
% Sum of Squared Errors
y = sum(sum((Measured - Predicted).^2));
%
%% Presentation of results
% Plot of the predicted product size distributions
% semilogx(x(1:n), p(:, 2:k), 'o-')
% xlabel('Particle size in mm')
% ylabel('Passing fraction')
% ------------------------------------------------------------------
```

A.3.4.3 Plotting particle size distributions – PlotResults.m

```
% Matlab function that plots particle size distributions with the
% following parameters:
% - Selection function parameters A and alpha
% - Breakage function parameteres beta, gamma, and phi
% The above parameters are those optimised using the Matlab
% function file 'BatchDataParam.m' following the Back-calculation
% method proposed by
% Austin, L.G., Klimpel, R.R., Luckie, P.T., 1984.
% Process Engineering of Size Reduction: Ball Milling. Society of
% Mining Engineers of the AIME, New York'
% ------------------------------------------------------------------
%% Definition of the PbmSearch function
function PlotResults(x)
% Extraction of variables
A = x(1); alpha = x(2); beta = x(3); gamma = x(4); phi = x(5);
%
%% Initial data
% Screen sizes used in the lab and extras for simulation purposes
x = [850; 600; 425; 300; 212; 150; 106; 75; 53; 45; 25; 19];
x = x/1000; % Sizes are converted to mm
% Input feed size distribution
f = [6.07 8.19 11.49 12.38 14.8 16.03 11.34 8.62 2.59 7.76 0.73];
f = f/100; % Mass fractions passing size class
% Input grinding times considered in batch milling test in min
t = [0 1 2 4 8 15 30];
```

```
%
%% Various calculations
% Number of size classes considered
n = length(x) - 1;
% ------------------------------------------------------------------
% Selection function values for the different particle sizes
S = A*(x(1:n).^alpha);
% ------------------------------------------------------------------
% Cumulative breakage function matrix B(i, j)
B = [diag(diag(ones(n))); zeros(1, n)];
for i = 2:n
   for j = 1:n-1
     if (i <= n) && (i > j)
       B(i, j) = phi*(x(i)/x(j+1))^gamma ...
                 + (1 - phi)*(x(i)/x(j+1))^beta;
     end
   end
end
% ------------------------------------------------------------------
% Primary breakage function matrix b(i, j)
b = tril(B(1:n, :) - B(2:n+1, :));
% ------------------------------------------------------------------
% Matrix a(i, j)
% Populate matrix a(i, j) with zeros
a = zeros(n);
% Case (i == j) && (j == 1)
a(1, 1) = f(1);
% Other cases
for i = 1:n
  for j = 1:n
    if (i < j)
      a(i, j) = 0;
    elseif (i == j) && (i ~= 1)
      a(i, j) = f(i) - sum(a(i, 1:j-1));
    elseif (i > j)
      a(i, j) = 1/(S(i) - S(j))* ...
              sum(S(j:i-1).*(b(i, j:i-1))'.*a(j:i-1, j));
    end
  end
end
% ------------------------------------------------------------------
% Mass fraction in each size interval for different grinding times
% Retained mass fractions
m = zeros(length(S), length(t));
for k = 1:length(t)
    m(:, k) = a*exp(-S*t(k));
end
%
% Correction of the retained mass in the sink fraction
m(n, :) = m(n, :) + (1-sum(m));
% ------------------------------------------------------------------
% Percent passing particle size
Predicted = 100*flipud(cumsum(flipud(m)));
% ------------------------------------------------------------------
%% Capture of 'MeasuredPsd' from the Matlab base workspace
Measured = evalin('base', 'MeasuredPsd');
% ------------------------------------------------------------------
%% Presentation of results
% Plot of the predicted product size distributions
```

```
semilogx(x(1:n), Predicted(:, 2:k))
hold on
% Plot of the measured product size distributions
semilogx(x(1:n), Measured(:, 2:k), 'o')
xlabel('Particle size in mm')
ylabel('Mass fraction passing in %')
hold off
% ------------------------------------------------------------------
```

A.4 Net power data for water and slurried ore

Table A.32 Net power data for water and slurried ore in Watts

Slurry filling U [-]	Net power draw [Watts]	
	Water	Slurried ore
0	74.4	74.4
0.5	76.3	79.1
1	78.6	84.2
1.2		81.9
1.4	75.5	77.9
1.6		76.0
1.8	73.1	75.5
2		74.0
2.2	73.5	74.8
2.4		74.1
2.6	72.4	74.4
2.8		72.6
3	71.6	71.0

A.5 Matlab scripts for power modelling

A.5.1 Bond's model

Listed below is the Matlab programme used for the determination of mill power according to Bond.

```
%% Description of the code
% This script is a Matlab version of the Bond's power model as
% reported in Moys, M.H., 1993. A model of mill power as affected
% by mill speed, load volume, and liner design, Journal of the
% South African Institute of Mining and Metallurgy, vol. 93,
% no. 6, pp. 135 - 141
%
%% Clearing the workspace
clear
% ------------------------------------------------------------------
%% Milling conditions
J = 0.2;
D = 0.552;
L = 0.4;
```

```
% ------------------------------------------------------------------
%% Bond's parameters
K = 0.1365; % K = 0.1365 is the best
RhoL = 4680; % Density of the charge, i.e. 7620 * 0.6
% Dynamic angle of repose = 37
alpha = unitsratio('radian', 'degree')*39;
beta = 0.937; % beta = 0.99 is appropriate
gamma = 6.5;
ksi = 0.1;
% ------------------------------------------------------------------
%% Speeds of the mill in percentage of critical
N = 0:140;
% ------------------------------------------------------------------
%% Calculation of power
% Bond's model
P = K * (D^2.3) * L * sin(alpha) * RhoL * J * (1 - beta*J)...
    * N.*(1 - (0.1)./(2.^(gamma-ksi*N)));
% Input raw data - Power measured in the lab
a = [0 24.57 35.54 46.86 56.96 62.83 67.38 72.14 77.48 89.91 ...
     106.09;
     0 135.59 210.02 299.01 363.05 392.20 405.18 410.05 398.45...
     268.38 29.25]';
plot(N, P, a(:,1), a(:,2), 'or')
% ------------------------------------------------------------------
P = P';
%
```

A.5.2 Moys' model

Below is the Matlab code that was used for the calculation of power as modelled using Moys' model:

```
%% Description of the Matlab code
% This script calculates mill power draw following Moys' model.
% For ample information, the user is referred to the papers below:
% Moys, M.H., 1993. A model of mill power as affected by mill
% speed, load volume, and liner design. Journal of the South
% African Institute of Mining and Metallurgy, vol. 93, no. 6,
% pp. 135 - 141
%
% van Nierop, M.A., Moys, M.H., 2001. Exploration of mill power
% modelled as function of load behaviour. Minerals Engineering,
% vol. 14, no. 10, pp. 1267 – 1276
% ------------------------------------------------------------------
%% Body of the Script
clear
% ------------------------------------------------------------------
J = 0.2;
D = 0.552;
L = 0.4;
% ------------------------------------------------------------------
nL = 18; % Number of lifters used
K = 0.1385; % K = 0.1365 is the best
RhoL = 4680; % Density of the charge
beta = 0.99; % beta = 0.99 is appropriate
% Dymanic angle of repose = 39
alpha = unitsratio('radian', 'degree')*39;
```

```
Nstar = 136;
% ------------------------------------------------------------------
N = 0:120; % Speeds of the mill in percentage of critical
DeltaJ = 3/nL; % -0.35 is the best value
DeltaN = 20.8 - 2.4*log(nL); % 17 is suitable for this parameter
% Thickness of centrifuged fraction
DeltaC = (J^DeltaJ)*exp(-(Nstar - N)/DeltaN);
Deff = (1 - 2*DeltaC)*D; % Effective diameter of the mill
Jeff = zeros(1, length(Deff)); % Matrix preallocation
for i = 1:length(DeltaC)
    if DeltaC(i) < 0.5*(1 - sqrt(1 - J))
        Jeff(i) = (J-4*DeltaC(i)*(1-DeltaC(i)))/(1-2*DeltaC(i)^2);
    else
        Jeff(i) = 0;
    end
end
Neff = N.*sqrt(Deff/D); % Speed factor
% ------------------------------------------------------------------
P = K*(Deff.^(2.3))*L*sin(alpha)*RhoL.*Jeff.*(1 -
beta*Jeff).*Neff;
% Input raw data - Power measured in the lab
a = [0 24.57 35.54 46.86 56.96 62.83 67.38 72.14 77.48 89.91 ...
     106.09;
     0 135.59 210.02 299.01 363.05 392.20 405.18 410.05 398.45 ...
     268.38 29.25]';
plot(N, P, a(:,1), a(:,2), 'or')
% ------------------------------------------------------------------
P = P';
%
```

A.5.3 Simplified torque-arm-based model

The application of this modelling scheme assumed that a wet overfilled mill takes the idealised profile depicted in Figure A.1. It is now a matter of integrating the pool of slurry and locating its centre of gravity about which its weight is applied. This way, the torque can be determined.

The calculation of the torque created by the pool (curved triangle IPT in Figure A.6) necessitates the knowledge of the abscissa x_G of its centre of gravity and the mass of slurry forming the pool. By definition, the x-coordinate of the centre of gravity is given by $x_G = \frac{1}{M_p}.\int_{\Omega} x.dm$ where Ω represents the curved triangle IPT defining the pool and M_p is the mass of slurry making up the pool.

The domain forming the pool is sliced following the Cartesian set of axes *Oxy* such that the infinitesimal mass element is defined as $dm = \sigma.dx.dy$ with σ being the specific density of the domain assumed here uniform.

Next, the sides of the curved triangle IPT can be geometrically defined as follows: The straight line IP is expressed as $y = -y_P$; the straight line TI which is the same as TS is given by $y - y_T = \tan\alpha.(x - x_T)$; and the circular segment PT is given by $y = -\sqrt{R^2 - x^2}$.

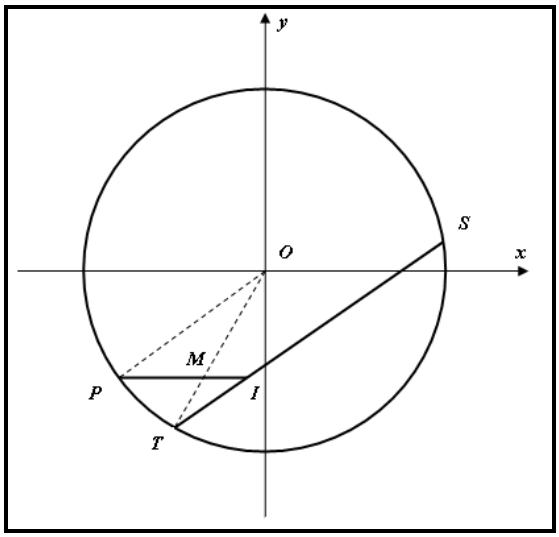

Figure A.1 Simplification of the load orientation of a wet mill

With all the above, *x*-coordinate of the centre of gravity becomes

$$x_G = \frac{1}{M_p}.\left[\int_{x=x_P}^{x_T}\sigma.x.dx\int_{y=-\sqrt{R^2-x^2}}^{y_P}dy + \int_{x=x_T}^{x_I}\sigma.x.dx\int_{y=y_T+(x-x_T).\tan\alpha}^{y_P}dy\right]$$

The last thing to do before dealing with the integral is the definition of the specific density σ of the domain of integration. With the assumption of uniform properties throughout the domain, one can write the following:

$\sigma = \frac{M_p}{A_{IPT}}$ where M_p and A_{IPT} are respectively the mass and surface area of the domain, i.e. the pool of slurry.

The surface area to be integrated can be calculated by subtracting triangle OMP from the circular sector OPT; afterwards, triangle IMT is added to the difference. Finally, with all the information above, the centre of gravity was found to be

$$x_G = \frac{1}{A_{IPT}}.\left[\frac{1}{2}y_P\left(x_T^2 - x_P^2\right) - \frac{1}{3}\left(R^2 - x_T^2\right)^{3/2} + \frac{1}{3}\left(R^2 - x_T^2\right)^{3/2} + \frac{1}{2}\left(y_P - y_T\right)\left(x_I^2 - x_T^2\right) - \frac{1}{3}\tan\alpha.\left(x_I^3 - x_T^3\right) + \frac{1}{2}x_T\left(x_I^2 - x_T^2\right)\right]$$

where $A_{IPT} = \frac{1}{2}R^2\left(\theta_T - \theta_P\right) - \frac{1}{2}y_P\left(x_P - x_M\right) + \frac{1}{2}\left(y_P - y_T\right)\left(x_I - x_M\right)$

and $x_M = \frac{y_P}{y_T}x_T$

The Matlab script that calculates numerically all the above equation and outputs mill power for given pool level is listed in the code below named **IndividualPooling.m**:

```
%% Description of the Matlab code
% The script calculates net power draw by combining physical and
% empirical understanding of the formation of the pool of slurry
%
%% Milling conditions
% Clearing the workspace
clear
% ---------------------------------------------------------------------
J = 0.2; % Degree of filling of the mill with grinding media
D = 0.552; % Diameter of the mill
L = 0.4; % Length of the mill
U = 0:0.1:3; % Range of slurry filling considered
% Dynamic angle of repose
alpha = unitsratio('radian', 'degree')*39;
%
%% Application of the empirical modelling scheme
% Mill speed in Percent of critical
%========|
N = 65; %| CHANGE ON A CASE BASIS
%========|
%
%% Orientation of the pool of slurry
% Angular position of the toe in degrees
%====================|
Toe = 140.85 + 90; %| CHANGE ON A CASE BASIS
%====================| [140.85 145.82 147.49 144.92 125.37]
%
ThetaT = unitsratio('rad', 'deg')*Toe; % in radians
%
% Coordinates of toe
xT = D/2*cos(ThetaT);
```

```
yT = D/2*sin(ThetaT);
% Parameter k in the pool model
%=============|
k = -0.3422; %| CHANGE ON A CASE BASIS
%=============| [-.3422 -.3515 -.3892 -.2937 -.3132]
%
% Angular position of the pool of slurry
Pool = (Toe - 90)*(U.^k) + 90; % in degrees
ThetaP = unitsratio('rad', 'deg')*(Pool); % in radians
% Coordinates of pool
xP = D/2*cos(ThetaP);
yP = D/2*sin(ThetaP);
% Coordinates of intersection of pool free surface
% and load rolling surface
xI = xT + (yP - yT)/tan(alpha);
%
%% Parameters of the pool of slurry
% Fraction of slurry by volume in rotating charge
f = zeros(1, length(U));
for i = 1:length(U)
    if U(i) <= 1
        f(i) = 1;
    else
        f(i) = 1/U(i);
    end
end
% Mass of slurry loaded in the mill
Mslurry = 4.7165*U; % 15.7216*U
% Mass of material forming the pool
Mpool = (1 - f).*Mslurry;
%% Contribution of the pool to power
% Gravity centre of the pool
xM = yP/yT*xT;
R = D/2;
Num = 1/2*yP.*(xT^2 - xP.^2) - 1/3*(R^2 - xT^2)^(3/2) ...
    + 1/3*(R^2 - xP.^2).^(3/2) + 1/2*(yP - yT).*(xI.^2 - xT^2) ...
    - tan(alpha)*(1/3*(xI.^3 - xT^3) - 1/2*xT*(xI.^2 - xT^2));
Den = 1/2*(R^2)*(ThetaT - ThetaP) - abs(1/2*yP.*(xM - xP)) ...
    + 1/2*(yP - yT).*(xI - xM);
Xpool = Num./Den;
%
g = 9.81; % Constant of gravity
Nc = 42.3/(sqrt(D - 0.01)); % Critical speed in rpm
Ns = 2*pi*(N/100)*Nc/60; % Speed rate in radians per sec
% Calculation of net power draw
Pp = Mpool*g.*Xpool*Ns;
Pp(1) = 0; % Ill-case
%% Empirical approach for 0 < U < 1
P = zeros(1, length(U));
% Detecting the position of U = 1 in the array
index = find(U == 1);
for i = 1:length(P)
    if i == 1
        % Measured net power for the dry mill, i.e. U = 0
        %==============|
        P(i) = 375.2; %| CHANGE ON A CASE BASIS
        %==============| [375.2 395.2 413.1 405.4 388.2]
    elseif (i > 1) && (i <= index)
        % Empirical consideration on slurry occupation of voids
```

```
        P(i) = P(1) + (6.2591*N - 373.77)*U(i);
    else
        % Model of Slurry pooling phenomenon
        P(i) = P(index) + Pp(i) ;
    end
end
%
%% Results
Filling = [0 0.5 1.0 1.1 1.2 1.3 1.4 1.5 1.6 1.8 2.0 2.2 2.4 ...
           2.6 2.8 3.0];
Power = [375.2 392.6 406.1 407.7 411.1 405.4 398.9 389.0 394.4 ...
    369.6 374.5 384.6 384.6 373.2 374.7 355.5;
    395.2 425.4 449.1 449.9 458.6 438.8 452.8 430.3 431.3 ...
    414.5 410.0 407.2 398.1 420.8 402.4 398.6;
    413.1 462.7 511.6 498.2 493.8 488.8 482.6 467.3 472.9 ...
    444.5 446.6 437.8 429.6 447.5 434.1 431.5;
    405.4 479.9 541.8 535.9 518.6 518.9 501.3 491.9 495.6 ...
    481.7 463.1 454.3 464.8 474.9 456.8 447.6;
    388.2 489.7 560.4 552.5 538.2 545.5 504.7 497.6 503.4 ...
    493.9 484.0 474.1 479.6 464.5 467.8 473.1];
%====================================|
plot(U, P, Filling, Power(1, :), 'o') %| CHANGE ON A CASE BASIS
%====================================|
grid on
```

A.5.4 Morrell's power model

Two Matlab codes were written for the calculation of power: the first was used on the dry mill charge while the second referred to the wet mill charge. Both were a Matlab implementation of the net power model proposed by Morrell (1993) in which net power was compared to the calculated one.

A.5.4.1 Dry mill load

```
%% Description of the program
% This Matlab code calculates net power draw of the Wits pilot
% mill loaded with ball media only after Morrell's model
% Reference
% Morrell, S., 1993. The prediction of power draw in wet tumbling
% mills. PhD. Thesis, University of Queensland (JKMRC), Australia
%
%% Clearing the workspace
clear
% ---------------------------------------------------------------
%% Load orientation
Phi = 0:0.001:1.2; % Fractional Speeds of the mill
Jt = 0.2; % Degree of filling of the mill
%
% Initial parameters for load orientation
A = 2.5307*(1.2796 - Jt);
B = 19.42;
PhiC = zeros(1, length(Phi));
for i = 1:length(Phi)
```

```
    if Phi(i) > 0.35*(3.364 - Jt)
        PhiC(i) = Phi(i);
    else
        PhiC(i) = 0.35*(3.364 - Jt);
    end
end
E = 0.3386 + 0.1041*Phi;
F = 1.54 - 2.5673*Phi;
% Load orientation according to Morrell
ThetaT = A.*(1 - exp(-B*(PhiC - Phi))) + pi/2;
ThetaS = pi/2 - (ThetaT - pi/2).*(E + F*Jt);
% ----------------------------------------------------------------
%% Geometry of the mill
D = 0.552; % Diameter of the mill
rm = D/2; % Radius of the mill
L = 0.4; % Length of the mill
% Constant of gravity
g = 9.81;
% Critical Speed in rpm
Nc = 42.3/(sqrt(D - 0.01));
% ----------------------------------------------------------------
%% In-mill geometry of the load
N = Phi*Nc; % Mill speeds in rpm
Nm = N/60; % Mill rotational rates in rev. per s
Nbar = Nm/2;
rbar = rm/2*(1 + sqrt(1 - (2*pi*Jt)./(2*pi + ThetaS - ThetaT)));
tc = (2*pi - ThetaT + ThetaS)./(2*pi*Nbar);
tf = sqrt(2*rbar.*(sin(ThetaS) - sin(ThetaT))/g);
beta = tc./(tc + tf);
ri = rm * sqrt(1 - (2*pi*beta*Jt)./(2*pi + ThetaS - ThetaT));
z = (1 - Jt)^(0.4532);
% ----------------------------------------------------------------
%% Prediction of mill power
RhoB = 7800; % Specific density of steel balls
RhoC = 7800*0.6; % Bulk density of the charge
Pnet = ((pi*g*L*RhoC*Nm*rm)./(3*(rm - z*ri)).*(2*(rm^3) ...
   - 3*z*(rm^2).*ri + (ri.^3)*(3*z - 2)).*(sin(ThetaS) ...
   - sin(ThetaT))) + L*RhoC*(((Nm*rm*pi)./(rm ...
   - z*ri)).^3).*(((rm - z*ri).^4) - (ri.^4)*((z - 1)^4));
% ----------------------------------------------------------------
%% Measured power
Speed = [0 24.57 35.54 46.86 56.96 62.83 67.38 72.14 77.48 ...
      89.91 106.09];
Power = [0 135.59 210.02 299.01 363.05 392.20 405.18 410.05 ...
      398.45 268.38 29.25];
% ----------------------------------------------------------------
%% Plot of Power versus Mill Speed
plot(Phi*100, Pnet, Speed, Power, 'o')
axis([0 110 0 500])
%
```

A.5.4.2 Wet mill load

```
%% Description of the Matlab code
% The script calculates the effects of slurry pool on net power:
% see Morrell, S., 1993. The prediction of net power draw in wet
% tumbling ball mills. PhD Thesis, University of Queensland,
```

```
% Australia
% -------------------------------------------------------------------
%% Clearing workspace
clear
% -------------------------------------------------------------------
%% Input initial data
% Choice of fractional speed
Index = 4; % Choose Index from 1 to 5
Speed = 0.65:0.05:0.85;
% Fractional speed of the mill
Phi = Speed(Index);
% Ball filling degree of the mill
Jb = 0.2;
% Densities of ore, grinding balls and water
Rho0 = 3470; RhoB = 7800; RhoW = 1000;
% Slurry fillings considered
U = 0:.01:3;
% Bed porosity and solids concentration
e = 0.4; s = 0.65;
% -------------------------------------------------------------------
%% Slurry properties
% Slurry concentration by volume
C = 1/(1/s + (3.49648/6.4935)*(Rho0*(1 - e) - RhoW)/RhoW);
% Masses of water and powder were 3.49648 and 6.4935 kg in the lab
% Slurry density
RhoS = C*Rho0 + (1 - C)*RhoW;
% -------------------------------------------------------------------
%% Rotating charge
% Fraction of slurry by volume in rotating mill charge
f = zeros(1, length(U));
for i = 1:length(U)
    if U(i) <= 1
        f(i) = 1;
    else
        f(i) = 1/U(i);
    end
end
% Mass of rotating mill charge
Vmill = 0.0920356; % Volume of the pilot mill in cubic meters
Mc = ((1 - e)*Jb*RhoB + e*Jb*f.*U*RhoS)*Vmill;
% Volume of rotating mill charge
Vc = ones(1, length(U)) * (Jb*Vmill);
% Average density of the rotating mill charge
RhoC = Mc./Vc;
% -------------------------------------------------------------------
%% Load behaviour
% Populate Jb matrix of same size as matrix U
Jb = Jb*ones(1, length(U));
% Exponent for pool model
pool = -[0.3422 0.3515 0.3892 0.2937 0.3132];
% Parameters for load orientation
A = 2.5307*(1.2796 - Jb);
B = 19.42;
PhiC = zeros(1, length(U));
for i = 1:length(U)
    if Phi > 0.35*(3.364 - Jb(i))
        PhiC(i) = Phi;
    else
        PhiC(i) = 0.35*(3.364 - Jb(i));
```

```
    end
end
E = 0.3386 + 0.1041*Phi;
F = 1.54 - 2.5673*Phi;
% Load orientation according to Morrell's description
ThetaT = A.*(1 - exp(-B*(PhiC - Phi))) + pi/2; % Toe
ThetaS = pi/2 - (ThetaT - pi/2).*(E + F*Jb); % Shoulder
ThetaP = zeros(1, length(U)); % Free surface of pool
for i = 1:length(U)
    if U(i) <= 1
        ThetaP(i) = ThetaT(i);
    else
        % Model of the pool position
        ThetaP(i) = pi/2 + (ThetaT(i) - pi/2)*U(i)^(pool(Index));
    end
end
% ---------------------------------------------------------------
%% Mill geometry and internal dynamics
rm = 0.276; % Radius of the mill
L = 0.4; % Length of the mill
g = 9.81; % Constant of gravity
Nc = 42.3/(sqrt(2*rm - 0.01)); % Critical Speed
Nm = Phi*Nc/60;
Nbar = Nm/2;
rbar = rm/2*(1 + sqrt(1 - (2*pi*Jb./(2*pi + ThetaS - ThetaT))));
tc = (2*pi - ThetaT + ThetaS)/(2*pi*Nbar);
tf = sqrt(2*rbar.*(sin(ThetaS) - sin(ThetaT))/g);
beta = tc./(tc + tf);
ri = rm * sqrt(1 - (2*pi*beta.*Jb)./(2*pi + ThetaS - ThetaT));
z = (1 - Jb).^(0.4532);
% ---------------------------------------------------------------
%% Calculation of power draw
% Theoretical net power draw
Pnet = pi*g*L*Nm*rm./(3*(rm - z.*ri)).*(2*(rm^3)-3*z*(rm^2).*ri...
    + (ri.^3).*(3*z - 2)).*(RhoC.*(sin(ThetaS) - sin(ThetaT)) ...
    + RhoS*(sin(ThetaT) - sin(ThetaP))) ...
    + L*RhoC.*((Nm*rm*pi./(rm - z.*ri)).^3).*(((rm - z.*ri).^4)...
    - (ri.^4).*(z - 1).^4);
% Measured power draw from the Wits pilot mill
filling = [0 0.5 1.0 1.1 1.2 1.3 1.4 1.5 1.6 1.8 2.0 2.2 ...
           2.4 2.6 2.8 3.0];
power = [375.2 392.6 406.1 407.7 411.1 405.4 398.9 389.0 ...
    394.4 369.6 374.5 384.6 384.6 373.2 374.7 355.5;
    395.2 425.4 449.1 449.9 458.6 438.8 452.8 430.4 431.3 ...
    414.5 410.0 407.2 398.1 420.8 402.4 398.6;
    413.1 462.7 511.6 498.2 493.8 488.8 482.6 467.3 472.9 ...
    444.4 446.6 437.8 429.6 447.5 434.1 431.5;
    405.4 479.9 541.8 535.9 518.6 518.9 501.3 491.9 495.6 ...
    481.7 463.1 454.3 464.8 474.9 456.8 447.6;
    388.2 489.7 560.4 552.5 538.2 545.5 504.7 497.6 503.4 ...
    493.9 484.0 474.1 479.6 464.5 467.8 473.1];
% Plotting outputs
plot(U, Pnet, filling, power(Index, :), 'o-'); grid on
```

A.5.5 Curve fitting power data of the wet mill

In the curve fitting exercise, it was decided to model the measured powers in Table A.17 using the following piece-wise function:

$y = f(x)$ with y and x representing respectively the gross power draw and slurry filling while f is the Matlab function '**powerdraw.m**' given below

where for $0 \le x \le 1$; $y = A_1 + A_2.x$ (linear function)

and for $1 < x \le 3$; $y = (A_1 + A_2).\ x^{-b}$ (power function similar the slurry pool model proposed in this thesis)

A_1, A_2, b are the curve fitting parameters to be optimised.

The chosen function is translated into the Matlab function script '**powerdraw.m**' listed below:

```
function y = powerdraw(x, xdata)
y = zeros(1, length(xdata));
for i = 1:length(xdata)
    if xdata(i) <= 1
        y(i) = x(1) + x(2)*xdata(i);
    else
        y(i) = (x(1) + x(2))*xdata(i)^(-x(3));
    end
end
```

The next step was to run a curve fitting algorithm in the least square sense. The following Matlab instructions were typed in the Command Window:

```
[x, resnorm] = lsqcurvefit(@powerdraw, Start, xdata, ydata)
y = powerdraw(coef, xdata);
plot(xdata, y, xdata, ydata, 'o')
```

A.6 Wits DEM Simulator

The simulator used for the DEM investigations presented in this thesis and some amongst other capabilities that come with the package is presented below. The DEM results pertaining to the research work are also reported. These are mill power, toe and shoulder positions of the media charge. Note that only the dry mill load was simulated.

A.6.1 The SimView interface

Wits SimView is essentially a Matlab based simulator for DEM purposes. Upon launching the simulator within Matlab®, a window similar to Figure A.2 pops up with several functionalities.

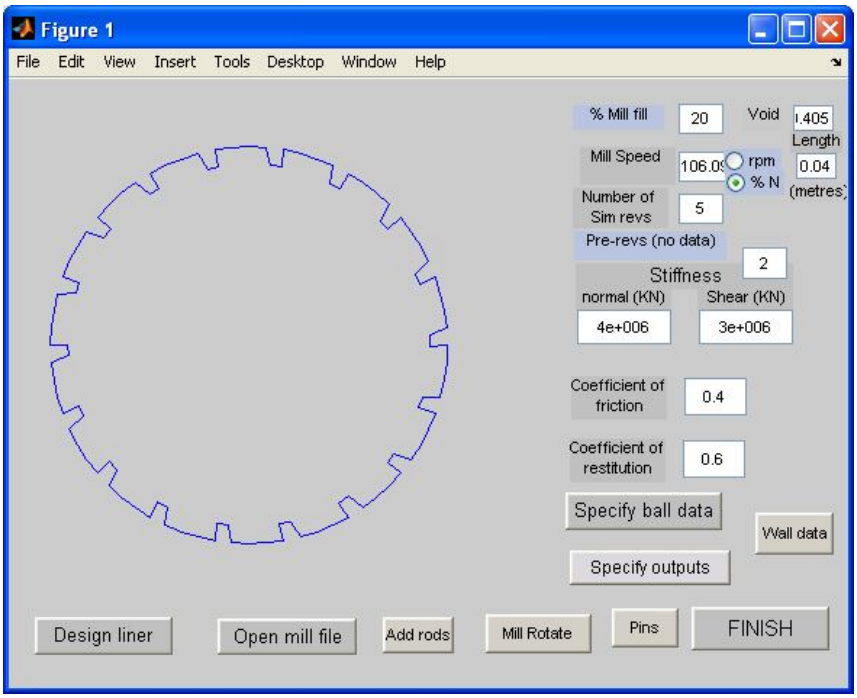

Figure A.2 SimView interface

Text boxes are quite self-explanatory and straightforward. However, one of the first things to do is to draw the profile of lifters to be used. To do that, click the '**Design liner**' button that will bring up Figure A.3 below.

A.6.2 The Design Liner interface

Figure A.3 shows the design liner window that was used to draw the lifter profile of the Wits pilot mill. The combination of the text boxes and push buttons in the lower left section of the window enables one to draw the lifter profile as shown in the plot area.

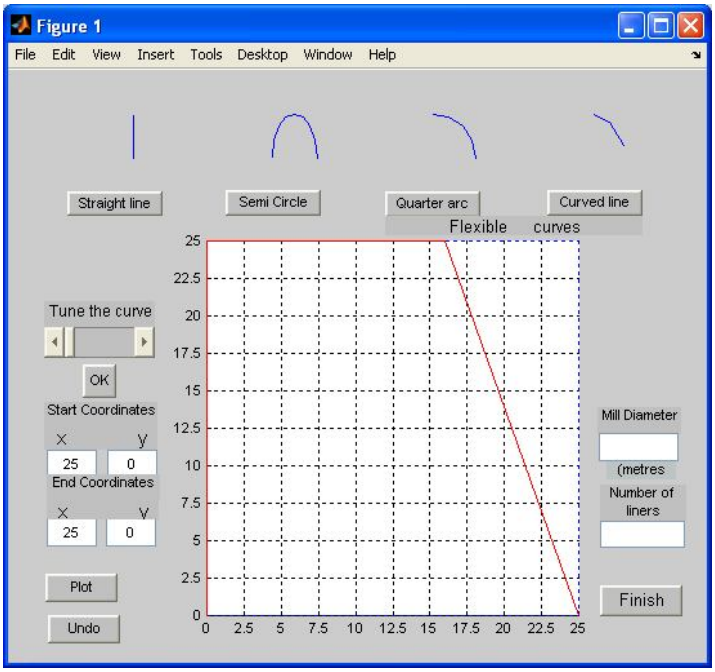

Figure A.3 Design of lifter profile

Once the profile of the lifter is designed, enter the **Mill Diameter** and the **Number of liners**, then press **Finish**.

A.6.3 Formatting Input and Output data

Upon termination of the design of lifters, Figure A.2 reappears in which text boxes on the right-hand side are to be filled with information pertaining to milling conditions and DEM parameters. Next, one can enter Ball size distribution used as well as Contacts Parameters by pressing the '**Specify ball data**' button in Figure A.2 to call Figure A.4 below.

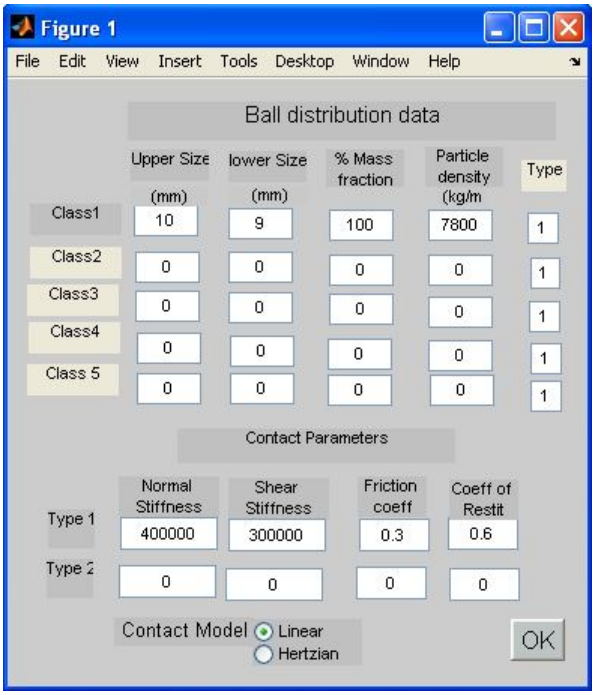

Figure A.4 Interface for entering Ball size distribution and DEM parameters.

The Window is called by the '**Specify ball data**' button

Figure A.5 Interface for entering the types of Energy data outputs.

The Window is called by the '**Specify outputs**' button.

The 'Specify outputs' in Figure A.2, on the other hand, invokes Figure A.5 in which DEM outputs are formatted. In this window, one can select the type of information to be outputted:

- Type of collision energy: impact, frictional and total energy
- Total number of collision events per energy type and per energy class range
- Number of frames to construct the animations
- Other outputs such as the Position plot distribution, velocity profile, ball trajectory, power draw per ball slices, total power draw, and alike.

A.6.4 The Simulator Viewer interface

The interface below (Figure A.6) makes it possible to view the results of the DEM calculation as a full animation. It has the capability of rendering animations frame after frame as the user clicks on the '**Frame Adv**' button. Animations can also be set to run in slow motion using the '**Speed Control**' option table. Animations can also be paused with the '**Pause**' button should one wish to capture a particular frame of the simulation for example.

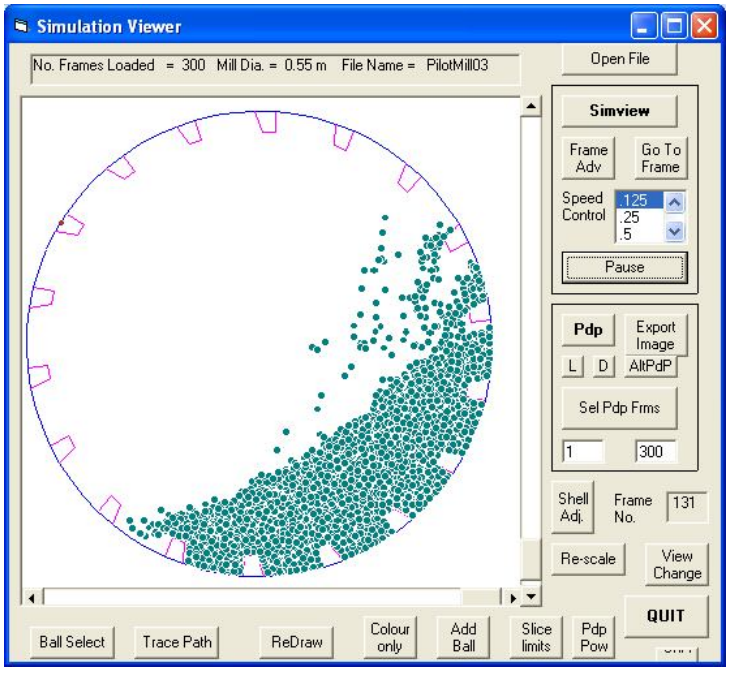

Figure A.6 Simulation Viewer interface

One other output the Simulation Viewer interface can supply is the particle trajectory. In order to generate it, one will click on the '**Trace Path**' button and then choose to plot the trajectories for as many consecutive frames as one wishes. The number of frames is of course limited by the maximum number of frames than the full animation can render. On top of that, one can also select the particles the trajectories of which should be plotted using the '**Ball Select**' button. As an illustration, Figure A.7 shows the complete trajectory followed by a single media within the load for the full simulation.

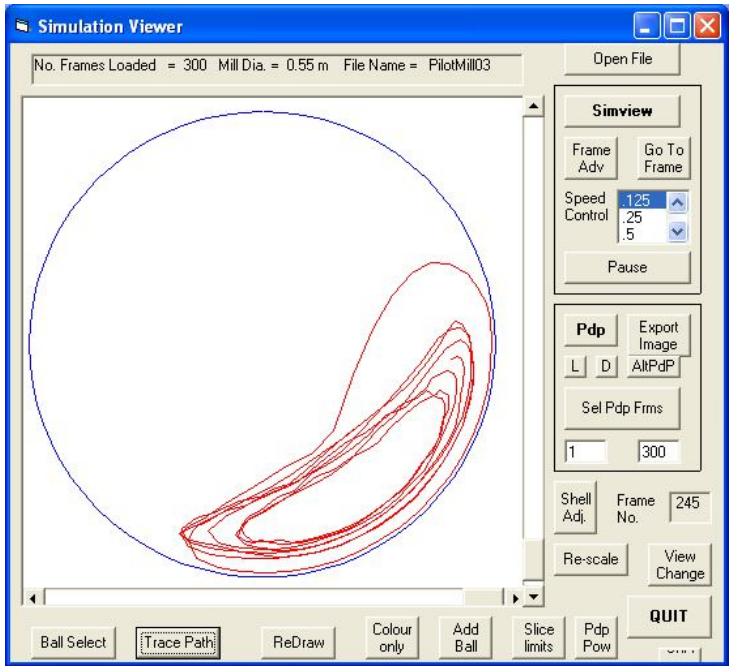

Figure A.7 Path of one single ball generated by the '**Ball Select**' button

In contrast to this, Figure A.8 presents the trajectories of all the grinding balls within the load for three consecutive frames. In the first instance (Figure A.7), the migration of particles from the cataracting to the cascading zone and vice-versa can be appreciated. Individual motions of particles can also be studied in detail from this type of information. In the next instance (Figure A.8), the velocity profile of the full load can be calculated from the length of the solid lines representing the trajectories if the time step between frames is known. Furthermore, the shape of the load is also viewed with a clear differentiation

between cascading, cataracting and centrifuging. The shoulder, toe, and dynamics angle of repose can all be easily measured here.

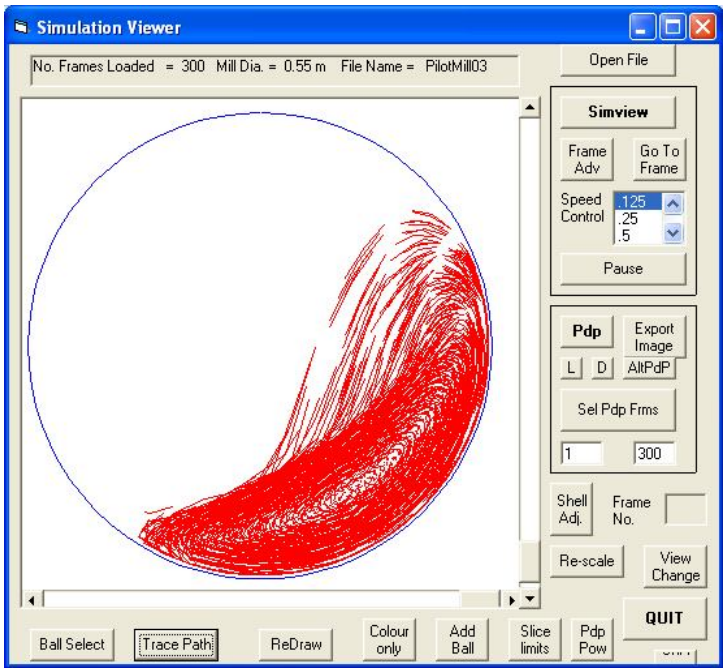

Figure A.8 Illustration of output generated by the '**Trace path**' button

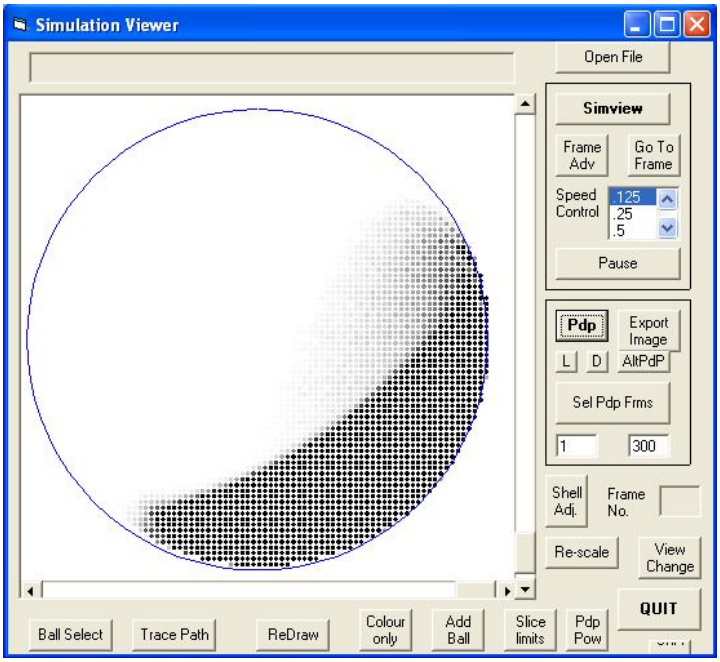

Figure A.8 Example of Particle density positions generated using the '**Pdp**' button

The last feature is the 'Particle density positions plot' or 'Pdp plot' for short. This output is basically the frequency plot of the occupancy by grinding media of each

pixel within the circle representing the mill. The number of time a pixel is occupied by a ball throughout the entire simulation is counted, and then converted to a colour-coded map of the mill using a grey scale (Figure A.9). The map can be made lighter or darker on the scale using the '**L**' and '**D**' buttons.
The Pdp plot provides a qualitative view of the load distribution in the mill. This is important specifically when one wishes to have an idea of how and where power is actually spent. Questions like the following can be answered: What behaviour (cascading or cataracting) is predominant inside a mill and to what extent?

The Wits DEM simulator offers more than is described in the Appendices. Its description has been limited to the functionalities extensively used in the thesis. But, the simulator provides information on the energy associated with friction, abrasion, etc. Net power per frame and per slice of the mill, forces of interaction, and number of collision per type and per energy class can also be obtained.

A.6.5 DEM predictions of mill power

Net powers obtained with the DEM simulator for the different combinations of DEM parameters used are listed below.

Table A.33 Net powers drawn by the mill as calculated by the DEM simulator

% N_c	**Simulated Net Power [Watts]**					
24.37	116.2		105.7	110.2	110.1	108.6
34.81	185.0	190.1		173.5		172.9
46.99	268.9	273.2		258.8		251.3
57.43	350.9	347.8	321.2	322.6	324.1	327.9
62.66	396.5			373.4		370.6
67.88	427.8			398.5		399.8
71.36	452.9	468.9	420.8	420.4	422.6	421.2
78.32	470.3			440.8		439.5
90.50	456.0			433.7		424.5
106.20	326.5	353.4	312.3	328.7	317.9	301.2
	DEM parameters used					
Friction	0.4	0.8	0.2	0.2	0.2	0.2
Ball-ball impact	0.6	0.6	0.6	0.6	0.8	0.75
Ball-wall impact	0.3	0.3	0.4	0.5	0.6	0.5